University of Exeter

Honeycombs with Structured Core for Enhanced Damping

Submitted by Marc-Antoine Cédric Jean Boucher, to the University of Exeter as a thesis for the degree of Doctor of Philosophy in Engineering

In September 2015.

It is a requirement of the project sponsor that the contents of this thesis are not made publicly available due to commercial sensitivities. The External Examiner will be required to sign a confidentiality agreement.

I certify that all material in this thesis which is not my own work has been identified and that no material has previously been submitted and approved for the award of a degree by this or any other University.

Signature :

Honeycombs with Structured Core for Enhanced Damping

Abstract

Honeycomb sandwich panels, formed by bonding a core of honeycomb between two thin face sheets, are in wide use in aerospace, automotive and marine applications due to their well-known excellent density-specific properties. There are many technological methods of damping vibrations, including the use of inherently lossy materials such as viscoelastic materials, viscous and friction damping and smart materials such as piezoelectrics. Some have been applied to damping of vibrations, in particular to sandwich panel and honeycomb structures, including viscoelastic inserts in the cell voids. Complete filling of the cell with foam, viscoelastic or particulate fillers have all been demonstrated to improve damping loss in honeycombs. However, the use of an additional damping material inside the core of a sandwich panel increases its mass, which is often deleterious and may also lead to a significant change in dynamic properties. The work presented in this thesis explores the competing demands of vibration damping and minimum additional mass in the case of secondary inserts in honeycomb-like structures.

The problem was tackled by initially characterising the main local deformation mechanism of a unit cell within a sandwich panel subjected to vibration. Out-of-plane bending deformation of the honeycomb unit cell was shown to be the predominant mode of deformation for most of the honeycomb cells within a sandwich panel. The out-of-plane bending deformation of the honeycomb cells results in relatively high in-plane deformation of the cells close to the skins of the sandwich panels. It was also highlighted that the magnitude and loading of the honeycomb unit cell are dependent on its location within the honeycomb or sandwich panel and the mode shape of the panel.

An optimisation study was carried out on diverse honeycomb unit cell geometries to find locations at which the relative displacement between the honeycomb cell walls of the void is maximal under in-plane loadings. These locations were shown to be dependant of the nature of the loading, i.e. in-plane tension/compression or in-plane shear loading of the honeycomb unit cell and the unit cell geometry.

3

Analytical expressions and finite element analyses were used to investigate the partial filling of the honeycomb unit cell with a damping material, in this case a viscoelastic elastomer, in the target locations identified previously where the relative displacement between the honeycomb cell walls is maximal. Damping inserts in the form of ligaments partially filling the honeycomb cell void have shown to increase the density-specific loss modulus by 26% compared to cells completely filled with damping material for in-plane tension/compression loading.

The form of the damping insert itself was then analysed for enhancement of the dissipation provided by the damping material. The shear lap joint (SLJ) damping insert placed in the location where the relative displacement between the honeycomb cell walls of the void is maximal under in-plane loadings was characterised with very significant damping improvements compared to honeycomb cells completely filled with viscoelastic material.

A case study of a cantilever honeycomb sandwich panel with embedded SLJ damping inserts demonstrated their efficiency in enhancing the loss factor of the structure for minimum added mass and marginal variation of the first modal frequency of the structure. Partial filling of the cells of the honeycomb core was shown to be the most efficient at increasing damping on a density basis.

Honeycombs with Structured Core for Enhanced Damping

Contents

Honeycombs with Structured Core for Enhanced Damping

6

Honeycombs with Structured Core for Enhanced Damping

7

Honeycombs with Structured Core for Enhanced Damping

8

Honeycombs with Structured Core for Enhanced Damping

List of Figures

9

Honeycombs with Structured Core for Enhanced Damping

10

Honeycombs with Structured Core for Enhanced Damping

11

Honeycombs with Structured Core for Enhanced Damping

Honeycombs with Structured Core for Enhanced Damping

13

Honeycombs with Structured Core for Enhanced Damping

14

Honeycombs with Structured Core for Enhanced Damping

Honeycombs with Structured Core for Enhanced Damping

Honeycombs with Structured Core for Enhanced Damping

List of Tables

Honeycombs with Structured Core for Enhanced Damping

Honeycombs with Structured Core for Enhanced Damping

Acknowledgements

I would like to thank Professor C. W. Smith, Professor F. Scarpa, Professor, K. E. Evans, and Dr W. Miller for their guidance and support throughout this project.

I gratefully acknowledge the support of Rolls-Royce Plc, especially the support provided by Dr R. Rajasekaran.

I have been honoured to have Dr Jem Rongong from the University of Sheffield and Prof Paul Reynolds from the University of Exeter examiners of my thesis, thank you.

I sincerely would like to thank all the friends I met during my PhD studies for their cheerfulness and all the good time spent together.

Last but not least, my warmest gratitude goes to my grandfather, General Jean-Pierre Chevillon, who introduced me to science and sparked the interest I have in science today. He sadly passed away in 2013 during my PhD research studies. I dedicate this PhD thesis to him.

Honeycombs with Structured Core for Enhanced Damping

20

Honeycombs with Structured Core for Enhanced Damping

Dissemination

During the course of this PhD a patent application has been filled, a paper has been published in a peer-reviewed journal and a conference presentation has been given.

Patent

M.-A. Boucher, C. W. Smith, F. Scarpa, R. Rajasekaran, K. E. Evans, 2013. Vibration Damping, Patent US20130264757 A1, 2013.

Publication

M.-A. Boucher, C. W. Smith, F. Scarpa, R. Rajasekaran, K. E. Evans, 2013. Effective Topologies for Vibration Damping Inserts in Honeycomb Structures, Composite Structures, Volume 106, Pages 1-14, ISSN 0263-8223.

Conference

M.-A. Boucher, C. W. Smith, F. Scarpa, R. Rajasekaran, K. E. Evans, 2012. High Damping Performance of Aluminium Honeycombs through the Use of Passive Inserts, *ICSS-10*, Nantes.

Honeycombs with Structured Core for Enhanced Damping

Chapter 1. Introduction and Literature Review

1.1 Introduction

Honeycomb core sandwich panels are formed by bonding two thin face-sheets to a low density honeycomb core, the properties of which are determined in the main by the geometry of their unit cells [1] [2]. Such sandwich panels are widely used in many applications, especially in transport, because of their excellent density-specific properties [3] [4]. For instance, these structures are used in airplane construction. Figure 1.1 shows the areas where sandwich structures are used in the Airbus A380 from the nose of the airplane to the turbine engine (Rolls-Royce Trent 900) [5]. Sandwich panels are, indeed, widely used in aircraft applications because they provide good strength properties and low-density structures, leading to fuel savings.
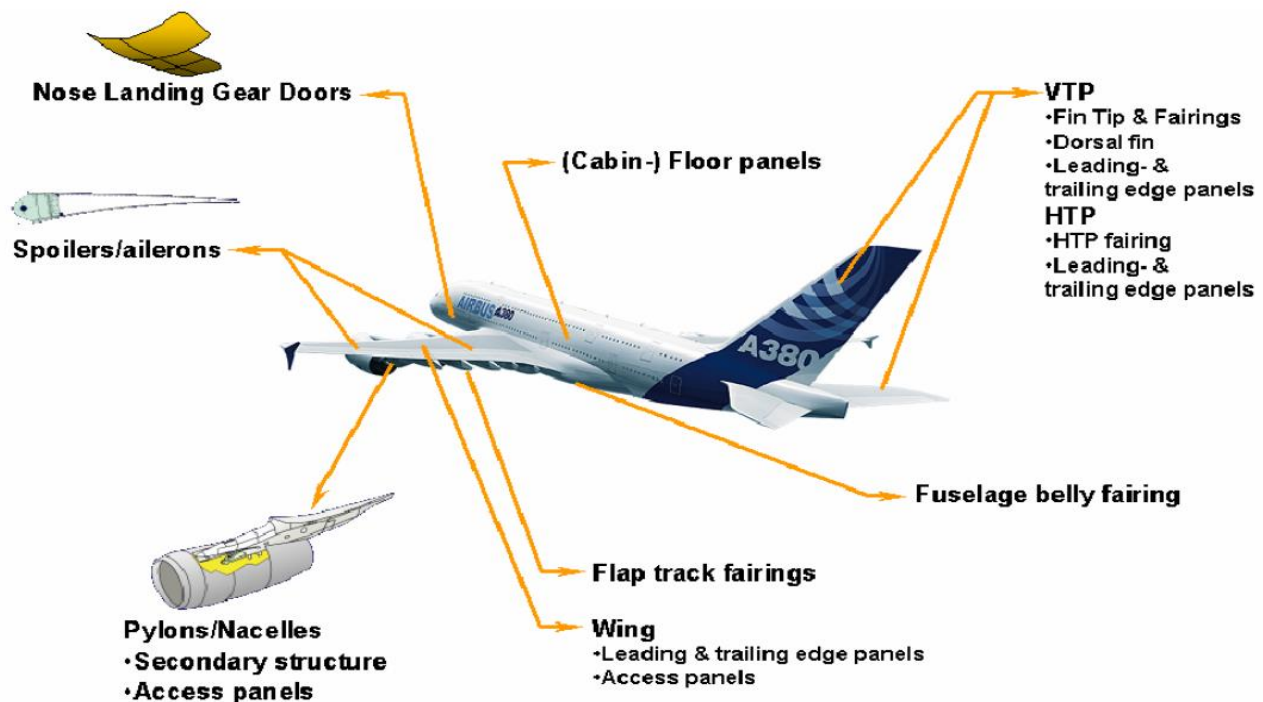
Figure 1.1: Airbus A380 sandwich applications [5].

Hence, in their application in the transport industry, honeycomb sandwich panels are used in vibration-rich environments. In aero-engines, for example, each blade is a source of excitation onto the fan case. Therefore, multiples of the shaft rotational

Honeycombs with Structured Core for Enhanced Damping

speeds are a source of excitation for the fan case, which can lead to resonance in numerous frequency ranges. Certification requirements and service cost reductions require a specific cycle life to be achieved, which is often minimal at the resonant frequencies of a system. When seeking to meet the allowable stress limits for a given fatigue life, damping can be added to a system. Many studies have sought ways to improve the damping properties of honeycombs, using either active or passive methods [6]. The active methods have used actuator materials such as piezoelectric or magnetostrictive materials, which are used to counteract structural deformations arising from vibrations from an external control system [7] [8]. However, the requirement for an external control system can, in some cases, be very difficult, especially in rotative components. Passive methods that do not require external control include many kinds of dissipative mechanisms: damping by 'friction ledge' [9], particle impact damping [10] and damping using viscoelastic inserts [11]. Shape memory alloys (SMAs) have also been postulated for use in damping roles, due to their high loss coefficients [12].

A literature survey encompassing honeycomb sandwich structures and solutions for improved damping properties is presented in this chapter, for application in high-vibration environments such as the rotating parts of a jet engine. The problems addressed by this thesis are subsequently defined at the end of this chapter.

1.2 Honeycomb Sandwich Structure

1.2.1 Uses of Sandwich Panel/Origins

Bitzer states that one of the earliest man-made sandwich panels dates back to 1845, with a wooden egg-crate core used as a very good compression panel for train applications [3]. Sandwich construction was then used by Fairbain in 1849 in the construction of the Britannia and Conway tubular bridges [23]. This sandwich panel was made with iron cores and a wood core.

With the development of aircraft applications, sandwich structures started to be used more widely because of their high density-specific properties. Therefore, the first plane with sandwich panels was built in 1919 for seaplane pontoons. Later on, von

Karman and Stock patented a glider that used sandwich panels in its fuselage [3]. A few years later, von Karman and Mautner designed a plane with sandwich elements in the wings. Sandwich panels were then introduced in the fuselage of several planes such as the Comet Race and the Albatross, and in the wings and the fuselage of the famous Mosquito, developed at the outbreak of World War II by the de Havilland Airplane Company. In these planes, the sandwich structure consisted of a balsa wood core and plywood skins [3]. A metal-wood sandwich was then applied in the floor of the older F27. In 1945, the first all-aluminium sandwich panel was produced. The use of the metal element for sandwich panels was an important step to avoid any degradation caused by the use of bio-degradable materials. However, the manufacturing of metal sandwich panels was the source of several problems, such as the bonding of the core and the face sheet using an adhesive [3].

Subsequent to World War II, during which time the development of aerospace technology and materials/structures such as sandwich panels was rapid, panels began to be used for a lot of different applications because of their attractive properties, especially in the fields of marine, aviation, building construction, and automotive. For example, sandwich panels were used in the Apollo project, which successfully landed on the Moon in 1969 [3].

Today, a large variety of sandwich materials are used in packaging applications using Kraft paper materials, to more advanced aircraft applications using metallic and composite materials [4].

1.2.2 Description of Sandwich Structure

A sandwich structure is formed by bonding thin, strong face sheets to a relatively thicker, lightweight core. A sandwich structure is composed of a skin, an adhesive film and a core, as illustrated in Figure 1.2 [13].

Honeycombs with Structured Core for Enhanced Damping
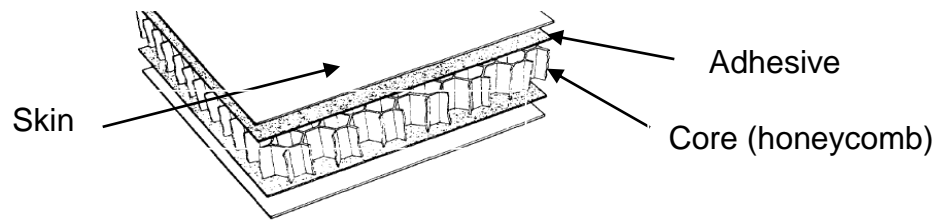
Figure 1.2: Representation of a sandwich panel [13].

a. Face-Sheet

In the sandwich panel structure, the face sheet handles the loads and deflection requirements, which influence the choice of the materials. A large range of materials are used in different industries, depending on the application for which the sandwich structure is designed. Packaging applications very often use Kraft paper as face sheets, whereas the aerospace industry tends to use materials with higher damage tolerance, such as composites [3]. The materials of the face sheets are chosen for properties such as strength, stiffness, damage tolerance, environmental conditions, appearance and cost.

b. Core Material

The core materials of sandwich structures are usually described as 'cellular solid' [2]. The term 'cellular solid' characterises structures made up of solid ribs or plates forming an interconnected network. Their internal architecture can form 'open-cells' or 'closed cells' and be 'deterministic' or 'stochastic'. Stochastic architectures are characterised by random cell parameters such as foams, whereas deterministic cells are defined by constant cell parameters forming a periodic arrangement of cells such as honeycomb panels. Figure 1.3 illustrates some examples of core materials used in sandwich structures: wood cores, foam cores, honeycomb cores, corrugated cores and textile cores [5].

Honeycombs with Structured Core for Enhanced Damping

Homogeneous core materials:
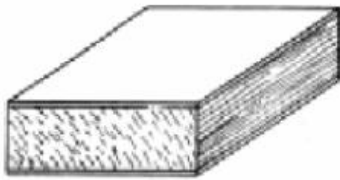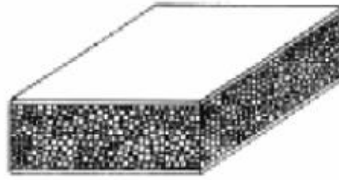
Wood cores   Foam cores

Structure core materials:
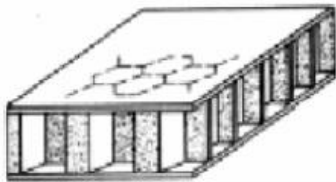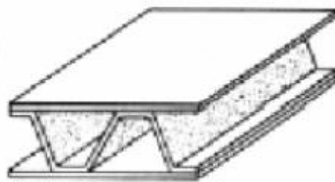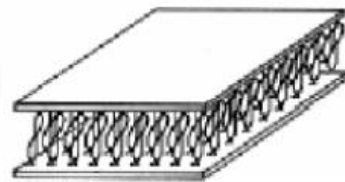
Honeycomb cores   Corrugated cores   Textile cores

Figure 1.3: Types of core in a sandwich panel [5].

Among the different cores that can be introduced in a sandwich panel, honeycombs are the most commonly used. It should be noted that an infinite number of honeycomb cell geometries can be defined given specific geometric cell parameters such as the number of walls, wall thickness and wall length, etc. Complex unit cells can be defined as illustrated in Figure 1.4, as opposed to more simplistic cells as in Figure 1.5 [18] [19]. The most commonly used honeycomb cell geometries are hexagonal or squared, one of the main reasons being the ease of manufacturing [3]. This thesis focuses on the hexagonal honeycomb core.

Honeycombs with Structured Core for Enhanced Damping
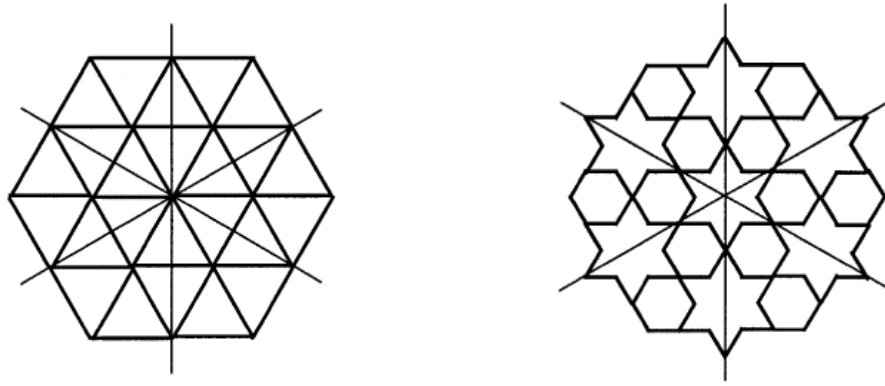
Figure 1.4: Representations of a triangular and a star-cell core [19].
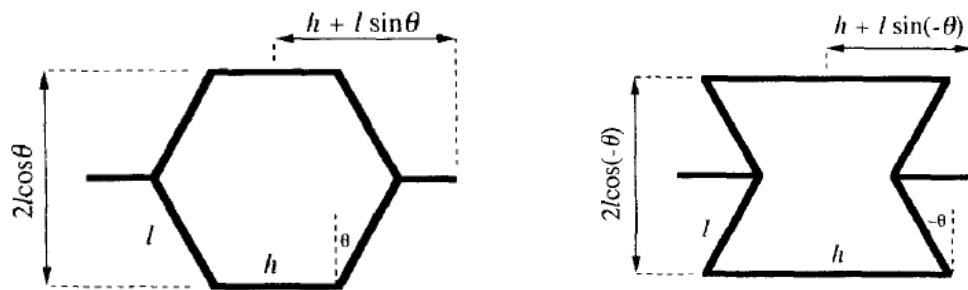
Figure 1.5: Representations of a hexagonal and a re-entrant cell core [18].

'Cellular solids' are used as core materials for sandwich panels because of their low relative density ρ^*/ρ_s, where ρ^* is the density of the core material and ρ_s is the density of the constituent material. Any material that can form 'cellular solids' can be used as a constituent material. For example, aluminium and steel can be used for metallic cores and fibreglass and Kraft paper can be used for non-metallic cores. The choice of the core material is based on its density and its application. It can be used for creating unidirectional fluid flows, for absorbing energy impacts, to impede thermal transport across the faces of sandwich panels and for acoustic damping [3] [16] [17].

c. Adhesive

The structural integrity of a sandwich panel is ensured by the bonding of the face sheet to the core material provided by the use of an adhesive. The choice of adhesive material depends on the skin/core properties and the environment/application for which the sandwich panel is designed [3]. Adhesives are

Honeycombs with Structured Core for Enhanced Damping

chosen conservatively in respect of the sandwich panel operating temperature range as their properties vary dramatically with temperature. Common adhesives used in sandwich panels are nitrile phenolic films, modified epoxy films, polyimide films, modified urethane pastes, core splicing adhesive pastes and tapes [22].

d. Manufacture of honeycomb sandwich structure

Many techniques are used to manufacture honeycomb cores depending on their constituent materials. Metallic honeycombs can be made by resistance welding, brazing, diffusion bonding, thermal diffusion and adhesive bonding, the latest being the most widely used in industry [3]. Two common manufacturing processes for honeycombs are illustrated in Figure 1.6. In the expansion process, thin metal sheets are cut into panels and strip bonded. These panels form after bonding to a block, which is cut and pulled apart to create an expanded panel. This method is widely used because the process is one of the cheapest to build honeycomb structures. However, this process requires high inter-sheet bond strengths to enable the sheet stretching. This can be done with low-density honeycombs. As the relative density of the honeycomb increases, the force needed to stretch the sheets can cause inter-sheet bond fracturing [15]. In this case, other manufacturing methods are required, such as the corrugation process. As presented in Figure 1.6, during the corrugation process a metal sheet is corrugated and cut into panels, then each corrugated panel is welded together to create the honeycomb structure.
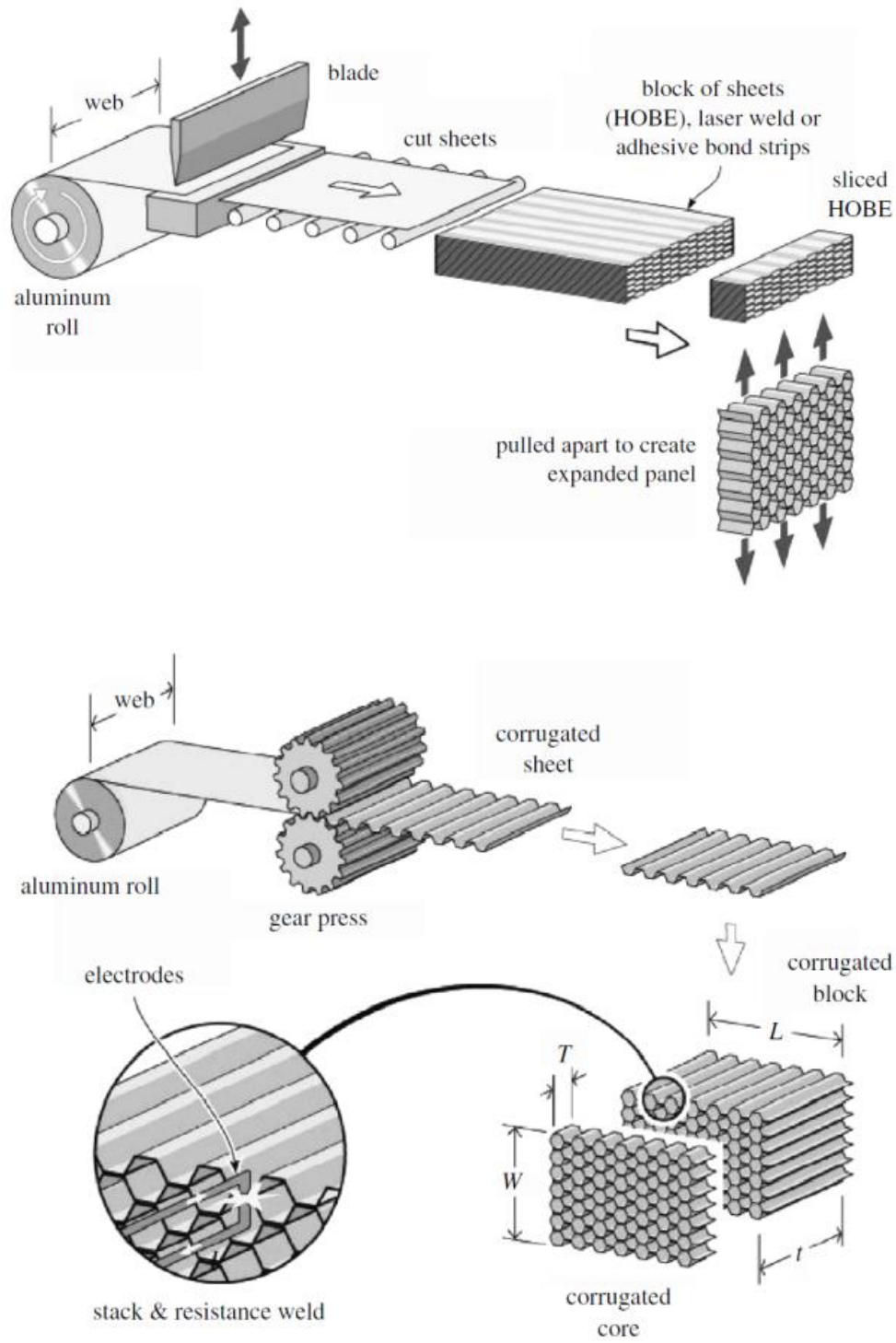
Figure 1.6: Representations of the expanded honeycomb manufacturing process (top) and the corrugation manufacturing process (bottom) [15].

Honeycombs with Structured Core for Enhanced Damping

Both the expanded and the corrugation processes can be applied to manufacture non-metallic honeycomb [3]. With the intensive development of 3D printers, fused deposition modelling (FDM) has become a quick and very effective method to manufacture complex honeycomb geometries [20].

1.2.3 Mechanical Properties of Sandwich Structures

Sandwich structures are characterised by their excellent density-specific properties. They exhibit especially high ratios between bending stiffness and mass; hence their application in aeronautic applications. The high bending stiffness of a sandwich structure is achieved by the separation of the face sheet with a core material, increasing the second moment of area of the structure. For illustration, Vinson compared the flexural and bending stiffness of an isotropic sandwich construction with a monocoque construction of the same skin mass (see Figure 1.7). The ratio between the bending stiffness of the sandwich structure and a monocoque construction is given in Equation 1.1 [1].
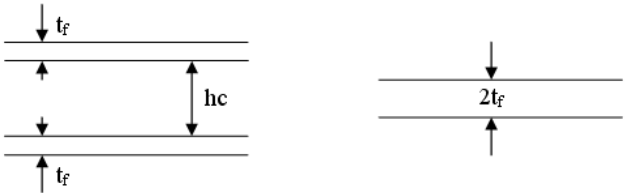
Figure 1.7: Cross-section of sandwich and monocoque constructions [1].

$$\frac{D_{sand.}}{D_{mon.}} = \frac{3}{4} \cdot \left(\frac{h_c}{t_f}\right)^2 + 1$$

<div align="right">Equation 1.1</div>

The primary function of the face sheet in a sandwich structure is to provide extensional and in-plane shear stiffness, whereas the core provides a through-thickness shear resistance and a through-thickness extensional resistance. Core properties are, therefore, characterised with high through-thickness shear modulus and Young's modulus [1]. Since most of core materials are cellular solids, much work has been undertaken to investigate their geometry-dependent properties. Equations

Honeycombs with Structured Core for Enhanced Damping

governing the mechanics of honeycombs have been derived by Gibson and Ashby using beam theory [2, 24]. For illustration, the expressions derived by Gibson and Ashby are shown in Equation 1.2 to Equation 1.4 respectively for the in-plane Young's Modulus in the x direction of the cell, $E_{x\ G\&A}$, the in-plane Young's Modulus in the y direction of the cell the of the cell, $E_{y\ G\&A}$, and the in-plane shear modulus, $G_{xy\ G\&A}$ of the cell illustrated in Figure 1.8. In these equations, bending of the honeycomb cell ribs is the predominant deformation mechanism of in-plane hexagonal honeycomb, which is a valid hypothesis for slender ribs (ratio between the thickness and length of the ribs < 0.1). More complex models have been derived accounting for examples of the stretching and hinging of the honeycomb cell walls [18].
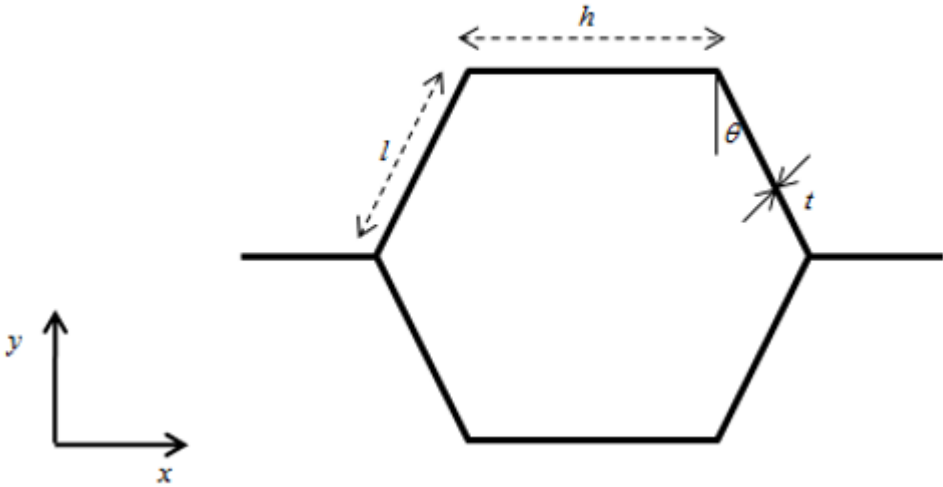
Figure 1.8: Honeycomb cell with its geometric parameters h, l, t and θ.

$$E_{x\ G\&A} = \left(\frac{t}{l}\right)^3 . \frac{E_{s.}(\frac{h}{l} + sin\theta)}{cos^3\theta}$$

Equation 1.2

Honeycombs with Structured Core for Enhanced Damping

$$E_{y\ G\&A} = \left(\frac{t}{l}\right)^3 . \frac{E_s.cos\theta}{\left(\frac{h}{l} + sin\theta\right).sin^2\theta}$$

<div align="right">Equation 1.3</div>

$$G_{xy\ G\&A} = \left(\frac{t}{l}\right)^3 . \frac{E_s.(\frac{h}{l} + sin\theta)}{\left(\frac{h}{l}\right)^2 .\left(2.\frac{h}{l} + 1\right).cos\theta}$$

<div align="right">Equation 1.4</div>

1.2.4 Strength of Sandwich Structures

The failure modes of sandwich structures depend on the properties of the face sheets, core materials, adhesive and the loading arrangement. Possible failure modes for a honeycomb sandwich panel consist of:

- Facing failure: generally caused by an insufficient panel thickness or facing strength, this mode of failure occurs when the normal tensile stresses due to the bending loads of the panel exceed the yield strength of the face sheet materials

- Transverse shear failure: caused by insufficient core shear strength or panel thickness

- Crushing of core: caused by excessive beam deflection or by low core compression strength

- General buckling: caused by insufficient core shear rigidity or insufficient panel thickness

- Intra-cell dimpling: occurs with very thin facings and large core cells, the face may fail by buckling where it is unsupported by the walls

- Shear crimping: occurs as a consequence of buckling of the panel and is generally caused by low core shear modulus or low adhesive shear strength

Honeycombs with Structured Core for Enhanced Damping

- Face wrinkling: occurs either in towards the core or outwards, depending on the stiffness of the core in compression and the adhesive strength. This mode of failure can be the origin of debonding between the face and the core

Figure 1.9 illustrates some of the possible modes of failure for a honeycomb sandwich panel [3] [25] [28].

Core shear   Local indentation

Face yielding   Intra-cell dimpling   Face wrinkling
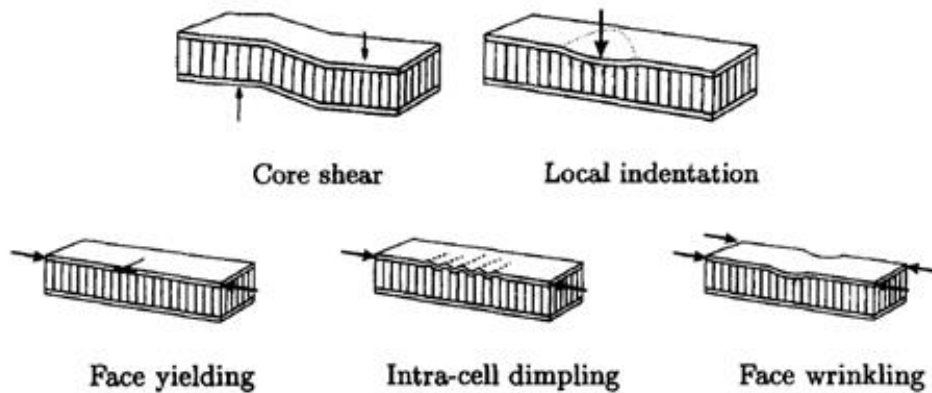
Figure 1.9: Modes of failure of a honeycomb sandwich panel [25].

To some extent, modes of failures can be classified in 'maps of failure', as illustrated in Figure 1.10 [26] [27].

Honeycombs with Structured Core for Enhanced Damping

$$t/L = 5 \cdot 10^{-4}$$
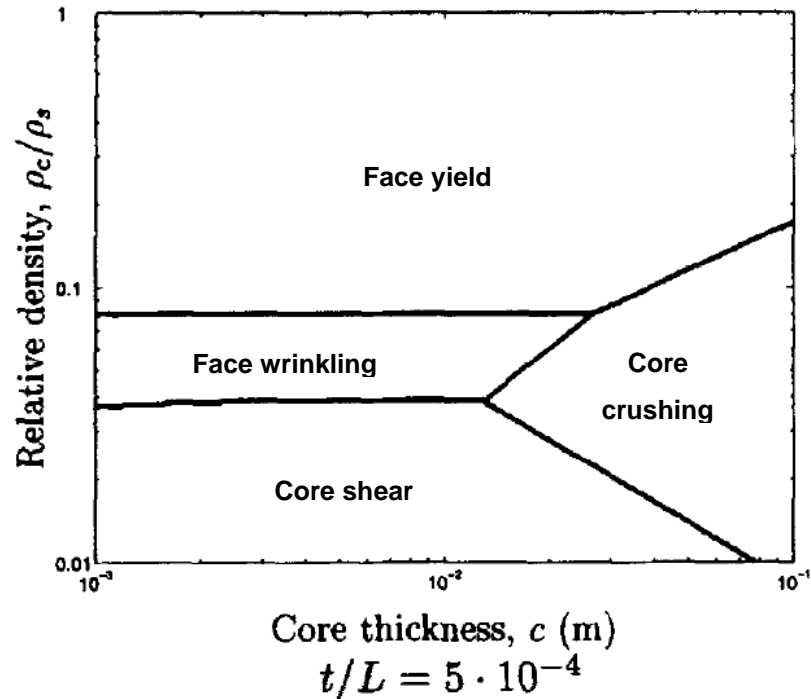
Figure 1.10: Map of failure of a honeycomb core [27].

1.3 Vibration Damping

1.3.1 Introduction to Vibration Damping

"Vibration is everywhere, and everything vibrates", Jones [29]. Vibrations are desirable for some applications, such as music instruments; but, in most cases, vibrations are an undesirable phenomenon leading to waste of energy and noise pollution. In structures, uncontrolled vibrations are often a source of mechanical failure, as illustrated in the collapse of the Tacoma Bridge in 1940. Vibrations are most critical when the natural frequency of a system matches the excitation frequency caused by external dynamic loads, as they induce resonance of the system. In an aero-engine, the response of the engine can be magnified up to 1,000 times at resonance [77]. Uncontrolled vibration can be limited with careful design, involving design iterations for mass, stiffness and damping of the system in order to avoid external driving frequencies. This will be discussed for a single degree of freedom system with viscous damping, as seen in Figure 1.11 [29] [30].

35
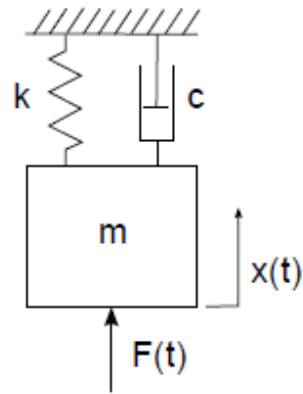
Figure 1.11: Single degree of freedom system with viscous damping.

The equation of motion for this system is shown in Equation 1.5, where m is the mass, c the coefficient of viscous damping, k the stiffness of the system and $F(t)$ the force excitation.

$$m.\ddot{x} + c.\dot{x} + k.x = F(t)$$

Equation 1.5

The natural frequency of the system, ω_0, depends of the stiffness and mass parameters of the system, as shown in Equation 1.6. Any modification to the stiffness and/or mass of the system is, therefore, a potential solution to avoid resonance induction at a specific external frequency.

$$\omega_0 = \sqrt{\frac{k}{m}}$$

Equation 1.6

However, most complex systems operate in a wide frequency range associated with multiple resonances. This is the case, for example, for an aero-engine in which the tuning of mass and stiffness parameters becomes almost impossible for avoidance of critical frequencies [78]. In order to reduce the response of a system, damping is

Honeycombs with Structured Core for Enhanced Damping

added to meet the required fatigue allowable. The objective of introducing damping in a system is to dissipate energy through each cycle of vibration by conversion into heat. As a result, resonance phenomena arising at the natural frequencies of a system are limited via energy dissipation. Equation 1.5 can be rearranged introducing the damping ratio, ζ, of the system, as shown in Equation 1.7. It should be noted that multiple measures of damping have been defined; the coefficient of viscous damping and the damping ratio are one of these measures. This will be presented in further detail in section 1.3.2.

$$\ddot{x} + 2.\zeta.\omega_0.\dot{x} + \omega_0{}^2.x = \frac{F(t)}{m} \quad \text{with} \quad \zeta = \frac{c}{2.\sqrt{k.m}}$$

<div align="right">Equation 1.7</div>

Figure 1.12 illustrates the impact of varying the damping ratio on the response amplitude of a single degree of freedom system with viscous damping subjected to a harmonic excitation. The amplitude response is reduced to increase the damping ratio to 1 (known as critical damping), where the resonance peak virtually disappears. The first modal frequency of a single degree of freedom viscously damped system is given in function of the natural frequency of the system ω_0 in Equation 1.8.

$$\omega_R = \omega_0.\sqrt{1 - \zeta^2}$$

<div align="right">Equation 1.8</div>

Honeycombs with Structured Core for Enhanced Damping
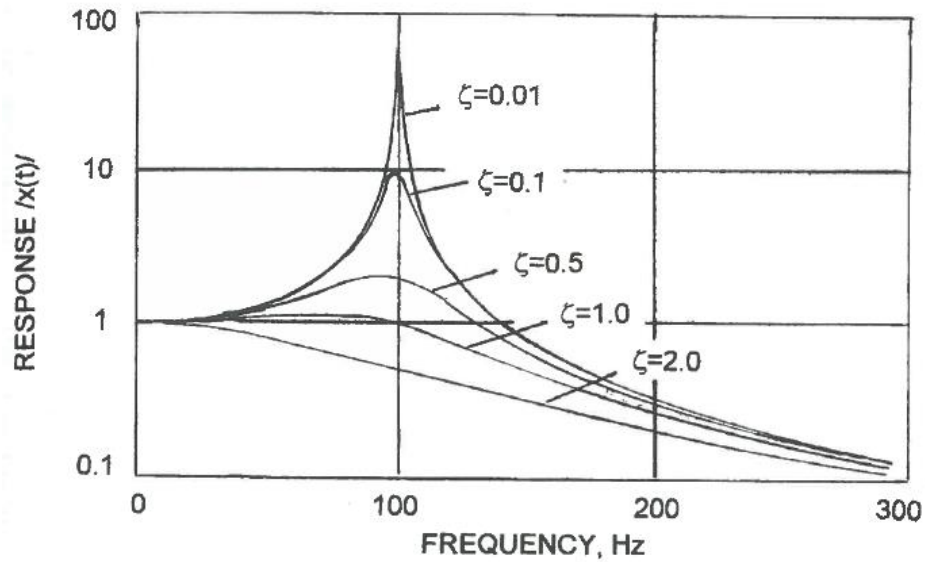
Figure 1.12: Time and harmonic response of the system with viscous damping [29].

1.3.2 Damping Parameters

In the previous paragraph, the damping ratio, ζ, and the coefficient of viscous damping, c, were introduced to define damping. The definition of the damping parameter is directly associated to the method used for measuring the damping properties of a system [79]. These methods can be classified in three categories:

1. Methods based on the transient response of a system: the logarithmic decrement, δ, is used to measure damping as defined in Equation 1.9, where q_i and q_{i+1} are heights of two subsequent peaks

$$\delta = \log\left(\frac{q_i}{q_{i+1}}\right)$$

Equation 1.9

2. Methods based on the harmonic response of a system: these methods use the definition of the Q factor to define the damping parameter at the resonance of a system

3. Methods based on energy dissipation: the loss factor, η, is used as a measure of energy dissipation, as defined in Equation 1.10, where U_{max} is

38

Honeycombs with Structured Core for Enhanced Damping

the maximum energy stored in the system and ΔU the energy loss per cycle

$$\eta = \frac{\Delta U}{2\pi.U_{max}}$$

<div align="right">Equation 1.10</div>

As a measure of damping, these parameters are related to each other as shown in Equation 1.11.

$$\eta = \frac{1}{Q} = 2.\zeta = \tan(\delta)$$

<div align="right">Equation 1.11</div>

1.3.3 Material Damping

Three primary mechanisms can be identified as sources of damping: internal damping, structural damping and fluid damping. Since the scope of the research presented in this thesis is to use material for improved damping properties of structures, material internal damping is discussed.

Material damping is a consequence of microstructural defects, crystal grain relative motions, dislocations in metals and molecular chain movements in viscoelastic materials causing energy dissipation through heat generation [31]. Damping of materials is usually quantified with loss factor, η, as defined in Equation 1.10. The loss factor represents the energy dissipation per loading cycle. The energy dissipation of a cycle of loading is illustrated in Figure 1.13.

Honeycombs with Structured Core for Enhanced Damping
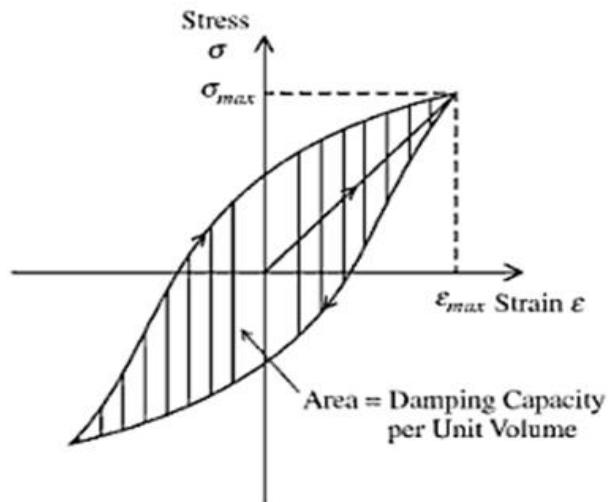
Figure 1.13: Representation of the hysteresis behaviour in a stress-strain curve introducing internal material damping.

The amount of energy lost per cycle is highly dependent on the material, as illustrated in Table 1.1. For instance, the energy dissipated during each cycle of vibration is extremely small for most metals unless the material is deformed beyond the yield point whereby the material starts to deform plastically [3]. Specific metallic alloys, for instance, shape memory alloy (SMA), exhibit higher damping properties from complex internal mechanisms of deformation [12].

Table 1.1: Loss factors of classic materials [76]

Material	Structural loss factor, η_s
Aluminium	1.0×10^{-4}
Brick, concrete	1.5×10^{-2}
Cast iron	1.0×10^{-3}
Copper	2.0×10^{-3}
Glass	1.0×10^{-3}
Plaster	5.0×10^{-3}
Plywood	1.5×10^{-2}
PVC	0.3
Sand (dry)	$0.02–0.2$
Steel	$1–6 \times 10^{-4}$
Tin	2.0×10^{-3}

Honeycombs with Structured Core for Enhanced Damping

Viscoelastic refers to polymers composed of long, intertwined and cross-linked molecular chains. The internal molecular interaction that occurs during the deformation and vibration of these materials provides damping by energy dissipation through heat generation. Viscoelastic materials encompass all rubber and gel materials [29]. Viscoelastic material properties are frequency and temperature dependent, as illustrated in Figure 1.14.
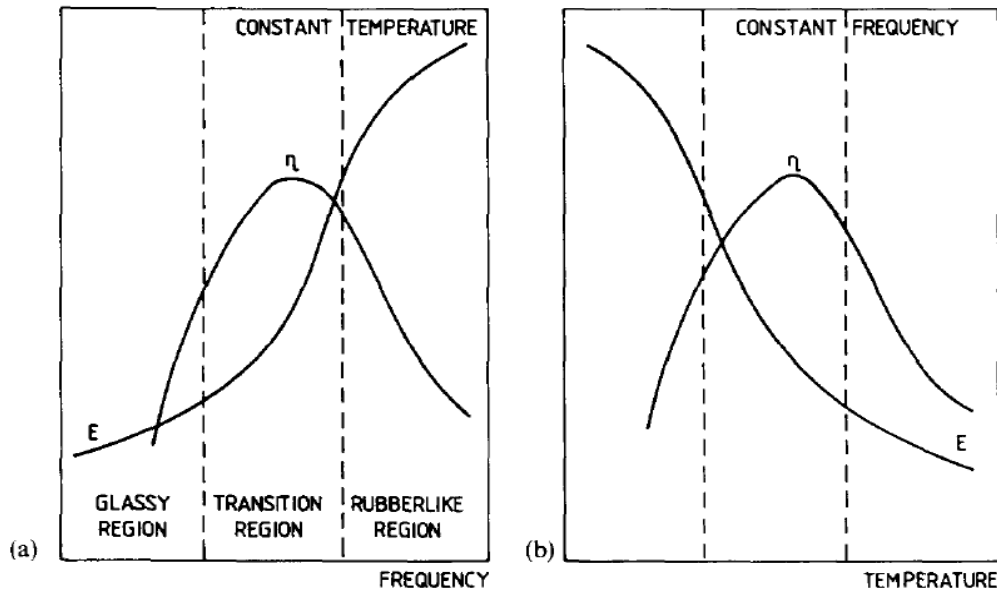
Figure 1.14: Material property of a viscoelastic material as a function of temperature (left) and frequency (right) [29].

For deformation below the yield strain of materials, metals exhibit an elastic behaviour characterised by Hooke's law. In contrast to purely elastic materials, viscoelastic materials exhibit an elastic and viscous behaviour under loading, enhancing energy dissipation. Figure 1.15 illustrates the stiffness loss map of Young's modulus versus damping for materials at ambient temperature [108]. With loss factor between 0.001 and 1 and Young's modulus between 0.01 MPa and 5 GPa, viscoelastic materials shows much higher damping capacity than metals. However, good damping performance of viscoelastic material is highly dependent on temperature and is only suitable for applications operating between -40°C to 150°C [80] [110].
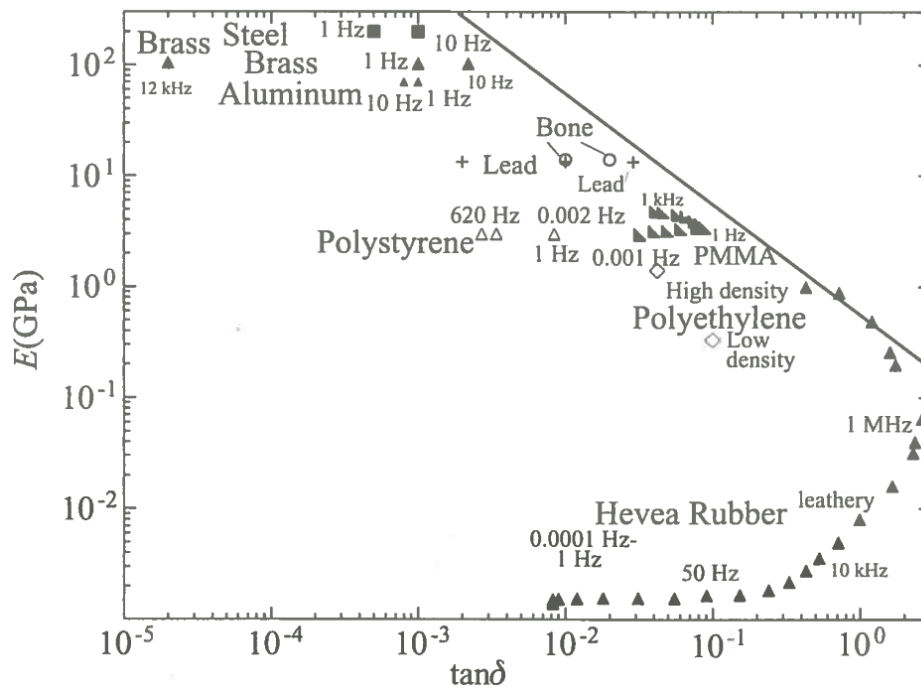
Figure 1.15: Stiffness loss map of Young's modulus versus damping for materials at ambient temperature [108].

Recently, enhanced damping has been achieved by tailoring material properties and design materials with a negative or null Poisson ratio [81] [89]. Materials with a negative Poisson ratio were first introduced by Lakes in 1987 with polyurethane foam. Materials with a negative Poisson ratio are known as 'auxetic', derived from the Greek word 'auxestos', meaning 'that which may be increased' [18] [86].

1.4 Damping of Sandwich Panels

Damping of sandwich panels falls in two categories: active and passive techniques [9].

Active damping deals with 'smart materials' such as piezoelectric materials, magnetostrictive materials and magneto rheological fluids [7] [8]. Piezoelectric materials provide an electric charge when mechanically stressed, and vice versa. These materials are, therefore, used as both sensors and actuators to control structures by providing an 'out of phase' signal to cancel unwanted deformations.

Passive damping encompasses all types of energy dissipation mechanism that do not require external control. Material damping is often used as an effective passive damping mechanism for structures relying on the damping capabilities of materials. As highlighted in the previous section, specific metals such as SMA and viscoelastic materials are suitable for passive damping applications. Passive damping can be achieved by friction and particle impact damping. Possible damping technologies are presented in Table 1.2.

Table 1.2: Damping technologies for sandwich panels.

Active Damping Technology	Passive Damping Technology
Electro and magnetorheological fluids Shunted piezoelectrics Shunted magnetostrictive	Thermoplastic cores Constraint layer Foam filling Friction (particles, ledge) Particle impact damping Tuned mass damping

For implementation inside jet engines, and especially rotating parts, active damping techniques are not a viable solution for damping improvement and, hence, not discussed in this thesis.

1.4.1 Viscoelastic Layer

Viscoelastic materials are commonly used as a layer treatment to enhance the damping properties of a mechanical component since they exhibit high material damping properties [4]. Since this technology is often applied in transportation industries such as automotive or aerospace, effective implementation of viscoelastic materials has been developed to limit weight increase. This is achieved by a local insertion of viscoelastic treatment where the viscoelastic material is most likely to be deformed, therefore increasing its internal energy dissipation. Layer damping treatments encompass free layer damping and constrained layer damping, as described subsequently.

Honeycombs with Structured Core for Enhanced Damping

1.4.1.1 Free Layer Damping or Coated Layer

Free layer damping consists of the application of a viscoelastic material with high damping properties on the surface of a base structure (see Figure 1.16). Under vibration, the viscoelastic layer follows the deformation of the base structure resulting in additional energy dissipation in the viscoelastic layer. Damping properties increase with the volume of viscoelastic material used as coating. However, this technique often leads to unwanted weight increase [4] [29].
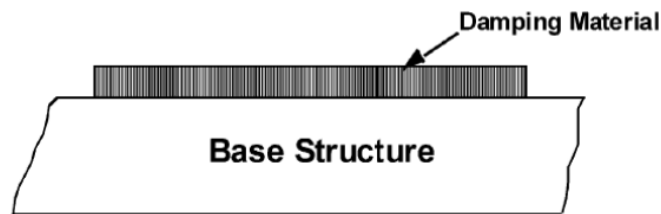
Figure 1.16: Illustration of a free layer damping system [4].

1.4.1.2 Constrained Layer Damping

Constrained layer damping (CLD) consists of an added viscoelastic material layer, sandwiched between two stiffer layers, as illustrated in Figure 1.17. Similarly to the free layer damping treatment, the viscoelastic layer follows the deformation of the based structure, enhancing the damping properties of the assembly. The damping performance of optimised CLD for a given weight increase of viscoelastic material is increased compared to free layer damping. The combined effect of the base structure and the constrained layer under vibration imposes a higher magnitude of shear deformation in the viscoelastic layer [4] [29] [32] [38].
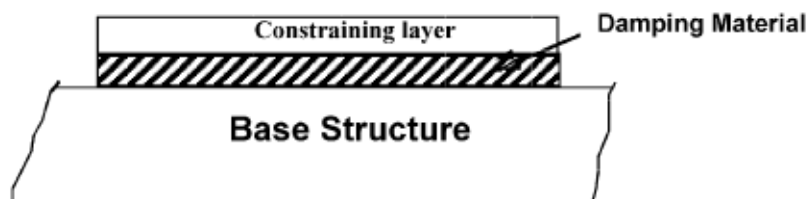
Figure 1.17: Illustration of a constrained layer damping system [4].

Honeycombs with Structured Core for Enhanced Damping

Since viscoelastic materials exhibit low stiffness compared to metals, the introduction of viscoelastic layers can potentially lead to unwanted low-frequency modes. Hybrid solutions using a honeycomb core parallel to the viscoelastic layer can be used to avoid such undesirable effects, as illustrated in Figure 1.18. Jung and Aref highlight that the global stiffness of the added layer treatment is governed by the honeycomb core [39].
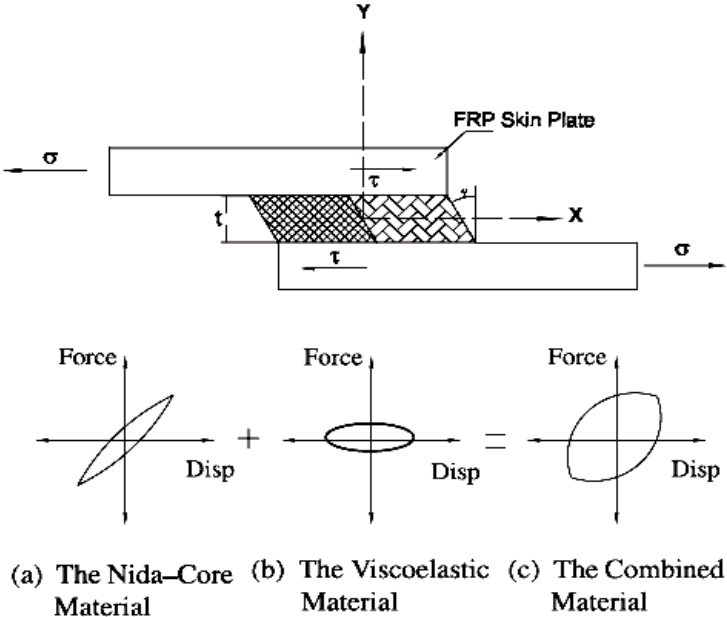
Figure 1.18: Schematic presentation of the idealised force-displacement relation of the concept developed by Jung and Aref [39].

1.4.2 Honeycomb Filling

Enhancement of the damping properties of the honeycomb sandwich panel can be provided through the use of a high damping performance material placed in the voids of the honeycomb structure. This can be achieved through simple filling of the honeycomb core with a lossy material or by use of particles inside the void of the honeycomb.

1.4.2.1 *Foam and Viscoelastic Filling*

Foam and viscoelastic filling is a damping solution that makes use of the internal voids of the honeycomb sandwich structure. The cell walls of the honeycomb core

Honeycombs with Structured Core for Enhanced Damping

are backed up by the viscoelastic or foam material so that the total surface allows external forces to dissipate more energy than the honeycomb core alone [11] [40] [41]. Experimental results with the foam filling of panels have shown an increase in the crushing strength and energy absorption capacity of a honeycomb sandwich panel up to 300% [46]. However, adding foam or viscoelastic material to the honeycomb sandwich panel significantly increases the total weight of the sandwich panel. Partial filling of the honeycomb core is a solution for reduced added mass, which can be achieved by filling target honeycomb cell voids within a sandwich panel, as presented by Woody and Smith [47], or by partially filling the honeycomb cell void as presented by Wayne et al. [98]. With partial foam filling, Woody and Smith obtained an improvement of almost 60% in damping for an added mass of less than 6% of the total structure [47]. Partial filling of the honeycomb unit cell with viscoelastic material has been shown to significantly enhance the damping properties of a honeycomb structure for a reduced weight penalty (see Figure 1.19) [98]. These partial filling methods consist of: i) an interlayer of viscoelastic material within the ribs of the cell; and ii) a viscoelastic material inserted in the form of fillets in the corner of the cell.
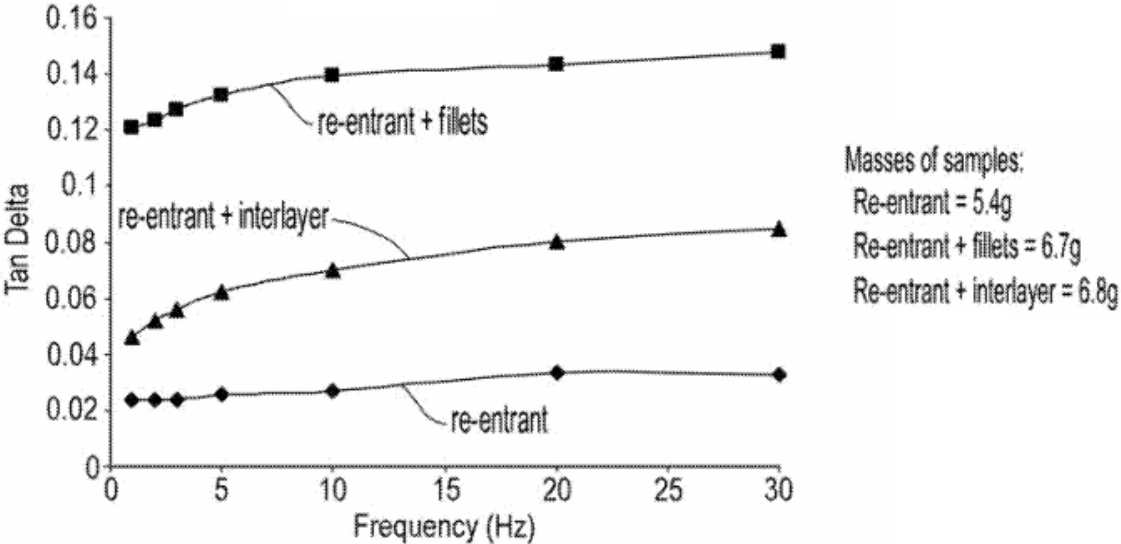
Figure 1.19: Tan delta plotted against frequency for three ABS honeycomb samples at -50C [98].

Honeycombs with Structured Core for Enhanced Damping

1.4.2.2 Particle Dampers

Structures filled with particles, generally small metallic or glass spheres, provide energy dissipation by non-elastic impact and friction damping to the vibrating structure. One of the advantages of this technique is to provide damping in any direction and over a wide frequency range. It also exhibits low influence on the stiffness of the structure, since the particles are not mechanically constrained by the structure [10] [48-57]. However, the added particles lead to weight increases. Michon et al. used viscoelastic particles for enhanced damping capacity provided by energy dissipation from viscoelastic deformation as well as impact and friction [10].

1.4.3 Shape Memory Alloy Honeycombs

Honeycomb cores for sandwich panels formed in entirety from SMA have been the object of recent study because they potentially combine both excellent density-specific mechanical properties and high damping loss coefficients [13] [14]. Shape memory alloys are two-phase alloys, with a martensitic phase predominating at a specific lower transition temperature, an austenitic phase predominating at a specific higher transition temperature, and both phases mixing at temperatures in between. The martensitic-austenitic transformation that occurs in SMAs (under mechanical or temperature loading) promotes high energy dissipation (or damping) in these materials [12]. This feature of SMAs has been applied to honeycomb structures as a route for improved damping by the author in previous work [67]. However, damping enhancement in SMA honeycombs appears effective only for a high magnitude of deformation to trigger the martensitic-austenitic phase transformation.

1.4.4 Friction Damping in Honeycomb Sandwich Structures

A friction damping mechanism can be applied to sandwich panels through the use of friction ledges alongside the honeycomb core, as illustrated in Figure 1.20 [9]. Vibrations cause friction between the ledge and the casing, enhancing energy dissipation and, therefore, damping.

47

Honeycombs with Structured Core for Enhanced Damping
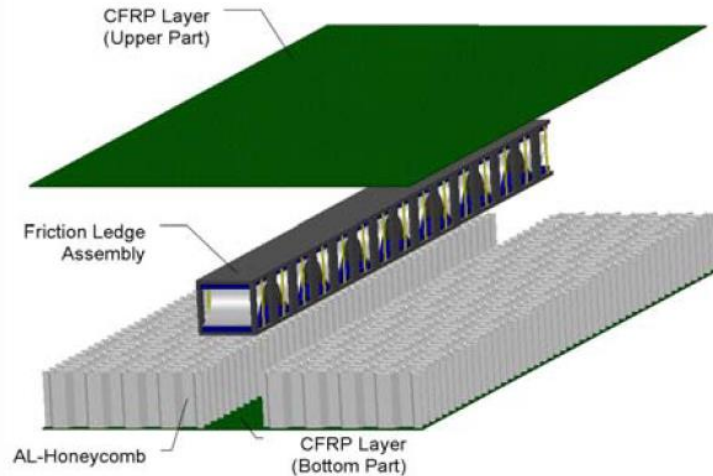
Figure 1.20: Representation of the friction damping system developed by Romberg [9].

1.5 Conclusion and Problematic Thesis Statement

Many technological methods have been identified for enhancement of the damping properties of the honeycomb sandwich panel. These technologies consist of the use of inherently lossy materials such as viscoelastic materials, friction damping, particle impact damping and the use of smart materials such as piezoelectrics [5-9]. Since this thesis focuses on rich vibration environments such as the rotating parts of a gas turbine engine, active methods have been discarded. Enhancement of the damping properties of sandwich panels via passive technologies have been identified through the use of free and constrained viscoelastic layers. However, these technologies do not benefit from the hollow structure of the honeycomb core of a sandwich panel. Viscoelastic and foam filling technologies as well as particle filling of the honeycomb core of a sandwich panel have been identified as benefiting from the hollow macro structure of the honeycomb core. However, the use of an additional damping material inside the core of a sandwich panel increases its mass, which is often deleterious and may also lead to a significant change in dynamic properties. Damping improvement has been recently highlighted on a density basis, filling target cells of the honeycomb core [47] and partially filling the honeycomb cell [98]. These methods appear well justified as the added damping material should be introduced

48

in a location where its loading is maximised for the best use of its dissipation capability.

This thesis focuses on the enhancement of vibration damping in a honeycomb sandwich panel and explores the competing demands between damping and the addition of extra mass. The objectives of the thesis are as follow:

- Determine the most influent loading direction in honeycomb panels subjected to vibration.
- Optimise the location of damping material within the honeycomb cell to limit mass increase.
- Optimise the mass increase given by the introduction of damping material within the honeycomb cell on a density basis.
- Optimise the geometry of the damping insert within the honeycomb cell to enhance damping capability on a density basis.
- Optimise the location and number of damping inserts within a honeycomb sandwich panel to limit mass increase.

Chapter 2 aims to identify the most influent loading directions of units cells within the honeycomb core of cantilever panels subjected to vibration. In this chapter, the influence of the location of the cell within the panels on the magnitude of deformation is also investigated.

Chapter 3 describes the optimal location for damping ligament inserts for use in the honeycomb cell void. In this chapter, several geometries of honeycomb ranging from 'auxetic' to regular cells are investigated.

Chapter 4 examines the use of viscoelastic damping inserts in both 'linear' and 'star' arrangements under in plane shear/axial loads for a regular honeycomb cell geometry. Young's modulus, loss factor and loss modulus as well than density specific loss modulus are quantified using finite elements analyses.

Chapter 5 examines the use of shear lap damping inserts under in plane shear/axial loads for a regular honeycomb cell geometry. Young's modulus, loss factor and loss

modulus as well than density specific loss modulus are quantified using finite elements analyses.

Chapter 6 investigates the use of the shear lap damping inserts on the damping properties of the first bending mode of a cantilever sandwich panel. A method for choosing targeted unit cells within the sandwich panel to limit the total mass increase of the panel is also presented in this chapter.

Chapter 7 discusses the findings of the study.

Finally, Chapter 8 concludes the thesis and provides to the reader recommendations for further work.

Honeycombs with Structured Core for Enhanced Damping

Chapter 2. Unit Cell Deformation Mechanism in Honeycomb and Sandwich Panels Subjected to Vibration

2.1 Introduction

In the process of designing a honeycomb sandwich panel, the honeycomb core is very often modelled as a continuum using homogenous properties, discarding the local deformation of the honeycomb unit cell geometry at a 'mesoscale' [2] [18]. This method is computationally inexpensive and is, therefore, very often used by engineers in the early design stage to size adequately a sandwich panel for a given application. However, this method cannot be used to establish the distribution of deformation, stress and strain in cells within a sandwich panel.

In this chapter, a discrete modelling approach for the honeycomb core using finite elements is taken so as to establish the distribution of deformation and principal loading directions in cells within a sandwich panel subjected to vibration.

The deformation of a unit cell within a panel subjected to vibration is a combination of multiple loads caused by the constraint given by surrounding cells and the skins of a honeycomb or sandwich panel. The first objective of this chapter is to identify the most predominant loading directions of unit cells within the honeycomb core of panels subjected to vibration.

The second objective of this chapter is to investigate if cells within a honeycomb and/or sandwich panel deform in a similar pattern independently from their locations within the panel for its first natural modes of deformation.

This analysis aims to narrow the complexity and number of load cases to account for optimising the mechanical and damping properties of honeycomb structures.

2.2 Methods

2.2.1 Modal Analysis of Cantilever Honeycomb and Sandwich Panels

Four different models of a cantilever honeycomb plate with and without face sheet have been simulated. The geometry of the honeycomb cell consists of a regular honeycomb cell with parameters $h = l = 10$ mm, $t = 0.2$ mm and $\theta = 30°$, as shown in Figure 2.1.
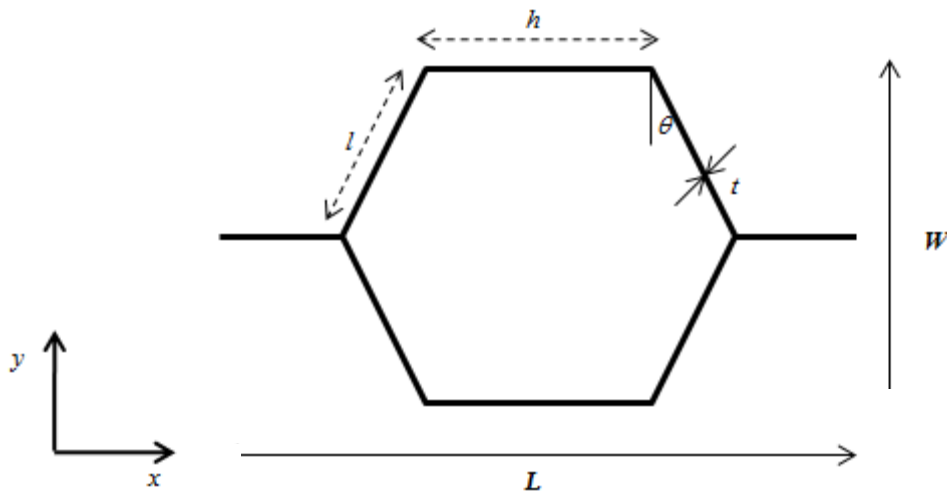
Figure 2.1: Honeycomb cell with its geometric parameters h, l, t and θ; and the cell orientation conventions L and W.

Models a, *and b* are illustrated in Figure 2.2. The number of cells along the x and y axes were chosen to investigate conventional principal cell orientations, L and W, for panels of approximately the same dimensions. The dimensions of the panel associated with *Models a* and *b* are 180 mm x 311.8 mm x 10 mm (6 cells along the x axis and 18 cells along the y axis) and those associated with *Models c* and *d* are 300 mm x 173.2 mm x 10 mm (10 cells along the x axis and 10 cells along the y axis).

52

Honeycombs with Structured Core for Enhanced Damping

(a)   (b)
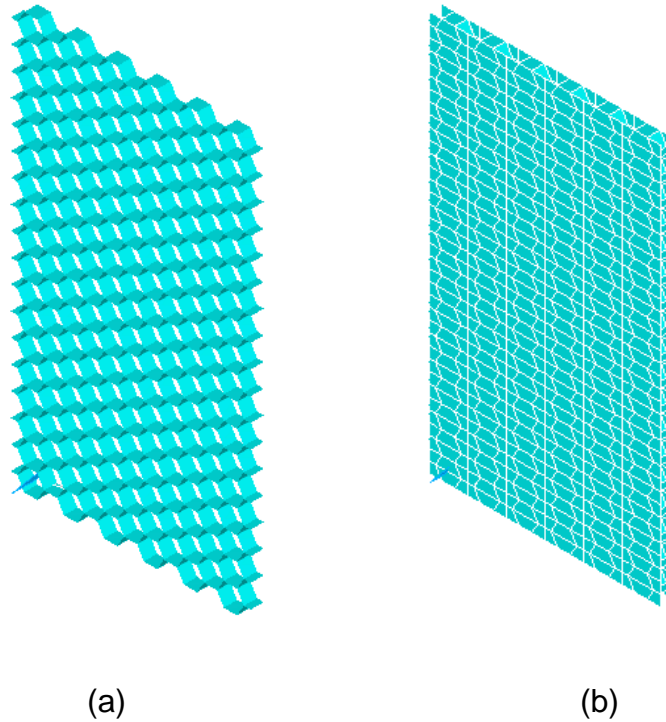
Figure 2.2: Illustration of the geometry of *Model a* and *b* representing respectively a honeycomb core and honeycomb sandwich panel.

Finite element analysis software ANSYS 13 [90] was used to simulate the behaviour of each of the models studied in this chapter. Four nodes linear elastic shell elements with both bending and membrane capabilities and with six degrees of freedom at each node (SHELL63 in ANSYS) were used to mesh the honeycomb core and face sheets. Shell elements were used instead of 3D brick elements because of the typically low ratio between the thickness and the length of the honeycomb cell walls and face sheets. The optimal number of elements required for each model was computed from convergence studies, and is reported in Table 2.1. Figure 2.3 shows detail of the mesh of a single honeycomb cell from *Model a,* with 10 elements along the core depth, while Figure 2.4 shows the mesh for a honeycomb cell and face sheets extracted from *Model b* with 14 elements along the core depth. In both cases, these are the unit cells tessellated to produce the entire structure.

Honeycombs with Structured Core for Enhanced Damping

Table 2.1: The number of shell elements used in each model.

	Elements
Model a	65,400
Model b	455,700
Model c	61,000
Model d	422,500
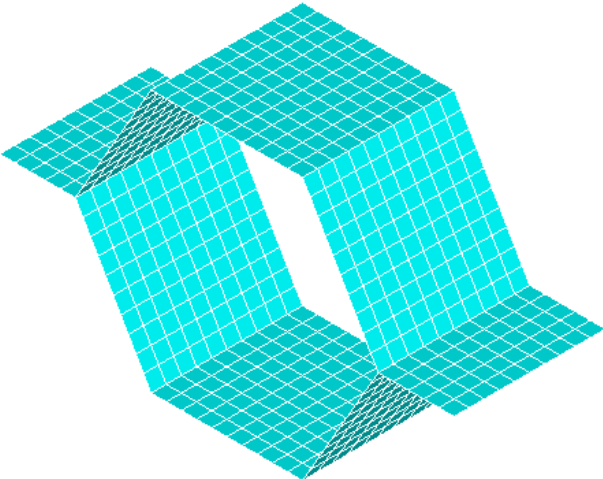
Figure 2.3: Mesh of a honeycomb unit cell from *Model a,* with 10 elements along the cell depth.

Honeycombs with Structured Core for Enhanced Damping
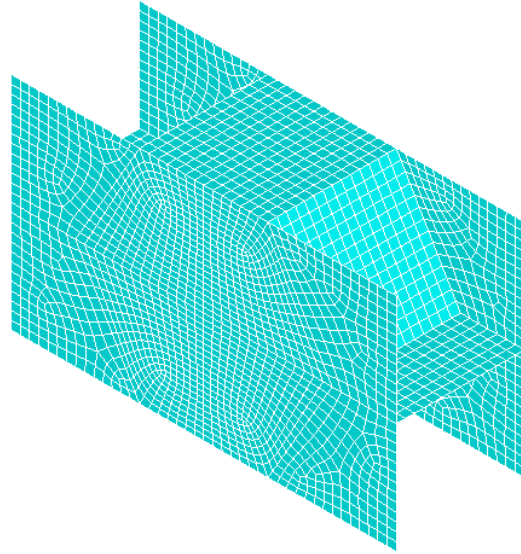
Figure 2.4: Mesh of a honeycomb unit cell with its facings from *Model b,* with 10 elements along the cell depth.

Cantilever boundary conditions were applied to each model. For the nodes located at one edge of the panel, all degrees of freedom were constrained to zero, as represented in Figure 2.5. Figure 2.5a shows the boundary conditions applied to *Models a* and *b* and Figure 2.5b those applied to *Models c* and *d*. Of note is the change in orientation of the cells between Figure 2.5a and Figure 2.5b.

Honeycombs with Structured Core for Enhanced Damping
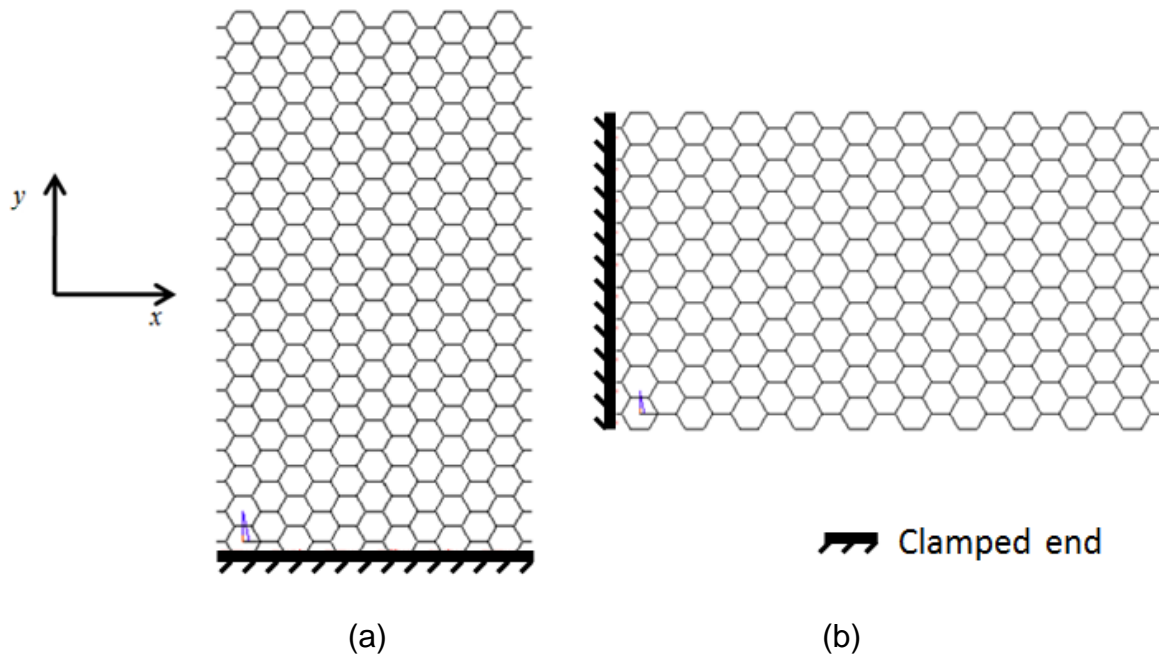
Figure 2.5: Cantilever boundary condition associated with *Models a* and *b* (a) and with *Models c* and *d* (b).

Both honeycomb core and facings were assumed to be made of aluminium, with material properties given as: Young's modulus $E = 70$ GPa, Poisson ratio $v = 0.33$ and density $\rho = 2700$ kg.m^{-3}.

A modal analysis was performed in the FE software to identify the first bending, torsion, shear and second bending modes. To reduce computational time, the block Lanczos method eigenvalue solver was used [90]. The models were generated with Ansys Parametric Design Language (APDL).

A normalisation of the node displacements between different models and vibration modes was required. Hence, the node undergoing the maximal displacement was identified and its displacement was set to 10 mm, from which scale factors were calculated to normalise the displacement of all the other nodes in that structure and for that vibration mode.

The total strain energy in each model under each of the first four modes was derived with an equivalent static analysis because the results of the normal mode analysis

Honeycombs with Structured Core for Enhanced Damping

are dimensionless. The normalised displacements of each node derived in the modal analyses were used as applied displacements in the static analyses for calculation of the strain energy associated to each mode shape.

2.2.2 Deformation Mechanism of Honeycomb Cells within Panel

The deformation of a honeycomb unit cell within a panel subjected to vibration (or any other loading) is caused by a combination of forces and moments acting on the periphery of the honeycomb unit cell. These loads and moments can be projected onto any specific coordinate system related to the honeycomb unit cell. As such, Gibson and Ashby identified two main modes of deformation: in-plane and out-of-plane deformations [2]. Figure 2.6 illustrates some of the typical in-plane and out-of-plane deformations of a honeycomb unit cell, namely in-plane tension/compression, in-plane shear, out-of-plane transverse shear and out-of-plane bending. The out-of-plane bending deformation of a honeycomb panel results in the in-plane deformation of the honeycomb cell as illustrated in Figure 2.7. In this case, one of the face of the honeycomb cell is loaded in in-plane tension while the opposite face is loaded in compression, passing through a zero deformation state in the neutral plane of the cell. As a result, the bending deformation of the honeycomb cell can be described by the in-plane tension/compression deformation through the depth of the cell. Of note, the out-of-plane transverse shear deformation of the honeycomb is much stiffer than the out-of-plane bending deformation because it involved significant axial or shear of the cell walls themselves [2].

Honeycombs with Structured Core for Enhanced Damping
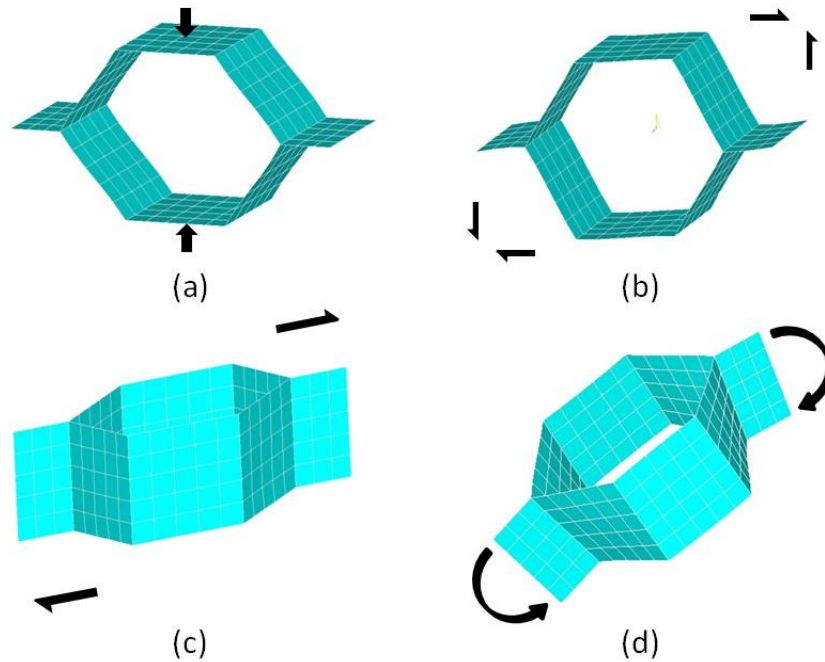
Figure 2.6: Deformation mechanisms of a honeycomb cell within a sandwich panel subjected to vibration: (a) in-plane tension/compression, (b) in-plane shear, (c) transverse shear through the core thickness, (d) bending.
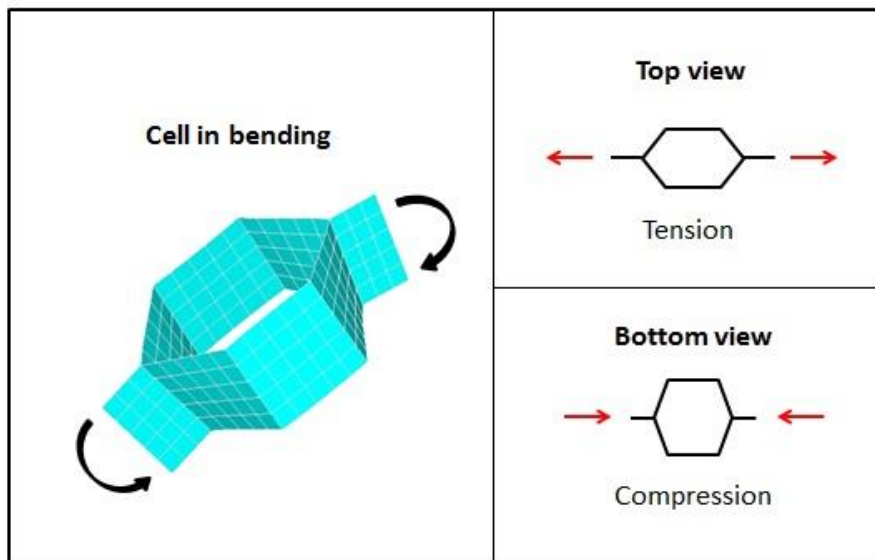
Figure 2.7: In-plane loading as associated with the out-of-plane bending of a unit cell.

Honeycombs with Structured Core for Enhanced Damping

2.2.2.1 In-plane Deformation

In-plane deformations of all cells which capture the out-of-plane bending deformation of the honeycomb cell as described in the previous paragraph, have been calculated along the three directions formed by the opposite edge of the honeycomb cell, as shown in Figure 2.8. In-plane strains ε_1, ε_2 and ε_3 have been derived from Equation 2.1 to Equation 2.3 where represents the length of vector $\vec{v}$ before deformation of the cell and is the length after deformation.

$$\varepsilon_1 = \frac{\left\|\overrightarrow{AB}\right\|_{bd} - \left\|\overrightarrow{AB}\right\|_{ad}}{\left\|\overrightarrow{AB}\right\|_{bd}}$$

Equation 2.1

$$\varepsilon_2 = \frac{\left\|\overrightarrow{CD}\right\|_{bd} - \left\|\overrightarrow{CD}\right\|_{ad}}{\left\|\overrightarrow{CD}\right\|_{bd}}$$

Equation 2.2

$$\varepsilon_3 = \frac{\left\|\overrightarrow{EF}\right\|_{bd} - \left\|\overrightarrow{EF}\right\|_{ad}}{\left\|\overrightarrow{EF}\right\|_{bd}}$$

Equation 2.3
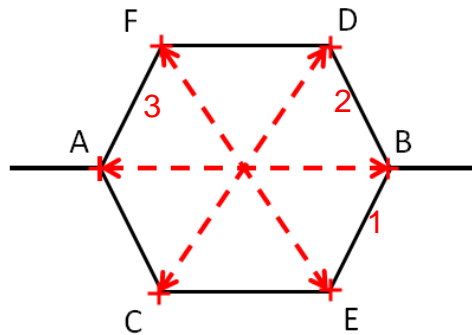
Figure 2.8: Vectors and directions inside the honeycomb cell defined to calculate in-plane strains ε_1, ε_2 and ε_3.

Honeycombs with Structured Core for Enhanced Damping

In-plane strains ε_1, ε_2 and ε_3 have been calculated for all models and mode shape studied at nodes located on the bottom face of the panels.

The variation of ε_1, ε_2 and ε_3 across the thickness of the core was investigated for a specific cell within *Models a* and *b* situated in the middle of the panel as shown in Figure 2.9, so as to consider the deformation of the cell as a continuum, i.e. away from edges and constraint.

The maximum tension/compression and in-plane shear strain have been defined by parameter $\varepsilon_i{}^*$ (see Equation 2.4).

$$\varepsilon_i{}^* = max_{all\_cells}(|\varepsilon_i|) \quad \text{with} \quad i = \{1,2,3\}$$

Equation 2.4
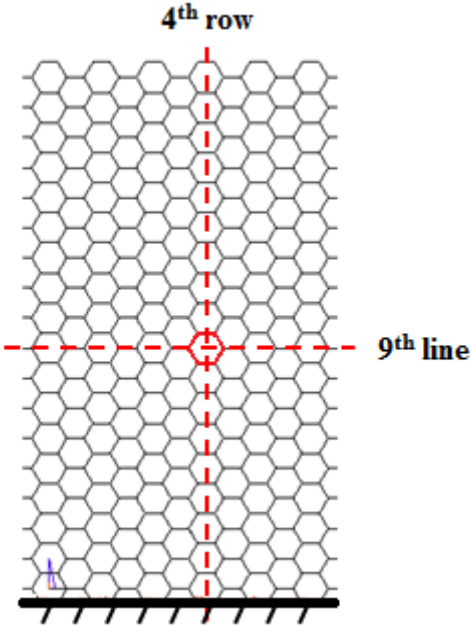
Figure 2.9: Cell location within *Model a* and *b* located away from the edge of the panel (4th row, 9th line).

2.2.2.2 Transverse Shear Out-of-plane Deformation

Out-of-plane transverse shear has been calculated in each edge of the honeycomb cell, as illustrated in Figure 2.10. The transverse shear strain γ has been derived

Honeycombs with Structured Core for Enhanced Damping

from Equation 2.5 where $\overrightarrow{OB}$ represents the vector after deformation of the cell wall through the thickness of the cell and $\overrightarrow{OC}$ the vector between the first two nodes at the bottom of the cell after deformation (see Figure 2.10). The vector $\overrightarrow{OC}$ was assumed to be locally collinear with the vector representing the cell wall through thickness before deformation. This convention was considered to be a good approximation as long as enough elements were used to model the core through thickness. Convergence tests showed that at least 10 elements were required through the thickness of the honeycomb panel without skin and 14 elements for those with skins, see Figure 2.11 and Figure 2.12 in the result section. The number of elements used to model the geometries studied was chosen from a convergence study on parameter γ.

$$\gamma = acos\left(\frac{\overrightarrow{OB}.\overrightarrow{OC}}{\|\overrightarrow{OB}\|.\|\overrightarrow{OC}\|}\right)$$

Equation 2.5

— Undeformed honeycomb cell

---- Transverse shear deformation of a honeycomb cell

• Nodes
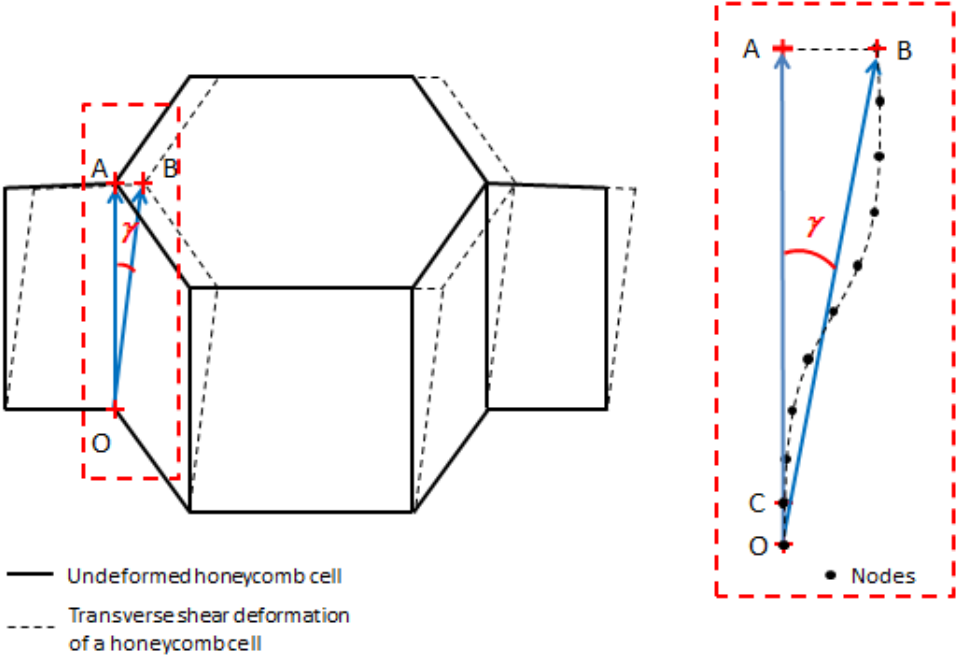
Figure 2.10: 3D view of a honeycomb cell and its deformed shape under transverse shear loading.

Honeycombs with Structured Core for Enhanced Damping

Parameter γ^* was defined to estimate the maximum transverse shear strain between all the cells of the panel (see Equation 2.6).

$$\gamma^* = max_{all\_cells}(|\gamma|)$$

<div align="right">Equation 2.6</div>

2.3 Results

2.3.1 Convergence Test

A convergence test is shown in Figure 2.11 for *Model a*, representing a 6x18 cell honeycomb panel without skin. The convergence study was carried out on the maximum strain ε_1^* and γ^*, respectively, the axial strain and the transverse shear strain from all the cells inside the sandwich structure. It can be seen that parameter ε_1 is not sensitive to the mesh refinement and accurate results are achieved by using only two elements along the thickness of the core (i.e. 10,464 elements for *Model a*). Parameter γ is, however, sensitive to the element size. Honeycomb panels without skin were modelled using 10 elements along the thickness of the core (i.e. 65,400 elements for *Model a*). This was found to be a good compromise between the accuracy of parameter γ and the computational time.

Honeycombs with Structured Core for Enhanced Damping
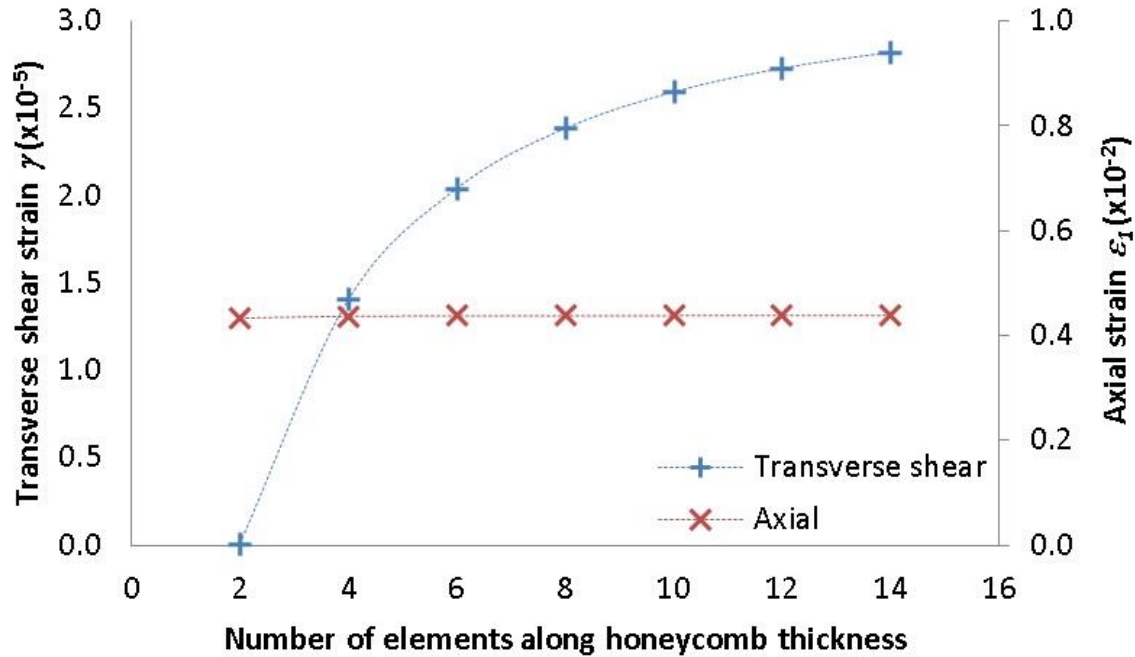
Figure 2.11: Transverse shear and in-plane axial strains in function of the number of elements along the core depth for *Model a*.

A convergence test is shown in Figure 2.12 for *Model b*, representing a 6x18 cell sandwich panel with skins. The convergence study was carried out as described previously for a honeycomb panel without skin. It can be seen that parameter ε_1 is not sensitive to the mesh refinement and accurate results are achieved using only two elements along the thickness of the core (i.e. 43,296 elements for *Model b*). Parameter γ is, however, sensitive to the element size of the mesh. It should be noted that more elements along the core thickness are required to achieve convergence of the transverse shear strain for a sandwich panel than for a honeycomb panel (without skins). Sandwich structures with skins were modelled using 14 elements along the thickness of the core (i.e. 455,748 elements for *Model b*). This was found to be an effective compromise between the accuracy of parameter γ and computational time.

63

Honeycombs with Structured Core for Enhanced Damping
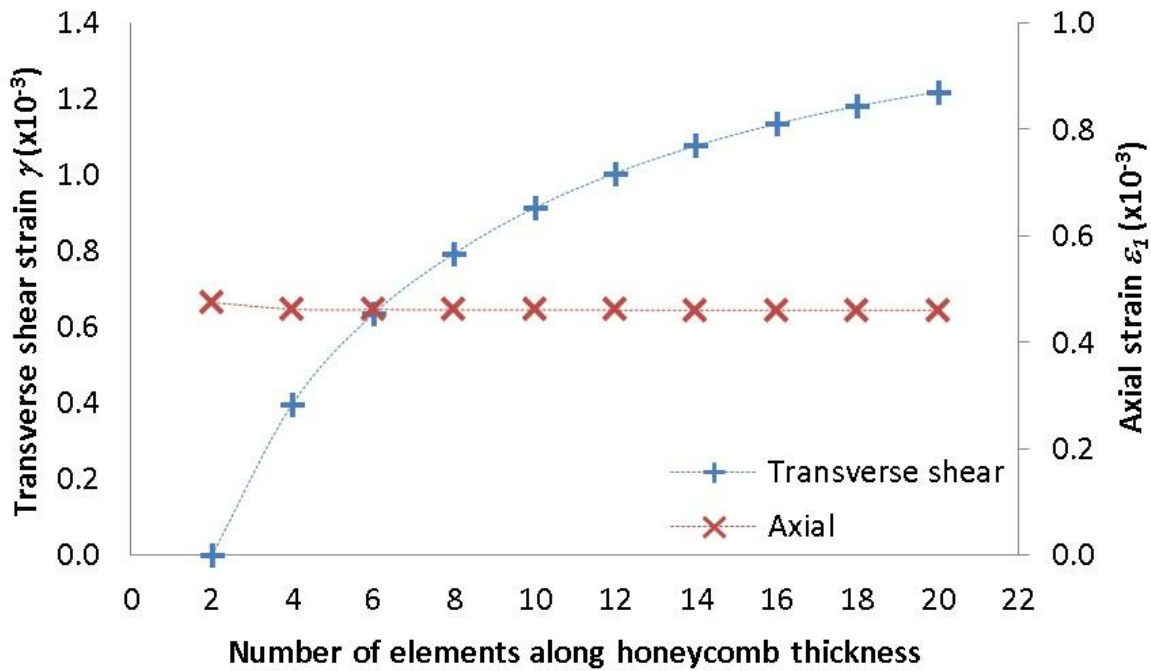
Figure 2.12: Transverse shear and in-plane axial strains against the number of elements along the core depth for *Model b*.

2.3.2 Modal Analysis of Cantilever Honeycomb and Sandwich Panels

The modal frequencies of the first four modes of the models studied are shown in Table 2.2. Frequencies associated to models with skins, i.e. *Models b* and *d,* are more than ten times higher compared to the models without skins, i.e. *Models a* and *c.* The natural frequencies between the two honeycomb panels, i.e. *Models a* and *c,* are within 10% differences; the same between the natural frequencies of the two sandwich panels, i.e. *Models b* and *c.*

Honeycombs with Structured Core for Enhanced Damping

Table 2.2: Modal frequencies (Hz) of the first four modes of vibration of *Models a, b, c* and *d*.

	Model a	*Model b*	*Model c*	*Model d*
Mode 1	9,0E+00	1,2E+02	1,0E+01	1,3E+02
Mode 2	1,6E+01	4,2E+02	1,8E+01	4,5E+02
Mode 3	3,5E+01	7,2E+02	3,5E+01	7,8E+02
Mode 4	4,9E+01	1,0E+03	5,2E+01	1,1E+03
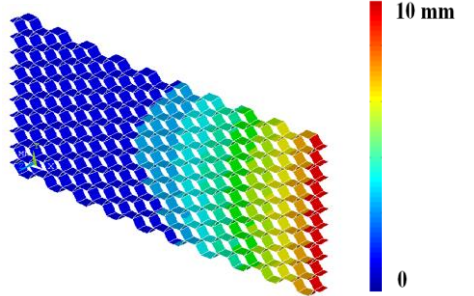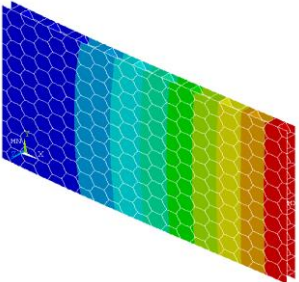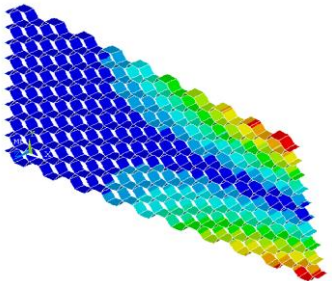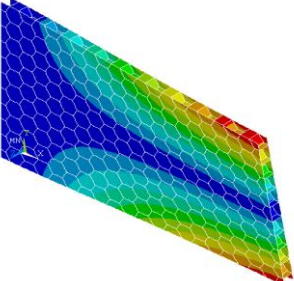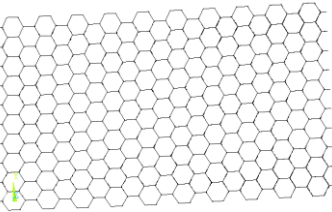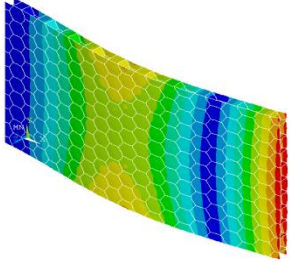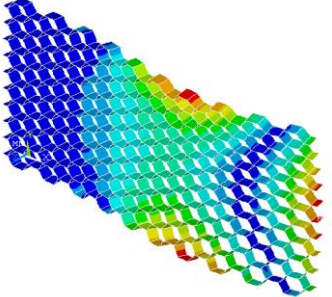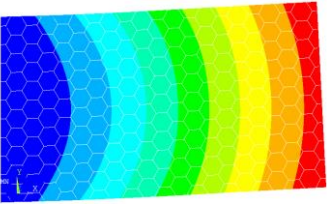
Table 2.3 shows the first four mode shapes of *Models a* and *b,* i.e. 6x18 cell honeycomb and sandwich panels. The first and second mode shapes correspond respectively to the first bending and first torsion mode of the structure. The third mode for *Model a*, i.e. panel without skins, is an in-plane shear mode whereas for *Model b*, i.e. panel with skins, the third mode is a second order bending mode; vice versa for the fourth mode. These mode shapes are consistent with those obtained for homogenous structures of similar geometry and under similar boundary conditions.

Honeycombs with Structured Core for Enhanced Damping

Table 2.3: Mode shapes of the first mode of vibration of *Models a* and *b*, i.e. 6x18 cell honeycomb and sandwich panels.

	Model a – 6x18 honeycomb panel	*Model b* – 6x18 sandwich panel
Mode 1		
Mode 2		
Mode 3		
Mode 4		

Honeycombs with Structured Core for Enhanced Damping

Table 2.4 shows the mode shapes associated with *Models c* and *d,* i.e. 10x10 cell honeycomb and sandwich panels, with similar observations made on the modal deformation shapes of *Models a* and *b*. Modes 1 and 2 are, respectively, a first bending and a first torsion mode. Mode 3 of *Model c* (without skins) is an in-plane shear mode whereas, for *Model d* (with skins), this mode is a second bending mode; and vice versa for Mode 4.

Honeycombs with Structured Core for Enhanced Damping

Table 2.4: Mode shapes of the first mode of vibration of *Models c* and *d*, i.e. 10x10 cell honeycomb and sandwich panels.

	Model c	*Model d*
Mode 1		
Mode 2		
Mode 3		
Mode 4		

Honeycombs with Structured Core for Enhanced Damping

2.3.3   In-plane Deformation of Honeycombs

2.3.3.1 Deformed Shape of Cells in Panels Subjected to Vibration

Typical in-plane deformations of the honeycomb cells with the honeycomb and sandwich panel have been illustrated respectively in Figure 2.13 and Figure 2.14 for the mode shapes studied in this chapter. The main directions of in-plane deformation are indicated with red arrows, and consist for all modes except the first in-plane shear mode of in-plane axial deformation caused by the bending of the honeycomb core. For the in-plane shear mode, the in-plane deformation of the cell is caused by the in-plane shear deformation of the honeycomb core.

(a)   (b)
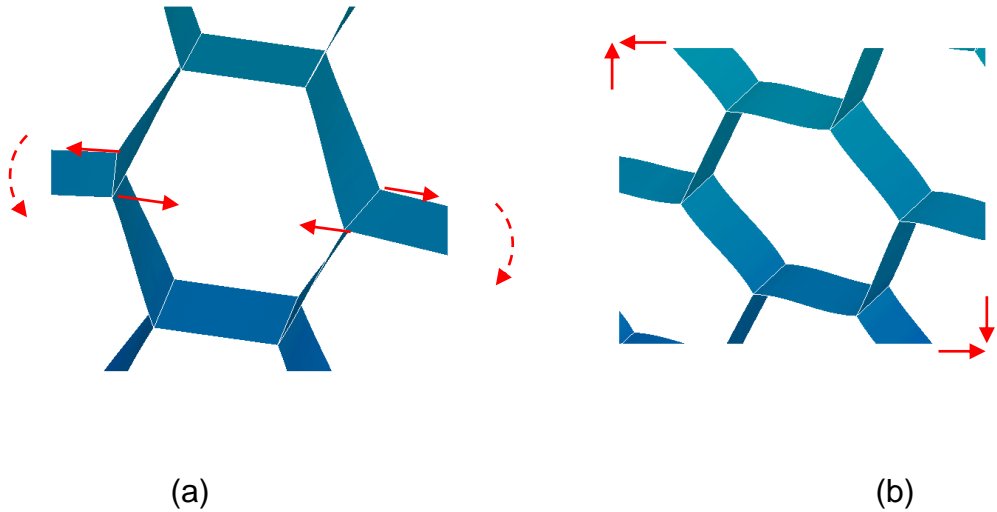
Figure 2.13: Deformation of a cell with the main local deformation highlighted with red arrows for the first bending mode (a) and the first in-plane shear mode (b) of *Model c.*

Honeycombs with Structured Core for Enhanced Damping

(a)	(b)
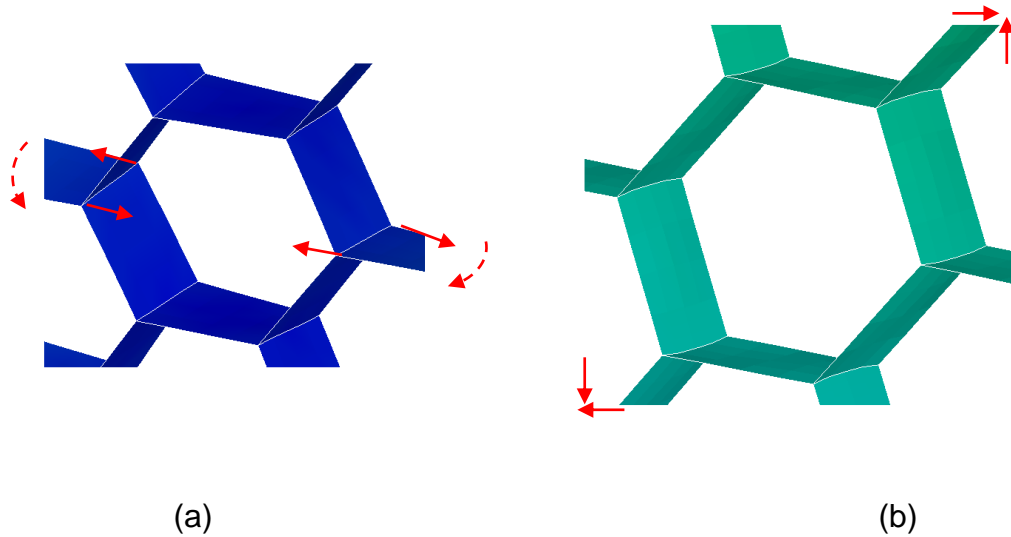
Figure 2.14: Deformation of a cell with the main local deformation highlighted with red arrows for the first bending mode (a) and the first in-plane shear mode (b) of *Model d.*

2.3.3.2 In-plane Deformation through the Honeycomb Core Depth

In-plane strains ε_1, ε_2 and ε_3 have been calculated in the middle cell of *Models a* and *b* for the first four vibration modes, as described in the method section of this chapter.

Figure 2.15 shows in-plane strains ε_1, ε_2 and ε_3 across the core depth of the middle cell without skins, i.e. *Model a,* normalised against their maximum magnitude $\varepsilon_{1\text{-}max}$, $\varepsilon_{2\text{-}max}$ and $\varepsilon_{3\text{-}max}$ for the first four modes of vibration. All strains vary linearly across the core depth. For all out-of-plane modes of vibration, i.e. the first bending, the first torsion and the second bending modes, the strains are increasing/decreasing across the core depth. For the first in-plane shear mode the strain is constant across the core depth.

Honeycombs with Structured Core for Enhanced Damping
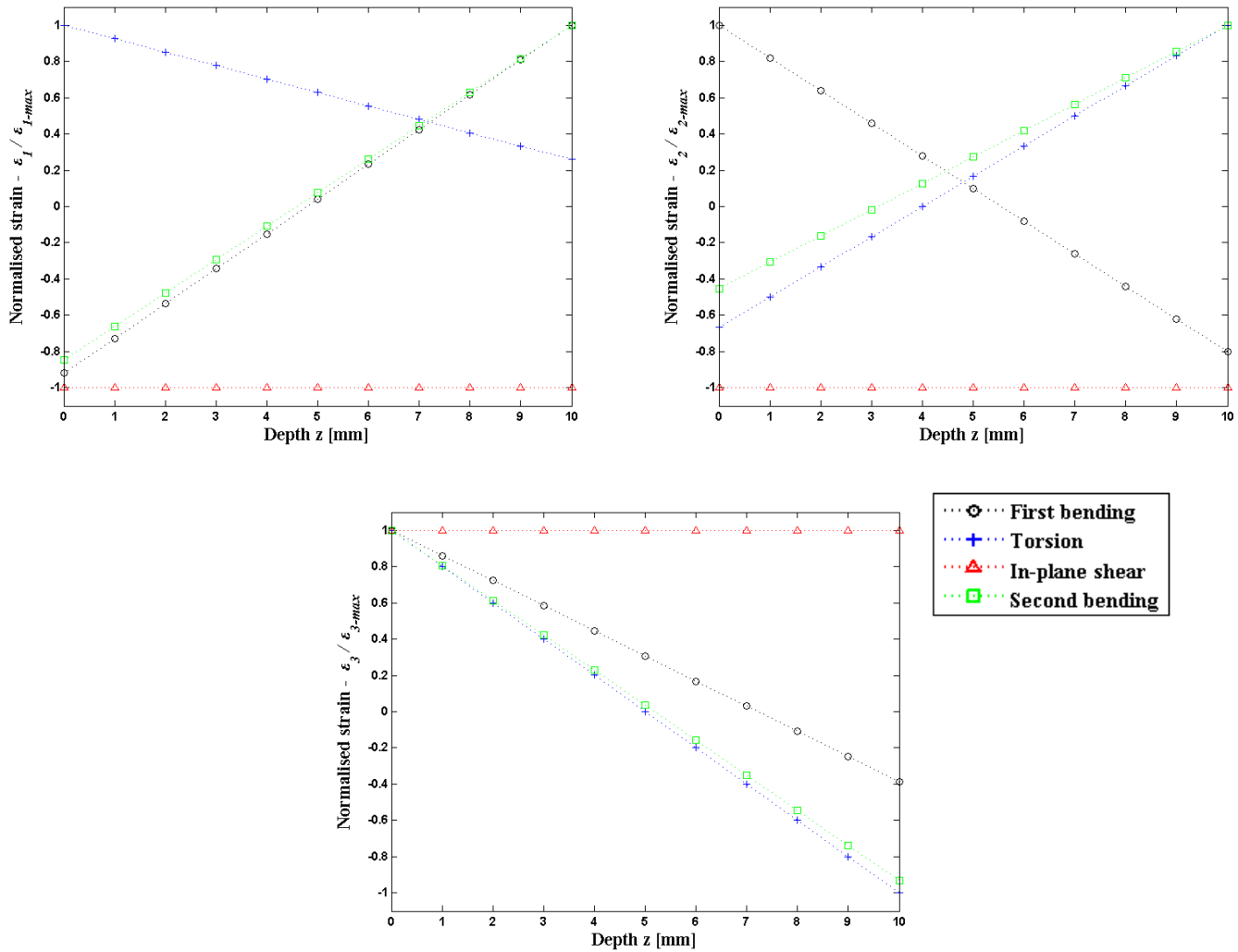
Figure 2.15: Normalised in-plane strains $\varepsilon_1/\varepsilon_{1-max}$, $\varepsilon_2/\varepsilon_{2-max}$ and $\varepsilon_3/\varepsilon_{3-max}$ in function of the core depth of a cell (4th row, 9th line) from *Model a*.

Figure 2.16 shows in-plane strains ε_1, ε_2 and ε_3 across the core depth of the middle cell with skins, i.e. *Model b,* normalised against their maximum magnitude ε_{1-max}, ε_{2-max} and ε_{3-max} for the first four modes of vibration. As opposed to the honeycomb panel, the strains do not vary linearly across the core depth. For all out-of-plane modes of vibration, i.e. the first bending, the first torsion and the second bending modes, the strains are increasing/decreasing across the core depth and the rate of change of the strains is reduced towards the minimal and maximal depth of the cells, i.e. the closest to the sandwich panel skins. For the first in-plane shear mode, the in-

71

Honeycombs with Structured Core for Enhanced Damping

plane strains are maximal towards the middle depth of the cell and decrease towards the sandwich panel skins.
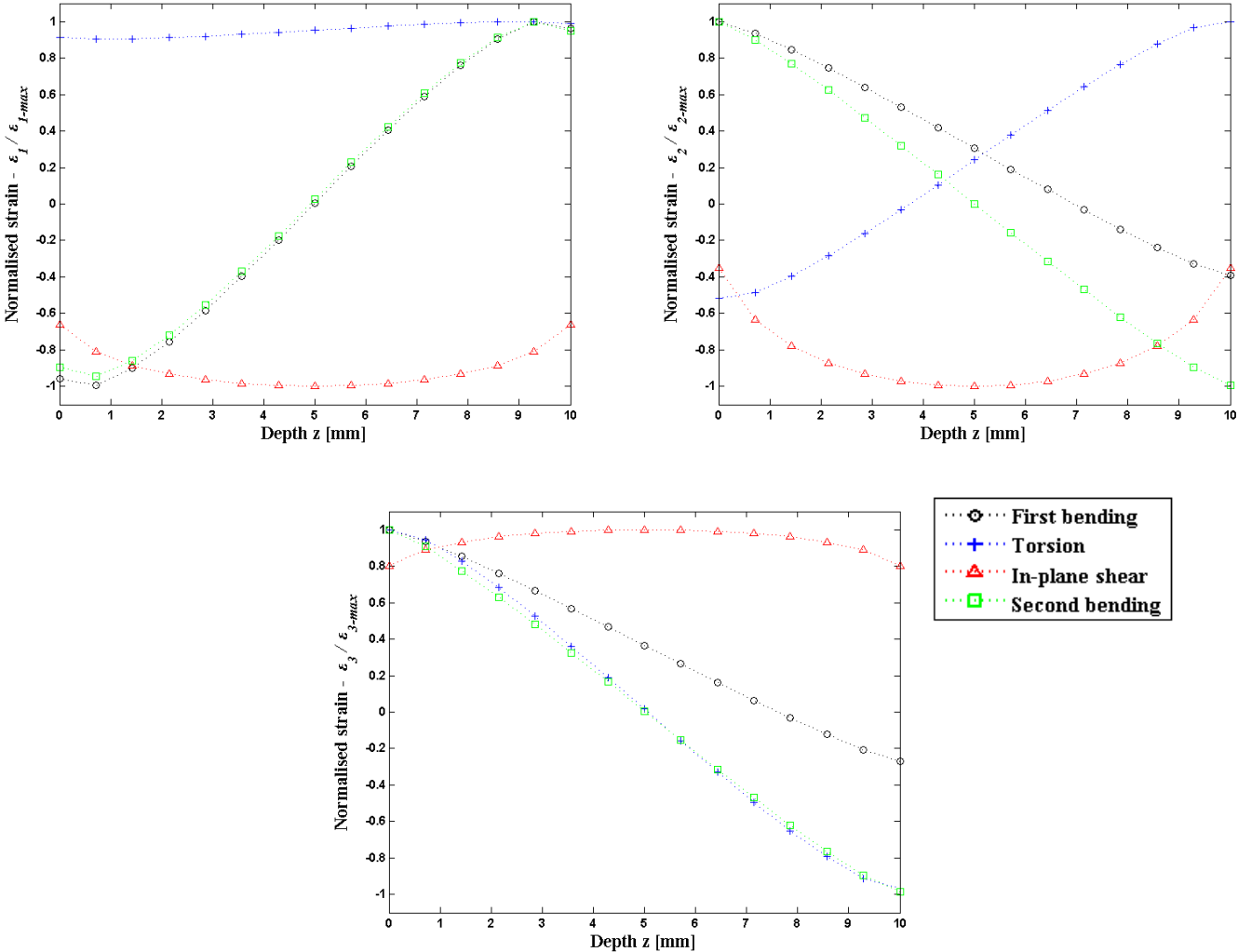
Figure 2.16: Normalised in-plane strains $\varepsilon_1/\varepsilon_{1\text{-}max}$, $\varepsilon_2/\varepsilon_{2\text{-}max}$ and $\varepsilon_3/\varepsilon_{3\text{-}max}$ in function of the core depth of a cell (4th row, 9th line) from *Model b*.

2.3.3.3 In-plane Deformation of Honeycomb Cells within Panel

Maps of in-plane strains ε_1, ε_2 and ε_3 are shown in Table 2.5 for all the cells of the first bending mode of *Model a*. The distribution of strain is symmetric for both strains ε_2 and ε_3, because of the symmetry of the geometry, the constraints and both strain

Honeycombs with Structured Core for Enhanced Damping

directions. Hence, the results for strain ε_3 have not been represented in the subsequent results.

Table 2.5: Map of in-plane strains ε_1, ε_2 and ε_3 from all cells within *Model a* for the first order bending mode.

Model a – Strain ε_1	*Model a –Strain ε_2*	*Model a – Strain ε_3*
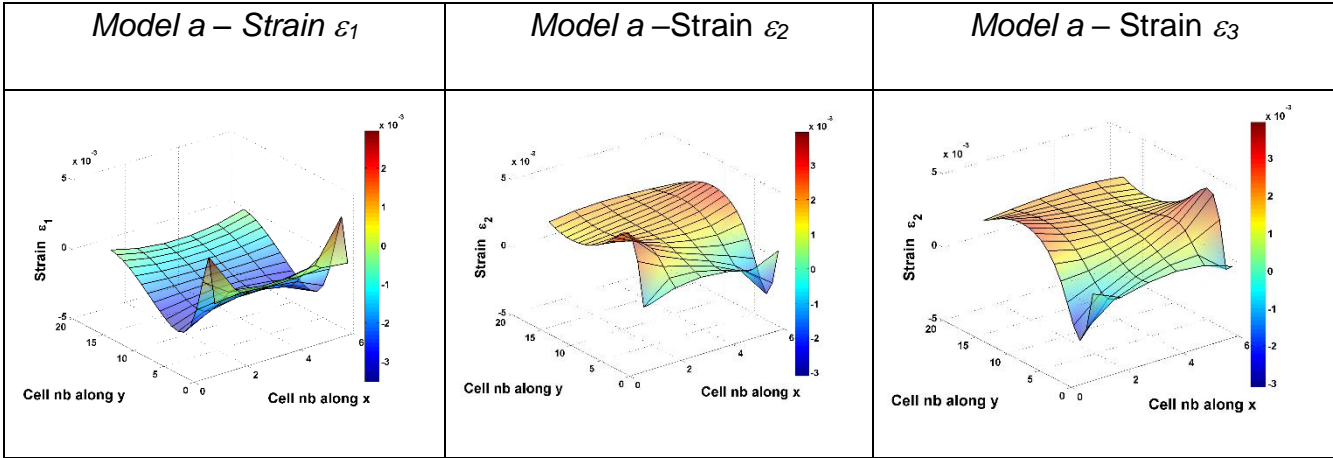
Table 2.6 to Table 2.9 show the magnitude of strains ε_1, ε_2 and γ at depth $z = 0$ mm for each cell within *Models a*, *b*, *c* and *d*, respectively, for the first bending mode, the first torsion mode, the first in-plane shear mode and the second bending mode. In each table, the scale of the graph remains constant. Cells with minimum strain are represented in blue and those with maximum strain are represented in red. Cells in tension exhibit positive strains and cells in compression negative strain. Similitude can be drawn for the location of maximum/minimum strain within panels with and without skins for the same modes of deformation and the same strain direction. It should be noted that the magnitude of deformation is higher for panels without skins compared to panels with skins. This is discussed subsequently. Apart from this similitude, the location of maximum/minimum strain is different for each mode and each strain direction.

73

Honeycombs with Structured Core for Enhanced Damping

Table 2.6: Maps of strains ε_1 and ε_2 of each cell inside *Models a*, *b*, *c* and *d* at depth $z = 0$ for the first bending mode.

First bending	Strain ε_1	Strain ε_2
Model a		
Model b		
Model c		
Model d		

Honeycombs with Structured Core for Enhanced Damping
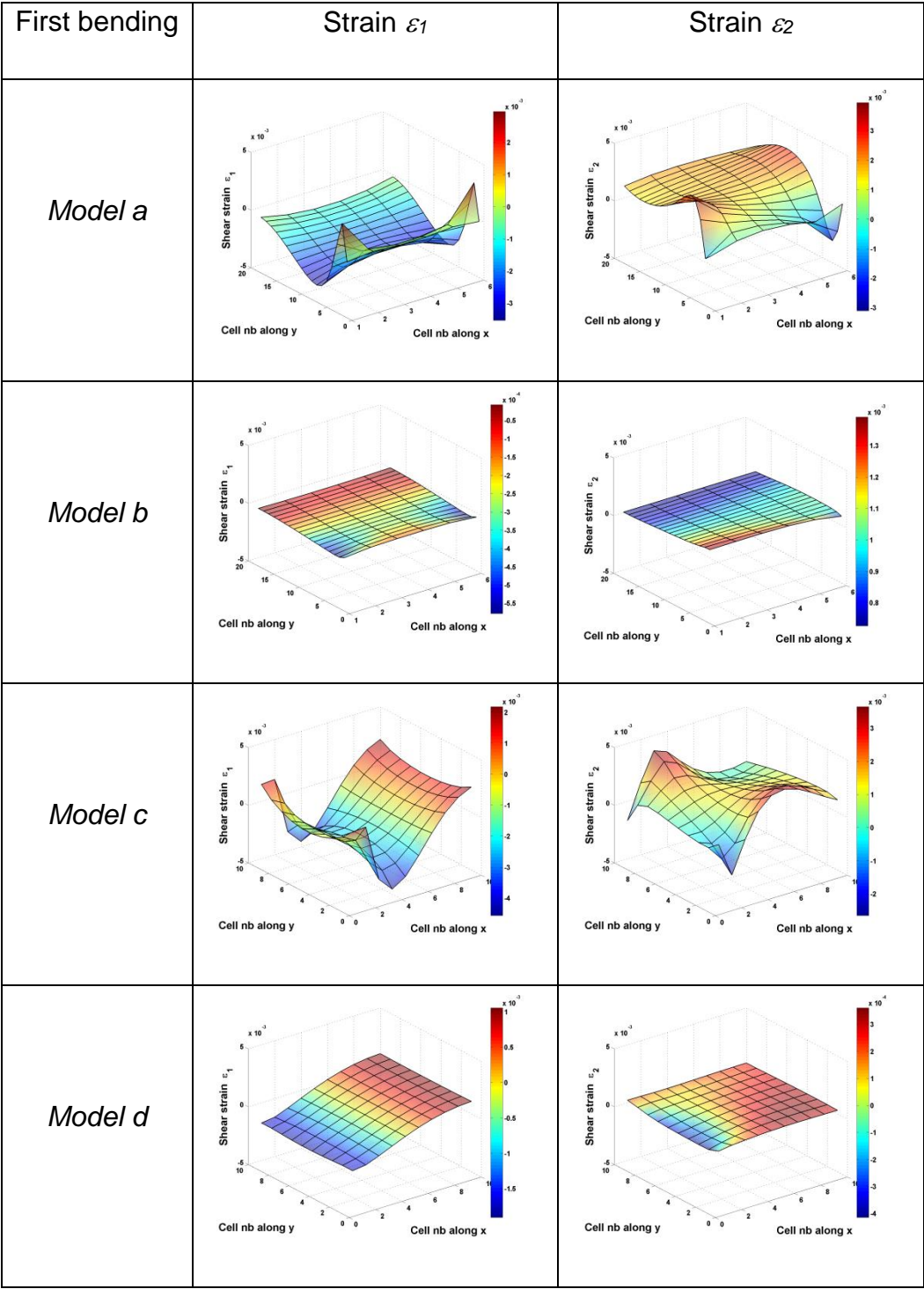
Table 2.7: Maps of strains ε_1 and ε_2 of each cell inside *Models a*, *b*, *c* and *d* at depth $z = 0$ for the first torsion mode.

Torsion	Strain ε_1	Strain ε_2
Model a		
Model b		
Model c		
Model d		

Honeycombs with Structured Core for Enhanced Damping
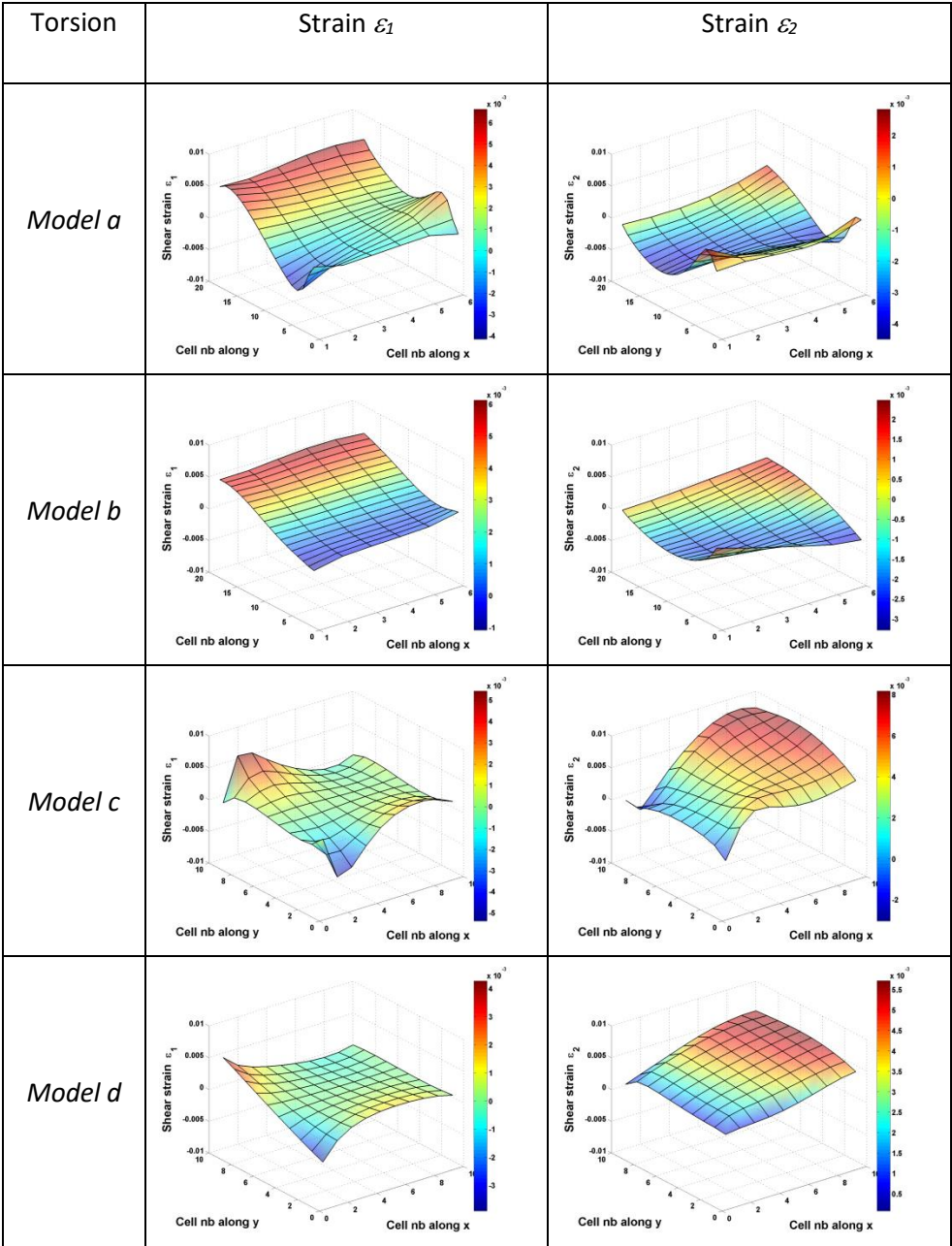
Table 2.8: Maps of strains ε_1 and ε_2 of each cell inside *Models a*, *b*, *c* and *d* at depth $z = 0$ for the first in-plane shear mode.

In-plane shear	Strain ε_1	Strain ε_2
Model a		
Model b		
Model c		
Model d		

Honeycombs with Structured Core for Enhanced Damping
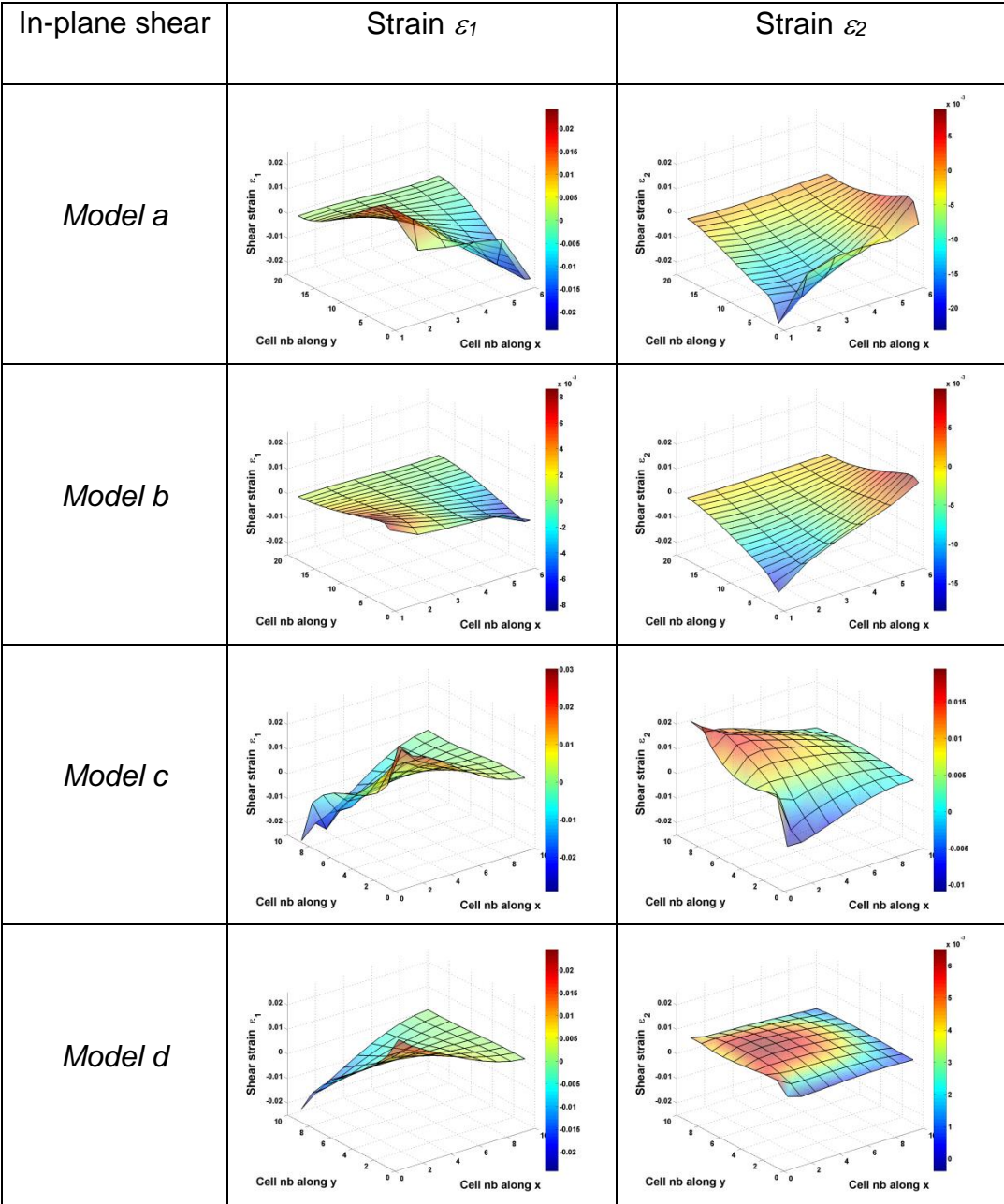
Table 2.9: Maps of strains ε_1 and ε_2 of each cell inside *Models a*, *b*, *c* and *d* at depth $z = 0$ for the second bending mode.

Second bending	Strain ε_1	Strain ε_2
Model a		
Model b		
Model c		
Model d		

Honeycombs with Structured Core for Enhanced Damping
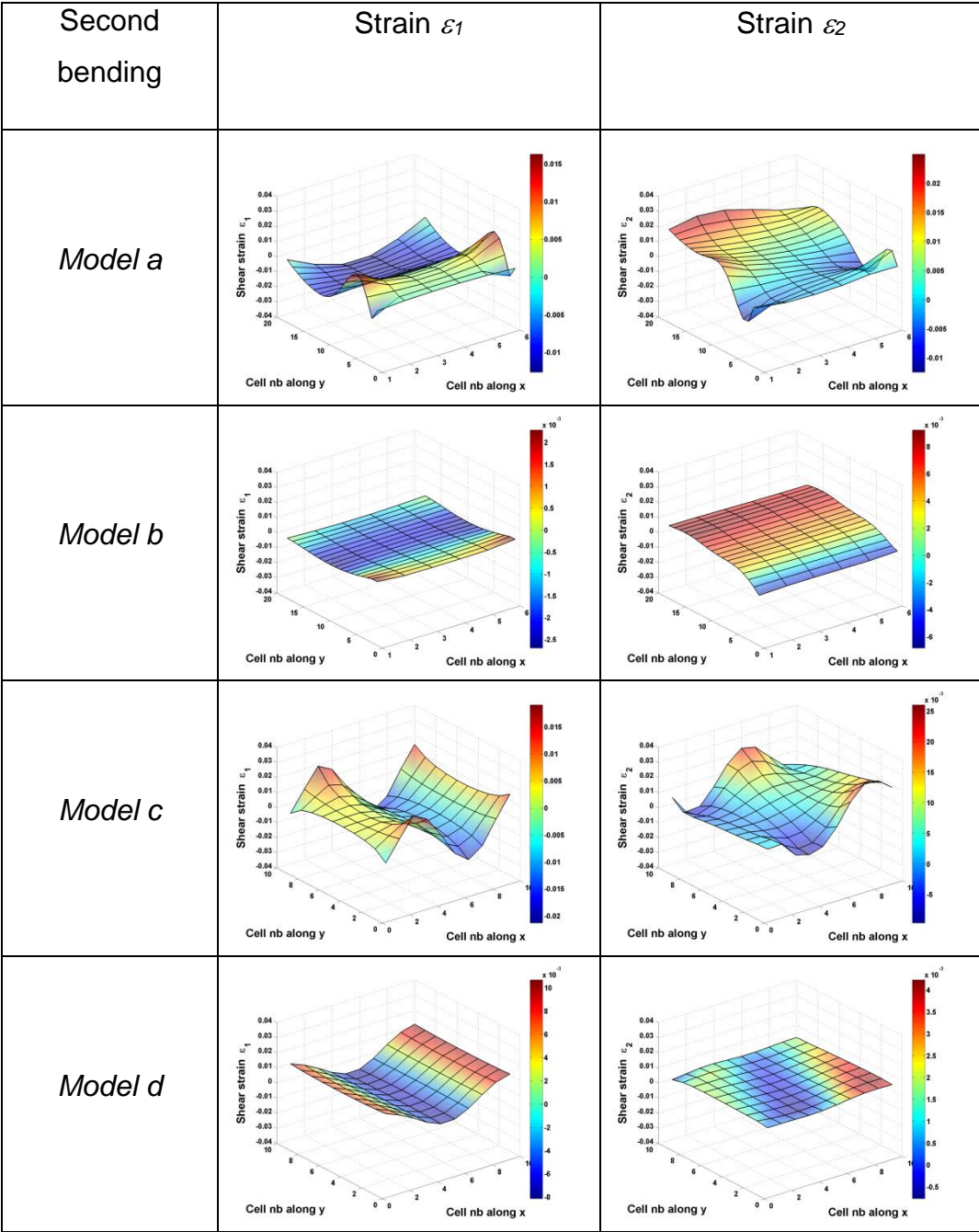
The maximum strains ε_1^* and ε_2^* at depth $z = 0$ mm between all the cells for each model and mode studied in this chapter are shown in Figure 2.17. The magnitude of strain is higher for the honeycomb panel (2.5%), i.e. *Models a* and *c*, than for the sandwich panel (2%), i.e. *Models b* and *c*, for all modes studied. The orientation of the cell within the panel, i.e. *L* or *W,* as shown in Figure 2.1, slightly influences the magnitude of maximal strain depending on the mode shape and strain orientation. Strain ε_1 is generally higher for *L*-orientated cells and strain ε_2 is generally higher for *W*-orientated cells. It should be noted that the maximum strain for each model was shown to be dependent on the mode shape of the structure in Figure 2.17. This last result is valid for the given assumption made in this chapter, i.e. each mode shape has been scaled to account for a maximal nodal displacement of 10 mm independently of the energy required to force the modal displacement. The strain energy stored in each model has been derived from a static analysis where the maximal nodal displacement has been set to 10 mm for each mode of vibration and is shown in Table 2.10, and was shown to be different for each mode, limiting the interpretation of this last result.
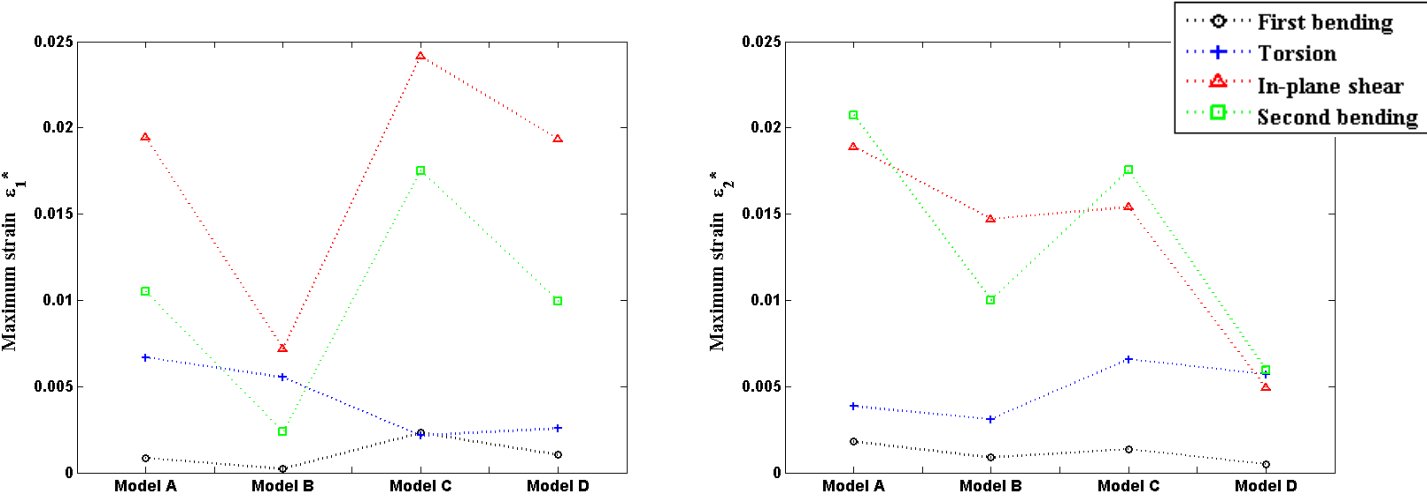
Figure 2.17: Maximum strain ε_1^* and ε_2^* for *Models a*, *b*, *c* and *d* and the mode of deformation studied.

Honeycombs with Structured Core for Enhanced Damping

Table 2.10: Total strain energy of each mode of vibration of the models studied. Results obtained from a static analysis where the maximal nodal displacement has been set to 10 mm for each mode of vibration.

Strain energy [N.m]	Model a (honeycomb only)	Model b (face sheets)	Model c (honeycomb only)	Model d (face sheets)
First bending	9.0E-04	6.9E-01	1.0E-03	7.5E-01
Torsion	1.9E-03	4.3E+00	2.1E-03	4.7E+00
In-plane shear	2.6E-02	5.6E+01	2.4E-02	5.6E+01
Second bending	2.2E-02	2.3E+01	2.3E-02	2.4E+01

2.3.3.4 Out-of-plane Deformation of Honeycomb

Typical out-of-plane transverse shear deformations of the honeycomb core are shown in Figure 2.18 for a panel with skins for its first torsion mode. This mode of deformation has not been visually captured for panels without skins, i.e. *Models a* and *c.*
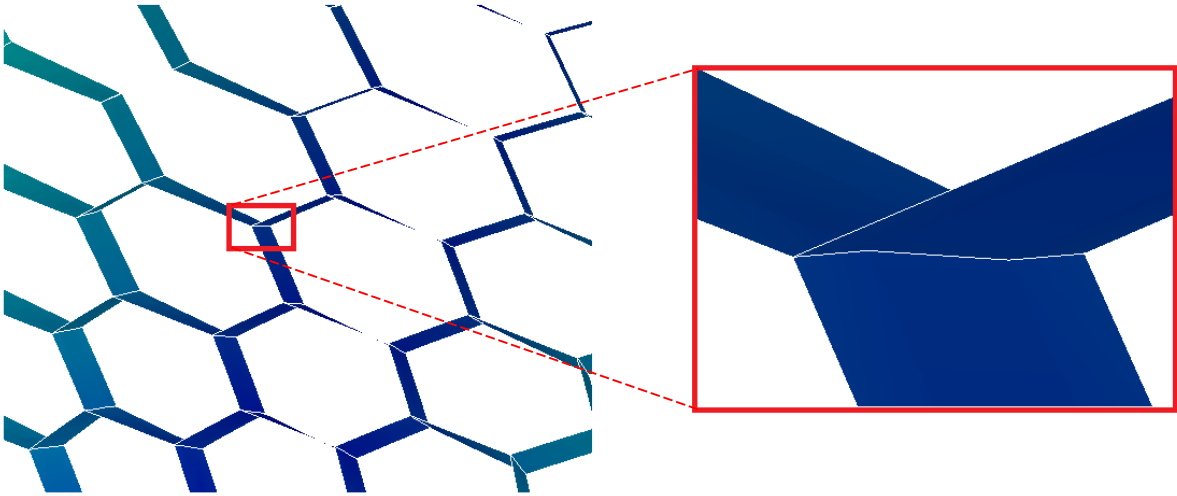
Figure 2.18: Deformed shape of cells of *Model d* for the torsion mode and a local view of the transverse shear deformation.

The maximum transverse shear strain γ^* as described in the methods sections is shown in Figure 2.19. As expected and discussed in the method section, the maximum transverse shear strain γ^* is quasi null for panels without skins, i.e. *Models a* and *c.* The highest transverse shear strain is 0.85% for sandwich panels.

Honeycombs with Structured Core for Enhanced Damping
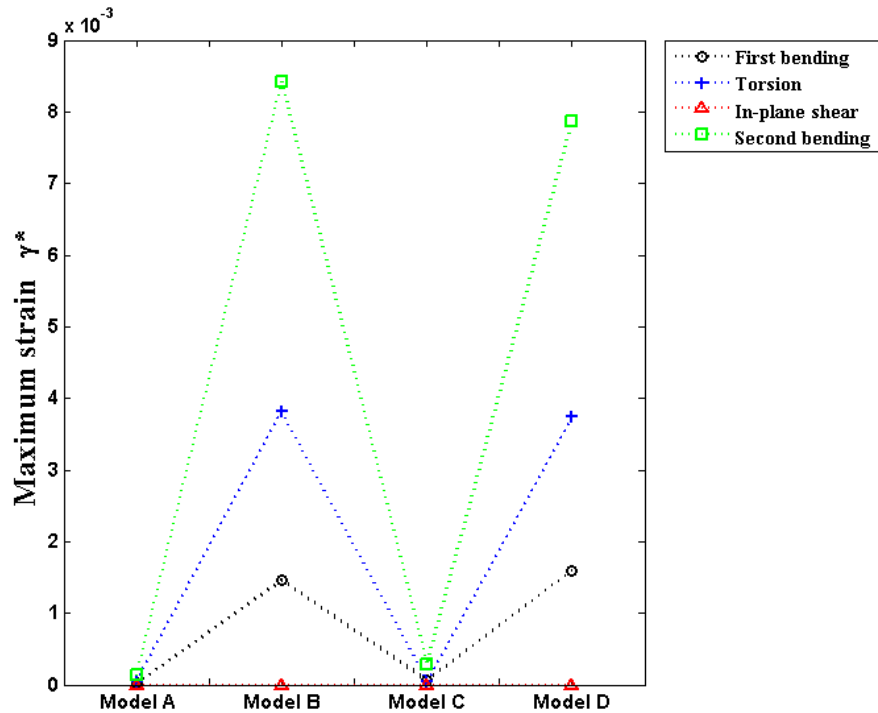
Figure 2.19: Maximum out-of-plane transverse shear strain γ^* for *Models a*, *b*, *c* and *d* and the mode of deformation studied.

2.4 Discussion

2.4.1 Dynamic Behaviour of Honeycomb and Sandwich Panels

The natural frequencies of the panels with skins, i.e. *Models b* and *d*, are at least ten times higher than the natural frequencies of the identical panels without skins, i.e. *Models a* and *c* (see Table 2.2). Sandwich panels are, indeed, much stiffer than the honeycomb core alone because the added skins contribute significantly to increasing the bending stiffness of the panel [1].

The first four modes have shown to be consistent for all the models studied and consisted of a first and second order bending mode, a first order torsion mode and a first in-plane shear mode (see Table 2.3 and Table 2.4). The second order bending mode and the in-plane shear mode were, respectively, the third and fourth natural modes for panel without skins, whereas the fourth and third for panels with skins.

Honeycombs with Structured Core for Enhanced Damping

This is because the added skins in the sandwich panel provide a higher increase in stiffness when deformed in in-plane shear than in bending.

The cell orientation, i.e. in the *L* or *W* direction, does not have a significant impact on the natural frequency of the panels (comparing *Model a* with *Model c* and *Model b* with *Model d*). This is a consequence of the in-plane isotropy of the regular honeycomb core in the models studied [2].

2.4.2 Local Deformation of Honeycomb Cells within a Panel Subjected to Vibration

The local deformation of a honeycomb cell within a honeycomb or sandwich panel subjected to vibration is predominated by an out-of-plane bending deformation of the cells resulting in the in-plane tension/compression of the cell through its depth. The in-plane deformation of the cell is dependent on the cell location within the panel and is maximal closer to the bottom and top skins of the sandwich panel.

The maximal out-of-plane transverse shear deformation for all the natural mode shapes studied in the honeycomb panel only is quasi null for the honeycomb panel only, as shown in Figure 2.19, as opposed to the maximal in-plane deformation that shows strain of around 2.5% (see Figure 2.17). This is because the honeycomb core without skins exhibit a low bending stiffness, hence result in significant bending deformation of the cells causing high in-plane tension/compression close to the top and bottom faces of the cells as illustrated in Figure 2.15. For the first order in-plane shear mode, the in-plane shear deformation of the honeycomb core is predominant due to the mode shape deformation, as shown in Table 2.7 and Table 2.8.

With skins on, i.e. for the sandwich panel, the out-of-plane transverse shear deformation of the honeycomb core reaches a maximum strain of 0.8%, which is significantly higher than the honeycomb panel without skins. This is because the core is loaded in shear by the deformation of the skins of the panel for all the out-of-plane modes of vibration studied. It should be noted that the transverse shear deformation of the sandwich panel is found to be null for the first in-plane shear mode of the panel (see Figure 2.19). In this mode of vibration the two skins of the panel

translate in the same direction with no relative displacement, hence the honeycomb core is not loaded in out-of-plane transverse shear. The maximum in-plane deformation within all modes of vibration studied is 2% for the sandwich panels studied (see Figure 2.17). This is higher than the maximum out-of-plane transverse shear deformation of 0.8%. As highlighted by Gibson and Ashby, this is because the stiffness of the honeycomb core is higher under transverse shear loading than in-plane loading [2]. Similarly to the honeycomb panel, in-plane deformation in the sandwich panel is maximal closer to the top and bottom skins of the panels (see Figure 2.16) and are caused by the bending deformation of the cell. However, the in-plane strains in the sandwich panel do not vary linearly from the top to the bottom face of the panel, as is the case for the honeycomb panel only (see Figure 2.15). This is because the added stiffness given by the skins of the panels limits the in-plane deformation of the honeycomb cells. In this case the maximal magnitude of strain is reduced by 0.5% for the sandwich panel.

The magnitude of in-plane strain of the honeycomb cell for both honeycomb and sandwich panels has been shown to be dependent on the location of the cell within the panel and the mode of vibration, as shown in Table 2.6 to Table 2.9. This is caused by the constraints, in this case a cantilever plate, edge effects and the particular mode shape deformation of the panel, which, at a unit cell level, is different for each individual cell within the panel.

The cell build-up convention within the panel, i.e. along the *L* or *W* direction, as shown in Figure 2.1, is slightly impacting the magnitude of maximal in-plane strain in the honeycomb cells, despite not having a significant impact on the natural frequency and mode shape of the panel because of the in-plane isotropy of the honeycomb core. As shown in Figure 2.17, the maximum in-plane strain for panels with build-up cells in the L direction is strain $\varepsilon_1{}^*$ with a magnitude of 2.5%, whereas the maximum in-plane strain in the W direction is 2%. This is because strain ε_1 matches the direction of the length of the panel, for panels with build-up cells in the L direction and, hence, is slightly more subject to deformation because of the inherent geometry of the panel.

Honeycombs with Structured Core for Enhanced Damping

It should be noted that, since the first order bending, torsion, shear and second order bending modes of vibration of honeycomb and sandwich panels have been investigated in this chapter, the findings can be extended to more complex deformation of the panel resulting in the combination of the mode shape studied or higher order mode of deformation.

2.5 Conclusions

The local in-plane and out-of-plane deformations of the honeycomb cell within honeycomb and sandwich panels subjected to vibration have been investigated in this chapter.

The predominant deformation mechanism of the unit cells consists of the out-of-plane bending of the cells for both honeycomb and sandwich panels. The out-of-plane bending of the cell results in high magnitude of in-plane strain close to the skins of the sandwich panels or close to the top and bottom faces of honeycomb panels. The in-plane strain are null in the neutral plane of deformation of the panel except for in-plane modes of the panels. The out-of-plane transverse shear loading of honeycomb panels is quasi null. For sandwich panels, the magnitude of out-of-plane transverse shear deformation is lower than for the in-plane loading.

The location of maximum in-plane deformation within the cells of a honeycomb or a sandwich panel is dependent of the position of the cell within the panel and the mode shape of the panel.

Honeycombs with Structured Core for Enhanced Damping

Chapter 3. Effective Topologies for Vibration Damping Inserts in Honeycomb Structures

3.1 Introduction

The behaviour of cellular core structures filled with viscoelastic materials was observed experimentally for the first time with a copper foam as a matrix and an elastomer as filling material [11]. The filling of hexagonal cores with foam was then demonstrated for improved energy and impact absorption [42] [93-95]. Foams have also been used to fill honeycomb structures with consequent improvement of damping properties [46, 47]. However, adding foam into honeycomb structures significantly increases the density of the sandwich panel, even if foams themselves exhibit relatively good density-specific properties. To avoid excessive increases in density, cells may be only partially filled with an insert. For example, Woody and Smith obtained an improvement of around 60% in damping loss factor by filling only selected cells within an array, adding less than 6% to the structure's mass [47].

Structures filled with particles, generally small metallic or glass spheres, provide energy dissipation by non-elastic impact and friction damping to the vibrating structure [53] [96] [97]. One of the advantages of this technique is to provide damping in any loading mode and over a wide frequency range, and with little change in stiffness of the structure [96]. However, this approach significantly increases the density of the sandwich. Depending on the application, different materials can be used as particle dampers, e.g. metals and polymers. Michon et al. proposed the use of viscoelastic particles [10], the dissipation of energy by viscoelastic deformation providing additional energy loss.

Complete occupation of a honeycomb cell void with a viscoelastic material has been shown to improve damping loss [11] [92]. Viscoelastic master curves for hexagonal and re-entrant honeycombs with viscoelastic filler have been illustrated [4]. It has also shown that the design of the insert has an important impact on the loss factor of a structure [40]. The more strain energy dissipated by the insert, the more efficient

85

the viscoelastic insert is. Designs of viscoelastic inserts inside honeycombs that improved the damping properties have been patented [98]. This patent describes the damping improvement of honeycombs with: i) a constrained layer of viscoelastic material within the ribs of the cell; and ii) a viscoelastic material inserted in the corner of the cell. Considering these results, it seems that the honeycomb filling method can be optimised with the use of specific core designs or specific inserts.

In order to minimise the added mass of honeycomb structures with damping inserts, the objective of this chapter is to find optimal locations for ligaments made from a high damping material within the void of honeycomb cells, allowing for different cell geometries, and under a variety of in-plane loading cases reflecting the deformation of core honeycomb cells in a range of possible structural vibration modes, as described in Chapter 2.

3.2 Methods

The approach taken was to explore the deformation and strain in a ligament connecting parts of a honeycomb cell, via closed form relations, and then to identify the location that gave rise to the largest strain of a viscoelastic ligament for a range of differently shaped honeycomb cells. The solutions were then validated using finite elements. An FE topological optimisation was also undertaken to check whether ligament stiffness, which was ignored in the analytical model, had an appreciable effect.

3.2.1 Parametric Analytical Study of Honeycomb Cells Loaded either Axially or in In-plane Shear

An analytical study was undertaken to identify the maximum relative displacement of the cell ribs inside various honeycomb unit cells, for in-plane axial and in-plane simple shear loading (see Figure 3.1), as a result of the findings from Chapter 2. The effectiveness of any damping insert will be maximised if it is subjected to the largest deformations and strains available. The honeycomb cell can, in this sense, amplify the local strain experienced by an insert.

Honeycombs with Structured Core for Enhanced Damping

This approach ignores the stiffness of the viscoelastic insert, assuming that the stiffness of the cell itself dominates, as supported by Abd El-Sayed et al. [99]. This will be invalid for cases where the very stiff or large inserts are used.
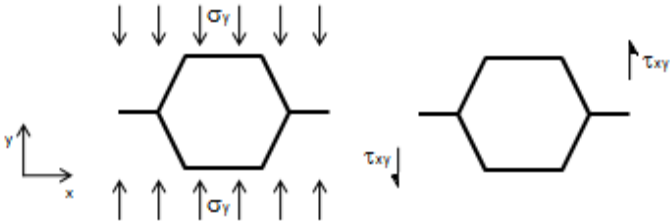
Figure 3.1: Loading modes considered in the analytical model, in-plane axial loading (left) and in-plane simple shear loading (right).

Following Gibson and Ashby [2], deflection of the cell ribs under in-plane axial loading of the honeycomb can be modelled as bending deformation of a cantilever guided at its end (*l* ribs in Figure 3.2). However, it must be noted that the bending-only deformation of the ribs described in [2] can be considered a valid assumption for slender cell walls and for internal angles θ not approaching 0°, at which point beam stretching dominates behaviour [18]. For cells where θ approaches 0°, the cells are effectively square, therefore highly anisotropic and, in practice, generally avoided. Equation 3.1 describes the vertical deflection of the rib, where *P* is the load normal to the beam, as represented in Figure 3.3, *l* the length of the beam, *E* the Young's modulus of the honeycomb material and *I* the second moment of area of the cell wall where *x* and *y* are lengths in the local coordinate system of ribs in Figure 3.3.

$$y = \frac{P.l.x^2}{4.E.I} - \frac{P.x^3}{6.E.I}$$

Equation 3.1

Honeycombs with Structured Core for Enhanced Damping
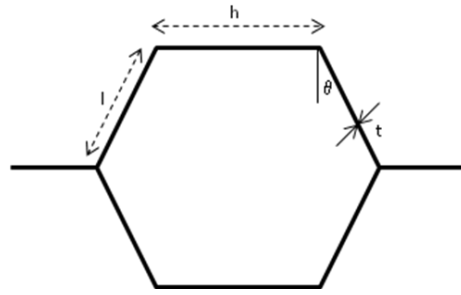
Figure 3.2: Honeycomb cell with its parameters: *h*, *l*, *t* and *θ*.
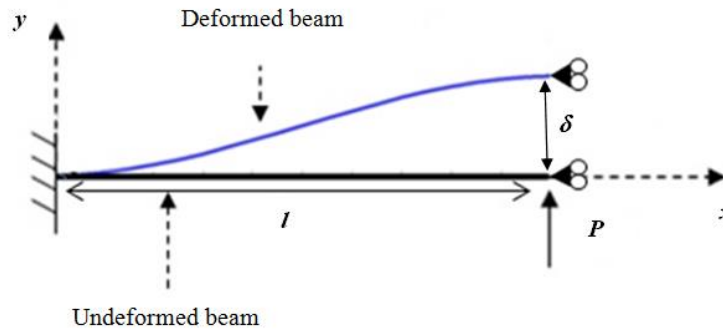
Figure 3.3: Bending deflection of a cantilever beam under guided end conditions.

In-plane simple shear in the honeycomb was modelled by the bending deformation of the horizontal *h* ribs of the honeycomb cells using Equation 3.1. The bending deformation of the oblique *l* ribs was not taken into consideration as its deformation is negligible compare to that of the horizontal *h* ribs in this specific loading [2].

Honeycomb cells were loaded under a global 1% strain ε_{global} both for the axial in-plane and shear loading. The load *P* for both in-plane axial and in-plane shear loading is given by Equation 3.2, where δ is the deflection of an Euler-Bernoulli beam in its local coordinate system, as shown in Figure 3.3.

$$P = \frac{\delta . 12 . E . I}{l^3 . sin\theta}$$

Equation 3.2

Honeycombs with Structured Core for Enhanced Damping

Equation 3.3 and Equation 3.4 show the expression of δ, respectively, for in-plane axial loading and in-plane shear.

$$\delta_{axial} = \frac{\varepsilon_{global}.\,l.\cos\theta}{\sin\theta}$$

<div align="right">Equation 3.3</div>

$$\delta_{shear} = \varepsilon_{global}.\,(h + l.\sin\theta)$$

<div align="right">Equation 3.4</div>

The deformations under these two loading modes were compared to the deformations obtained with FE models. For this purpose, an FE model of a regular honeycomb was constructed with the commercial FE software Ansys 13. Twenty uniaxial elements with tension, compression, torsion and bending capabilities were used to model each beam of the cell (Ansys BEAM4 element [90]).In-plane axial, in-plane simple shear and in-plane pure shear boundary conditions were considered. Figure 3.4a shows the deformed shape of the honeycomb cells under 1% strain for the loading modes considered (displacement magnified by a factor of 10). Of note, the deformed shapes of the cells presented in Figure 3.4 is valid for all regular honeycomb cells independently of their cell ribs dimension for cells with slender cell walls (*t<<l*). This is because the ratio between the beam deflection δ and the characteristic length of the cell for both in-plane axial loading, i.e. *l.cos(θ),* and in-plane shear loading, i.e. *h+l.sin(θ)* is independent of the cell ribs dimensions *h*, *l* and *t*. For both in-plane axial and shear loading conditions, the analytical model matches the FE results, validating the hypotheses made. Figure 3.4b shows, in particular, that the deformed shape of the honeycomb cell when loaded in in-plane simple or pure shear at the same strain is identical.

Honeycombs with Structured Core for Enhanced Damping
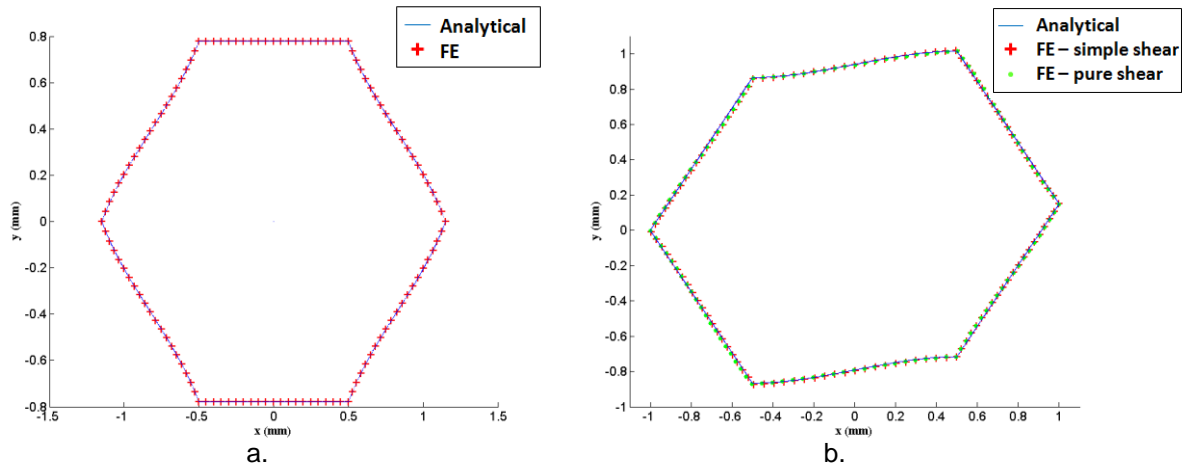
Figure 3.4: A deformed honeycomb cell predicted by the analytical and FE models under in-plane axial loading (a.) and, similarly, a cell under in-plane simple shear and in-plane pure shear (b.).

A parametric search of all possible insert ligament locations was undertaken to identify the locations of the ligaments with maximal strain. This process is described in the following three steps.

Step 1. Ligaments are straight and may connect any two points of the cell ribs. Cells were divided up into approximately 300 seed nodes in the cell void, and for each of these seed nodes 35 vectors were defined passing through that node, with angles to the horizontal at 5° increments, i.e. between 0° and 175°. This defines all the allowable vectors that pass through all the seed nodes in the cell void. This process was repeated for all seed nodes in each cell considered.

Step 2. The deformation of a ligament was assumed to be the relative displacement of two points on the cell ribs connected by a vector. The deformation of the cell ribs was calculated by considering them as beams, as described before. This gave a profile of displacement at any point along the length of the cell ribs. The strain of all ligaments passing through all seed nodes was calculated by considering these displacements as the deformations of the ligaments. This makes the assumption that the extra stiffness associated with the presence of the ligament did not affect the deformation of the cell rib, and is examined in detail later. Symmetry for axial cell

Honeycombs with Structured Core for Enhanced Damping

deformation meant that only a quarter of the void space needs be considered, and half the void space needs be considered for shear. Trials with smaller intervals of seed node location and ligament rotation made little or no difference to the results.

Step 3. The strain in all ligaments was calculated in post-processing and the value of the maximum strain at each seed node was recorded. For each honeycomb cell geometry, the seed nodes with the largest strain values would lie along the same vector as the ligament with maximal strain. Thus, the optimal locations of ligaments with the highest strain energies are defined.

As shown in Figure 3.5 and Figure 3.6, for each position inside the void space, the relative strain of ligaments, ε_{insert}, was calculated from Equation 3.5, where L_i and L_f were the ligament lengths before and after (respectively) the global cell deformation.

$$\varepsilon_{insert} = \frac{|L_i - L_f|}{L_i}$$

Equation 3.5
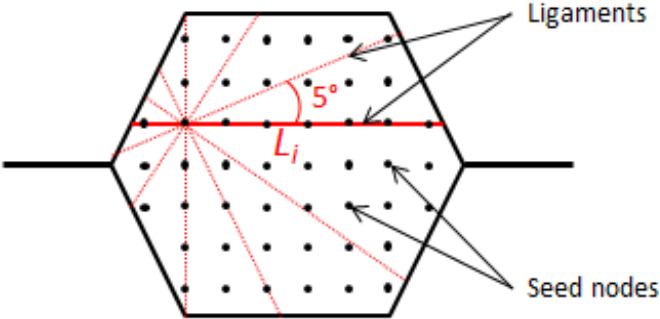
Figure 3.5: The seeds nodes in an undeformed honeycomb cell. Also shown are a small number of the ligaments for one particular node, notably one with length L_i.

Honeycombs with Structured Core for Enhanced Damping
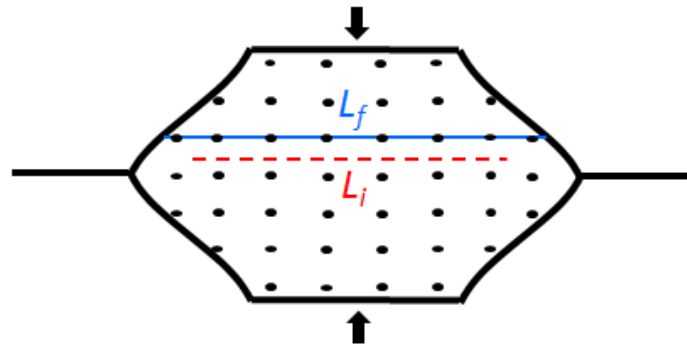
Figure 3.6: A deformed honeycomb cell loaded axially as shown, in which the ligament shown in Figure 3.5 has lengthened to L_f.

Maps of the maximum relative strain ε_{insert_max} across all ligament orientations for each node location inside the void of the honeycomb were then constructed post-process (in Matlab 2009 [101]).

Different honeycomb geometries were investigated by varying α, the ratio between the length of the horizontal h ribs and the oblique l ribs, between 0.2 (a markedly squat cell) and 2.0 (a markedly thin cell). The internal angle θ of the honeycomb cell was varied between $\theta = 30°$ (a 'regular' honeycomb) and $\theta = -20°$ (a 're-entrant' honeycomb) (see Figure 3.2) [99]. Investigation of parameters α and θ provides the full description of the honeycomb in-plane geometric parameters as defined by Gibson and Ashby [2]. The effect of the cell ribs' thickness in the present model is provided by the second moment of area I used in Equation 3.1 and Equation 3.2. Substituting P from Equation 3.2 into Equation 3.1, the second moment of area I disappears and, therefore, the thickness of the cell rib. This assumption is valid for β values, the ratio between the thickness of the cell ribs t and the oblique l ribs, lower than 0.2 to neglect possible contributions from the shear deformation of the ribs' cross-section [2]. Relative density-specific quantities presented in the result section have been derived for $\beta = 0.1$. The density ratio of the honeycomb $\rho_{rel} = \rho/\rho_c$ is defined in Equation 3.6 where ρ is the density of the honeycomb, and ρ_c the density of the constituent material of the honeycomb.

Honeycombs with Structured Core for Enhanced Damping

$$\rho_{rel} = \frac{\rho}{\rho_c} = \beta . \frac{2 + \alpha}{2.(\alpha + sin\theta).cos\theta}$$

<div align="right">Equation 3.6</div>

3.2.2 FE Analysis of In-plane Loadings

A 2D FE model of a regular honeycomb cell *(α=1, h=1 mm, β=t/l=0.02,* and *θ=30°)* and a re-entrant cell *(θ=-20°)* was constructed using 10 Beam4 elements per ribs with aluminium material properties (Young's modulus of 70 GPa and Poisson ratio of 0.3). Similarly, the realistic boundary conditions for in-plane axial and shear under 1% strain were applied to the FE model of the cell so as to be a fair comparison of the analytical model. The displacements of all element nodes were recorded for each model and the relative strain between each element node, i.e. the strain of a hypothetical ligament placed between them ε_{ij}, was calculated from Equation 3.7, where di_{ij} and df_{ij} are the distances between element node *i* and element node *j* before and following applied deformation. Locations of maximum relative displacements for all the element nodes of the structure were then identified during post-processing.

$$\varepsilon_{ij} = \frac{\left|di_{ij} - df_{ij}\right|}{di_{ij}}$$

<div align="right">Equation 3.7</div>

3.2.3 Topological Optimisation of Honeycomb Cells Completely Filled with Viscoelastic Material

A topological optimisation was undertaken with Ansys 13, of a 2D honeycomb unit cell model of a regular aluminium honeycomb cell *(α = 1* and *θ = 30°)* and a 're-entrant' cell *(α = 1* and *θ = -20°).* The unit cell is a representative volume element (RVE) for the honeycomb core. The objective of the optimisation was to minimise the compliance of the honeycomb cell, which was initially completely filled with a viscoelastic material. The constraint of the optimisation problem was to reduce the volume of the viscoelastic material in the honeycomb cell by 80%. The viscoelastic

material in solutions with smaller compliances carry a greater proportion of total load borne by the cell, and, therefore, are under a higher strain and likely to carry more strain energy. By minimising compliance, this process ensured that the viscoelastic material carried more strain energy and, therefore, damped more vibration energy. The model was initially completely filled with a viscoelastic material and loaded in the in-plane axial and in-plane pure shear directions to 1% strain. The viscoelastic material was modelled with a Young's modulus of 0.1 MPa and a Poisson ratio of 0.35 (the maximum value of Poisson ratio that can be assigned to elements in a topological optimisation in the FE software used). Symmetry boundary conditions were applied to the RVE cell to represent a continuum of cells. The model consisted of approximately 1,000 PLANE82 8-node bilinear plane elements with plane strain behaviour. The compliance of the cell structure was defined as the rate of deformation with respect to load.

The results of this optimisation study were compared with the results from the analytical models, in which the stiffness of the ligaments was not considered. Four honeycomb cell geometries were considered, as shown in Table 3.1: Geometry 1 in which the native honeycomb had a Young's modulus similar to that of the viscoelastic material, and geometry 2 in which the cell had a Young's modulus of more than 10 times the viscoelastic material. Geometries 3 and 4 represent a 're-entrant' cell configuration.

Table 3.1: Honeycomb cell dimensions in topological optimisation study.

	Geometry 1	Geometry 2	Geometry 3	Geometry 4
Honeycomb parameters				
l (mm)	1	1	1	1
h (mm)	1	1	1	1
t (mm)	0.01	0.02	0.01	0.02
□	30	30	-20	-20
Material properties				
Honeycomb Young's Modulus (MPa) [2]	0.16	1.29	0.86	6.84
Viscoelastic Young's Modulus (MPa)	0.1	0.1	0.1	0.1

3.3 Results

3.3.1 Parametric Analytical Study of Honeycomb Cells Loaded either Axially or in In-plane Shear

The relationship between the maximum relative strain ε_{insert_max} of all possible ligaments and the honeycomb internal angle θ is shown in Figure 3.7 for an in-plane axial deformation mode. In this case, the honeycomb parameters were set at $\alpha = 1$ and $h = 1$. Honeycombs with internal angles close to 0 achieve the highest maximum ligament strains, with a discontinuity around $\theta = 0°$ because the deformation of the oblique ribs (*l*) becomes predominantly axial rather than flexural. The location of the maximum ligament strain for three different honeycomb cells is shown in Figure 3.8. The magnitude of the ligament strain is indicated by colour for each location in the cell, and those ligaments with highest strain (shown in red) tend to form axes across the middle of the cell for all three geometries. These axes of maximal ligament strain locations indicate the orientation of the ligament of maximum strain, e.g. the ligament with the highest strain would lie across the mid axis of the cell in Figure 3.8. This is, therefore, the optimal ligament location and orientation.
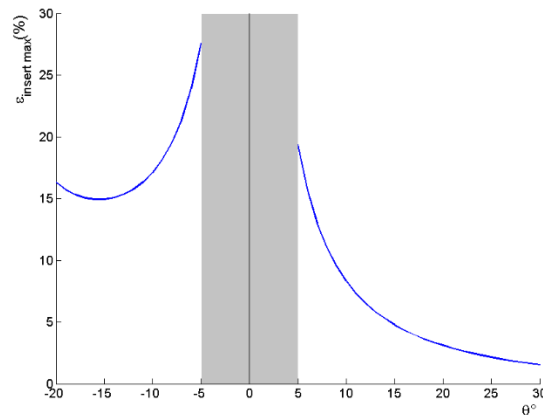
Figure 3.7: The maximum relative strain, $\varepsilon_{insert\ max}$, of all possible ligaments as a function of the honeycomb internal angle, θ under in-plane axial loading.

Honeycombs with Structured Core for Enhanced Damping
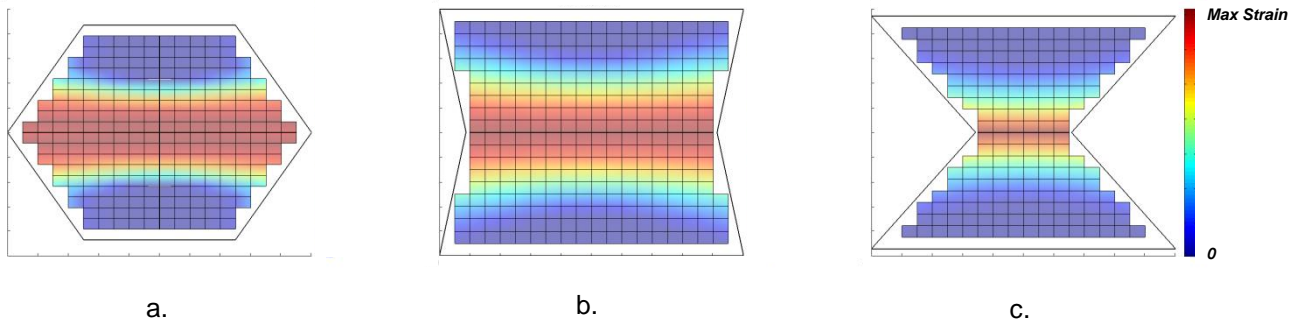
Figure 3.8: Strain map of the ligaments in three different honeycomb cell geometries under in-plane axial deformation, (θ=and 30° in a., -5° in b and -20° in c.).

Similarly, Figure 3.9 shows the relationship between maximum relative strain ε_{insert_max} of all possible ligaments, for different internal angles, but for the case of in-plane simple shear. The honeycomb cell parameters were as above (α=1 and h=1). The maximal ligament strain in simple shear is lower than the maximal ligament strain in axial loading (0.74 opposed to 27), see Figure 3.7 and Figure 3.9, and the maximal values are achieved at extreme internal angle values, i.e. θ= -20° and θ= 30°. The minima for ligament strain are found at internal angles of θ = -12° and θ = 12°, with no discontinuity at θ = 0°. The magnitude of the maximal ligament strain is indicted graphically in Figure 3.10 for five different cell geometries, though this data was obtained for all cases. For cells with internal angles between -20° and -12° (see Figure 3.10), the optimal ligaments lie along axes across the middle of the cells (see Figure 3.9 for an example cell with θ = -20°). This was in common with the case of axial loading (see Figure 3.8). In contrast, for cells with internal angles between -12° and 12°, the optimal ligaments formed symmetric cross structures in the upper and lower sections of the cell (see Figure 3.10). For cells with internal angles greater than 12°, the optimal ligaments formed a single cross structure extending across the full height of the cell (see Figure 3.10).

Honeycombs with Structured Core for Enhanced Damping
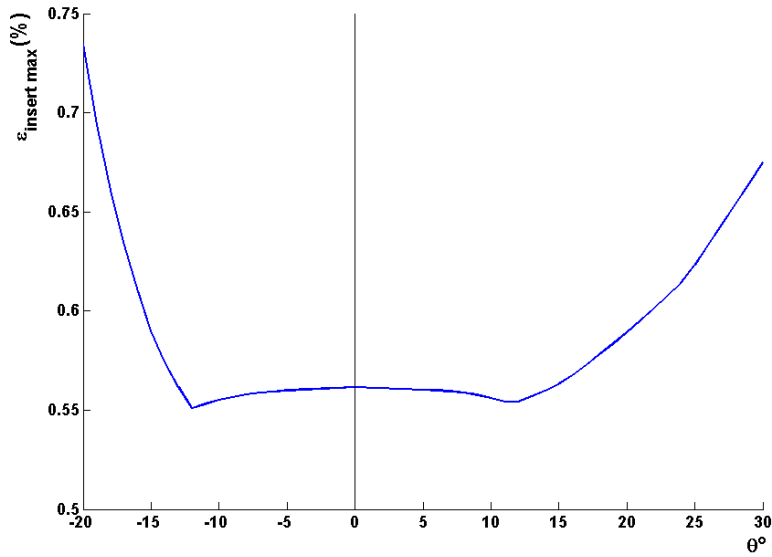
Figure 3.9: Maximal ligament strain, $\varepsilon_{insert\ max}$, of ligaments inside the cell void as a function of the honeycomb internal angle, θ under in-plane shear loading.

a.

b.

c.

d.

e.
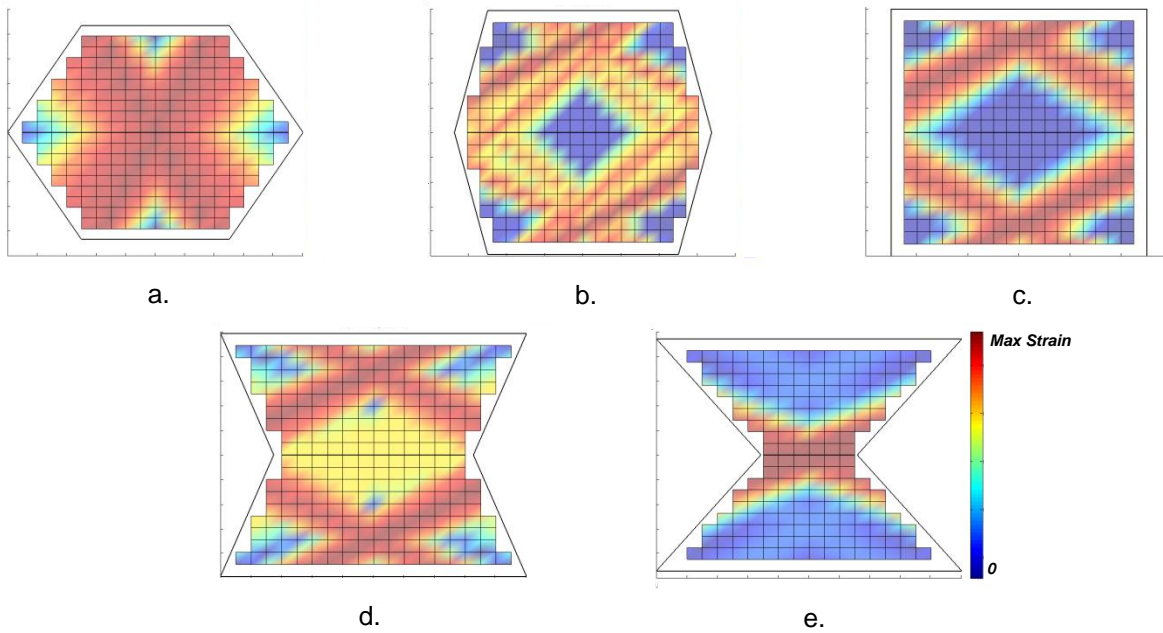
Figure 3.10: The strain of the ligaments in three different honeycomb cell geometries under in-plane shear deformation ($\theta = 30°$ in a., 10° in b., 0° in c., -10° in d. and -20° in e.).

97

Honeycombs with Structured Core for Enhanced Damping

The influence of the parameter α, the ratio of the lengths *h* and *l*, of the honeycomb cell on the maximal ligament strain is presented in Figure 3.11, for both in-plane axial and shear loading cases. For these data, the internal angle θ was set to 30° (a regular honeycomb), the length *h* was varied between 0.2 mm and 2 mm, while *l* remained constant at 1 mm ($\alpha = 0.2$ to 2). For $\theta = 30°$, i.e. a regular honeycomb, the maximal ligament strain for in-plane axial loading appears to be only approximately twice the value for in-plane simple shear, unlike for other cell angles where it can be an order of magnitude. The parameter α has a minimal effect upon the magnitude of the maximal ligament strain, with maximum strain values reached at minimal values of α. However, Figure 3.12 and Figure 3.13 indicate that the location of ligaments with maximal strain does depend on parameter α. For in-plane axial loading and parameter $\alpha \leq 1.6$, most of the ligaments with maximal strain are located across the middle of the cell (see Figure 3.12). Note that, upon close inspection, there is more than one optimal ligament and they lie on two parallel axes near to the cell mid-line (see Figure 3.12a). These axes tend to move closer to one another as the value of α increases. For values of $\alpha > 1.6$, the optimal ligaments switch to two parallel vertical ligaments between the oblique *l* ribs. When loaded in-plane simple shear (see Figure 3.13), the optimal ligaments are located in the corners between the *h* and *l* ribs for $0.2 < \alpha < 0.6$. For values of $\alpha > 0.6$, the optimal ligaments form diagonal crosses extending between the *h* ribs.

Honeycombs with Structured Core for Enhanced Damping
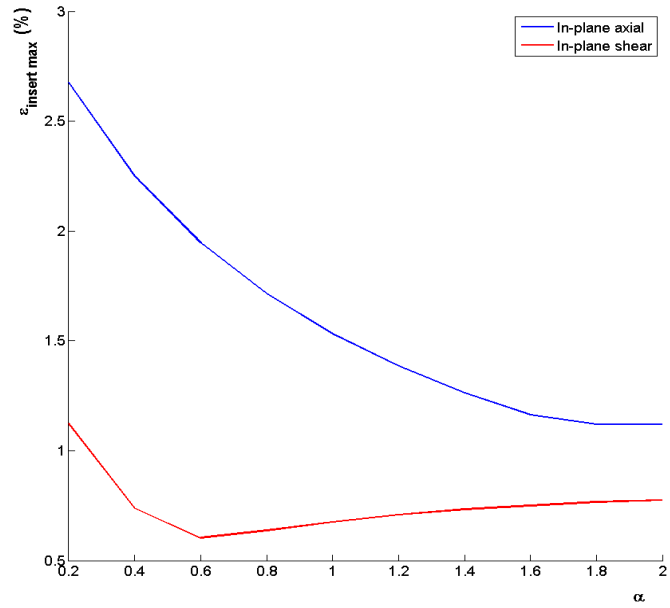
Figure 3.11: Maximum strain, $\varepsilon_{insert\ max}$, of all ligaments as a function of the aspect ratio of the ribs $\alpha = h/l$.

a.

b.

c.

d.

e.
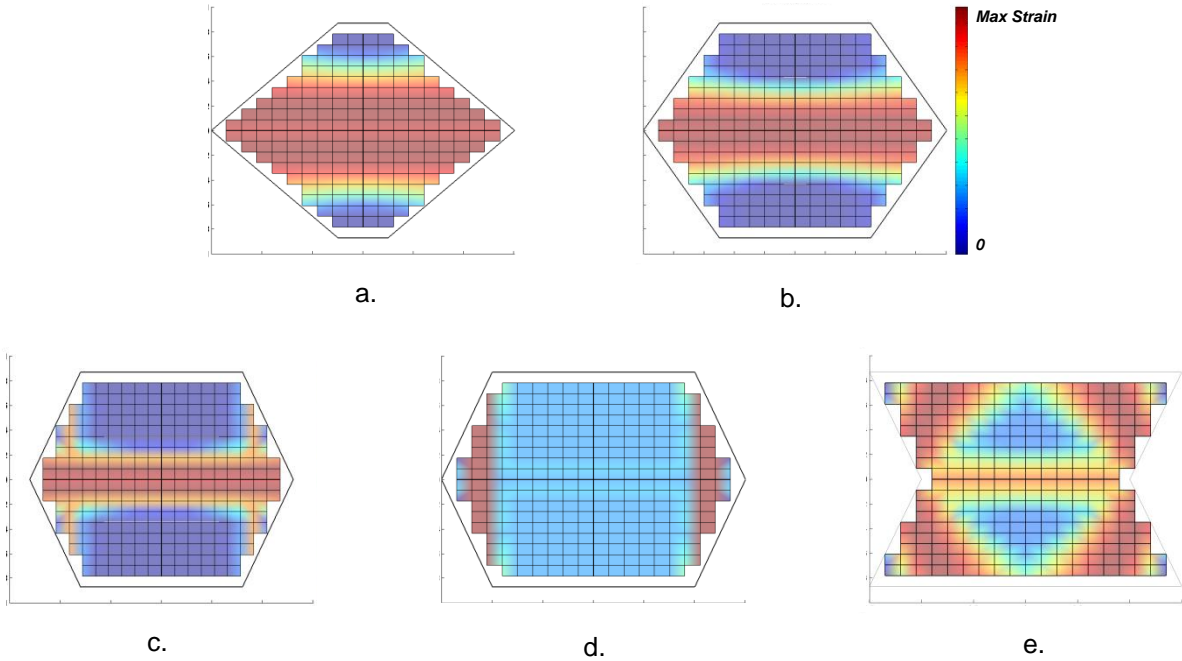
Figure 3.12: The strain of the ligaments in four different honeycomb cell geometries under in-plane axial deformation ($\theta = 30°$ and $\alpha = 0.2$ in a., 1 in b., 1.6 in c., 2 in d. and $\theta = -20°$ and $\alpha = 2$ in e.).

Honeycombs with Structured Core for Enhanced Damping
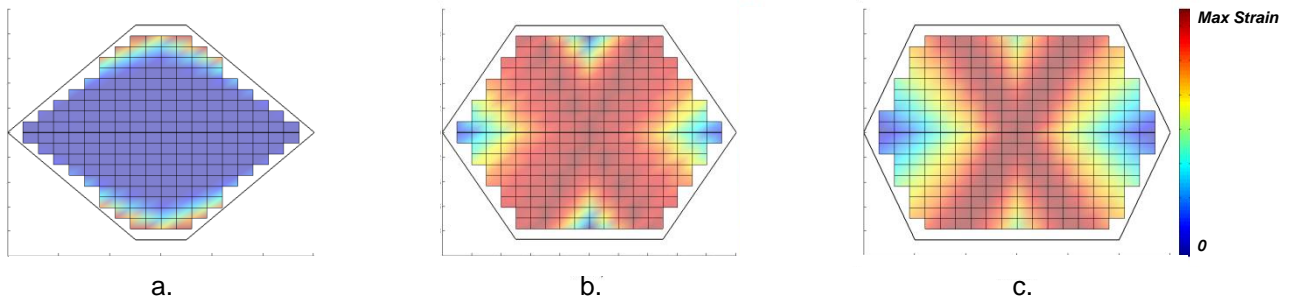
Figure 3.13: The strain of the ligaments in three different honeycomb cell geometries under in-plane shear deformation ($\alpha = 0.2$ in a., 1 in b. and 2 in c.).

The magnitude of the maximum ligament strain ε_{insert_max} for honeycombs with varying internal angle θ and length ratio α under axial loading is shown in Figure 3.14. Similarly, the magnitude is shown in Figure 3.15 but normalised to the density ratio $\rho/\rho c$ of the honeycomb. The highest ligament strain is achieved for cell geometries with internal angles θ of near to 0 and with the lowest length ratio α. In contrast, when considering the relative density, the length ratio α has a negligible effect on the magnitude of the optimal ligament strain.
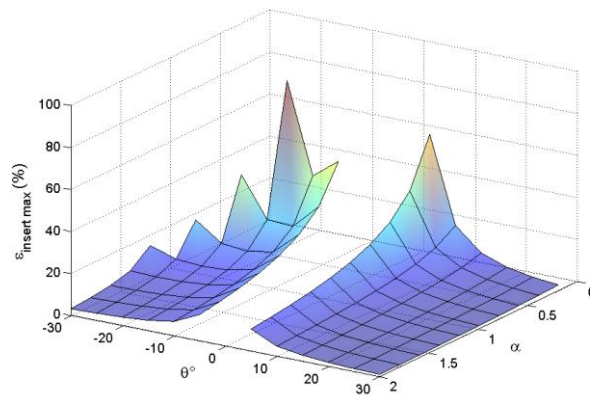
Figure 3.14: Maximum strain, $\varepsilon_{insert\ max}$, of all possible ligaments as a function of the ratio between ribs, $\alpha=h/l$ and the honeycomb internal angle θ under in-plane axial deformation.

Honeycombs with Structured Core for Enhanced Damping
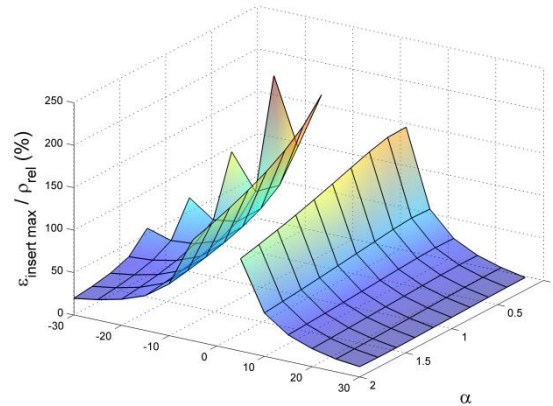
Figure 3.15: Maximum strain, $\varepsilon_{insert\ max}$, normalised to the density ratio, $\rho/\rho c$, of the honeycomb of all possible ligaments as a function of the ratio between ribs α and the honeycomb internal angle θ under in-plane axial deformation.

For simple shear loading, the maximum ligament strain, ε_{insert_max}, for a range of honeycomb geometries is shown in Figure 3.16. Again, this data is shown normalised to relative density $\rho/\rho c$ in Figure 3.17. The highest ligament strain is achieved for cell geometries with both large negative internal angle θ and low length ratio α. This is reversed when considering relative density, where higher positive values of internal angle θ and length ratio α perform optimally.

Honeycombs with Structured Core for Enhanced Damping
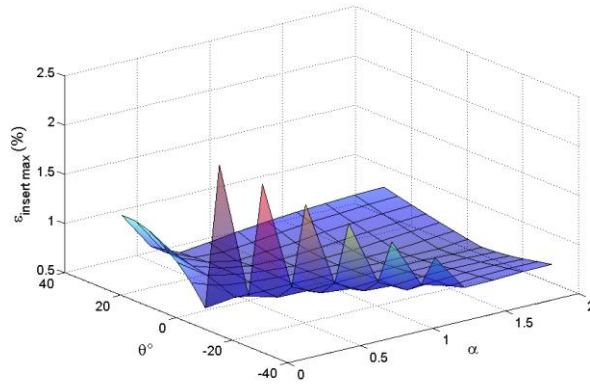
Figure 3.16: Maximum strain, $\varepsilon_{insert\ max}$, of all possible ligaments as a function of the ratio between ribs $\alpha=h/l$ and the honeycomb internal angle θ under in-plane shear deformation.
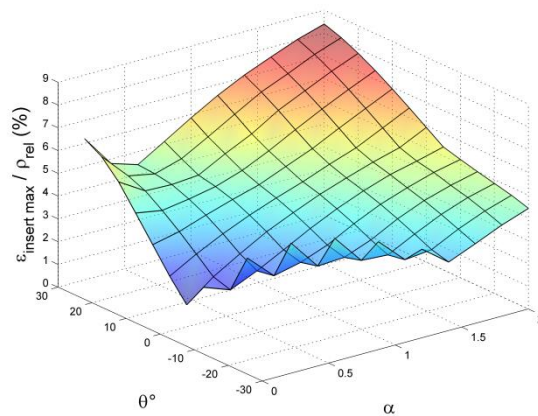
Figure 3.17: Maximum strain, $\varepsilon_{insert\ max}$, normalised to the density ratio $\rho/\rho c$ of the honeycomb of all possible ligaments as a function of the ratio between ribs α and the honeycomb internal angle θ under in-plane shear deformation.

3.3.2 FE Analysis

Optimal locations of ligaments between nodes of the FE model of a regular and a re-entrant honeycomb cell are shown in Figure 3.18 and Figure 3.19 for the different loading cases studied (in-plane axial and in-plane simple shear). Ligaments between nodes reaching at least 98% the strain of the ligament with the highest strain in the

Honeycombs with Structured Core for Enhanced Damping

cell have been represented in these figures. When loaded axially, the optimum location of ligaments forms an axe across the middle of the regular honeycomb cell. For in-plane shear deformation, this location forms a single cross structure extending across the full height of the cell. For the "re-entrant" cell, ligaments of highest strain form an axe across the middle of the cell for both in-plane axial and shear deformation.
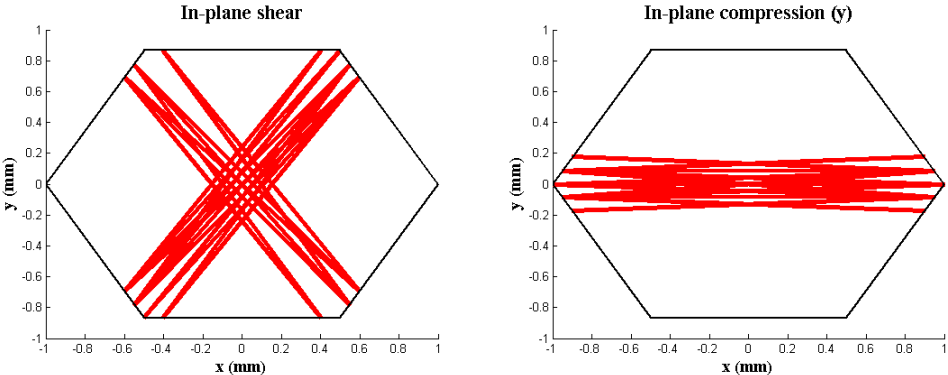
Figure 3.18: Ligaments reaching at least 98% of the maximal ligament strain are shown located in the cell. The ligaments connect nodes in the finite element model of the regular cell, and their spacing is thus discontinuous.
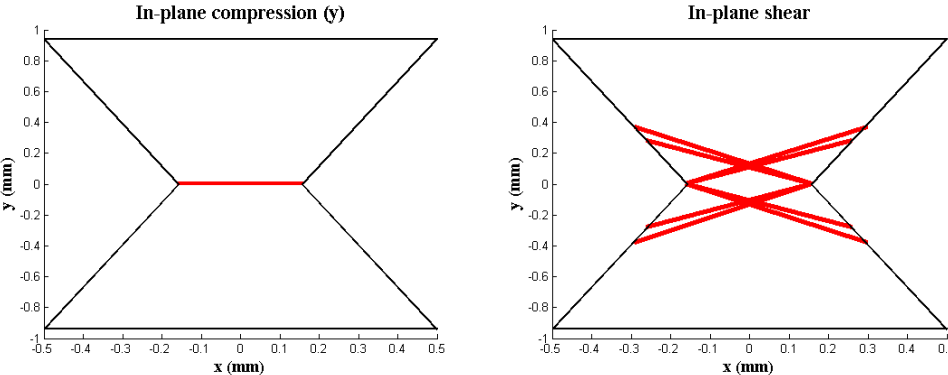
Figure 3.19: Ligaments reaching at least 98% of the maximal ligament strain are shown located in the cell. The ligaments connect nodes in the finite element model of the re-entrant cell, and their spacing is thus discontinuous.

103

Honeycombs with Structured Core for Enhanced Damping

3.3.3 Topological Optimisation of Honeycomb Cells Completely Filled with Viscoelastic Material

The results of the topological optimisation set to maximise the global stiffness of the structure for an 80% volume reduction of the viscoelastic material used to fill the void of the cell are shown in Figure 3.20 for geometries 1 to 4 (methodology) loaded axially. The results of the optimisation highlight a location forming a horizontal ligament in the middle of the cell.

Figure 3.21 shows the result of the topological optimisation for the geometries studied for in-plane pure shear loading. For geometries 1 and 2, two different locations have been formed by two crossed ligaments in the middle of the honeycomb cell. For geometries 3 and 4, the results of the optimisation highlight a location forming a horizontal ligament in the middle of the cell.
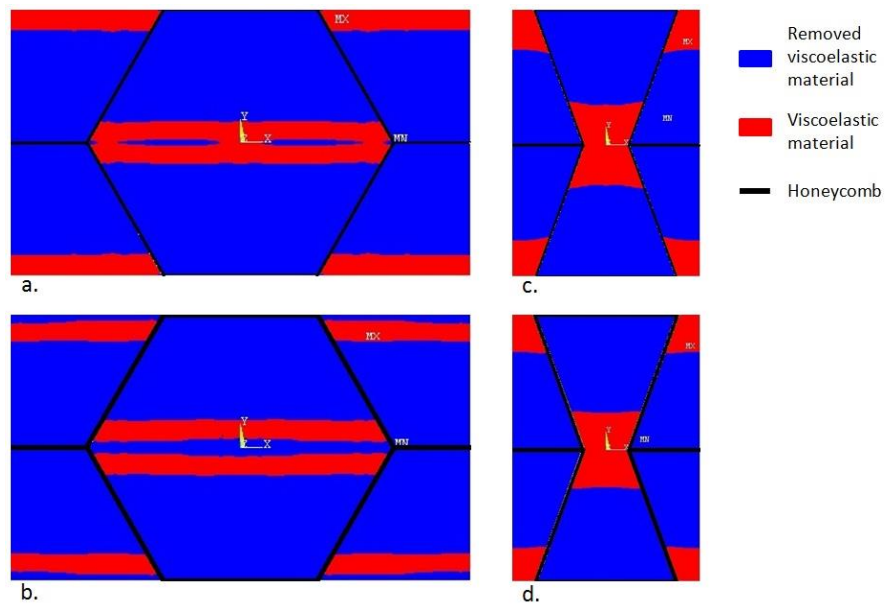
Figure 3.20: Topological optimisation of the stiffness of a honeycomb cell filled with a viscoelastic material under in-plane axial deformation (a. corresponds to geometry 1, b. to geometry 2, c. to geometry 3 and d. to geometry 4).

Honeycombs with Structured Core for Enhanced Damping
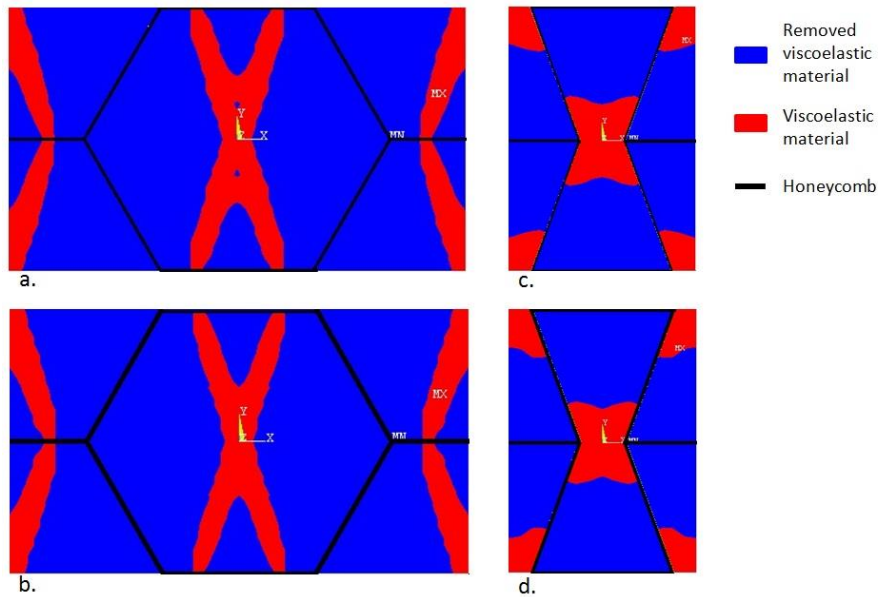
Figure 3.21: Topological optimisation of the stiffness of a honeycomb cell filled with a viscoelastic material under in-plane shear deformation (a. corresponds to geometry 1, b. to geometry 2, c. to geometry 3 and d. to geometry 4).

3.4 Discussion

3.4.1 In-plane Axial Loading

When loaded axially, optimal locations of inserts tend to form a horizontal axis across the middle of the cell, and this is independent of the internal honeycomb angle θ. In this loading case, the maximum displacement between the cell ribs arises near to the vertices between adjacent *l* ribs. However, the optimal ligament does not lie at the *l* rib vertices because the beams are rigidly connected at their ends and are thus considered to be 'guided' cantilevers (see Figure 3.3). Considering the geometry of the honeycomb cells, the highest absolute values of optimal ligament strains are found in cells with internal angle θ approaching 0° (see Figure 3.7). This is because the rate of change of the internal angle is greatest as it approaches 0°. Notably, cells with negative internal angles exhibited higher maximal values of strain in their optimal ligaments because the distance between *l* rib vertices is smaller in the re-entrant cells.

Honeycombs with Structured Core for Enhanced Damping

The influence of the cell aspect ratio α is clear in Figure 3.12, i.e. that as the *h* rib begins to exceed the *l* rib by 60% or more the optimal rib swaps to lying between adjacent rather than opposing *l* ribs. This is because the initial value of the distance between opposing *l* rib vertices increases with α, also explaining why the highest value of maximum relative strain is reached for the lowest value of α (Figure 3.12). On a density-specific basis, α has less influence since it is also a factor in the density (see Figure 3.15).

The results of the FE analysis of a regular honeycomb under axial loading, Figure 3.18, also shows similar optimal ligament locations, agreeing well with the results from the analytical model. Similarly, the results obtained from the topological optimisation agree, and go some way to validating the assumption in section 2.1 that, for the range of cases studied here, the compliance of the ligament can be neglected and that the deformed shape of the honeycomb is mainly driven by the constituent material of the ribs. This assumption is likely to become invalid for cases where the cell ribs are much thinner or more compliant or the ligament material is much stiffer.

3.4.2 In-plane Shear Loading

For in-plane shear, locations of the optimal ligaments are mainly determined by the internal honeycomb angle θ. These location are classified in three categories: i) as shown in Figure 3.10, for cells with internal angles between -20° and -12°, optimal ligaments form an axis across the cell middle; ii) for internal angles between -12° and 12°, the optimal ligaments form a double cross structure; iii) for cells with internal angles of greater than 12° the optimal ligaments form a single cross structure across the full height of the cell. The reason the location and form of the optimal ligament changes is because the initial distance between *l* rib vertices changes with the cell shape, increasing as the angle θ increases. From these three different highlighted locations, the most efficient appears to be the locations described for θ between -20° and -12° and between 12° and 30°, as shown in Figure 3.10.

The influence of the ratio α on locations of the optimal ligaments can be seen in the two distinct categories, as shown in Figure 3.13. From $\alpha = 0$ to $\alpha = 0.6$, optimal

ligaments are located in the vertices between *h* and *l* ribs. In fact, the optimal ligament runs between points on the *l* ribs parallel and near to the *h* rib. At a critical value of cell aspect ratio, $\alpha = 0.6$, the increase of *h* reduces the ligament strain, and thus there is a change to a new configuration of optimal ligaments of a single cross.

Figure 3.16 shows that higher optimal ligament strains are achieved for structures with the low values of angle θ and ratio α. If the base sheet material forming the honeycomb is similar as θ and α change, the density will change markedly. The effect of this is shown in Figure 3.17, and it is clear that the higher density of the cells with low θ and α values outweighs the benefits of higher strains in the ligament. It would of course be possible to alter the thickness of the constituent sheet material, t, so as to keep the density constant as both θ and α vary, in which case inclusion of density would not change the shape of Figure 3.16.

Comparison of Figure 3.14 (for axial deformation) and Figure 3.16 (for shear deformation) shows that the absolute strain values in the optimal ligaments are higher in axial loading than in shear loading (87% *vs* 2%, respectively), despite the applied global strain being 1% in both cases. The structure of the cell magnifies the global strain in axial loading much more than in shear.

The FE model of cell deformation agrees well with the predictions of the analytical analysis, at least for the cases studied, i.e. a regular honeycomb cell ($\alpha = 1$, $\theta = 30°$) and a re-entrant cell ($\alpha = 1$, $\theta = -20°$). The topological optimisation also agrees with the analytical and FE model of cell deformation, despite the topological model's inclusion of the ligament's stiffness in calculation of the structure's deformation.

3.5 Conclusion

The best location for inclusion of a ligament damping insert within the void of a honeycomb cell is the location where the relative displacement between the wall of the cell is maximal so as to maximise the deformation of the damping insert, hence its damping capacity.

The best locations are very specific to the geometry of the honeycomb cell and the in-plane loading direction. For most cases, a ligament between the two opposite edges of the honeycomb cell is the best location for ligament damping insert subject to axial loading. In all cases, complete occupation of the void is not the best solution for optimising the axial strain deformation of the damping material within the void of the cell.

In the particular case of regular honeycomb cells, horizontal ligaments between the opposite edges of the cell void are best for in-plane axial loading and double cross ligaments across the two diagonal opposite edges of the honeycomb for in-plane shear loading.

Honeycombs with Structured Core for Enhanced Damping

Chapter 4. Viscoelastic Damping Inserts

4.1 Introduction

In-plane axial and shear loading were identified in Chapter 2 as the main deformation mechanisms of honeycomb unit cells inside a sandwich panel subjected to vibration. Best locations of damping material inside the void of the honeycomb cell have been investigated in Chapter 3 for both loadings. Different geometries of damping insert have been identified depending of the geometry of the cell and its loading.

Complete occupation of the honeycomb cell void with damping material such as viscoelastic material has been shown to improve damping loss [11]. However, the weight penalty of this solution is considerable, making it not suitable for lightweight structures. Enhancement of the damping performance with partial filling of the cell void has been investigated for auxetic honeycombs, involving the use of viscoelastic material in the corner of the honeycomb cell [98]. The use of an auxetic honeycomb panel is, however, not common in industry because of the difficulties of manufacturing an auxetic core [3] [15].

The objective of this chapter is to quantify the density-specific damping properties of partially filled regular honeycombs with viscoelastic damping inserts located in the locations highlighted in Chapter 3 for both in-plane axial and shear loadings. Only regular honeycomb cells are investigated in this chapter because of their common use in industry [3].

Analytical expression of the loss modulus and FE analyses have been used to quantify the loss modulus of the different geometry of damping inserts studied in this chapter. The loss modulus, the product of the structural modulus and the loss factor of a structure, is the figure of merit for composite material using viscoelastic material [86]. The damping properties of honeycomb with damping inserts have been quantified through static analyses using the modal strain energy (MSE) method [100] [102] [103].

Honeycombs with Structured Core for Enhanced Damping

4.2 Methods

4.2.1 Analytical Model

4.2.1.1 Mechanical and Damping properties of a honeycomb cell with a ligament insert

The mechanics of honeycomb structures have been widely studied and several analytical models have been developed to calculate their mechanical properties. Models of different complexities have been derived. Mechanical properties such as Young's modulus or Poisson's ratio can be calculated taking account of the bending deformation of the cell walls [2]. More complex expressions have been derived for thicker cell walls ($t/l > 0.2$), taking into account their shear deformation [2]. More complex expressions have been derived taking into account the stretching/compression and hinging of the cell walls [18]. For low-density honeycomb loaded at small strain, expressions derived by Gibson and Ashby, taking account only of the bending deformation of the cell walls, represent well the mechanical properties of honeycombs. Their approach has been used in this section to derive the mechanical and damping properties of honeycombs with a damping insert across their middle (see Figure 4.1).
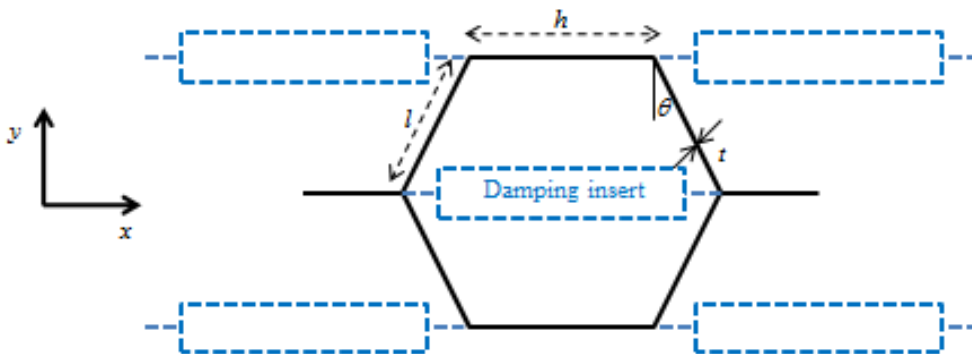
Figure 4.1: Honeycomb unit cell with damping insert partially filling the honeycomb cell void.

Honeycombs with Structured Core for Enhanced Damping

Analytical expressions of Young's modulus E, loss factor η and loss modulus E^* have been derived for in-plane uniaxial loading in the y direction to understand the mechanical behaviour of the honeycomb with a damping insert. The honeycomb cell is defined by parameters l, h, t and θ, as represented in Figure 4.1, and b representing the honeycomb depth. The damping insert is defined by parameters l_{insert} and h_{insert}, as represented in Figure 4.2.
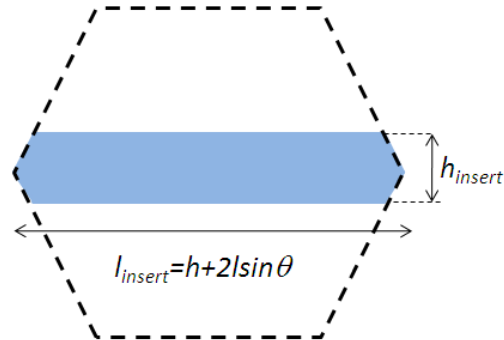
Figure 4.2: Dimension of a horizontal ligament damping insert located within the void of a honeycomb cell.

For uniaxial in-plane loading, it was assumed that the deformation mechanism consisted of the bending deformation of the honeycomb l walls due to the compression of the cell in the y direction [2] and the force introduced by the damping insert. Considering the symmetry of the model represented in Figure 4.1, a quarter of the cell can be isolated to derive the mechanical properties of the honeycomb cell with a damping insert. Loads resulting from the uniaxial loading along the y direction are represented in Figure 4.3 in a free body diagram. The moment M causing the bending of the cell walls is defined in Equation 4.1, where P is the force resulting from the stress σ_y (see Equation 4.2), and F_{insert} the force of the damping insert. Giving the geometry of the honeycomb with the damping insert and the symmetry of the uniaxial loading in the y direction, the damping insert is loaded in tension/compression along the x direction. Using beam theory, the force of the damping insert, F_{insert}, is given in Equation 4.3, where $2.\delta.cos\theta$ is the displacement

Honeycombs with Structured Core for Enhanced Damping

of the damping insert and K_{insert} the stiffness of the damping insert (see Equation 4.4), where E_{insert} is the Young's modulus of the material of the damping insert.
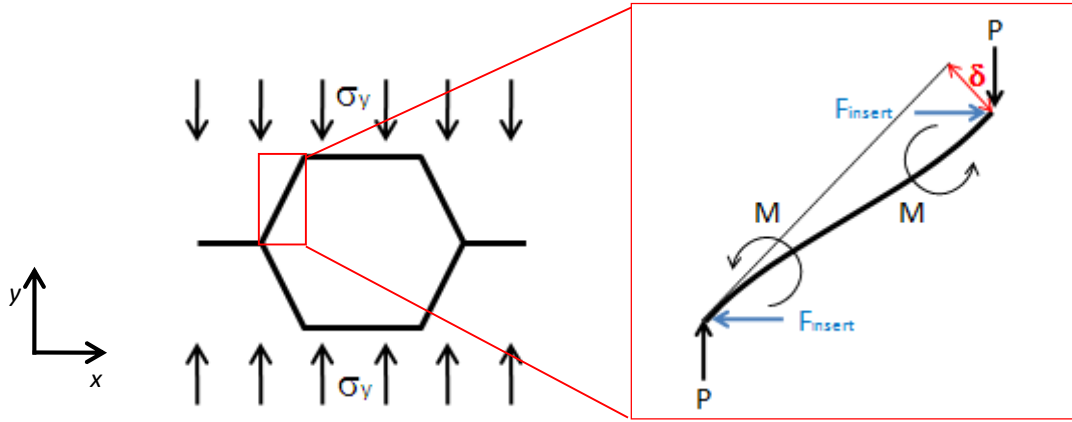
Figure 4.3: Force body diagram of the l walls of a honeycomb cell subject to a compressive load in the y direction.

$$M = \frac{P.l.sin\theta + F_{insert}.l.cos\theta}{2}$$

Equation 4.1

$$P = \sigma_y.(h + l.\sin\theta).b$$

Equation 4.2

$$F_{insert} = -K_{insert}.2.\delta.cos\theta$$

Equation 4.3

$$K_{insert} = \frac{E_{insert}.h_{insert}.b}{l_{insert}}$$

Equation 4.4

From standard beam theory [104], the deflection δ of the walls is given in Equation 4.5, where E_s is the Young's modulus of the honeycomb constituent material and I is the second moment of area of the cell wall (for a wall of uniform thickness t, $I=bt^3/12$).

112

Honeycombs with Structured Core for Enhanced Damping

$$\delta = \frac{2.M.l^2}{12.E_s.I}$$

<div align="right">Equation 4.5</div>

Substituting *M* from Equation 4.1 into Equation 4.5, and rearranging the terms, the deflection δ is given from the geometric parameters and materials used in Equation 4.6.

$$\delta = \frac{P.sin\theta.l^3}{12.E_s.I + 2.K_{insert}.cos^2\theta}$$

<div align="right">Equation 4.6</div>

The strain of the honeycomb with its damping insert, ε_y, is given in Equation 4.7.

$$\varepsilon_y = \frac{y_{displacement}}{y_{length}} = \frac{\delta.sin\theta}{l.cos\theta}$$

<div align="right">Equation 4.7</div>

Substituting δ from Equation 4.6 into Equation 4.7, the strain ε_y is given from the geometric parameters and materials used in Equation 4.6.

$$\varepsilon_y = \frac{P.l^2.sin^2\theta}{cos\theta.(12.E_s.I + 2.K_{insert}.l^3.cos^2\theta)}$$

<div align="right">Equation 4.8</div>

Assuming a linear elastic deformation of the walls, i.e. small strain, the Young's modulus E_y of the structure can be derived from Hooke's law (see Equation 4.9). The first term in the expression of the Young's modulus depends only on the parameters of the honeycomb structure and corresponds to the expression found of the Young's modulus of the honeycomb cell without damping insert, $E_{y\ G\&A}$, as derived by Gibson and Ashby in [100] (see Equation 4.10).

Honeycombs with Structured Core for Enhanced Damping

$$E_y = \frac{\sigma_y}{\varepsilon_y} = \frac{12. E_s. I. cos\theta}{\left(\frac{h}{l} + sin\theta\right). sin^2\theta. l^3. b} + \frac{2. K_{insert}. cos^3\theta}{\left(\frac{h}{l} + sin\theta\right). sin^2\theta. b}$$

<div align="right">Equation 4.9</div>

$$E_{y\ G\&A} = \frac{12. E_s. I. cos\theta}{\left(\frac{h}{l} + sin\theta\right). sin^2\theta. l^3. b}$$

<div align="right">Equation 4.10</div>

The damping parameters of the honeycomb with its damping insert were calculated from the modal strain energy method [100] [102] [103]. This method approximates the loss factor of a structure as the sum of the ratio between the strain energy stored in each constituent material of the structure multiplied by its material loss factor over the total strain energy stored in the structure. The loss factor η of the structure derived from the MSE method is presented in Equation 4.11, where U_{tot} is the total strain energy of the structure (Equation 4.12), η_{insert} is the loss factor of the material of the damping insert, U_{insert} is the strain energy of the damping insert (Equation 4.13) and $U_{honeycomb}$ is the strain energy of the honeycomb (Equation 4.14).

$$\eta = \eta_{insert}. \frac{U_{insert}}{U_{tot}} + \eta_{honeycomb}. \frac{U_{honeycomb}}{U_{tot}}$$

<div align="right">Equation 4.11</div>

$$U_{tot} = \frac{1}{2}. E_y. \varepsilon_y{}^2. V_{cell}$$

<div align="right">Equation 4.12</div>

With:

$$V_{cell} = 4. l. cos\theta. (h + l. sin\theta). b$$

Honeycombs with Structured Core for Enhanced Damping

$$U_{insert} = \frac{1}{2} \cdot E_{insert} \cdot \varepsilon_{insert}{}^2 \cdot V_{insert}$$

With:

$$V_{insert} = l_{insert} \cdot h_{insert} \cdot b$$

$$\varepsilon_{insert} = \frac{2 \cdot \delta \cdot cos\theta}{l_{insert}}$$

$$U_{honeycomb} = U_{tot} - U_{insert}$$

The MSE method is applied in this study for static loadings. This is correct for frequency independent material properties such as most metals but not strictly for viscoelastic materials since they exhibit frequency-dependent material properties. In the particular case of this study, the MSE method is used to compare the damping properties provided by the introduction of a viscoelastic damping insert inside the void of a honeycomb cell, hence justifying its validity as a method for comparing the damping properties of honeycomb cells with different geometries of damping inserts.

The loss modulus E^*, the product of the loss factor η and the Young's modulus E of the structure are deduced from Equation 4.9 and Equation 4.11 (see Equation 4.15).

$$E_y{}^* = \eta \cdot E_y$$

4.2.1.2 Limiting condition of the insert

The load transferred to the ligament insert of a honeycomb cell loaded in tension compresses the ligament insert. As a result, the ligament insert will buckle if the

condition in Equation 4.16 is met [111], invalidating the equations derived in the previous section.

$$-F_{insert} > \frac{\pi^2 . E_{insert} . I_{insert}}{l_{insert}} \text{ with } I_{insert} = \frac{b . h_{insert}{}^3}{12}$$

Subtracting the expression of I_{insert}, Equation 4.3 and Equation 4.4 into Equation 4.16, a limiting condition on the thickness of the insert h_{insert} can be derived. The limiting condition of the thickness of the insert h_{insert} to avoid buckling is shown in Equation 4.17 after simplification.

$$h_{insert} > \sqrt{\frac{24 . l_{insert} . \varepsilon}{\pi^2}}$$

4.2.2 Finite Element Analysis of Honeycomb Structure with Damping Inserts

Mechanical and damping properties of regular honeycomb with damping inserts have been investigated with a finite element analysis using Ansys 13. Six models have been studied under different loading conditions.

4.2.2.1 Damping Insert Geometries

Geometries for damping inserts have been chosen to investigate the best locations of inserts for a regular honeycomb found in Chapter 3. The six geometries studied are represented in Figure 4.4. A regular honeycomb without insert (Figure 4.4a.) and one completely filled (Figure 4.4f.) with the damping material have been studied for comparison with the damping insert geometries studied. Figure 4.4b. shows a regular honeycomb with a horizontal ligament insert across the middle of the cell void; this location was found to be the most efficient for honeycombs loaded in in-plane tension/compression. Figure 4.4d. shows a honeycomb with a double cross ligament inside the cell void; this location was found to be the most efficient for

regular honeycombs loaded in in-plane shear. Figure 4.4c. shows a regular honeycomb cell with a single ligament insert across the diagonal of the cell; this location was thought to be an adaption of the horizontal ligament for in-plane shear loading. Figure 4.4e. shows a regular honeycomb unit cell with a star ligament configuration combining the best location of damping insert found for both in-plane tension/compression and shear loadings.

Honeycombs with Structured Core for Enhanced Damping

a.

b.

c.

d.

e.

f.
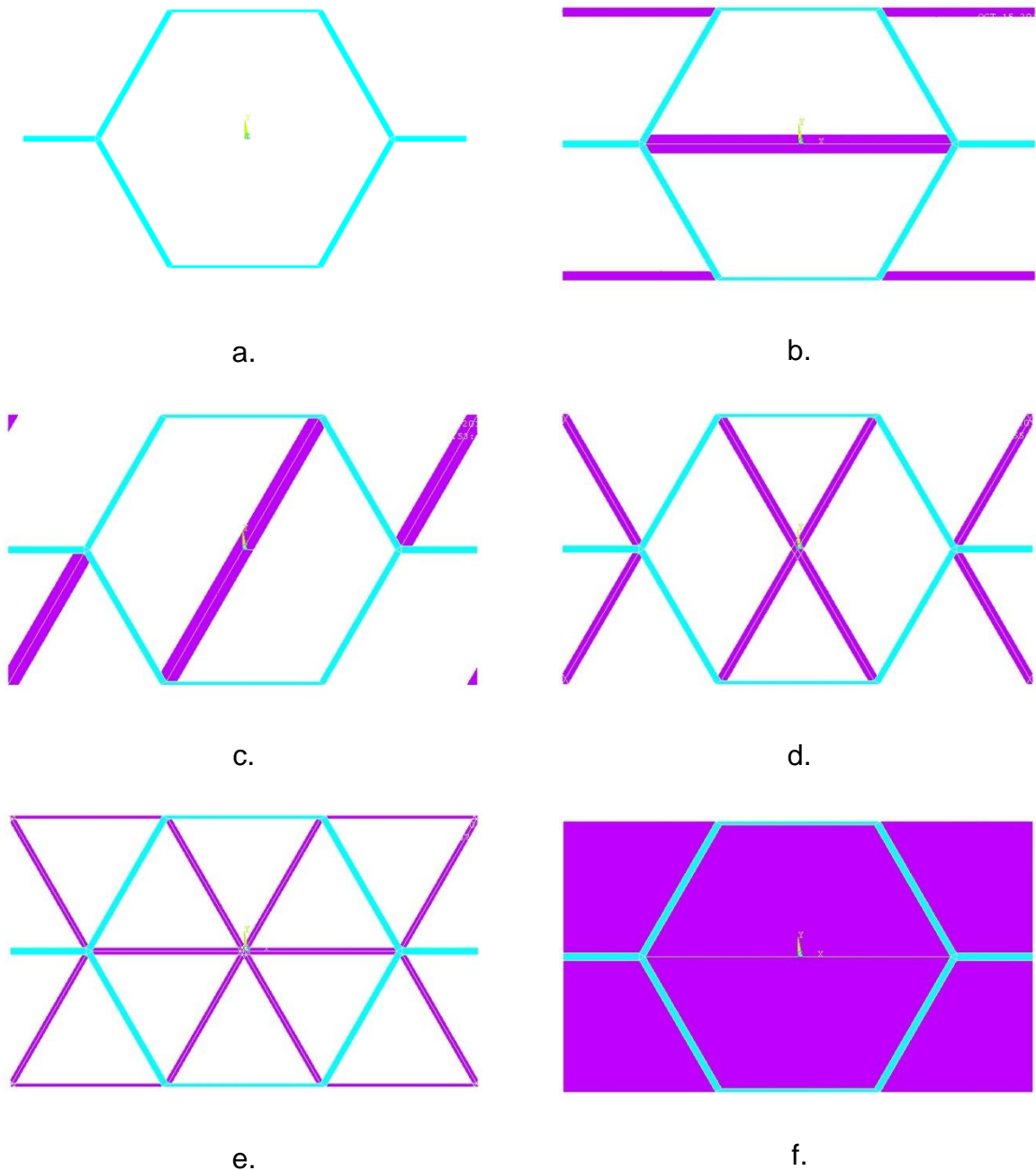
Figure 4.4: Honeycomb unit cells in blue with geometries of viscoelastic damping inserts in purple.

Honeycomb geometric parameters have been set as follows: $l = h = 1$ mm, $\theta = 30^{\circ}$ and $t = 0.0433$ mm for a honeycomb cell relative density, $\rho^* = 0.05$ (see Equation 4.18). Relative density of 0.05 matches with commonly used, '1/16 inch' honeycombs from HEXCEL [105].

Honeycombs with Structured Core for Enhanced Damping

$$\rho^* = \frac{t}{l} \cdot \frac{(\frac{h}{l} + 2)}{2.\cos\theta.(\frac{h}{l} + \sin\theta)}$$

<div align="right">Equation 4.18</div>

Table 4.1: HEXCEL Honeycomb Designation - 5052 Alloy Hexagonal Aluminium Honeycomb [105].

Cell Size [in]	Foil Gauge	Nominal Density [g/cc]	Relative Density
1/16	0.0007	0.104120012	0.038534423
1/16	0.001	0.147369863	0.05454103
1/16	0.0015	0.198628946	0.073511823

Each damping insert geometry has been studied from 5% to 95% filling of the honeycomb cell void by 5% increments. The volume occupied by the inserts $V_{ligament}$ is defined in Equation 4.19 for the ligament insert geometries (Figure 4.4b. and c.) without considering the overlap of the honeycomb structure. $h_{ligament}$ is the thickness of the ligament insert. Giving the geometry of the insert, $V_{ligament}$ was calculated as four times area A_1 and A_2, as shown in Figure 4.5. The volume of the double cross ligament was considered to be the one of two separate ligaments and the star ligament, three separate ligaments. This assumes that the overlapping of the ligaments in the middle of the cell was neglected. This assumption is valid for low filling of the honeycomb void (up to 20%). For higher filling, the volume was corrected manually using the exact volume computed from the FE software.

Honeycombs with Structured Core for Enhanced Damping
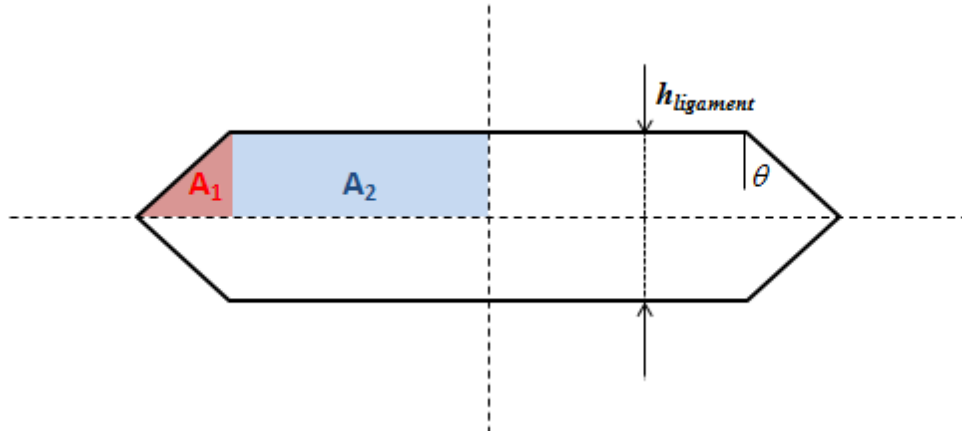
Figure 4.5: Ligament insert geometry subdivided in four sections of equal area A_1 and A_2.

$$V_{ligament} = \frac{h_{ligament}^2 \cdot \tan\theta}{2} + h_{ligament} \cdot (2.l.\sin\theta + h_{ligament} - h_{ligament} \cdot \tan\theta)$$

Equation 4.19

4.2.2.2 Loadings and Associated Boundary Conditions

In-plane tension/compression, and in-plane pure shear boundary conditions have been applied to the geometries studied. These loading conditions correspond to the noticeable deformations of honeycomb cells in a sandwich structure as highlighted in Chapter 2.

Boundary conditions associated to the in-plane tension/compression loading are shown in Figure 4.6. Nodes on the bottom edge of the unit cell were constrained in the y direction and nodes on the left edge were constrained in the x direction. Nodes on the right edge of the cell were constrained to remain parallel in the x direction. A displacement was applied to nodes of the top edge in the y direction, loading the cell at $\varepsilon_y = 0.1\%$ strain.

Honeycombs with Structured Core for Enhanced Damping
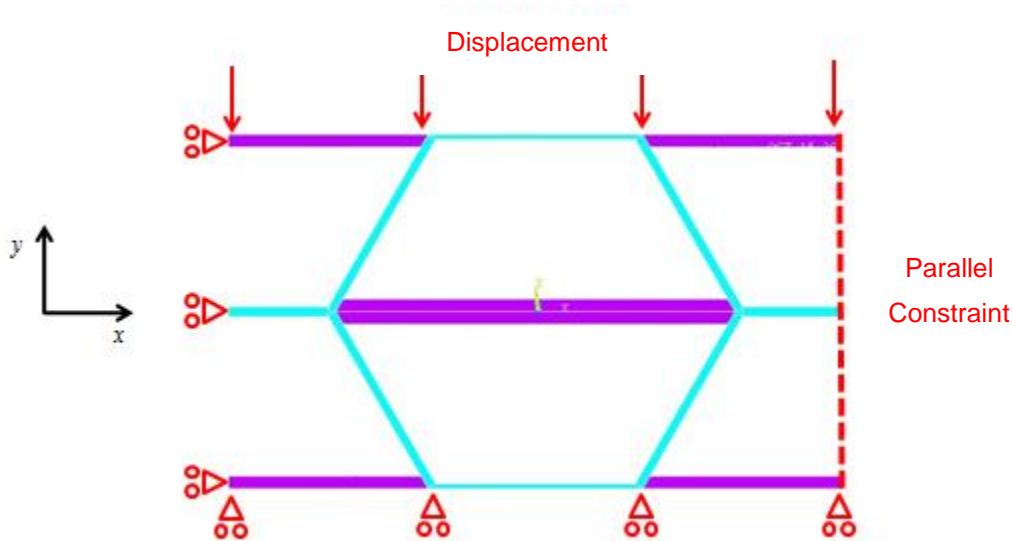
Figure 4.6: Loading and boundary conditions of a honeycomb unit cell with damping insert in simulating the compression of the cell along the *y* direction.

The in-plane tension/compression boundary conditions associated to the geometry representing the diagonal ligament across the cell (Figure 4.4c.) have not been applied to the unit cell but to a 9x9 cell array. This has been carefully chosen from a convergence study due to the discontinuity of the model of the unit cell, as highlighted in Figure 4.7.
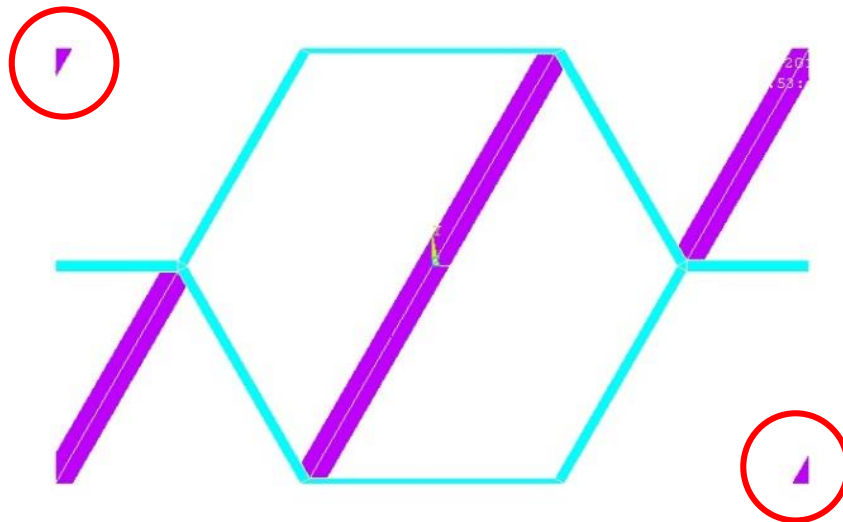
Figure 4.7: Honeycomb unit cell with a diagonal ligament insert. Discontinuity of the ligament insert for the type of unit cell chosen is highlighted within the red circles.

Honeycombs with Structured Core for Enhanced Damping

Boundary conditions associated to the in-plane shear loading were applied to a 15x15 cell array to satisfy periodicity and symmetry conditions of the centre cell of the panel, as shown in Figure 4.8. The size of the panel studied was chosen from a convergence study to avoid over-constraining the edge of the unit cell [106] [107]. Nodes on the bottom edge of the unit cell were constrained in the *x* direction and nodes on the left edge were constrained in the *y* direction. Displacement *dx* has been applied to nodes on the top edge in the *x* direction and displacement *dy* to nodes on the right edge in the *y* direction. Displacements *dx* and *dy* have been fixed to load the panel at γ_{xy} = 0.1% strain (see Equation 4.20 and Equation 4.21), with *nb_cell_x* and *nb_cell_y* the number of cells of the panel, respectively, in the *x* and *y* direction.
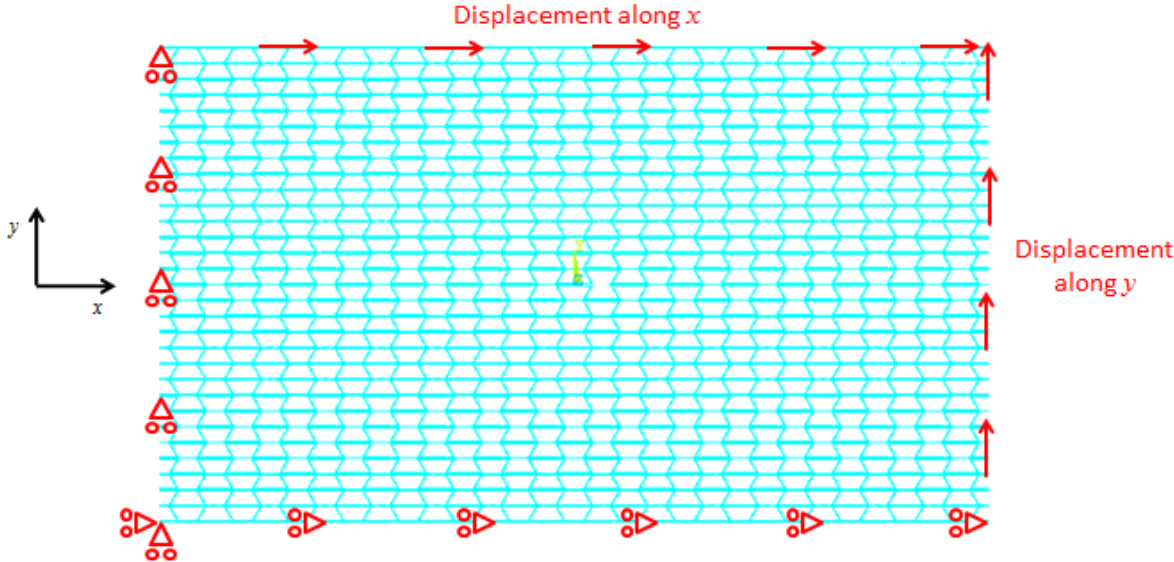
Figure 4.8: In-plane pure shear loading and boundary conditions of a honeycomb panel (15x15 cells) with ligament damping inserts.

$$dx = \gamma_{xy} . 2 . l . cos\theta . nb\_cell\_y$$

Equation 4.20

$$dy = \gamma_{xy} . 2 . (h + l . sin\theta) . nb\_cell\_x$$

Equation 4.21

Honeycombs with Structured Core for Enhanced Damping

Both in-plane axial and shear boundary conditions have been validated against analytical expressions of the Young's modulus, $E_{y\ G\&A}$, and shear modulus, $G_{xy\ G\&A}$, derived by Gibson and Ashby for a regular honeycomb (see Equation 1.3 and Equation 1.4) [2].

4.2.2.3 Elements Definition

The finite element mesh consists of 2D bilinear structural PLANE82 elements (plane strain formulation). Numbers of elements have been carefully chosen from a convergence study. Models with a damping insert filling 5% of the honeycomb cell void had a minimum of 3,000 elements (see Figure 4.9), and models with a damping insert filling 95% of the cell void numbered around 35,000 for a single unit cell.
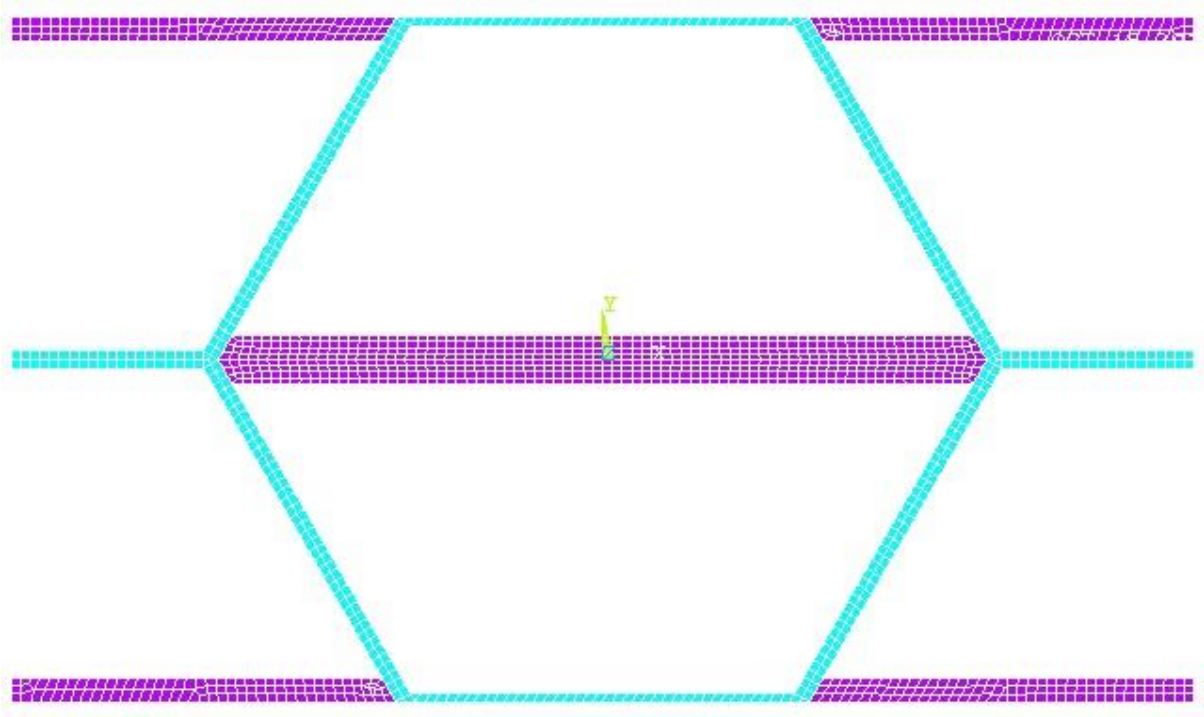
Figure 4.9: FE mesh of the honeycomb unit cell with a horizontal ligament damping insert filling 10% of the void space of the honeycomb.

4.2.2.4 Material Properties

Two material properties have been defined. The constituent material of the honeycomb has been modelled with aluminium properties, with a set of linear and

Honeycombs with Structured Core for Enhanced Damping

isotropic elastic constant (E_{al} = 70000 MPa, v_{al} = 0.3, pal = 2.7 g.cm^3 and η_{al} = 0.0001 [76]). The damping insert has been modelled with arbitrary material properties representing a viscoelastic material, with a set of linear and isotropic elastic constant (E_{visco} = 1MPa, v_{visco} = 0.45, ρ_{visco} = 1.25 g.cm3 and η_{visco} = 0.1 [108]).

The density of the honeycomb cell partially filled with viscoelastic material, ρ, is derived in Equation 4.22 where V_{al} is the volume of the constituent material of the honeycomb cell (aluminium), V_{cell} is the volume of the unit cell defined in Equation 4.12 and V_{visco} is the volume of the viscoelastic material forming the damping insert defined in Equation 4.19.

$$\rho = \frac{\rho_{al}.V_{al} + \rho_{visco}.V_{visco}}{V_{cell}}$$

Equation 4.22

4.2.2.5 FE Analysis

Mechanical and damping properties of the models and loadings described previously have been calculated using a linear static analysis with Ansys 13 [90]. The Young's modulus E_y and the shear modulus G_{xy} have been calculated in the centre cell of each model from, respectively, Equation 4.23 and Equation 4.24, where U_{total} is the total strain energy of all the elements in the centre cell, ε_y is the strain of the cell loaded axially, γ_{xy} is the shear strain of the cell loaded in pure shear and V_{cell} is the total volume of the cell.

$$E_y = \frac{2.U_{total}}{\varepsilon_y{}^2.V_{cell}}$$

Equation 4.23

$$G_{xy} = \frac{2.U_{total}}{\gamma_{xy}{}^2.V_{cell}}$$

Equation 4.24

Honeycombs with Structured Core for Enhanced Damping

Loss factors and loss moduli of the structure for both loading cases have been derived from Equation 4.11 based on the MSE method. The MSE method is applied in this study for static loadings. This is correct for frequency-independent material properties such as most metals but not for viscoelastic materials since they exhibit frequency-dependent material properties [108]. In the particular case of this study, the loading frequency of the viscoelastic material is imposed by the recipient honeycomb structure independently of the damping insert geometry. Therefore, the MSE method is valid for comparison of each damping insert's damping properties. This assumes that the loadings frequencies and the surrounding temperature of the damping insert are suitable for viscoelastic materials.

4.3 Results

4.3.1 Convergence Study

A convergence test is shown in Figure 4.10 for different sizes of aluminium regular honeycomb panels of relative density $\rho^* = 0.05$. The convergence study performed on the FE computed Young's Moduli E_y and G_{xy} normalised against their analytical expression $E_{y\_G\&A}$ and $G_{xy\_G\&A}$ from [2] (see Equation 1.3 and Equation 1.4). The FE computed Young's modulus, E_y, is constant for honeycomb panels of different sizes, whereas the FE computed shear modulus, G_{xy}, is 60% higher for a 3x3 cell panel.

Honeycombs with Structured Core for Enhanced Damping
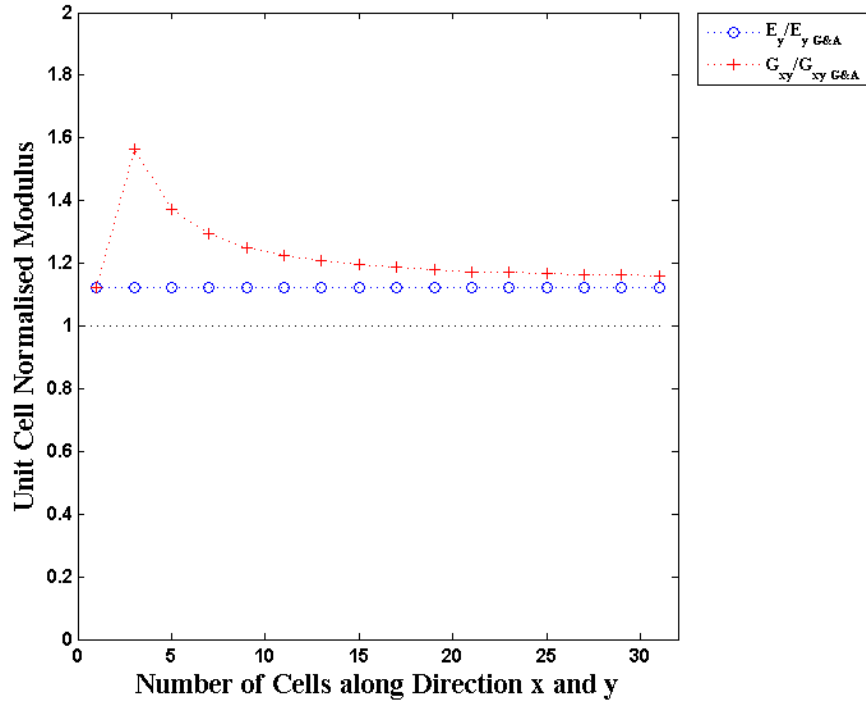
Figure 4.10: FE predicted unit cell Young's and shear moduli for different sizes of honeycomb panels normalised against their respective analytical expression from Gibson and Ashby [2].

Figure 4.11 shows the deformed shape of a regular aluminium honeycomb unit cell of relative density ρ^*= 0.05 (a.), a 3x3 honeycomb panel (b.) and a 9x9 honeycomb panel (c.) loaded in in-plane shear. The unit cell deformation appears to be consistent with the plane of symmetry of the geometry *(xOz* and *yOz)*. Horizontal walls of the honeycomb are deformed in bending as predicted in [2]. For larger arrays, the symmetry is broken where the boundary conditions have been applied, as shown in Figure 4.11 b. and Figure 4.11 c. As opposed to the rest of the model, the horizontal walls where the boundary conditions have been applied are not deformed in bending. Symmetry is recovered in the middle of the 9x9 honeycombs panel (further away from the application of the boundary conditions).

Honeycombs with Structured Core for Enhanced Damping
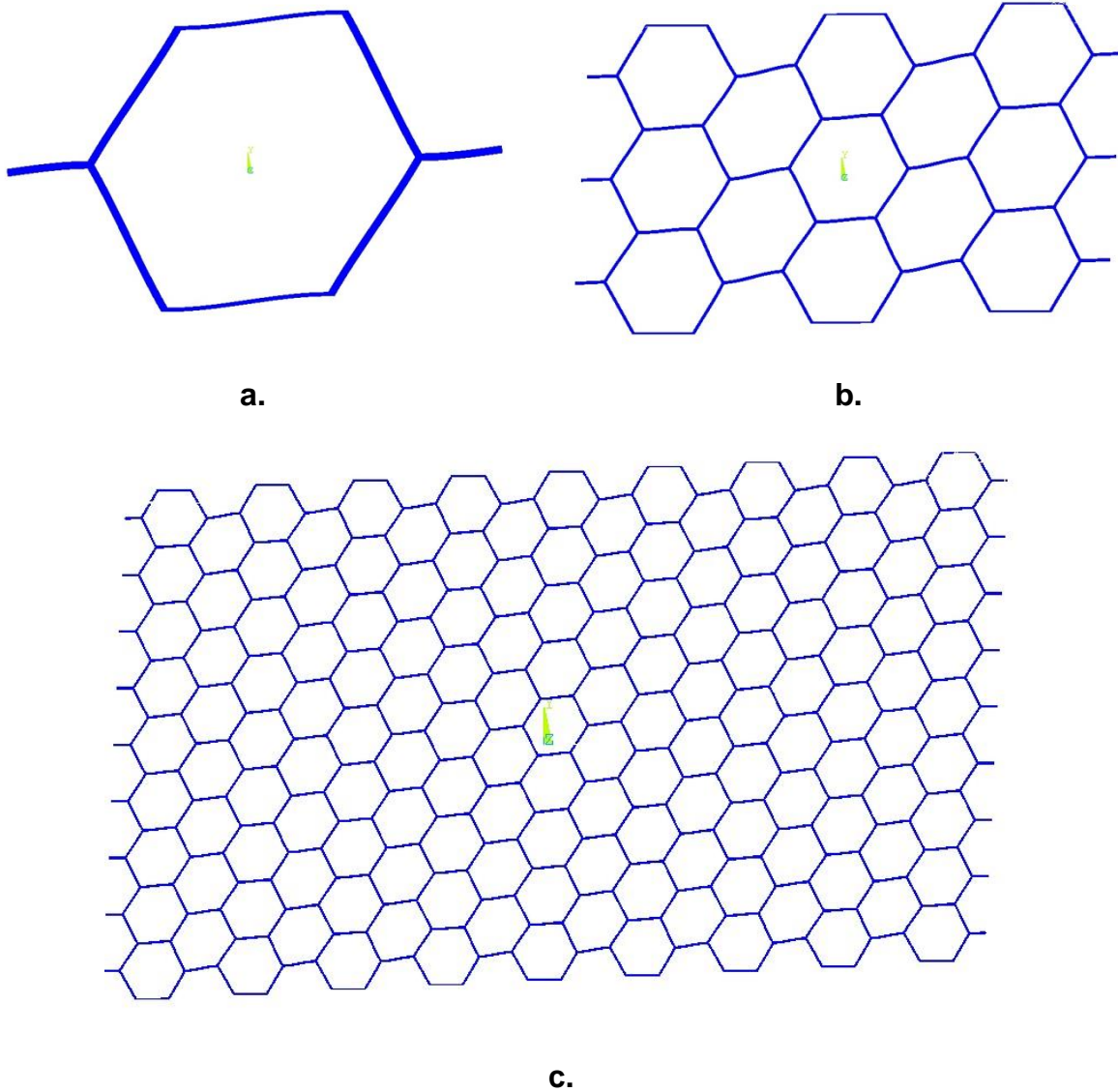
Figure 4.11: In-plane shear deformation of a honeycomb unit cell (a.), a 3x3 honeycomb cell array (b.), and a 9x9 honeycomb cell array (c.).

A convergence study has been performed on honeycomb panels with the four architectures of damping inserts occupying 10% of the honeycomb cell void to verify the consistency of the boundary conditions applied to the FE models. The strain energy stored in the viscoelastic material of the middle cell of the honeycomb panel (one of the parameters used to calculate structural modulus, loss factor and loss modulus of the cell with damping insert) is presented in Figure. The strain energy stored in the viscoelastic material is constant in in-plane axial loading independently

Honeycombs with Structured Core for Enhanced Damping

of the number of cells of the panel. For in-plane shear loading, convergence of the strain energy stored in the viscoelastic material is achieved for a 15x15 cell panel.

a.   b.
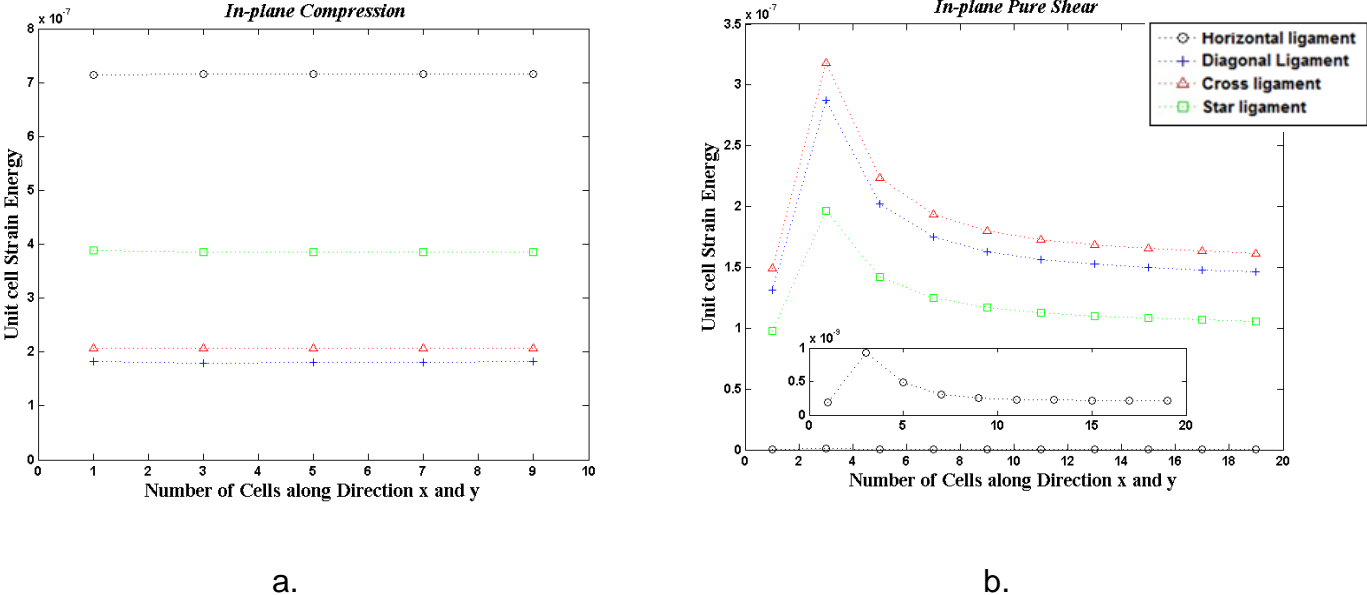
Figure 4.12: Strain energy (J) stored in the middle cell of different honeycomb panel sizes under in-plane compression (a.) and in-plane pure shear loading (b.).

4.3.2 In-plane Axial Damping Performance of Honeycomb with Viscoelastic Damping Inserts

The elastic equivalent Von Mises strain [90] of the viscoelastic insert geometries is illustrated in Figure 4.13 for a 10% filling of the void of a regular honeycomb unit cell and for a completely filled unit cell under a compression loading of 0.1% strain. The highest magnitude of strain forms a horizontal ligament across the completely filled cell. A higher magnitude of strain is achieved for the horizontal ligament geometry and the star ligament geometry compared to other geometries of damping inserts analysed.

Honeycombs with Structured Core for Enhanced Damping
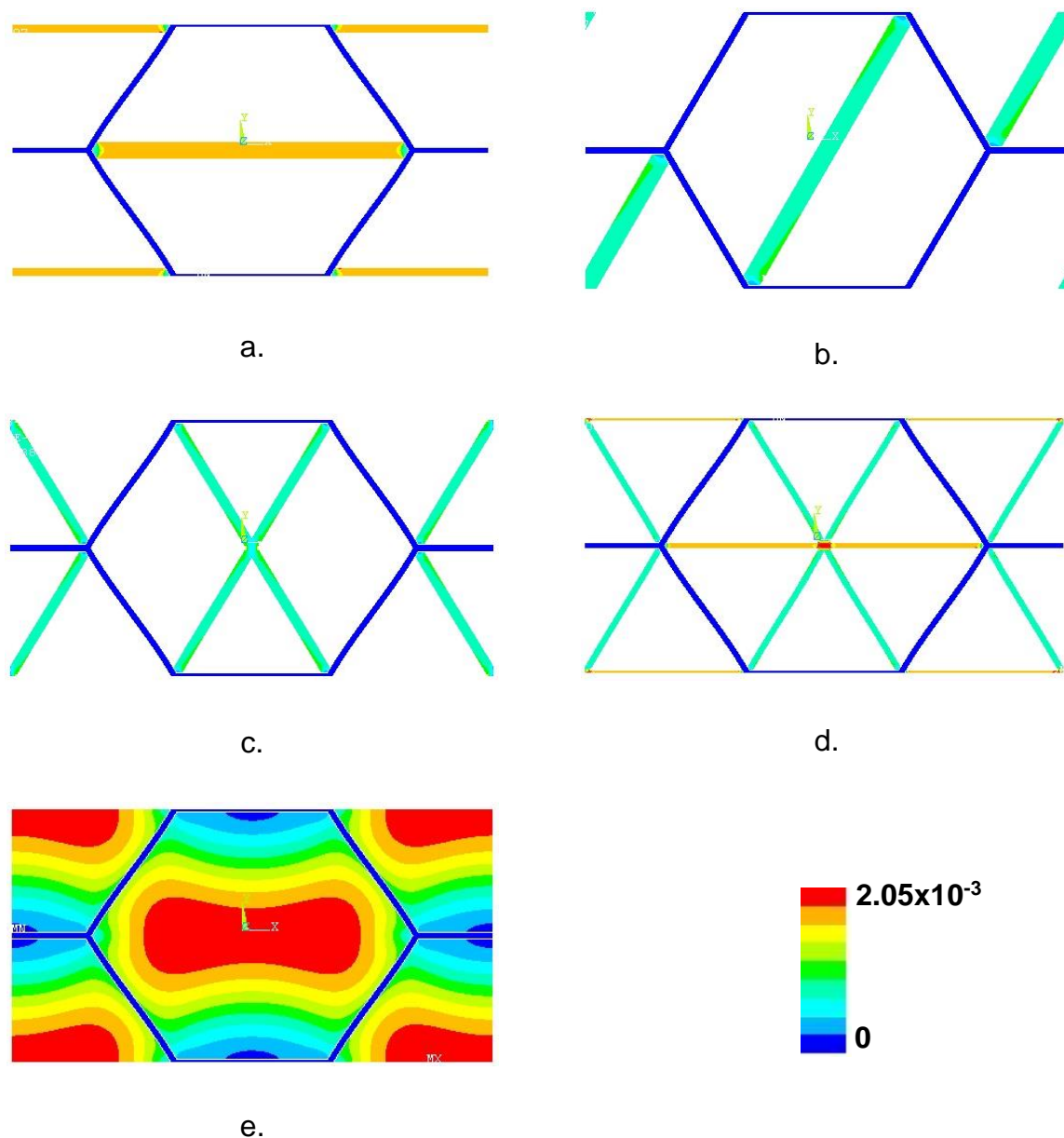
Figure 4.13: Elastic equivalent Von Mises strain of the different viscoelastic insert geometries filling 10% of the void of a regular honeycomb unit under compression loading of 0.1% strain.

The elastic equivalent Von Mises strain [90] of a regular honeycomb unit cell with a horizontal viscoelastic ligament filling, respectively, 10%, 30%, 50% and 70% of the honeycomb cell void and a completely filled honeycomb cell loaded at 0.1% strain in compression is presented in Figure 4.14. The magnitude of strain in the viscoelastic

Honeycombs with Structured Core for Enhanced Damping

ligament is high and almost uniform at 10% filling of the honeycomb void. A higher magnitude of strain is achieved locally for larger ligaments that are balanced with localised magnitude of strain lower than that achieved for the ligament filling 10% of the honeycomb cell void.

a.

b.

c.

d.

e.

2.05x10^{-3}

0
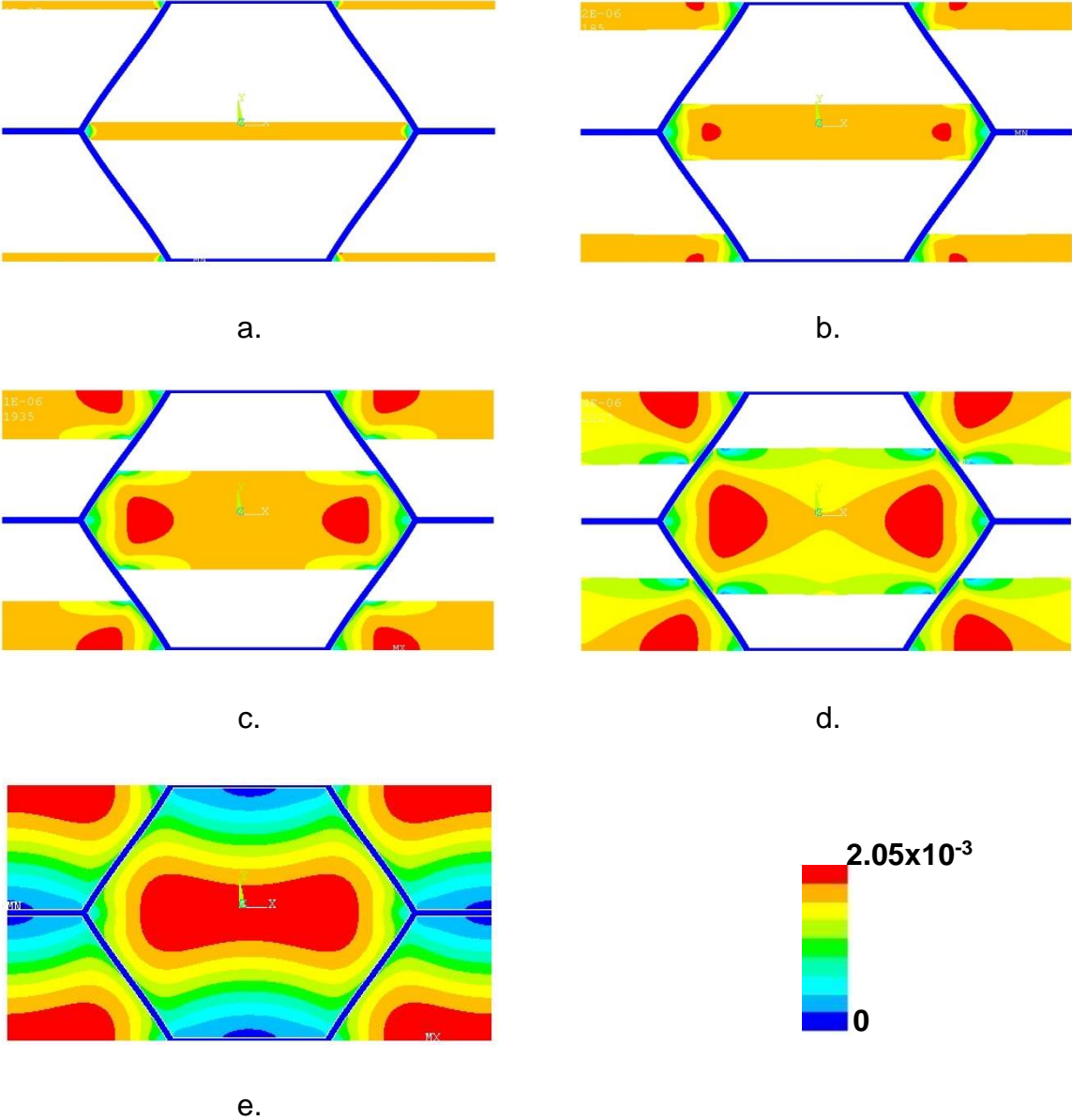
Figure 4.14: Elastic equivalent Von Mises strain of horizontal ligament damping inserts filling 10% (a.), 30% (b.), 50% (c.), 70% (d.) and 100% (e.) of the void of a honeycomb unit cell under compression loading of 0.1% strain.

Honeycombs with Structured Core for Enhanced Damping

The in-plane Young's modulus E_y is represented as a function of the volume fraction occupied by the viscoelastic damping insert over the void space of the honeycomb cell in Figure 4.15, i.e. the cell void filling with viscoelastic material for all viscoelastic insert geometries. The Young's modulus of a cell completely filled with viscoelastic material and a honeycomb cell without damping insert are also represented in Figure 4.15. The analytic expression of the in-plane Young's modulus of the honeycomb cell with a horizontal ligament geometry derived in Equation 4.9 is superposed to the FE results. The Young's modulus increases with the filling of the cell, from the Young's modulus of the empty cell (14.69 MPa), i.e. an aluminium honeycomb, to the magnitude reached with a completely filled cell (16.65 MPa). Between the viscoelastic insert geometries analysed, the Young's modulus magnitude varies less than 10% for a given cell filling; among those, the horizontal ligament insert exhibits the highest magnitude. The analytical expression of the Young's modulus of the honeycomb cell with a horizontal ligament is of the same magnitude than the FE computed Young's modulus and varies linearly with the cell void filling. For cell void filling below 55% the Young's modulus is slightly underestimated analytically (1 MPa for 5% cell filling), whereas above 55% cell void it is slightly overestimated (1.7 MPa for 95% filling).

Honeycombs with Structured Core for Enhanced Damping
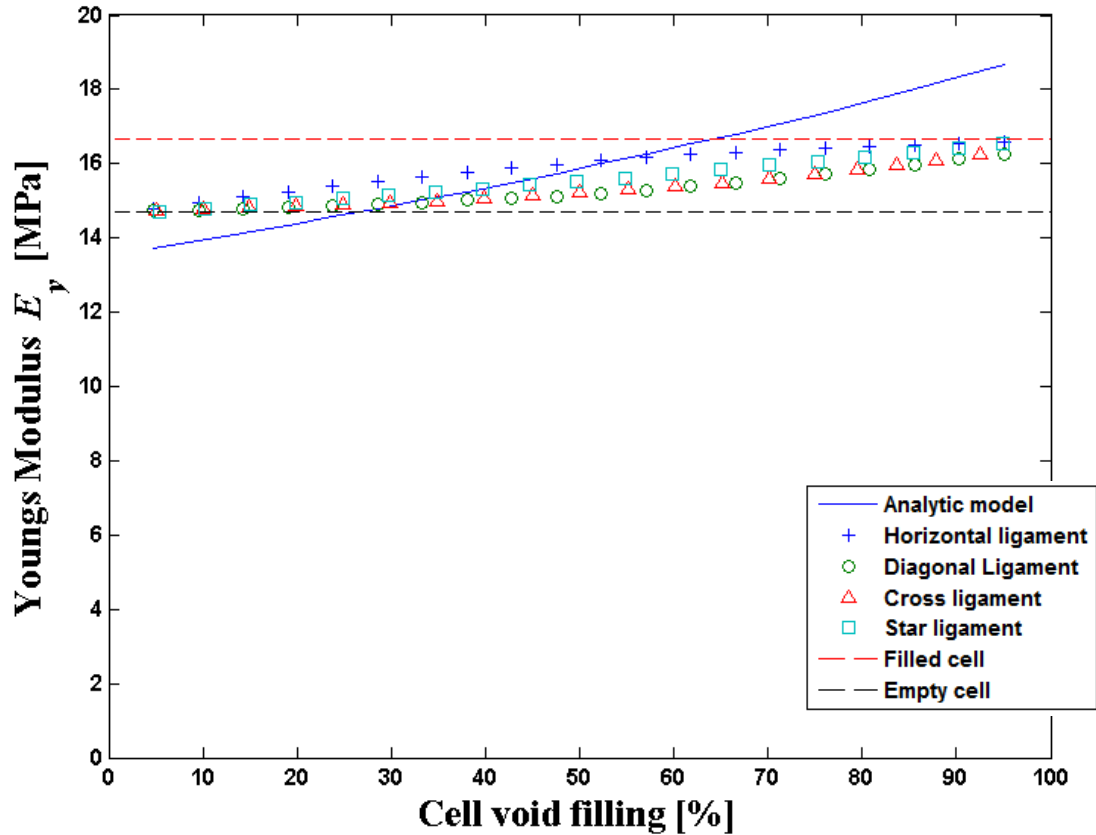
Figure 4.15: Analytical and FE computed Young's modulus E_y of a honeycomb cell of relative density $\rho^* = 0.05$ with different geometries of ligament damping inserts represented in function of the cell void filling of the damping insert.

The loss factor η derived from the MSE method under in-plane compressive strain of 0.1% of the honeycomb unit cell, for all viscoelastic insert geometries, a completely filled and an empty honeycomb cell is represented in Figure 4.16 as a function of the filling of the honeycomb cell void. The analytic expression of the loss factor η of the honeycomb cell with a horizontal ligament geometry is derived in Equation 4.11. Equation 4.9 is superposed to the FE results. The loss factor increases with the filling of the cell, from the magnitude of the empty cell (1e-4), i.e. a pure aluminium honeycomb, to the magnitude reached with a completely filled cell (1.18e-2). Between the viscoelastic insert geometries analysed, the loss factor magnitude varies largely for a given cell filling; among those, the horizontal ligament

Honeycombs with Structured Core for Enhanced Damping

insert exhibits the highest magnitude and the diagonal ligament insert the lowest. The analytical expression of the loss factor of the honeycomb cell with a horizontal ligament matches well the FE predictions for cell void filling up to 35%. Above 35% cell void filling, the analytical expression of the loss factor overestimates the FE predictions.
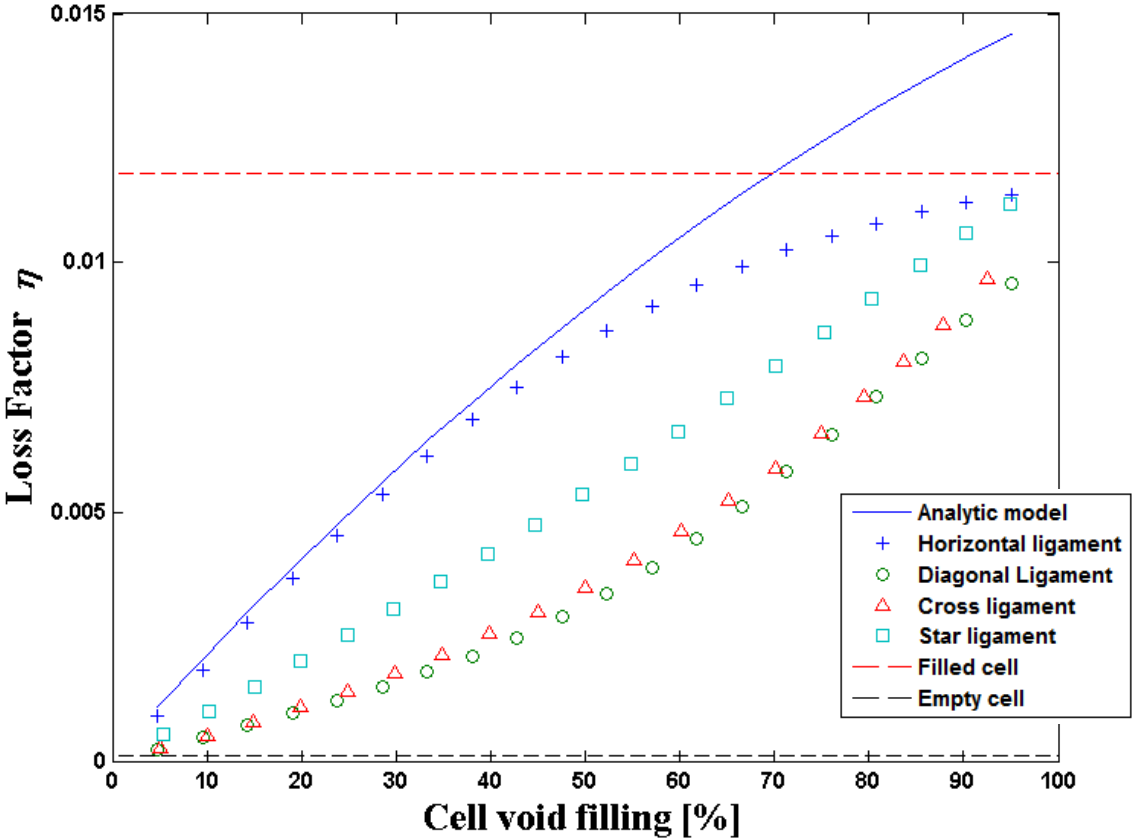
Figure 4.16: Analytical and FE computed loss factor η of a honeycomb cell of relative density ρ^*= 0.05 with different geometries of ligament damping inserts represented in function of the cell void filling of the damping insert.

The in-plane loss modulus E_y^* for all viscoelastic insert geometries, a completely filled and an empty honeycomb cell, is represented in Figure 4.17 as a function of the filling of the honeycomb cell void. The analytic expression of the in-plane loss modulus E_y^* of the honeycomb cell with a horizontal ligament geometry derived in

Honeycombs with Structured Core for Enhanced Damping

Equation 4.15 is superposed to the FE results. The loss modulus follows the same trends described for the loss factor with the horizontal ligament exhibiting the highest loss modulus for a given cell filling. The analytical expression of the loss modulus of the honeycomb cell with a horizontal ligament matches well the FE predictions for cell void filling up to 50%. Above 50% cell void filling, the analytical expression of the loss factor overestimates the FE predictions.
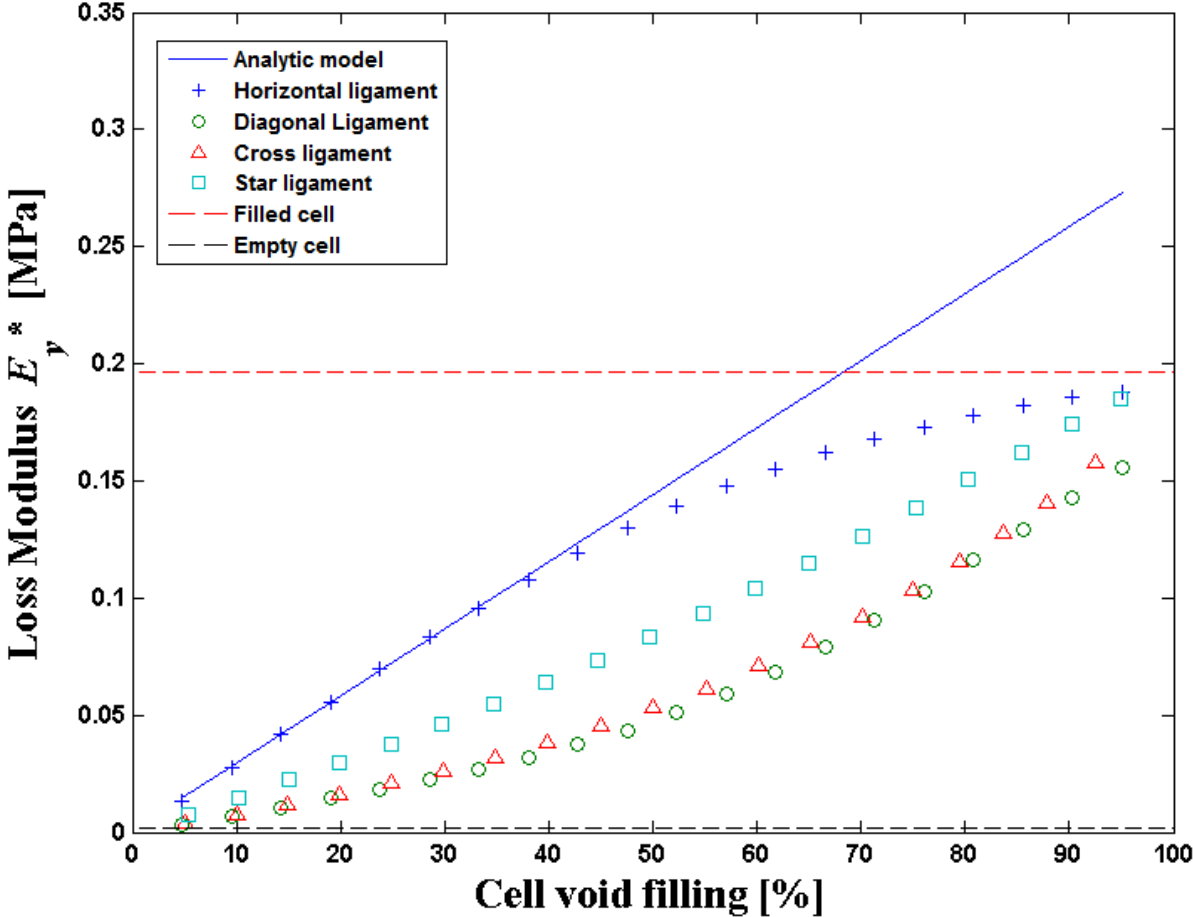
Figure 4.17: Analytical and FE computed loss modulus E_y^* of a honeycomb cell of relative density $\rho^* = 0.05$ with different geometries of ligament damping inserts represented in function of the cell void filling of the damping insert.

The in-plane density-specific loss modulus E_y^*/ρ for all viscoelastic insert geometries, a completely filled and an empty honeycomb cell is represented in

Honeycombs with Structured Core for Enhanced Damping

Figure 4.18 as a function of the filling of the honeycomb cell void. Except for the horizontal ligament insert, the density-specific loss modulus increases with the filling of the cell, from the magnitude of the empty cell to the magnitude of the completely filled cell. The horizontal ligament insert exhibits higher density-specific modulus from 20% filling of the cell. The highest magnitude is reached at 45% filling of the cell. The density-specific loss modulus decreases progressively to the magnitude of the cell completely filled with viscoelastic material.
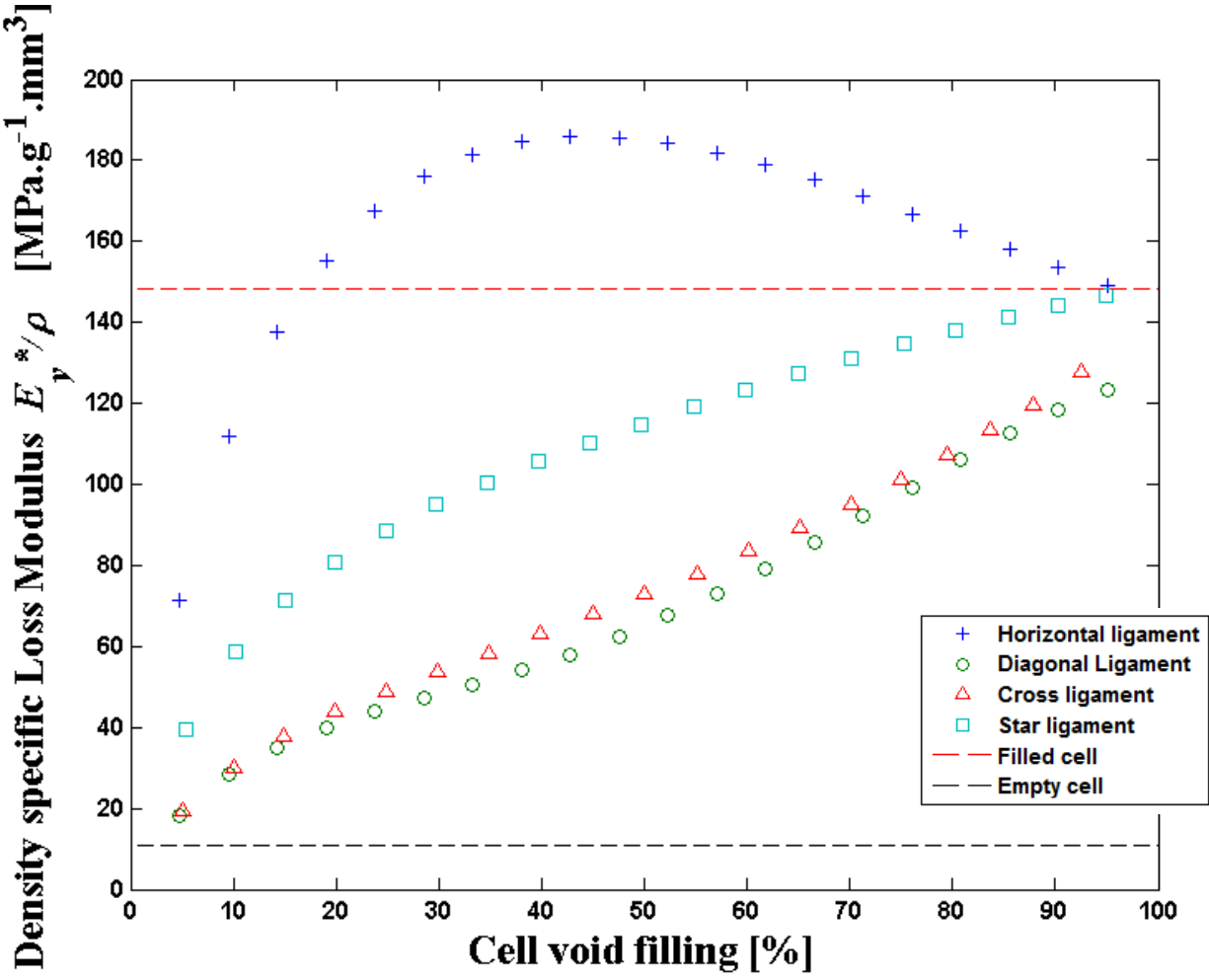
Figure 4.18: FE computed density-specific loss modulus E_y^*/ρ of a honeycomb cell of relative density $\rho^* = 0.05$ with different geometries of ligament damping inserts represented in function of the cell void filling of the damping insert.

Honeycombs with Structured Core for Enhanced Damping

The density ρ of the honeycomb as a function of the cell void filling with viscoelastic material is illustrated in Figure 4.18. The density varies linearly with the percentage of cell filling from 1.90e^{-4} g/mm^3 for a filling of 5% to 1.3e^{-3} for a filling of 95%.
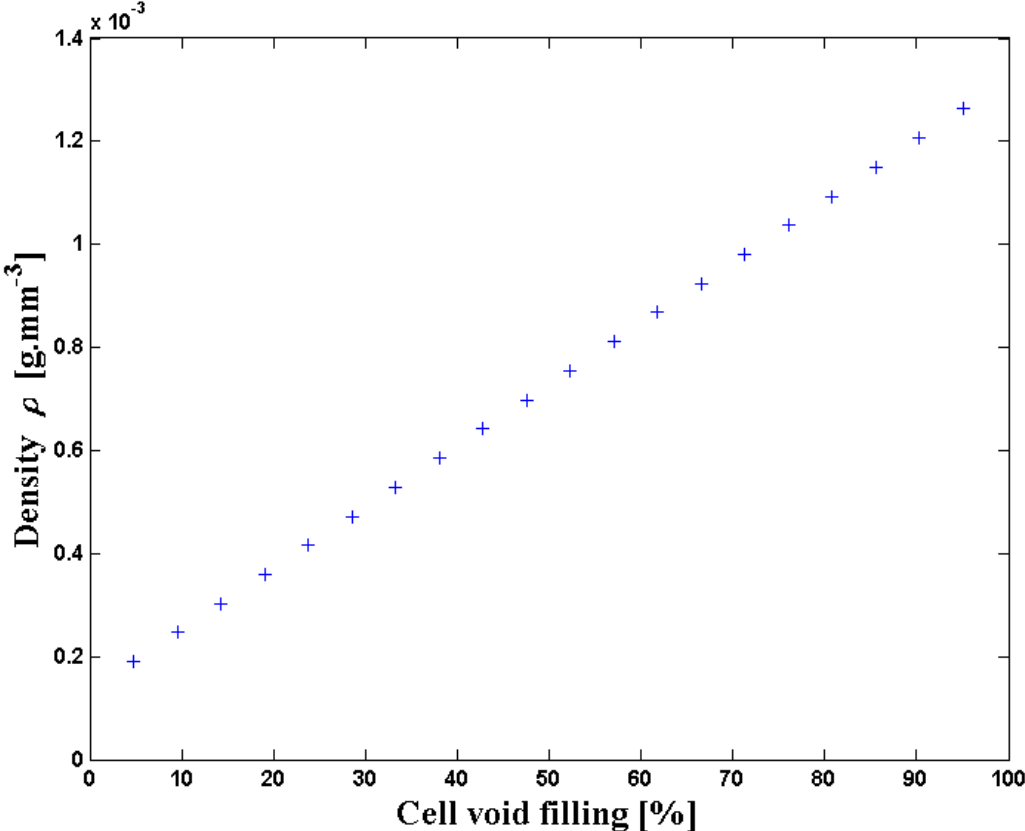
Figure 4.19: Density ρ of a honeycomb cell of relative density ρ^*= 0.05 in function of the cell void filling with viscoelastic material.

4.3.3 In-plane Shear Damping Performance of Honeycomb with Viscoelastic Damping Inserts

The elastic equivalent Von Mises strain [90] of the viscoelastic insert geometries is illustrated in Figure 4.20 for a 10% filling of the void of a regular honeycomb unit cell and for a completely filled unit cell under in-plane shear loading at 0.1% strain. The highest magnitude of strain forms a vertical ligament across the middle section of the completely filled cell. A higher magnitude of strain is achieved for insert geometries with diagonal ligament inserts across the cell void. As shown in Figure

136

Honeycombs with Structured Core for Enhanced Damping

4.20 a. and Figure 4.20 c., the strain in the horizontal ligament insert is negligible for in-plane shear loading.

a.

b.

c.

d.

e.
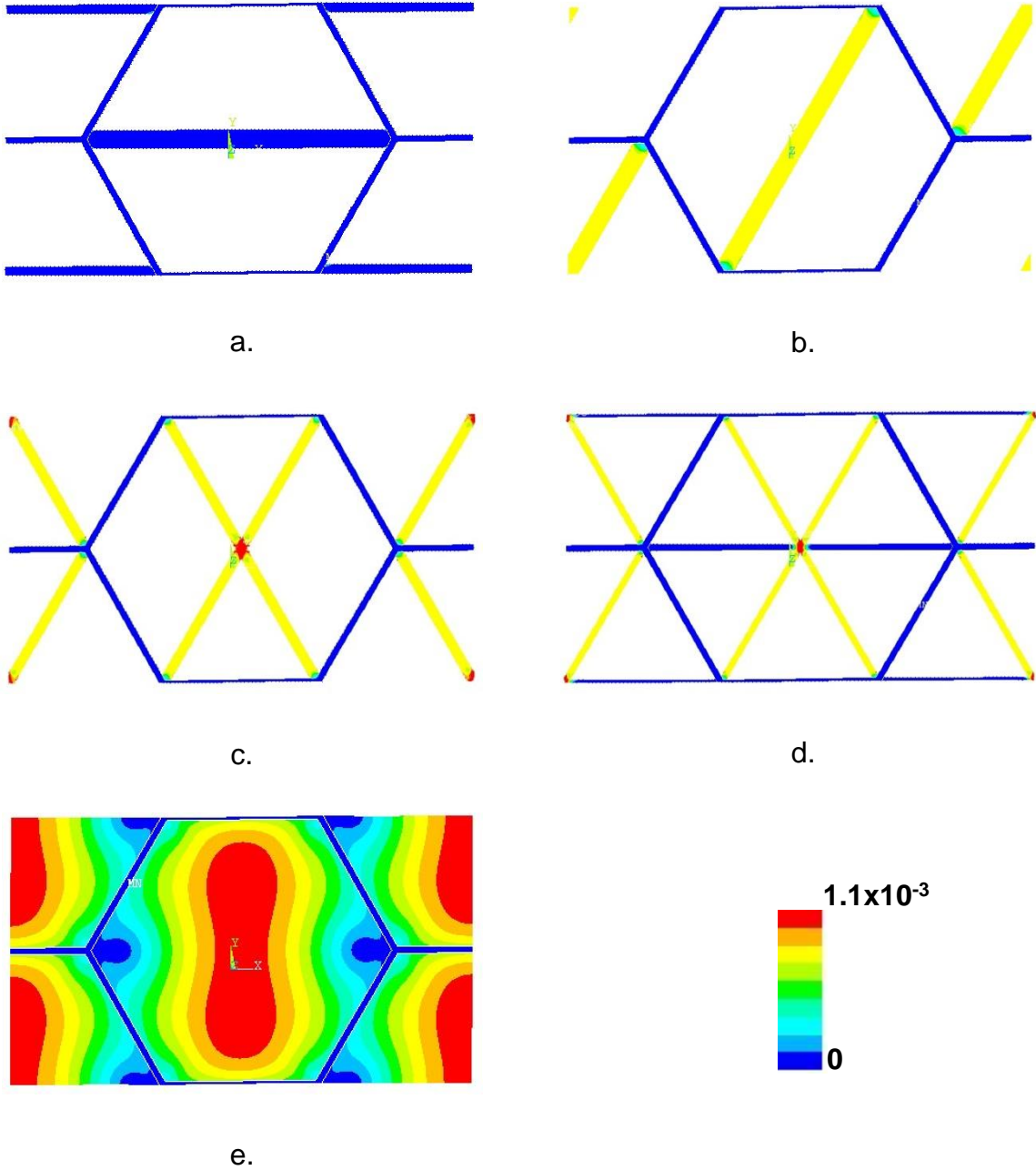
Figure 4.20: Elastic equivalent Von Mises strain of the different viscoelastic insert geometries filling 10% of the void of a regular honeycomb unit cell under in-plane pure shear loading of 0.1% strain.

Honeycombs with Structured Core for Enhanced Damping

The in-plane density-specific loss modulus, Gxy^*/ρ, for all viscoelastic insert geometries, a completely filled and an empty honeycomb cell is represented in Figure 4.21 as a function of the void filling percentage with viscoelastic material of the honeycomb unit cell. Except for the cross ligament insert, the density-specific loss modulus of all ligament inserts is lower than the magnitude reach of the completely filled cell. The cross ligament insert exhibits a higher density-specific modulus from 35% filling of the cell; the highest magnitude is reached at 75% filling of the cell and then decreases to the magnitude of the cell completely filled with viscoelastic material. The diagonal ligament increases within 10% of the density-specific modulus of the completely filled cell from 35% filling of the cell voids; its magnitude remains almost constant for a higher percentage of filling. The density-specific loss modulus of the star ligament increases progressively to the magnitude of the completely filled cell. The density-specific loss modulus of the horizontal ligament geometry is lower than that of a pure aluminium honeycomb for a filling up to 35%, then it increases to 75% of the density-specific loss modulus of the completely filled cell at 95% filling of the honeycomb cell void.

Honeycombs with Structured Core for Enhanced Damping
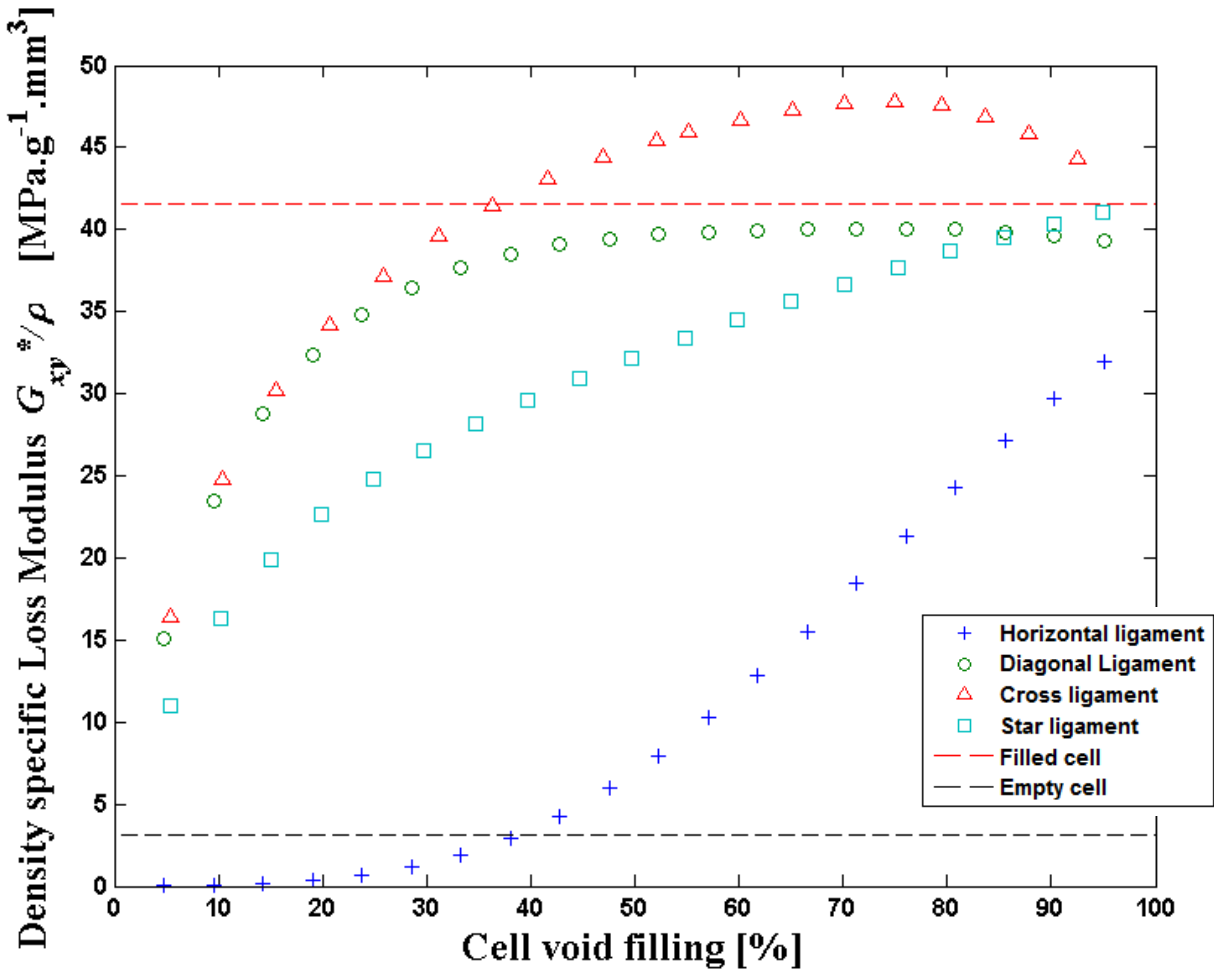
Figure 4.21: FE computed density-specific loss modulus *Gxy*/ρ* of a honeycomb cell of relative density ρ*= 0.05 with different geometries of ligament damping inserts represented in function of the cell void filling of the damping insert.

4.4 Discussion

4.4.1 Boundary Conditions

The consistency of the boundary conditions applied to the FE models representing a honeycomb unit cell have been verified by comparing the FE computed moduli of the honeycomb cell for both in-plane axial and shear loading with their respective analytical expression derived by Gibson and Ashby [2]. The boundary conditions applied on the edge of the honeycomb unit cells are consistent for in-plane axial loading but not for in-plane shear loading. The FE computed shear modulus is 60%

higher than the predicted shear modulus by Gibson and Ashby when the boundary conditions are applied to the edge of a 3x3 cell panel and converge to the predicted shear modulus for larger panels (see Figure 4.10). This characteristic has been observed in [106], particularly for shear loading, and is the consequence of over-constraining boundary conditions. The strain energy in the viscoelastic material follows the same pattern described for Young's and shear moduli (see Figure 4.12). As a result, the boundary conditions have been applied to a unit cell model for in-plane axial loading and to a 9x9 cell panel for in-plane shear loading.

The converged magnitude of the FE moduli in both in-plane axial and shear is slightly higher than its predicted magnitude from the expression derived by Gibson and Ashby (< 10%) (see Figure 4.10). The expressions derived by Gibson and Ashby assume only bending deformation of the cell walls of the honeycomb cell, which is valid for honeycombs with slender walls (t/l<<1) [2]. Stretching and shear deformation of the walls of the honeycomb are not considered in their expressions, explaining the differences with the FE computed moduli.

4.4.2 In-plane Axial Damping Performance of Honeycomb with Viscoelastic Damping Inserts

The mechanical and loss properties of honeycombs progressively filled with viscoelastic material have been described in Figure 4.15 to Figure 4.17 for all geometries of inserts. The geometry with the honeycomb cell completely filled with viscoelastic material exhibits higher modulus, loss factor and loss modulus and the geometry without viscoelastic material exhibits the minimum ones. The viscoelastic material inside the completely filled cell increases the stiffness of the cell and its loss properties due to its high loss properties. For the partially filled cell, the mechanical and loss properties vary from those of a pure aluminium cell for low filling of the void and converge progressively to the properties of the completely filled cell for higher filling of the honeycomb cell void. The convergence rate to reach the properties of the completely filled cell is dependent on the damping ligament geometry, as highlighted in Figure 4.15 to Figure 4.17. The horizontal ligament geometry exhibits higher mechanical and damping properties than the star ligament geometry, which

Honeycombs with Structured Core for Enhanced Damping

exhibits higher properties than the cross and diagonal ligament geometries for the same percentage of filling of the honeycomb cell void. This is caused by the location of the damping ligament insert inside the honeycomb geometry. As highlighted in Figure 4.13, the Von Mises strain is higher in the horizontal ligament geometry than in the diagonal ligament geometry. Since the horizontal ligament insert is loaded at higher strain, it provides higher resistance than the other insert geometries upon axial loading, therefore exhibiting higher mechanical properties. Since the damping properties are dependent on the strain in the viscoelastic material, the horizontal ligament insert also exhibits higher damping properties. The Von Mises strain is higher in the horizontal ligament insert because of the cell geometry. The section of a regular honeycomb unit cell is characterised by parameters h, l, t and θ, and forms a rectangular section of length $2.(h+l.sin(\theta))$ along its horizontal axis (x) and height $2.l.cos(\theta)$ along its vertical axis (y) (see Figure 4.1). Since a regular honeycomb cell exhibits a Poisson ratio of one, the horizontal displacement of the cell is larger than the vertical displacement upon in-plane axial loading. Therefore, the horizontal ligament is loaded at higher strain (see ε_{insert} in Equation 4.13), because the relative displacement of opposite walls of the unit cell is higher for horizontal walls than for diagonal walls. This has been discussed in further detail in the previous chapter.

Correlation with the analytical model of the horizontal insert derived in the methodology correlates well with the FE results for filling of the cell void below 60%. The Young's modulus is slightly underestimated in the analytical model since it accounts only for the bending deformation of the honeycomb cell walls. Correlation for filling higher than 60% is limited because of the assumptions made in the analytical model. The length of the viscoelastic ligament l_{insert} is assumed to be the distance between the two opposite horizontal walls of the honeycomb unit cell (see Figure 4.2). Since the l walls of the honeycomb form an angle θ with the vertical axis, the effective length of the horizontal insert varies with the percentage of filling of the cell, which is not accounted for in the analytical model. Furthermore, the horizontal ligament is squeezed between the two l walls of the honeycomb cell, which is not

Honeycombs with Structured Core for Enhanced Damping

accounted for in the analytical model and is not negligible at high percentages of filling of the cell (see Figure 4.14).

Since the enhancement of the mechanical and damping properties implies an increase of the total weight of the honeycomb unit cell caused by the additional filling with viscoelastic material, the density-specific loss modulus of honeycombs loaded axially with different ligament insert geometries have been compared in Figure 4.18. A honeycomb with a horizontal ligament insert filling 40% of its void exhibits the highest density-specific loss modulus, 26.7% higher than the honeycomb cell completely filled with viscoelastic material, which exhibits the higher loss modulus. The density-specific loss modulus is higher than that of the honeycomb completely filled with viscoelastic material from a filling of 20% to 100% of the honeycomb cell void. As highlighted previously, the loss modulus of the ligament insert converges from the value of the loss modulus of the empty cell to that of the cell completely filled with viscoelastic material. Low filling of the cell void exhibits small increases of the Young's modulus, loss factor and loss modulus. Despite the smaller density, which varies linearly with the filling of the cell as shown in Figure 4.19, the additional damping provided by the added material is not enough to outweigh the added damping of the completely filled cell. Other geometries of inserts, star, diagonal and cross ligaments exhibit higher density-specific loss modulus compared to the empty cell but lower compared to the completely filled cell. This is because these geometries of damping inserts have diagonal ligament inserts across the cell void and are not effective under axial loading, as explained previously.

4.4.3 In-plane Shear Damping Performance of Honeycomb with Viscoelastic Damping Inserts

The mechanical and damping properties of honeycombs with damping insert loaded in shear are also dependent on the insert geometry. The horizontal ligament performs better in axial loading than the diagonal ligament, as discussed previously. For in-plane shear loading, the diagonal ligament performs better than the horizontal ligament, as shown in Figure 4.21. A honeycomb with a cross ligament insert (two diagonal ligaments) filling 75% of its void exhibits the highest density-specific loss

Honeycombs with Structured Core for Enhanced Damping

modulus, 16% higher than the honeycomb cell completely filled with viscoelastic material. The density-specific loss modulus is higher than that of the honeycomb completely filled with viscoelastic material from a filling of 35% to 100% of the honeycomb cell void. The density-specific loss modulus of the single diagonal ligament geometry remains within 10% of the difference of that of the completely filled honeycomb from 35% filling of the honeycomb cell void. The star ligament reaches 10% of the density-specific loss modulus of the completely filled cell at 85% filling of the cell void. The horizontal ligament geometry has a lower density-specific loss modulus than the empty cell for a filling up to 35% and then increases to 75% of the density-specific loss modulus of the completely filled cell at 95% filling. Von Mises strain plots of the honeycombs with different damping inserts in Figure 4.20 shows that diagonal ligament inserts are loaded at much higher strains than horizontal ligaments. This is because the relative displacement of the diagonal opposite walls across the middle of the cell is higher than that between the horizontal walls for in-plane shear, as opposed to in-plane axial loading (Chapter 3). This has been discussed in further detail in the previous chapter. The Von Mises strain plot of the horizontal ligament geometry shows that it is barely loaded under in-plane shear loading. This is the reason why the density-specific loss modulus of the horizontal insert geometry is lower than the cell with no damping insert for filling up to 35%. The added material is not loaded sufficiently to provide efficient damping on a density basis.

4.5 Conclusion

The geometry of damping inserts for use inside a regular honeycomb cell void have been derived from Chapter 3 for best use of the damping capacity of the damping material upon loading. These geometries consist of a horizontal ligament insert across the cell void, a diagonal ligament insert, a cross ligament insert and a star ligament insert.

The density-specific damping capability of each insert has been compared to an aluminium regular honeycomb cell and a cell completely filled with damping material; a viscoelastic material in this case.

143

The density-specific damping capability of each insert has been shown to be dependent on both the geometry of the insert and the loading of the cell. Partial filling of the honeycomb cell with damping insert exhibited the best density-specific damping capability compared to honeycomb cells without damping insert or honeycomb cells completely filled with a viscoelastic material.

Under in-plane axial loading the horizontal ligament insert performs best and gives a 26.7% increase of the density-specific loss modulus of the honeycomb compared to a completely filled honeycomb cell. Under in-plane shear loading the cross ligament insert performs best and gives a 16% increase of the density-specific loss modulus of the honeycomb compared to a completely filled honeycomb cell.

Honeycombs with Structured Core for Enhanced Damping

Chapter 5. Shear Lap Joint Damping Insert

5.1   Introduction

The use of viscoelastic material for enhanced damping properties in a structure is often applied as a free layer treatment or a constrained layer treatment. In a free layer treatment, the damping material is sprayed or bonded to the base structure. In constrained layer damping treatments, the damping material is sandwiched between the base structure and a constraining layer. Under bending loading, the damping material in the free layer treatment deforms primarily in extension/compression in planes parallel to the base structure whereas, in the constrained layer treatment, the damping material deforms in shear. Constrained layer damping has shown to be more effective than free layer damping since the damping material is loaded at higher strain and, therefore, dissipates more energy [4].

The viscoelastic damping inserts presented in the previous chapter have been shown to increase the damping properties of the honeycomb cell. The damping loss provided by the viscoelastic material has been shown to be dependent on the insert geometry and the nature of loading. This is because the honeycomb host structure loads the insert in extension/compression; leading to increased energy dissipation. The damping characteristics of the viscoelastic damping insert can, therefore, be compared to the damping characteristics of a free layer coating of viscoelastic material in a structure. As mentioned previously, constrained layer damping has been shown to be a more effective method to implement damping in structures than free layer damping. The objective of this chapter is to analyse shear lap joint (SLJ) damping inserts for honeycomb structures and quantify their density-specific properties.

Geometries of SLJ inserts are presented based on the optimum location for damping inserts found in Chapter 3. Analytical expressions and FE analysis have been used to quantify the mechanical and damping properties of the different geometries of damping inserts studied in this chapter. The loss modulus, product of the structural modulus and the loss factor of a structure are the figures of merit for composite

Honeycombs with Structured Core for Enhanced Damping

material using viscoelastic material [86]. The damping properties of honeycomb with damping inserts have been quantified through static analyses using the MSE method [100] [102] [103].

5.2 Methods

5.2.1 Shear Lap Joint Damping Insert Concept

The geometry of SLJ damping inserts for use inside honeycomb unit cells are illustrated in Figure 5.1 and consist of a constraining structure and a damping material, which can be a viscoelastic material with high damping capability. As per convention, the dual material single shear lap joint is referenced as the SSLJ damping insert and the dual material double shear lap joint as the DSLJ damping insert.
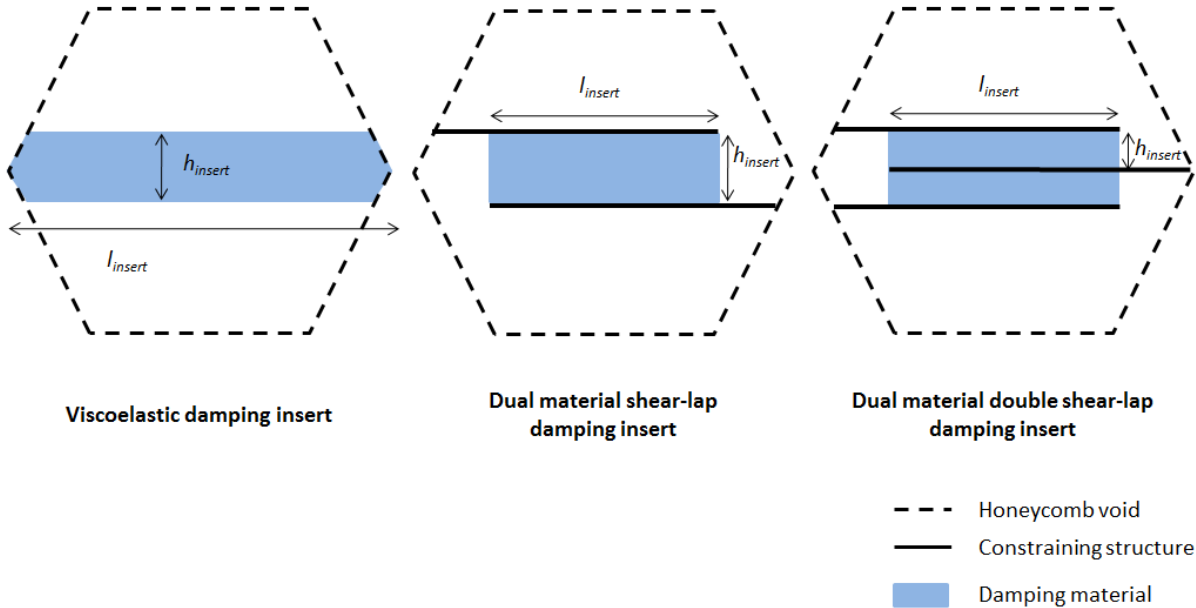
Figure 5.1: Honeycomb cell void with a viscoelastic damping insert, a dual material shear lap damping insert (SSLJ) and a dual material double shear lap damping insert (DSLJ).

As presented in section 4.2.1, under in-plane axial loading the viscoelastic damping insert is loaded in extension/compression and, therefore, strain energy is stored in

Honeycombs with Structured Core for Enhanced Damping

the damping material (see Figure 5.2). A portion of this strain energy is then dissipated, enhancing the damping capacity of the honeycomb structure.
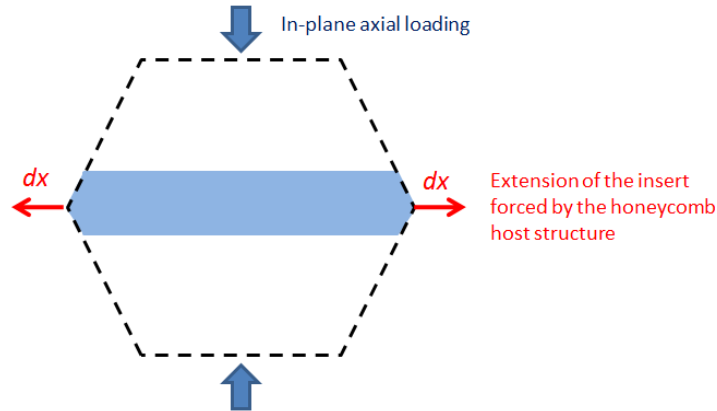
Figure 5.2: Deformation mechanism of a damping insert within a honeycomb cell void subject to in-plane axial loading.

In the case of in-plane axial loading, the strain energy stored in the damping insert is a function of the strain inside the insert squared, assuming uniaxial deformation of the insert. The function of the constraining structure inside the SSLJ and the DSLJ damping inserts (Figure 5.1) is to force shear deformation of the damping material for increased energy dissipation. This is described in further detail subsequently.

5.2.2 Analytical Model

5.2.2.1 Mechanical and damping properties of a honeycomb cell with a SSLJ and DSLJ inserts

Analytical expressions of the Young's modulus E_y, loss factor η and loss modulus $E_y{}^*$ derived for the viscoelastic damping insert in section 4.2.1 using standard beam theory and assuming linear elasticity are identical for the SSLJ and the DSLJ insert geometries, and are presented, respectively, in Equation 5.1 to Equation 5.3. This assumes a uniaxial deformation mechanism of the damping insert.

Honeycombs with Structured Core for Enhanced Damping

$$E_y = \frac{\sigma_y}{\varepsilon_y} = \frac{12.E_s.I.cos\theta}{\left(\frac{h}{l} + sin\theta\right).sin^2\theta.l^3.b} + \frac{2.K_{insert}.cos^3\theta}{\left(\frac{h}{l} + sin\theta\right).sin^2\theta.b}$$

<div align="right">Equation 5.1</div>

$$\eta = \eta_{insert}.\frac{U_{insert}}{U_{tot}} + \eta_{honeycomb}.\frac{U_{honeycomb}}{U_{tot}}$$

<div align="right">Equation 5.2</div>

$$E_y{}^* = \eta.E_y$$

<div align="right">Equation 5.3</div>

Assuming that the constraining structure of the damping insert does not deform under axial loading, the stiffness of the SSLJ insert K_{insert}, derived in Equation 5.4, is a consequence of the shear deformation of the damping material. G_{insert} is the shear modulus of the damping material of the insert; l_{insert} and h_{insert} are the geometric parameters of the insert, as illustrated in Figure 5.3; b is the through thickness depth of the insert.

$$K_{insert} = \frac{G_{insert}.l_{insert}.b}{h_{insert}}$$

<div align="right">Equation 5.4</div>
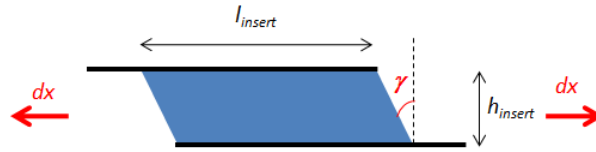
Figure 5.3: Axial deformation of an SSLJ insert.

Assuming, under in-plane axial loading of the honeycomb, that the damping material is loaded at a constant shear strain γ resulting from the displacement dx imposed by the honeycomb structure at each end of the damping insert (see Figure 5.3), the

Honeycombs with Structured Core for Enhanced Damping

strain energy stored upon loading in the damping insert, U_{insert}, is derived in Equation 5.5.

$$U_{insert} = \frac{1}{2} . G_{insert} . \gamma^2 . V_{insert}$$

With:

$$V_{insert} = l_{insert} . h_{insert} . b$$

$$\gamma = \frac{2 . dx}{h_{insert}}$$

Defining geometric parameters of the DSLJ insert, as illustrated in Figure 5.4, i.e. l_{insert} representing the length of the damping material and h_{insert} the distance between two constraining structures, stiffness and total strain energy of the insert can be derived from Equation 5.4 and Equation 5.5. The stiffness of the DSLJ insert is two times that of the shear lap insert. The strain energy stored in the dual shear lap insert is two times that of the SSLJ insert for the same deflection.
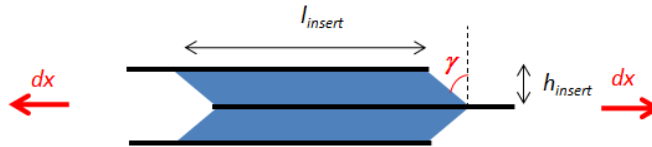
Figure 5.4: Axial deformation of DSLJ insert.

5.2.2.2 Limiting condition of the insert

It has been assumed in the previous section that the stiffer component of the SSLJ and DSLJ inserts do not deform while the insert is loaded axially in tension / compression. This hypothesis is valid when the stiffness of the viscoelastic insert loaded in shear is lower than the stiffness of the stiff part of the insert, as shown in Equation 5.6, where K_{insert_visco} is the stiffness of the viscoelastic layer of the insert and K_{insert_stiff} the stiffness of the stiff part of the insert. In Equation 5.7, the stiffness

149

of the viscoelastic layer and stiff part of the insert are substitute by their analytical expression dependant of the parameters of the insert.

$$K_{insert\_visco} < K_{insert\_stiff}$$

<div align="right">Equation 5.6</div>

$$\frac{G_{insert\_visco} \cdot l_{insert} \cdot b}{h_{insert}} < \frac{E_{insert\_stiff} \cdot h_{insert} \cdot b}{l_{insert}}$$

<div align="right">Equation 5.7</div>

Equation 5.7 simplifies itself so as to give a limiting condition on the thickness of the viscoelastic layer of the insert, h_{insert}, and is shown in Equation 5.8.

$$h_{insert} > \sqrt{\frac{G_{insert\_visco} \cdot l_{insert}^2}{E_{insert\_stiff}}}$$

<div align="right">Equation 5.8</div>

5.2.3 Finite Element Analysis of Honeycomb Structure with SLJ Damping Inserts

5.2.3.1 SLJ Damping Insert Geometries

The damping insert geometries studied in this chapter consist of dual material single shear lap joint (SSLJ) and dual material double shear lap joint (DSLJ) damping inserts, as illustrated in Figure 5.5.

Honeycombs with Structured Core for Enhanced Damping
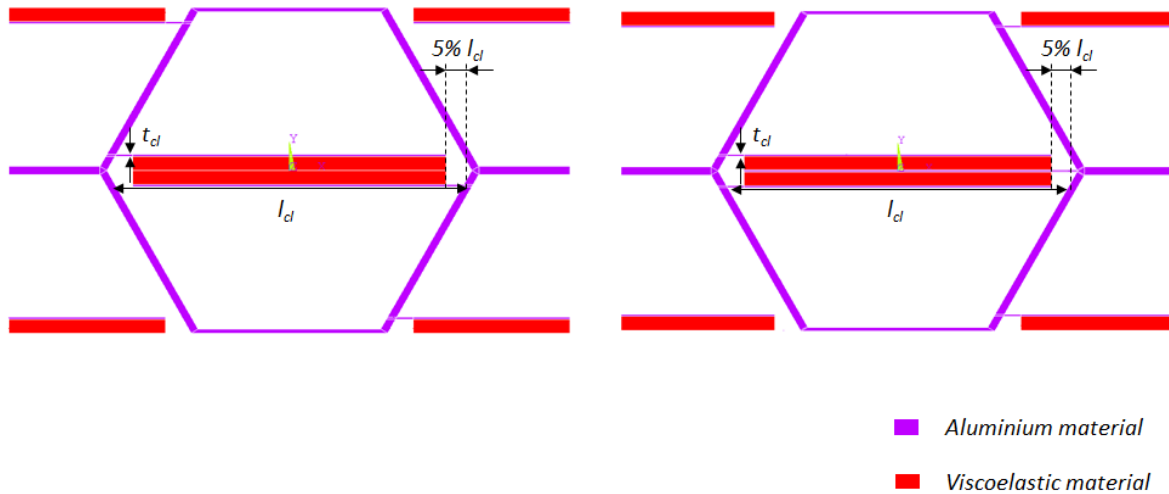
Figure 5.5: Unit cell models of a honeycomb cell with an SSLJ insert (left) and with a DSLJ insert (right).

Honeycomb geometric parameters has been set as follows, identically to the parameters of the honeycomb geometry used in Chapter 4: $l = h = 1$ mm, $\theta = 30°$ and $t = 0.0433$ mm for a honeycomb cell relative density $\rho^* = 0.05$.

A parametric model of damping insert has been created using Ansys Parametric Design Language (APDL) [90], and geometries of damping insert filling 5% to 40% of the cell void by 5% increments have been studied. The thickness of the constraining layer t_{cl} has been set to 0.01 mm. The length of the constraining layer l_{cl} has been set so as to leave a minimum gap of 5% between the viscoelastic material and walls of the honeycomb cell, as highlighted in Figure 5.5.

5.2.3.2 Loadings and Associated Boundary Conditions

In-plane tension/compression and in-plane pure shear boundary conditions have been applied to the geometries studied. These loading conditions correspond to the noticeable deformations of honeycomb cells in a sandwich structure, as highlighted in Chapter 2. Identical boundary conditions described in section 4.2.2.2, have been applied for in-plane tension/compression and in-plane shear. The boundary conditions have been applied to a 15x15 cell panel. This has been chosen from a

Honeycombs with Structured Core for Enhanced Damping

convergence study to account for the surrounding deformation of the cells around the middle cell of the panel.

The analysis made in Chapter 4 highlighted that the horizontal ligament performs best for in-plane axial loading than the diagonal ligament across the cell void and the opposite for in-plane shear loading. These results have been accounted for in the analysis. Shear lap insert geometries are positioned horizontally across the void of the unit cell for in-plane axial loading and diagonally across the unit cell for in-plane shear loading.

5.2.3.3 Elements Definition

The finite element mesh consists of 2D bilinear structural PLANE82 elements (plane strain formulation). Models with a damping insert filling 5% of the honeycomb cell void had a minimum of 1,500 elements (see Figure 4.9), and models with a damping insert filling 40% of the cell void had around 5,000 for a single unit cell. Figure 5.6, shows the finite element mesh of the honeycomb unit cell with a DSLJ insert filling 10% of the cell void; 2,162 elements have been used in this model.

Honeycombs with Structured Core for Enhanced Damping
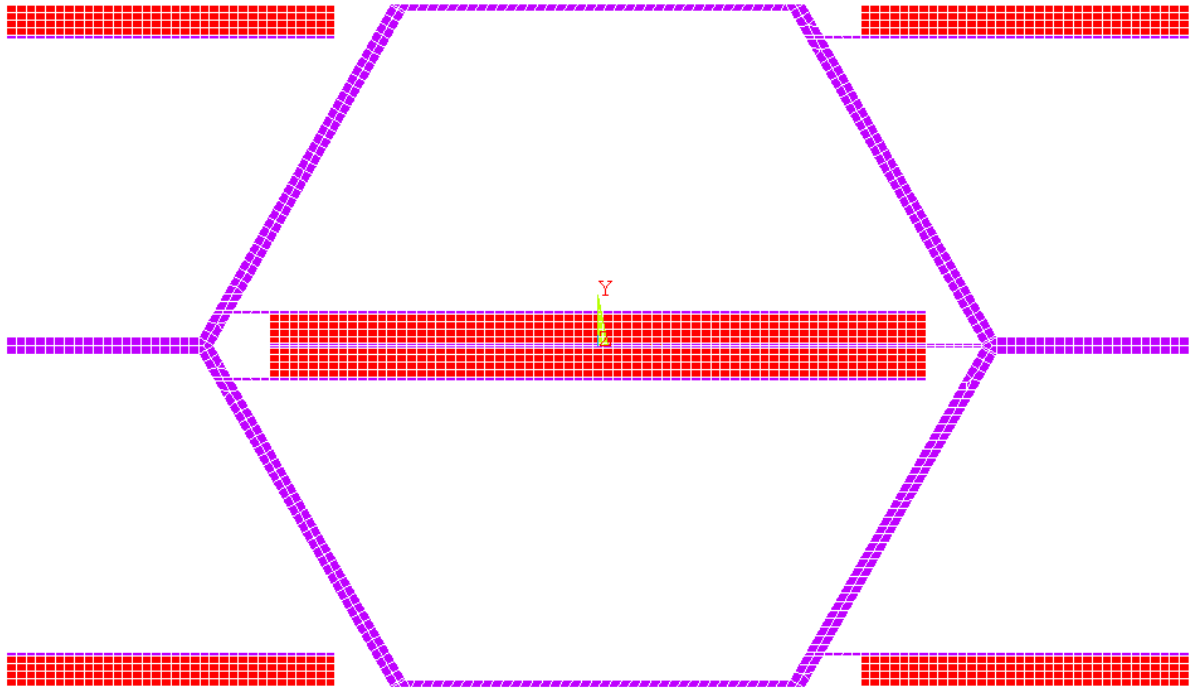
Figure 5.6: FE mesh of the honeycomb unit cell with a DSLJ insert filling 10% of the void space of the honeycomb.

5.2.3.4 Material Properties

Two material properties have been defined. The constituent material of the honeycomb and the constraining layers of the damping inserts have been modelled with aluminium properties, with a set of linear and isotropic elastic constants (E_{al} = 70000 MPa, ν_{al} = 0.3, ρ_{al} = 1.25 g.cm^3 and η_{al} = 0.0001 [76]). The damping insert has been modelled with arbitrary material properties representing a viscoelastic material, with a set of linear and isotropic elastic constants (E_{visco} = 1MPa, ν_{visco} = 0.45, ρ_{visco} = 2.7 g.cm^3 and η_{visco} = 0.1 [108]).

5.2.3.5 FE Analysis

Mechanical and damping properties of the models and loadings described previously have been calculated using a linear static analysis with Ansys 13[90]. Young's modulus E_y and shear modulus G_{xy} have been calculated in the centre cell of each model from, respectively, Equation 5.9 and Equation 5.10, where U_{total} is the total strain energy of all the element in the centre cell, ε_y is the strain of the cell loaded

Honeycombs with Structured Core for Enhanced Damping

axially, γ_{xy} is the shear strain of the cell loaded in pure shear and V_{cell} is the total volume of the cell.

$$E_y = \frac{2.U_{total}}{\varepsilon_y{}^2.V_{cell}}$$

<div align="right">Equation 5.9</div>

$$G_{xy} = \frac{2.U_{total}}{\gamma_{xy}{}^2.V_{cell}}$$

<div align="right">Equation 5.10</div>

Loss factors and loss moduli of the structure for both loading cases have been derived from Equation 5.2 based on the MSE method, similarly to Chapter 4.

5.3 Results

5.3.1 Convergence Study

The influence of the surrounding cells on the strain energy stored in the viscoelastic material is presented in Figure 5.7 and Figure 5.8, in order to verify the consistency of the boundary conditions applies to the FE models. These figures show the total strain energy stored in the viscoelastic material of the middle honeycomb cell with damping insert filling 10% of the honeycomb cell void for different sizes of panel, respectively, for in-plane axial loading and in-plane shear loading. Convergence of the strain energy stored in the viscoelastic material is achieved for a 15x15 cell panel for the SSLJ insert and both loading directions. Convergence of the strain energy stored in the viscoelastic material is achieved for a 3x3 cell panel for the DSLJ insert when loaded axially and a 15x15 cell panel when loaded in shear. The viscoelastic strain energy in both models where boundary conditions have been applied to the boundary of the unit cell were shown to be underestimated.
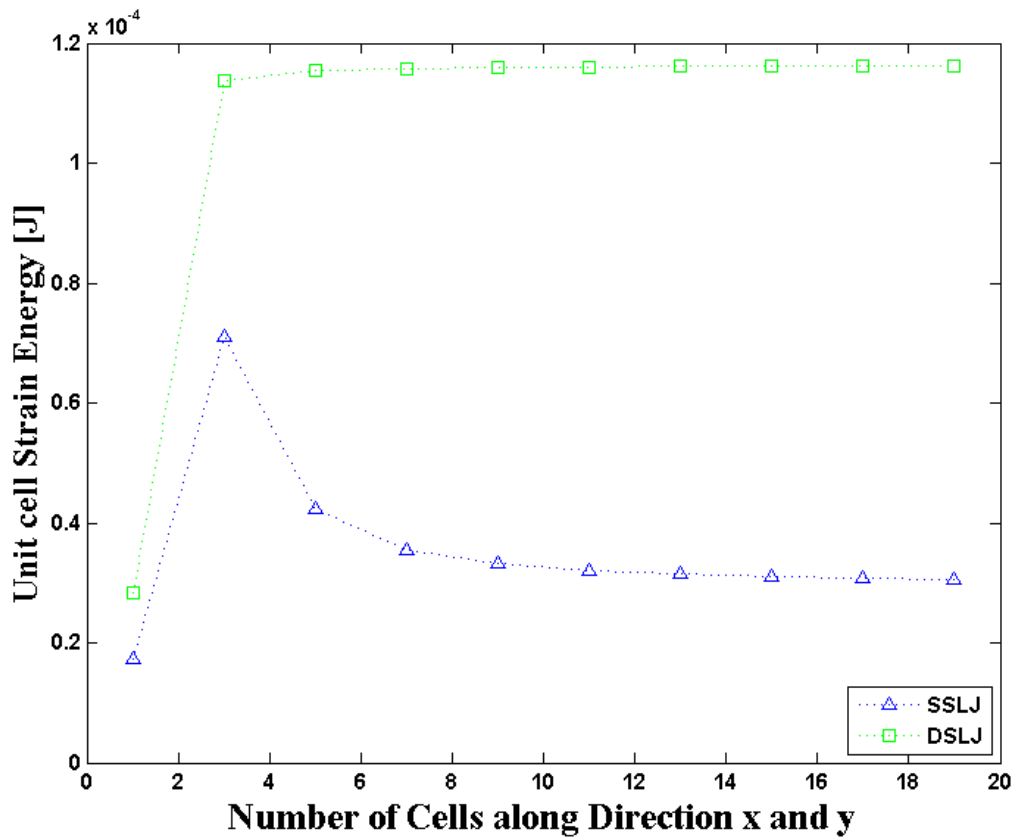
Figure 5.7: Strain energy (J) stored in the middle cell of different honeycomb panel sizes filled with SSLJ and DSLJ inserts under in-plane compression loading of 0.1% strain.

Honeycombs with Structured Core for Enhanced Damping
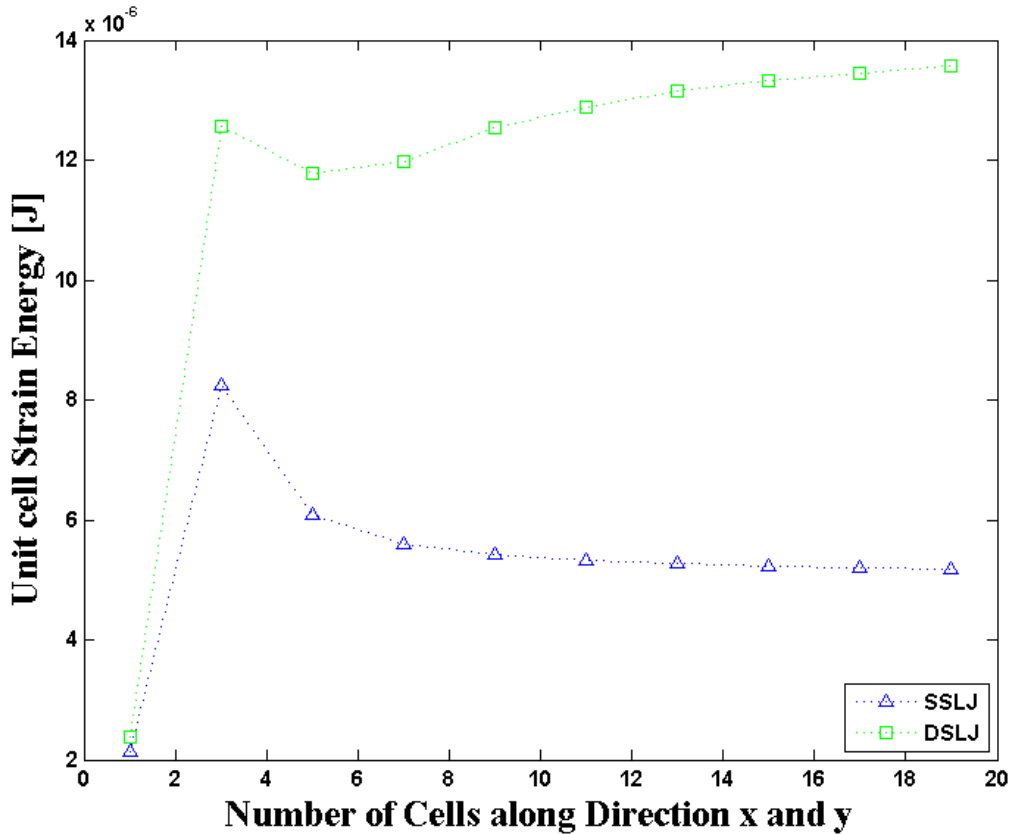
Figure 5.8: Strain energy (J) stored in the middle cell of different honeycomb panel sizes filled with SSLJ and DSLJ inserts under in-plane pure shear loading of 0.1% strain.

5.3.2 In-plane Axial Damping Performance of Honeycomb with SLJ Damping Inserts

The elastic equivalent Von Mises strain [90] of the SSLJ and DSLJ damping insert geometries filling 10% of the honeycomb cell void is illustrated in Figure 5.9 for a 0.1% strain compression loading. The magnitude of strain in the DSLJ insert is twice that of the SLJ insert.

Honeycombs with Structured Core for Enhanced Damping
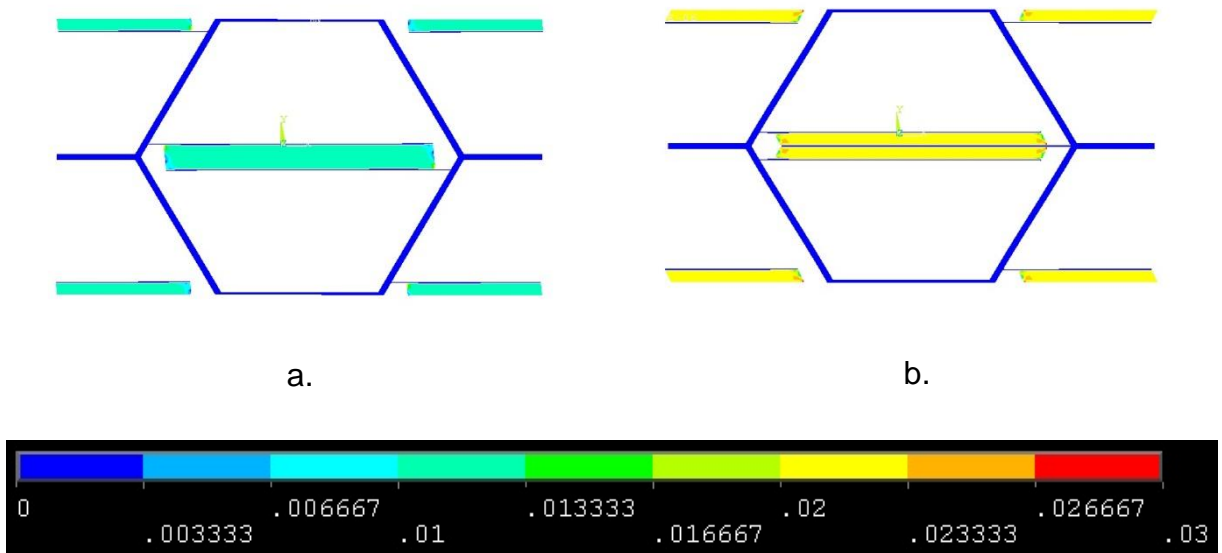
Figure 5.9: Elastic equivalent Von Mises strain of SSLJ and DSLJ damping insert geometries filling 10% of the honeycomb cell void under compression loading of 0.1% strain.

The elastic equivalent Von Mises strain [90] of the DSLJ damping insert filling, respectively, 10%, 20%, 30% and 40% of the honeycomb cell void is illustrated in
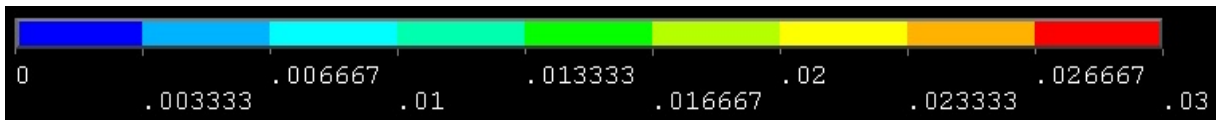
Figure 5.10 for a 0.1% strain compression loading. The equivalent Von Mises strain inside the viscoelastic material decreases with increasing damping insert size.

Honeycombs with Structured Core for Enhanced Damping
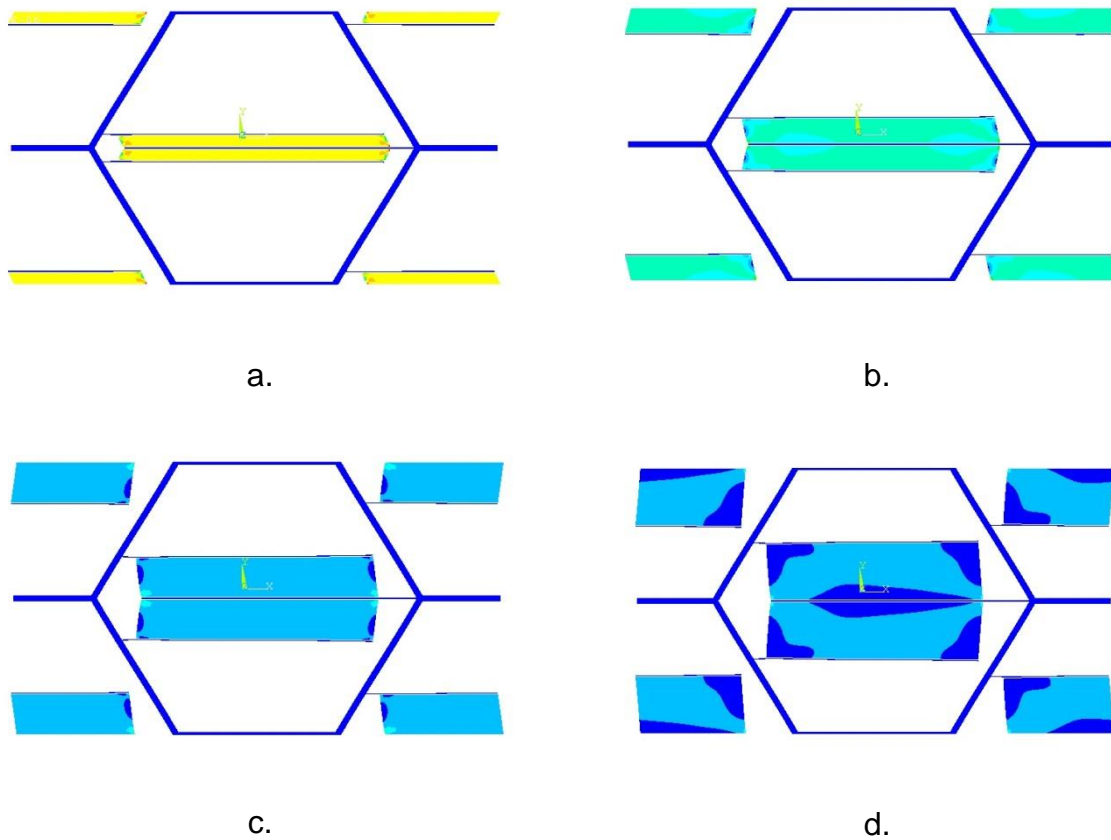
Figure 5.10: Elastic equivalent Von Mises strain of DSLJ inserts filling 10% (a.), 20% (b.), 30% (c.), and 40% (d.) of the void of a honeycomb unit cell under compression loading of 0.1% strain.

The in-plane Young's modulus E_y of the SSLJ and DSLJ damping insert geometries is represented in Figure 5.11 in function of the honeycomb cell void occupation of the insert. The analytic expressions of the in-plane Young's modulus of the honeycomb cell derived in Equation 5.1 for the SSLJ and DSLJ inserts is superposed to the FE results. The analytical expressions of the Young's modulus derived for both SSLJ and DSLJ match well the FE predictions. For both insert geometries, the Young's modulus decreases with the increasing size of the damping insert and converges to the Young's modulus of the cell completely filed with viscoelastic material. The SSLJ insert occupying 5% of the honeycomb cell void has a Young's

Honeycombs with Structured Core for Enhanced Damping

modulus of 49.6 MPa, which represents a 198% increase of the Young's modulus of a honeycomb completely filled with viscoelastic material. The DSLJ insert occupying 5% of the honeycomb cell void has a Young's modulus of 133 MPa, which represents a 698% increase of the Young's modulus of a honeycomb completely filled with viscoelastic material.
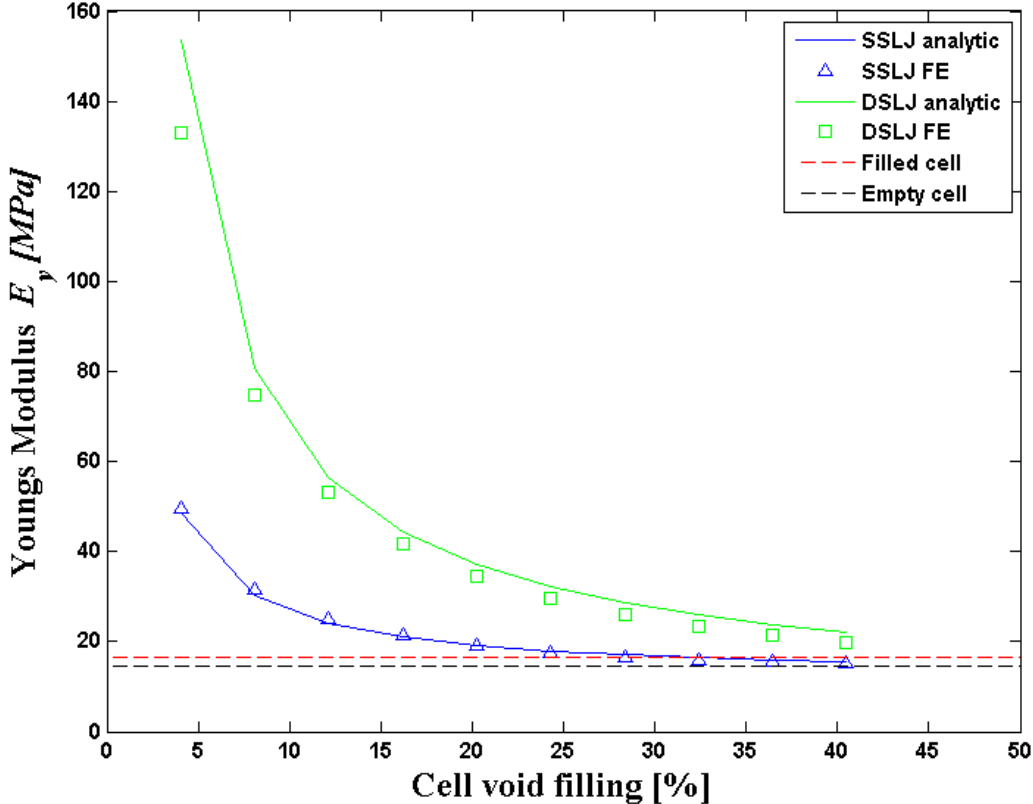
Figure 5.11: Analytical and FE computed Young's modulus E_y of a honeycomb cell of relative density $\rho^* = 0.05$ with SSLJ and DSLJ inserts represented in function of the cell void filling of the damping insert.

The loss factor η derived from the MSE method under in-plane compressive loading at 0.1% strain of the SSLJ and DSLJ damping insert geometries is represented in Figure 5.12 in function of the honeycomb cell void occupation of the insert. The analytic expressions of the loss factor of the honeycomb cell derived in Equation 5.2 for the SSLJ and DSLJ inserts is superposed to the FE results. The analytical

Honeycombs with Structured Core for Enhanced Damping

expressions of the loss factor of honeycomb cell with SSLJ and DSLJ inserts are of the same magnitude than the FE computed loss factor and decrease with the cell void filling of the cell so as the FE predictions. For both insert geometries, the loss factor decreases with the increasing size of the damping insert. The honeycomb cell with a SSLJ insert occupying 5% of the honeycomb cell void has a loss factor of 6.59%, which represents a 458% increase of the loss factor of a honeycomb completely filled with viscoelastic material. The honeycomb cell with a DSLJ insert occupying 5% of the honeycomb cell void has a loss factor of 7.65%, which represents a 548% increase of the loss factor of a honeycomb completely filled with viscoelastic material.
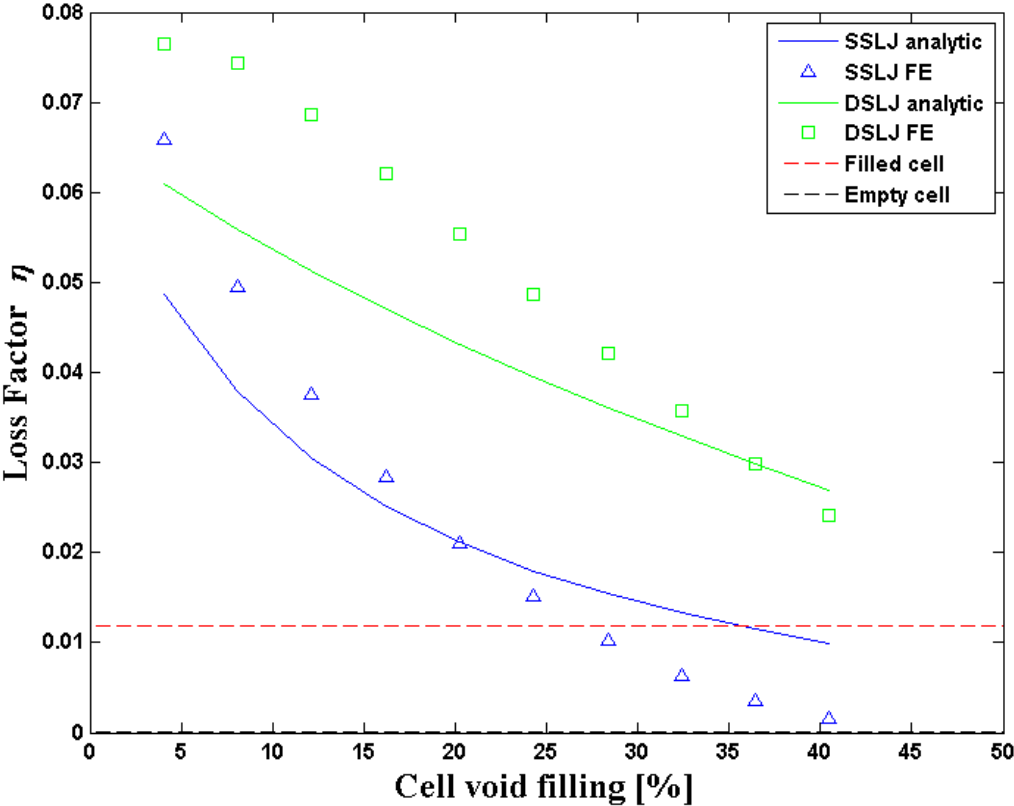
Figure 5.12: Analytical and FE computed loss factor η of a honeycomb cell of relative density $\rho^* = 0.05$ with SSLJ and DSLJ inserts represented in function of the cell void filling of the damping insert.

Honeycombs with Structured Core for Enhanced Damping

The in-plane loss modulus E_y^* of the SSLJ and DSLJ damping insert geometries is represented in Figure 5.13 in function of the honeycomb cell void occupation of the insert. The analytic expressions of the in-plane loss modulus of the honeycomb cell derived in Equation 5.3 for the SSLJ and DSLJ inserts is superposed on the FE results. The analytical expressions of the loss modulus derived for both SSLJ and DSLJ slightly underestimate the FE predictions cell void filling below 20% and overall match well the FE predictions. For both insert geometries, the loss modulus decreases with the increasing size of the damping insert and converges to the Young's modulus of the cell completely filed with viscoelastic material. The honeycomb cell with a SSLJ insert occupying 5% of the honeycomb cell void has a loss modulus of 3.27 MPa, which represents a 1,566% increase of the loss modulus of a honeycomb completely filled with viscoelastic material. The honeycomb cell with a DSLJ insert occupying 5% of the honeycomb cell void has a loss modulus of 10.17 MPa, which represents a 5,085% increase of the loss modulus of a honeycomb completely filled with viscoelastic material.

Honeycombs with Structured Core for Enhanced Damping
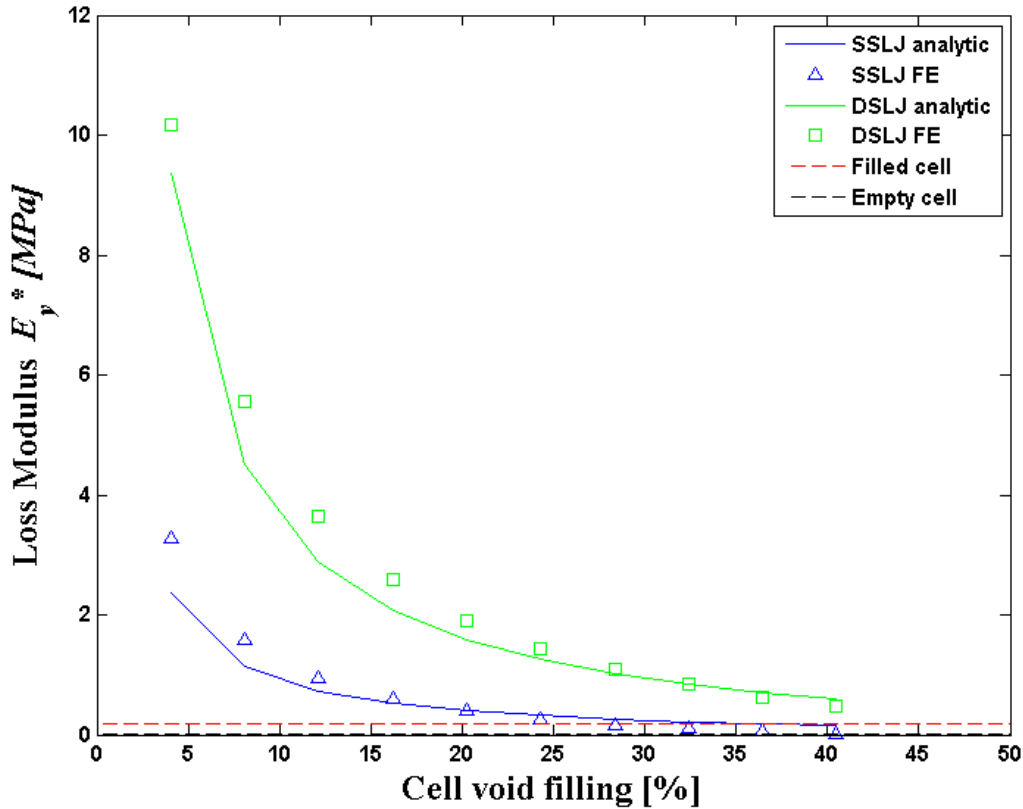
Figure 5.13: Analytical and FE computed loss modulus Ey^* of a honeycomb cell of relative density $\rho^*= 0.05$ with SSLJ and DSLJ inserts represented in function of the cell void filling of the damping insert.

The in-plane density-specific loss modulus Ey^*/ρ of the SSLJ and DSLJ damping insert geometries is represented in Figure 5.13 in function of the honeycomb cell void occupation of the insert. For both insert geometries, the density-specific loss modulus decreases with the increasing size of the damping insert and converges to the density-specific loss modulus of the cell completely filed with viscoelastic material. The honeycomb cell with a SSLJ insert occupying 5% of the honeycomb cell void has a density-specific loss modulus of 14900 MPa.g^{-1}.mm^3, which represents a 9,950% increase compared to the honeycomb completely filled with viscoelastic material. The honeycomb cell with a DSLJ insert occupying 5% of the honeycomb cell void has a density-specific loss modulus of 42700 MPa.g^{-1}.mm^3,

Honeycombs with Structured Core for Enhanced Damping

which represents a 28,600% increase compared to the honeycomb completely filled with viscoelastic material.
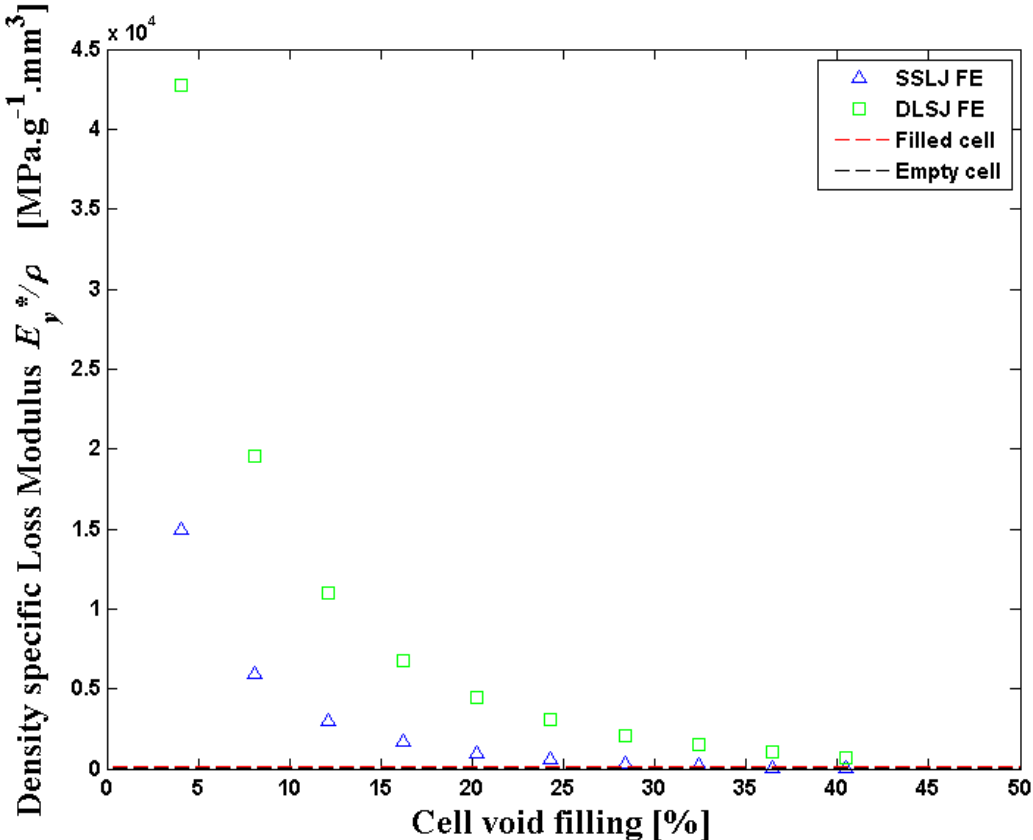
Figure 5.14: FE computed density-specific loss modulus Ey^*/ρ of a honeycomb cell of relative density $\rho^*= 0.05$ with SSLJ and DSLJ inserts represented in function of the cell void filling of the damping insert.

5.3.3 In-plane Shear Damping Performance of Honeycomb with Viscoelastic Damping Inserts

The elastic equivalent Von Mises strain [90] of the damping insert geometries filling 10% of the honeycomb cell void is illustrated in Figure 5.15 for a 0.1% strain shear loading. The magnitude of strain in the DSLJ insert is almost twice that of the SSLJ insert.

Honeycombs with Structured Core for Enhanced Damping

<table>
<tr><td>a.</td><td>b.</td></tr>
</table>
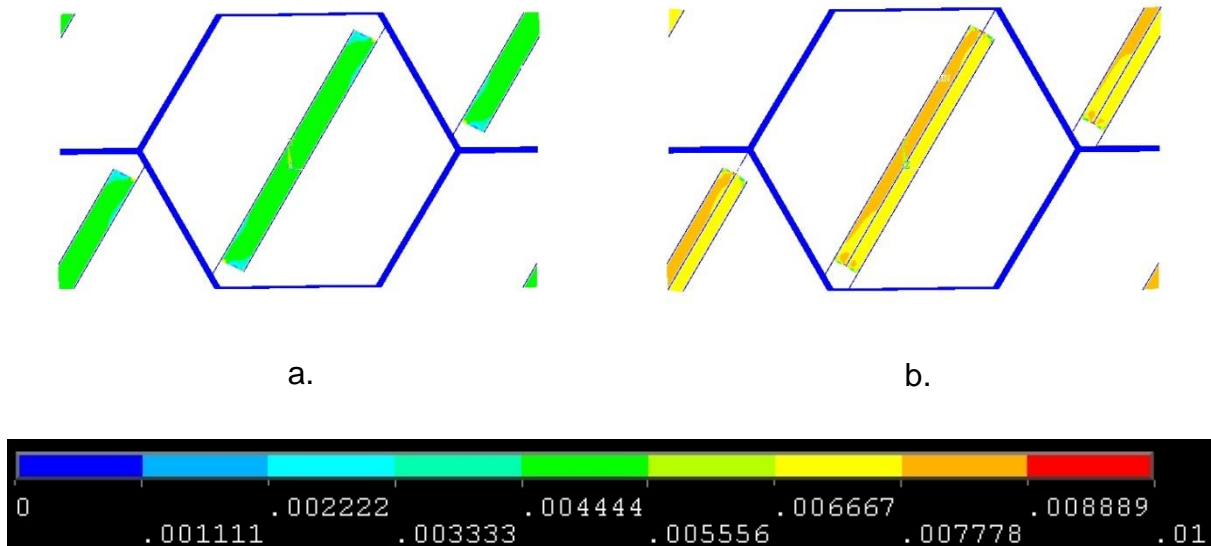
Figure 5.15: Elastic equivalent Von Mises strain of SSLJ and DSLJ damping insert geometries filling 10% of the honeycomb cell void under in-plane pure shear loading of 0.1% strain.

The in-plane density-specific loss modulus Gxy^*/ρ of the honeycomb cell with a SSLJ or DSLJ damping insert geometries is represented in Figure 5.16 in function of the honeycomb cell void occupation of the insert. For both insert geometries, the density-specific loss modulus decreases with the increasing size of the damping insert and converges to the density-specific loss modulus of the cell completely filed with viscoelastic material. The honeycomb cell with a SSLJ insert occupying 5% of the honeycomb cell void has a density-specific loss modulus of 1885 MPa.g^{-1}.mm^3, which represents a 4,435% increase compared to the honeycomb completely filled with viscoelastic material. The honeycomb cell with a DSLJ insert occupying 5% of the honeycomb cell void has a density-specific loss modulus of 4265 MPa.g^{-1}.mm^3, which represents a 10,160% increase compared to the honeycomb completely filled with viscoelastic material.

Honeycombs with Structured Core for Enhanced Damping
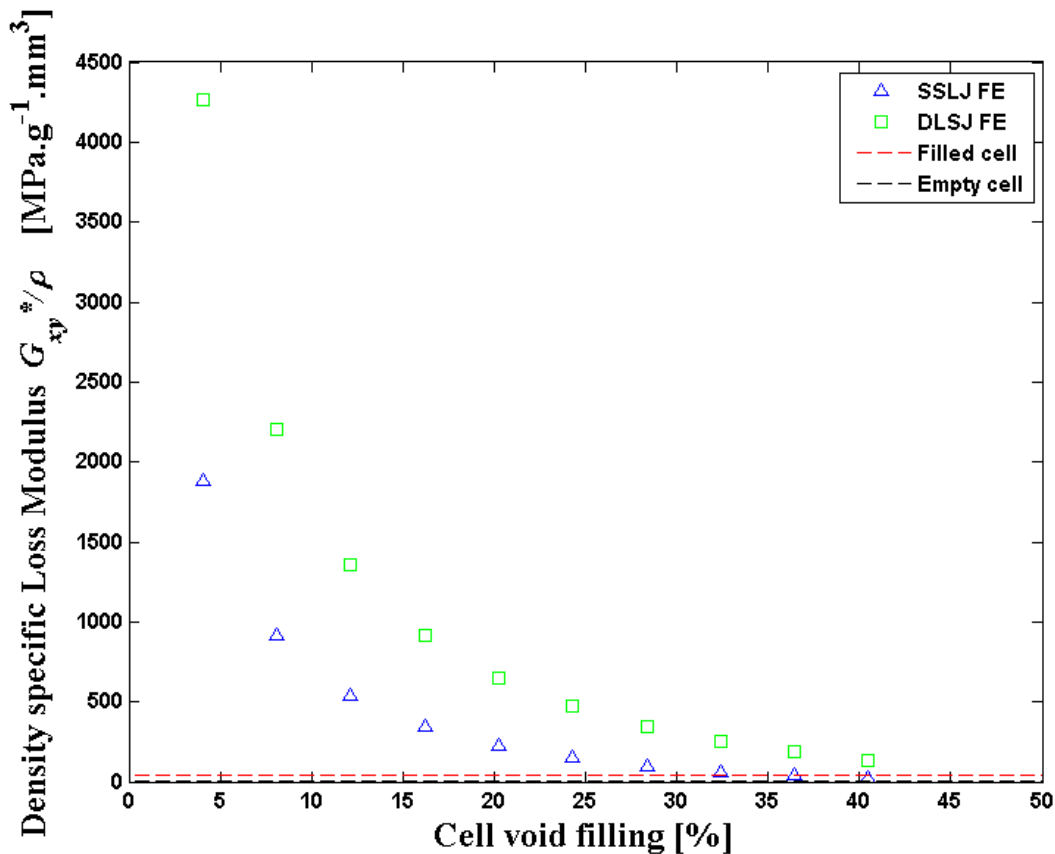
Figure 5.16: FE computed density-specific loss modulus $Gxy*/\rho$ of a honeycomb cell of relative density $\rho* = 0.05$ with SSLJ and DSLJ inserts represented in function of the cell void filling of the damping insert.

5.4 Discussion

5.4.1 Boundary Conditions

Boundary conditions applied to the edge of the honeycomb unit cell with damping insert have shown to underestimate the strain energy of the damping insert (see Figure 5.7 and Figure 5.8). Convergence of the strain energy for most damping inserts geometries and loadings occurs when boundary conditions are applied further away from the middle cell of the panel from which mechanical and damping properties are calculated. This is caused by the geometric discontinuity of the honeycomb unit cell, as represented in Figure 5.5. The honeycomb unit cell with damping inserts presents a quarter of the damping insert in each one of its four

Honeycombs with Structured Core for Enhanced Damping

corners. Application of the boundary conditions to the edge of the honeycomb unit cell is, therefore, not appropriate for the SSLJ and DSLJ insert geometries, because the damping inserts are not correctly loaded by the surrounding cells in each corner of the unit cell model. Convergence of the strain energy inside the damping insert has shown to be achieved in all cases for panels of 15x15 cells. The strain energy is overestimated for smaller panel sizes (from 3x3 cells) because of over-constraining boundary conditions, as observed by [106], and in Chapter 4.

5.4.2 In-plane Axial Damping Performance of Honeycomb with Viscoelastic Damping Inserts

The mechanical and loss properties of honeycombs with SSLJ and DSLJ damping inserts have been described in Figure 5.11 to Figure 5.13 for in-plane axial loading. The Young's modulus, loss factor and loss modulus are significantly enhanced through the use of both inserts. Maximum enhancement of the mechanical and damping properties is achieved for the minimum size of damping insert studied in this chapter, filling 5% of the honeycomb cell void. The DSLJ damping insert has been shown to increase the Young's modulus E_y of the unit cell by 698%, its loss factor η by 548% and its loss modulus E_y^* by 5,085% compared to a honeycomb cell completely filled with the same viscoelastic material, which has been characterised to have the highest Young's modulus, loss factor and loss modulus compared to the ligament inserts made from a single viscoelastic material studied in Chapter 4. Maximum enhancement is achieved for the minimum size of damping insert because of the shear lap geometry of the insert. Under in-plane axial loading, the constraining layers of the insert force shear deformation of the viscoelastic material of the damping insert. Since the shear stiffness of the damping insert is inversely proportional to its thickness (see Equation 5.4), the insert with minimal thickness and, therefore, minimum size provides the maximum resistance upon loading, i.e. maximum Young's modulus. Consequently, strain energy is maximal for the minimum size of insert. Since the energy dissipation of the insert is proportional to its total strain energy, maximum loss factor and loss modulus are provided by SSLJ and DSLJ inserts of minimum size. This result has been illustrated in Figure 5.10 for

different sizes of insert. Analytical expressions of Young's modulus, loss factor and loss modulus derived in Equation 5.1 to Equation 5.3 correlate with the results of the FE analyses, and provide further understanding of mechanical and damping enhancement given by the SSLJ and DSLJ inserts. The Young's modulus is dependent on the stiffness of the damping insert that is inversely proportional to the thickness of the insert. The loss factor is dependent on strain energy stored inside the viscoelastic material that is proportional to the strain squared in the viscoelastic material; given the internal architecture of the damping insert, the constraining layers of the insert impose a shear strain inside the viscoelastic material that is inversely proportional to the thickness of the insert (see Equation 5.5). Therefore, the insert with minimum thicknesses provides the maximum enhancement of the mechanical and damping properties. This also explains why the DSLJ insert exhibits higher Young's modulus, loss factor and loss modulus than the SSLJ insert, since its viscoelastic layer thickness is half the thickness of the viscoelastic layer within the SSLJ insert for a damping insert of the same size. This is illustrated in Figure 5.9, where the strain inside the DSLJ insert is twice the strain inside the SSLJ insert.

In theory, shear lap inserts with viscoelastic layers of infinitesimal thicknesses will result in honeycombs with infinite Young's modulus, loss factor and loss modulus. However, the thickness of the viscoelastic layer is likely to be limited by the manufacturing methods used to construct such inserts and the strength properties of the constituent material of the insert.

Since there is an inverse relationship between the thickness of the viscoelastic layer in the shear lap insert and its loss modulus, its density-specific loss modulus is many times greater than that of the completely filled honeycomb; for example, 280 times in Figure 5.14.

5.4.3 In-plane Shear Damping Performance of Honeycomb with Viscoelastic Damping Inserts

The analysis made in Chapter 4 highlighted that diagonal ligament inserts perform best for in-plane shear loading. This is because the insert is located between the two

opposite corners of the honeycomb which exhibit the maximum relative displacement between all the locations inside the void of the honeycomb. As a result, the SSLJ and DSLJ located in these locations are mainly loaded axially, hence behave similarly than SSLJ and DSLJ horizontal inserts of a honeycomb cell loaded axially.. Density-specific loss modulus is enhanced by more than 10,000% compared to the honeycomb completely filled with viscoelastic material. This has been illustrated in Figure 5.16.

5.5 Conclusion

Shear lap joint insert consist of a damping material constrained between two or several constraint layers, so as to enforce deformation of the damping material similarly to constrained layer damping technologies [4]. Deformation of a honeycomb cell with a SLJ insert forces the damping material of the insert into shear deformation which proved to efficiently enhanced the mechanical and damping properties of the overall honeycomb cell.

The two forms of SLJ insert, i.e. SSLJ and DSLJ, both outperformed by far the ligament damping inserts investigated in Chapter 4 and honeycomb cell completely filled with a damping material, in term of both mechanical and damping performance.

Between the SSLJ and DSLJ, the DSLJ insert is the best damping insert in term of both mechanical and damping enhancements of the overall honeycomb cell

Analytical expressions and FE analysis have been used to quantify the mechanical and damping properties of the SLJ inserts. These inserts exhibit very high mechanical and damping enhancement properties. Compared to a honeycomb cell completely filled with viscoelastic material, SLJ inserts enhanced the density-specific in-plane axial loss modulus E_y^* by more than 28,000% and the density-specific in-plane shear loss modulus G_{xy}^* of the honeycomb structure by more than 10,000%.

Honeycombs with Structured Core for Enhanced Damping

Chapter 6. Sandwich Panel with Double Shear Lap Joint Damping Inserts

6.1 Introduction

The behaviour of cellular core structures filled with viscoelastic materials was observed experimentally in [11] for the first time with a copper foam as a matrix and an elastomer as a filling material. The filling of hexagonal cores with foam was then demonstrated for improved energy and impact absorption [42] [93-95]. Foams have also been used to fill honeycomb structures, with consequent improvement of damping properties [46] [47]. However, adding foam into honeycomb structures significantly increases the density of the sandwich panel, even if foams themselves exhibit relatively good density-specific properties. To avoid excessive increases in density, cells may be only partially filled with an insert. For example, Woody and Smith obtained an improvement of around 60% in damping loss factor by filling only selected cells within an array, adding less than 6% to the structure's mass [47].

Geometries of SLJ damping inserts for use inside honeycomb unit cells have been shown to significantly enhance the loss modulus in in-plane tension/compression and in-plane shear loadings in Chapter 5. These inserts consist of a constraining structure and a damping material, which can be a viscoelastic material with high damping properties. As the viscoelastic constrained layer damping system in structure [4], the constraining layer of the insert is forcing high shear deformation of the damping material, providing high energy dissipation by the insert, therefore, enhancing damping properties of the honeycomb structure.

In a sandwich structure, made from two face sheets and a honeycomb core, each honeycomb unit cell deformation is a combination of in-plane loading introduced by the out-of-plane bending deformation of the sandwich panel, and out-of-plane transverse shear deformation, as highlighted in Chapter 2.

Since geometries of inserts, as studied in Chapters 4 and 5, are dependent on the main loading direction of the honeycomb unit cell, an engineered method for

Honeycombs with Structured Core for Enhanced Damping

localisation of an SLJ damping insert is introduced in this chapter to investigate a partial filling solution of sandwich panels with damping inserts, choosing the best orientation of the damping insert inside the honeycomb void.

Enhancement of the damping loss factor of the first bending mode of a honeycomb sandwich panel with DSLJ damping inserts is investigated in this chapter. The damping properties of the sandwich panel with damping inserts have been quantified through static analyses using the MSE method.

6.2 Methods

6.2.1 Location and Orientation of DSLJ Damping Inserts Inside a Honeycomb Sandwich Structure

When subjected to vibration, each honeycomb unit cell of a sandwich structure deforms as a combination of in-plane and out-of-plane loadings. The intensity of each loading direction is dependent of the unit cell location within the sandwich structure and the vibration mode exited, as discussed in Chapter 2. Since it has been highlighted in Chapter 5 that SLJ damping inserts are most efficient in dissipating energy when loaded axially, the location and orientation of the damping insert within the honeycomb unit cell of a sandwich structure have an impact on the damping performance of the insert. For best use of the damping insert characteristics, it needs to be located where relative displacement between opposite walls of the honeycomb unit cell is maximal within the sandwich panel.

The methodology developed in this section for the location of an SLJ damping insert within a sandwich panel is derived from the response of a honeycomb sandwich panel without damping insert. The modal deformation of the panel is analysed and locations for damping inserts are derived for the unit cells exhibiting maximum relative displacement between their opposite walls (parameters ε_1, ε_2 and ε_3 derived in Chapter 2). Given a number of SLJ damping inserts to be used in the sandwich structure, which is driven by the maximum weight increase allowable for the structure, damping inserts are located in cells exhibiting maximum relative displacement between their opposite walls. The input/output diagram of this process

is illustrated in Figure 6.1. This methodology assumes that the SLJ damping insert does not modify the response of the sandwich structure. This approach ignores the stiffness of the viscoelastic insert, assuming that the stiffness of the cell itself dominates, as supported by Abd El-Sayed et al. [99]. This will be invalid for cases where very stiff or large inserts are used.
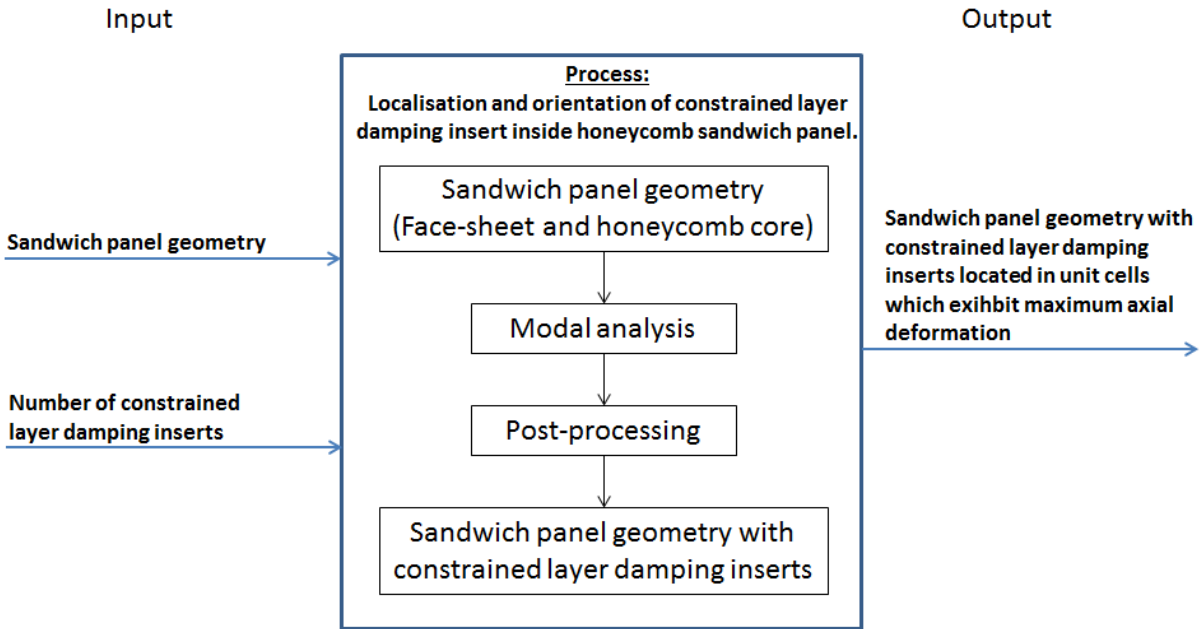
Figure 6.1: Input/output diagram of the process used to localise and orientate damping inserts within a sandwich panel.

6.2.2 Geometries Studied

The sandwich panel geometries studied in this chapter share an identical host structure for the SLJ damping inserts. This host structure is composed of two aluminium face sheets of thicknesses $t = 0.2$ mm, and a honeycomb core structure of 10 mm depth formed by six regular honeycomb unit cells along the x axis and 18 unit cells along the y axis, as described in Figure 6.2. The parameters of the honeycomb unit cells are $h = l = 10$ mm, $t = 0.2$ mm and $\theta = 30°$.

Honeycombs with Structured Core for Enhanced Damping
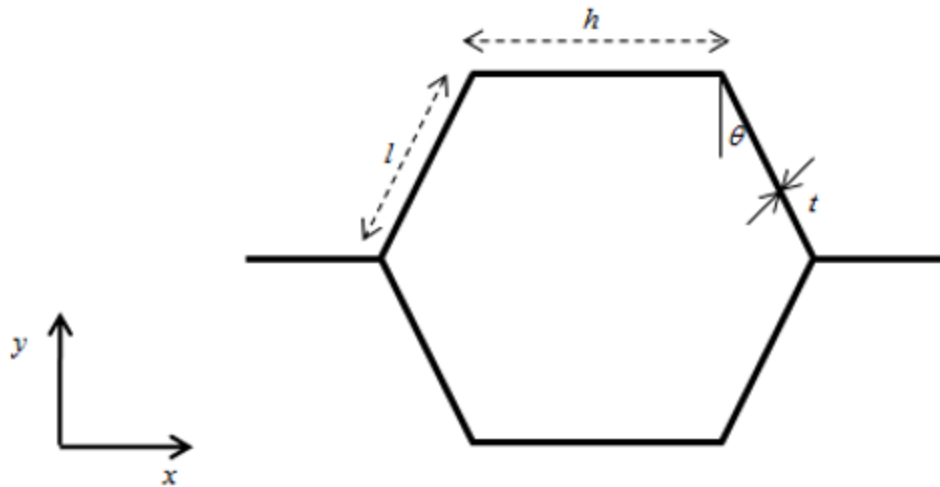
Figure 6.2: Honeycomb cell with its geometric parameters h, l, t and θ.

The DSLJ damping insert consists of a dual material double shear lap joint insert made from aluminium and viscoelastic material, as described in Chapter 5, see section 5.2.1. Constraint layers of the insert have a thickness $t = 0.2$ mm. The two viscoelastic layers of the insert both have 0.365 mm. The damping insert occupies 5% of the middle void of the honeycomb unit cell. The damping insert does extend through the full depth of the unit cells. It stops at a distance $d = 0.5$ mm from the outer surfaces of the honeycomb unit cell, which are connected to the face sheets of the sandwich panel, as illustrated in Figure 6.3. This is to avoid increase of the panel stiffness caused by the addition of the DSLJ insert as the aim of the insert is to improve the damping properties of the panel without large modification of its structural properties. Of note, it was identified in Chapter 2 that the best location for forcing in-plane deformation is the closest to the skins of the panel. As such, the geometry of the DSLJ insert studied in this chapter could be improved even further so as for the insert to not occupy the neutral plane of deformation of the targeted mode of deformation.

Honeycombs with Structured Core for Enhanced Damping
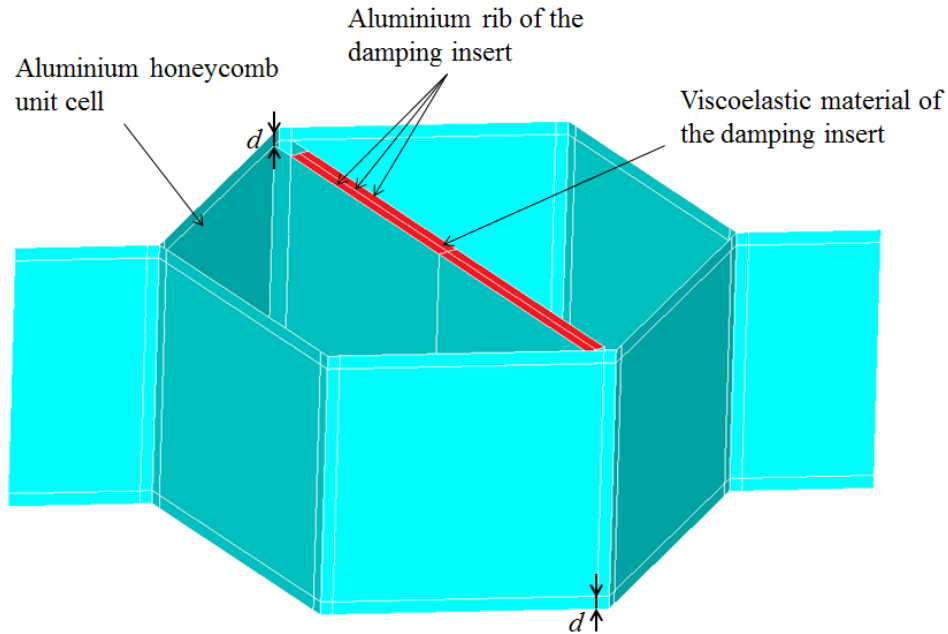
Figure 6.3: 3D model of a honeycomb unit cell filled in its middle with one DSLJ insert.

Twenty-two different geometries have been studied in this chapter. One consists of the sandwich panel host structure with no embedded damping insert and the last consists of the sandwich panel host structure completely filled with viscoelastic material. In between, twenty geometries with increasing numbers of DSLJ inserts have been studied. The description of the sandwich panel geometries, including the location and orientation of damping inserts, is illustrated in Table 6.1. The location and orientation of the damping inserts have been derived from the methodology presented in section 6.2.1 for improving the damping properties of the first bending mode of the panel. The first mode of the panel exhibits the largest effective mass participation which is often the most damaging of a structure.

Honeycombs with Structured Core for Enhanced Damping

Table 6.1: Sandwich panel core geometries investigated in this chapter. A honeycomb core without damping inserts, a series of cores filled with 10 to 193 DSLJ inserts, and a honeycomb core completely filled with viscoelastic material.
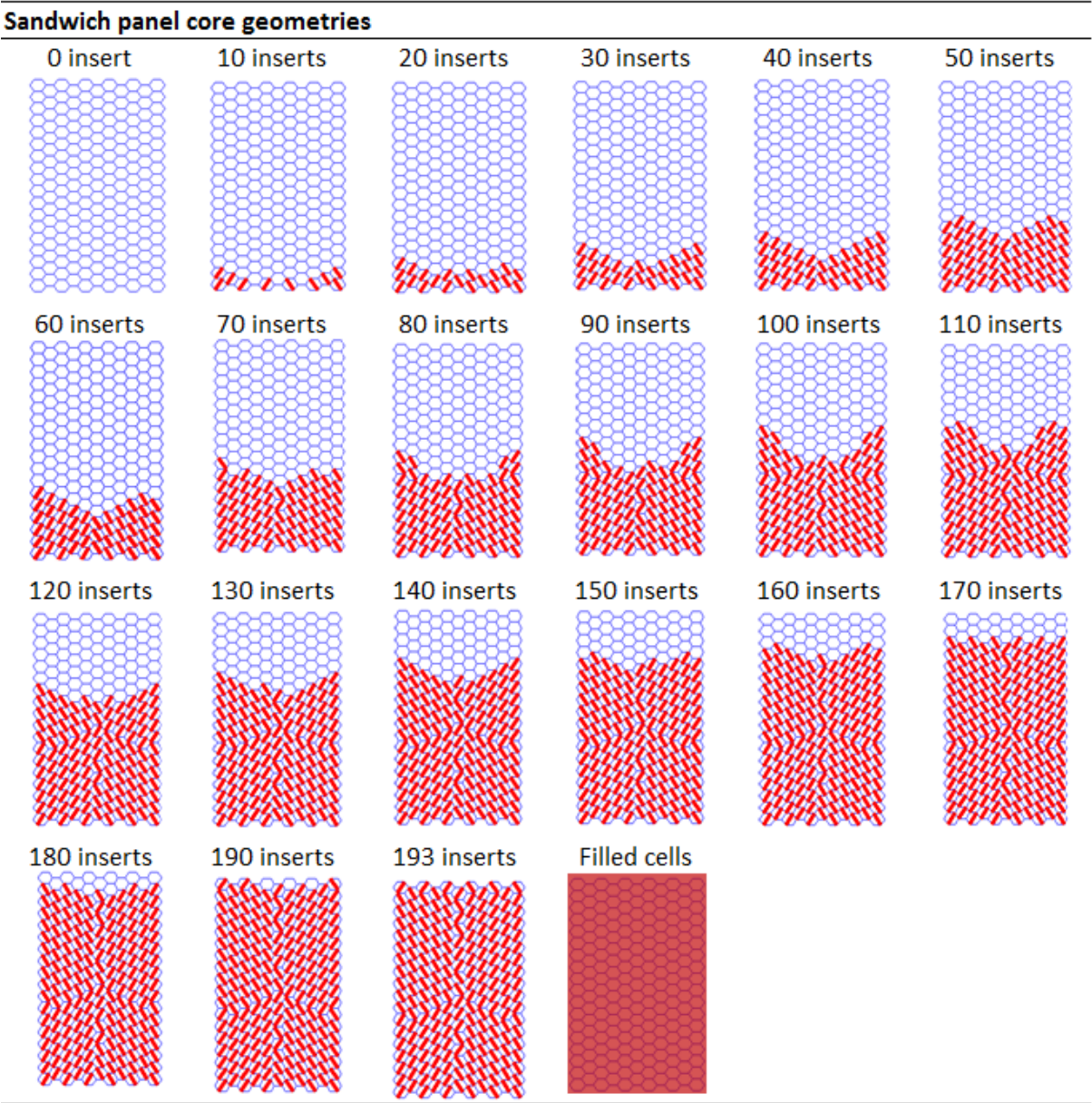
6.2.3 FE Models

Finite element analysis software ANSYS 13 [90] was used to create and simulate the behaviour of models defined in Table 6.1. Four node SHELL63 elastic shell elements with both bending and membrane capabilities have been used to mesh the

Honeycombs with Structured Core for Enhanced Damping

face sheets, the honeycomb core and the thin aluminium rib of the damping insert. Height nodes SOLID45 elastic solid elements have been used to mesh the viscoelastic material of the damping insert. Each unit cell is meshed with 2,107 shell elements. The damping insert is meshed with 846 shell and solid elements. The number of finite elements used in each model varies between approximately 100,000 to 300,000, depending on the number of damping inserts embedded in the honeycomb host structure. Figure 6.4 illustrates the finite element mesh of the honeycomb sandwich panel with embedded damping inserts.

a.

b.

c.
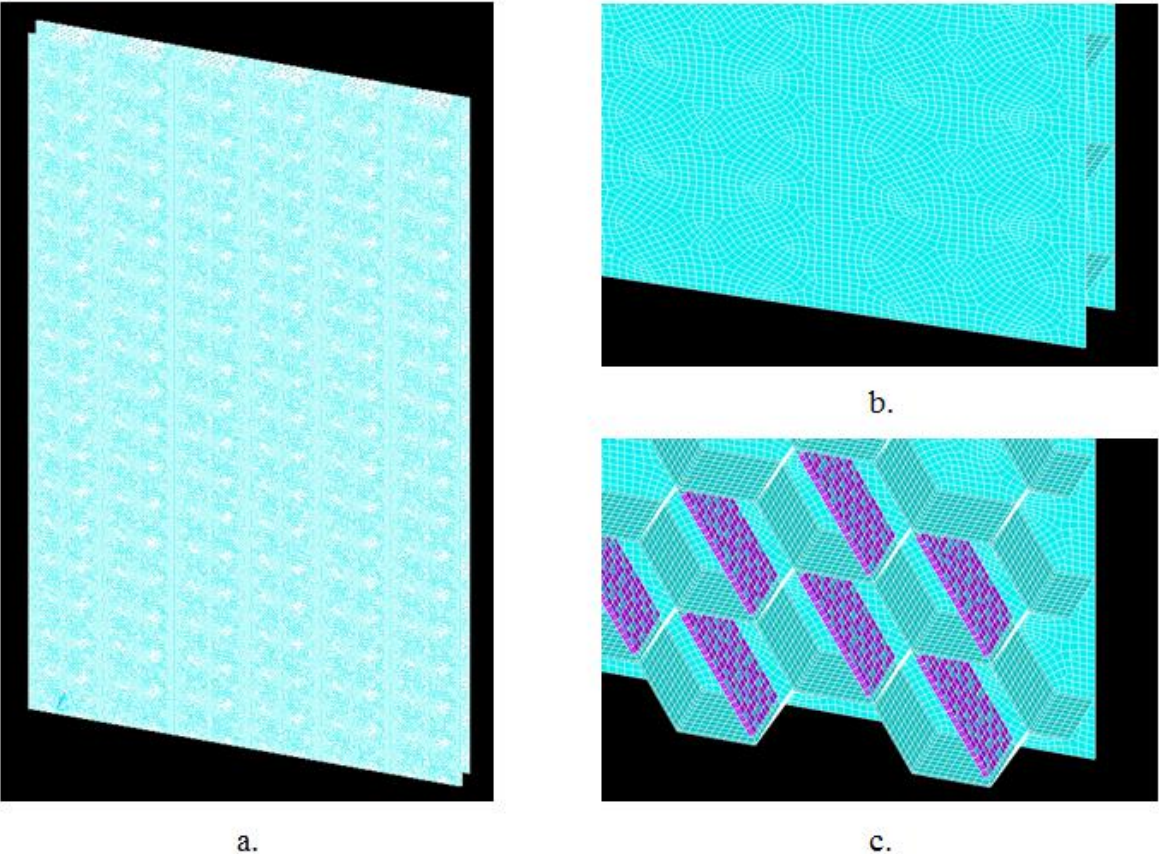
Figure 6.4: FE model of the sandwich panel filled with 20 DSLJ inserts, as studied in this chapter.

6.2.4 Material Properties

Two material properties have been defined. The constituent material of the honeycomb has been modelled with aluminium properties, with a set of linear and

isotropic elastic constants (E_{al} = 70000 MPa, v_{al} = 0.3, ρ_{al} = 2.7 g.cm^3 and η_{al} = 0.0001 [76]). The damping insert has been modelled with arbitrary material properties representing a viscoelastic material, with a set of linear and isotropic elastic constants (E_{visco} = 1MPa, v_{visco} = 0.45, ρ_{visco} = 1.25 g.cm3 and η_{visco} = 0.1 [108]).

6.2.5 FE Analyses

Cantilever boundary conditions were applied to each model described in Table 6.1. All degrees of freedom of nodes located at one edge of the panel were constrained as represented in Figure 6.5.

A normal modal analysis has been performed with ANSYS 13, using the block Lanczos method eigenvalue solver for reduced computational time, to compute the first modal frequency and mode shape of each model.

Bending stiffness and damping properties associated to the first bending mode of each model have been computed from a linear static analysis. A force F of 1 N has been equally distributed to nodes lying on the opposite constrained edge of the sandwich structure in the transverse direction, as illustrated in Figure 6.5. It is assumed that the static deformation of the panel subject to the force F is similar to the deformation of the first bending mode of this panel. The damping properties have been derived using the modal strain energy method [100] [102] [103].
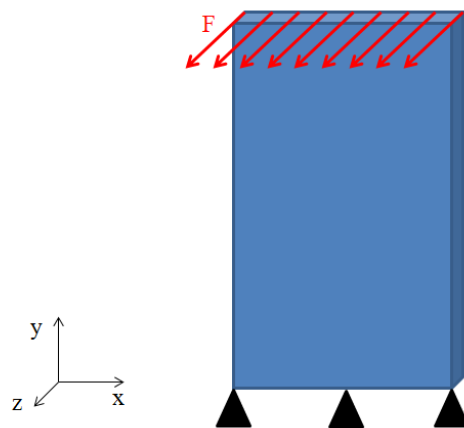
Figure 6.5: Loading and boundary conditions of the sandwich panel.

176

Honeycombs with Structured Core for Enhanced Damping

6.3 Results

Table 6.2 shows the first bending mode frequency, weight, bending stiffness and loss factor of all sandwich panel geometries studied. Table 6.3 shows the variation of these parameters against the sandwich panel with no damping inserts.

The first bending mode frequency of the sandwich panel with DSLJ damping inserts varies up to 5% for geometries with less than 130 inserts. For geometries with a higher number of embedded inserts, the frequency decreases up to 25% for geometries with voids filled with DSLJ damping inserts. The sandwich panel with no damping insert but completely filled with a viscoelastic material presents the maximum frequency variation with a reduction of 64% the frequency of the sandwich panel with no inserts.

The mass of one DSLJ damping insert is approximately 10 g. Therefore, the weight of the sandwich panel with an increasing number of damping inserts is increasing, with an increase of up to 82% compared to the host sandwich panel structure. The sandwich panel with no damping insert but completely filled with a viscoelastic material presents the maximum weight variation with an increase of 1,436% of the frequency of the sandwich panel with no inserts.

The bending stiffness of the sandwich structure slightly increases with the number of DSLJ damping inserts, with an increase of up to 1% compared to the structure completely filled with damping inserts. The bending stiffness of the sandwich panel with no damping insert and the panel completely filled with viscoelastic material are similar.

The loss factor of the sandwich panel with damping inserts increases significantly with the number of DSLJ damping inserts, with an increase of up to 824% compared to the sandwich panel with no embedded inserts. The loss factor of the sandwich structure filled with viscoelastic material is increased by 420% compared to the sandwich panel with no embedded inserts. The loss factor increase of the sandwich structure filled with viscoelastic material is achieved with 40 DSLJ inserts, as illustrated in Figure 6.6.

177

Honeycombs with Structured Core for Enhanced Damping

The modal effective mass of the first bending mode of the geometries studied increases with the number of DSLJ damping inserts. The variation of the modal effective mass remains below 10% for sandwich panel with up to 70 embedded damping inserts compared to the sandwich panel with no damping inserts. The rate of variation increases with added damping inserts. The modal effective mass of the sandwich panel with a damping insert in each of its cells (193 inserts) is increased by 80%. Maximum effective mass variation compared to the sandwich panel with no insert is achieved for the sandwich panel filled with viscoelastic material (691% increase).

Honeycombs with Structured Core for Enhanced Damping

Table 6.2: Frequency, weight, bending stiffness, loss factor and effective mass of a sandwich panels with cores exhibiting various numbers of DSLJ inserts and a core completely filled with viscoelastic material.

Geometry	Frequency [Hz]	Weight [kg]	Bending stiffness [N.m−1]	Loss factor [%]	Effective mass (z direction) [%]
0 insert	1.2E+02	9.5E−02	1.4E+04	1.0E−02	6.2E+00
10 inserts	1.2E+02	9.9E−02	1.4E+04	2.3E−02	6.2E+00
20 inserts	1.2E+02	1.0E−01	1.4E+04	3.4E−02	6.2E+00
30 inserts	1.2E+02	1.1E−01	1.4E+04	4.4E−02	6.3E+00
40 inserts	1.2E+02	1.1E−01	1.4E+04	5.2E−02	6.3E+00
50 inserts	1.2E+02	1.2E−01	1.4E+04	5.9E−02	6.5E+00
60 inserts	1.2E+02	1.2E−01	1.4E+04	6.5E−02	6.6E+00
70 inserts	1.2E+02	1.2E−01	1.4E+04	7.0E−02	6.8E+00
80 inserts	1.2E+02	1.3E−01	1.4E+04	7.4E−02	7.1E+00
90 inserts	1.2E+02	1.3E−01	1.4E+04	7.8E−02	7.4E+00
100 inserts	1.2E+02	1.4E−01	1.4E+04	8.1E−02	7.7E+00
110 inserts	1.1E+02	1.4E−01	1.4E+04	8.4E−02	8.2E+00
120 inserts	1.1E+02	1.4E−01	1.4E+04	8.6E−02	8.5E+00
130 inserts	1.1E+02	1.5E−01	1.4E+04	8.8E−02	8.9E+00
140 inserts	1.1E+02	1.5E−01	1.4E+04	8.9E−02	9.4E+00
150 inserts	1.0E+02	1.6E−01	1.4E+04	9.0E−02	9.8E+00
160 inserts	1.0E+02	1.6E−01	1.4E+04	9.1E−02	1.0E+01
170 inserts	9.8E+01	1.6E−01	1.4E+04	9.2E−02	1.1E+01
180 inserts	9.4E+01	1.7E−01	1.4E+04	9.2E−02	1.1E+01
190 inserts	9.0E+01	1.7E−01	1.4E+04	9.2E−02	1.1E+01
193 inserts	8.9E+01	1.7E−01	1.4E+04	9.2E−02	1.1E+01
Filled cell	4.2E+01	1.5E+00	1.4E+04	5.2E−02	4.9E+01

Table 6.3: Frequency, weight, bending stiffness, loss factor and effective mass variations of a sandwich panels with cores exhibiting various numbers of DSLJ inserts and a core completely filled with viscoelastic material.

Geometry	Frequency variation [%]	Weight variation [%]	Bending stiffness variation [%]	Loss factor variation [%]	Effective mass variation (z direction) [%]
0 insert	0.00E+00	0.00E+00	0.00E+00	0.00E+00	0.00E+00
10 inserts	1.00E−01	4.27E+00	1.60E−01	1.28E+02	2.61E−02
20 inserts	1.88E−01	8.53E+00	3.05E−01	2.40E+02	2.78E−01
30 inserts	2.48E−01	1.28E+01	4.30E−01	3.36E+02	9.99E−01
40 inserts	2.70E−01	1.71E+01	5.35E−01	4.18E+02	2.25E+00
50 inserts	2.45E−01	2.13E+01	6.27E−01	4.88E+02	4.06E+00
60 inserts	1.43E−01	2.56E+01	7.03E−01	5.48E+02	6.56E+00
70 inserts	−8.58E−02	2.99E+01	7.69E−01	5.97E+02	9.90E+00
80 inserts	−5.41E−01	3.41E+01	8.23E−01	6.40E+02	1.42E+01
90 inserts	−1.19E+00	3.84E+01	8.71E−01	6.77E+02	1.92E+01
100 inserts	−2.11E+00	4.27E+01	9.12E−01	7.09E+02	2.48E+01
110 inserts	−3.36E+00	4.69E+01	9.52E−01	7.39E+02	3.15E+01
120 inserts	−4.58E+00	5.12E+01	9.79E−01	7.60E+02	3.72E+01
130 inserts	−6.47E+00	5.54E+01	1.00E+00	7.78E+02	4.40E+01
140 inserts	−8.71E+00	5.97E+01	1.02E+00	7.92E+02	5.07E+01
150 inserts	−1.12E+01	6.40E+01	1.03E+00	8.03E+02	5.73E+01
160 inserts	−1.40E+01	6.82E+01	1.04E+00	8.11E+02	6.34E+01
170 inserts	−1.73E+01	7.25E+01	1.05E+00	8.17E+02	6.98E+01
180 inserts	−2.02E+01	7.68E+01	1.06E+00	8.20E+02	7.44E+01
190 inserts	−2.35E+01	8.10E+01	1.06E+00	8.23E+02	7.90E+01
193 inserts	−2.45E+01	8.23E+01	1.06E+00	8.25E+02	8.03E+01
Filled cell	−6.44E+01	1.44E+03	0.00E+00	4.21E+02	6.92E+02

179
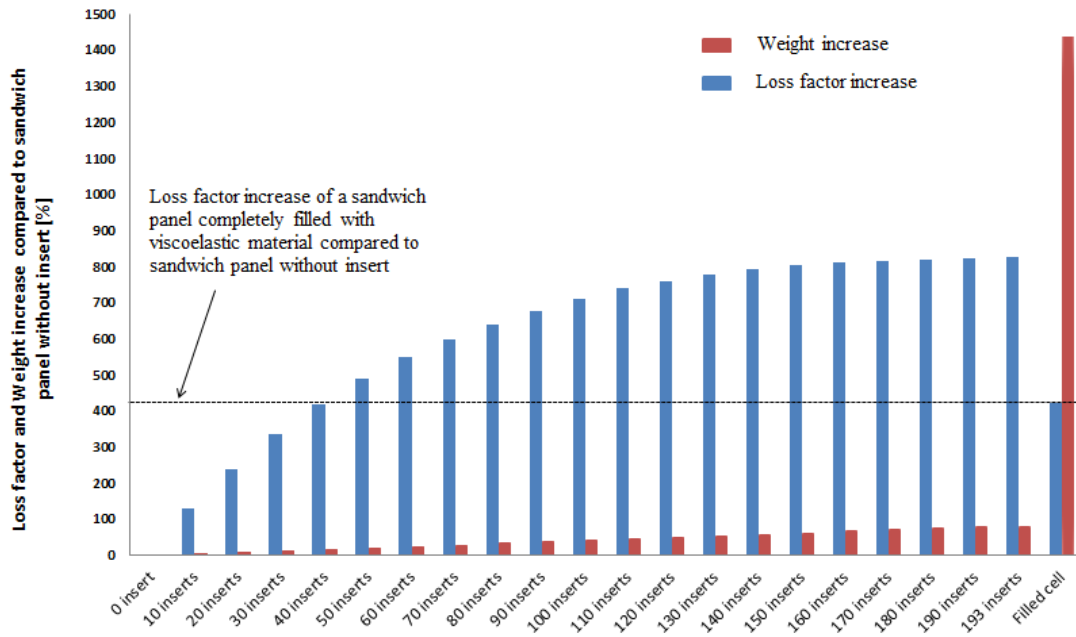
Figure 6.6: Loss factor and weight increase of a sandwich panel with cores exhibiting various numbers of DSLJ inserts and a core completely filled with viscoelastic material compared to the same sandwich panel without damping insert.

Figure 6.7 shows the weight-specific bending stiffness, the ratio between the bending stiffness and the total weight of the geometries studied. The weight-specific bending stiffness decreases with increasing number of embedded damping inserts and is minimal for the sandwich panel completely filled with viscoelastic material.

Honeycombs with Structured Core for Enhanced Damping
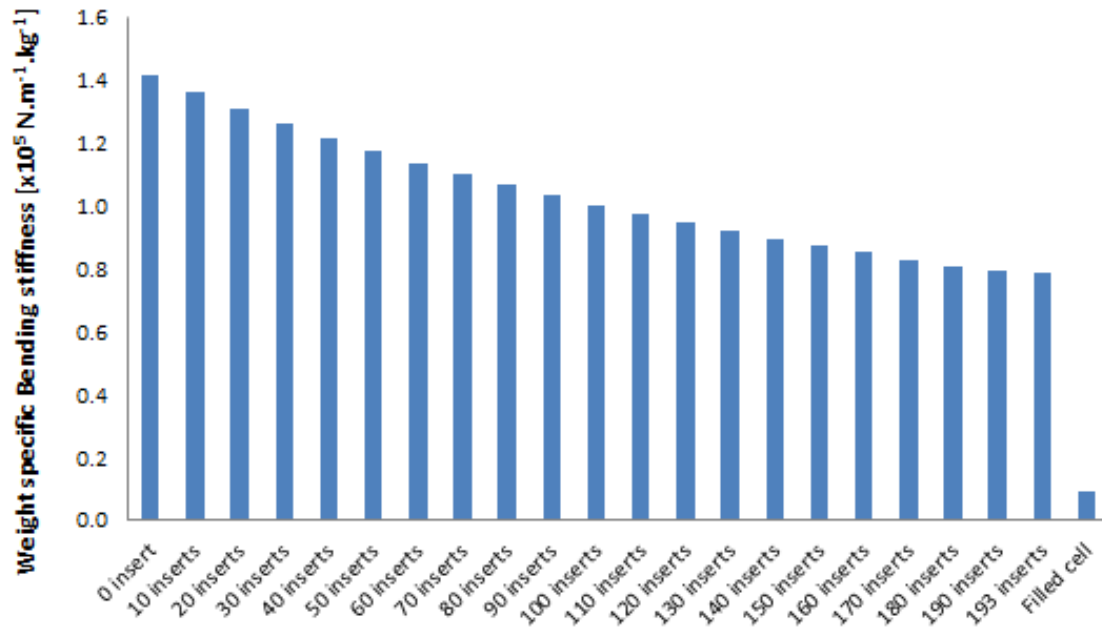
Figure 6.7: Weight-specific bending stiffness of a sandwich panel with cores exhibiting various numbers of DSLJ inserts and a core completely filled with viscoelastic material.

Figure 6.8 shows the weight-specific loss factor, the ratio between the loss factor and the total weight of the geometries studied. The weight-specific loss factor is increasing with the number of embedded DSLJ damping inserts and is maximal for 110 inserts. The weight-specific loss factor decreases for a higher number of DSLJ damping inserts (471% increase compared to the sandwich panel with no insert). Minimum weight-specific loss factor is achieved by the sandwich panel completely filled with viscoelastic material (66% decrease compared to the sandwich panel with no insert).

Honeycombs with Structured Core for Enhanced Damping
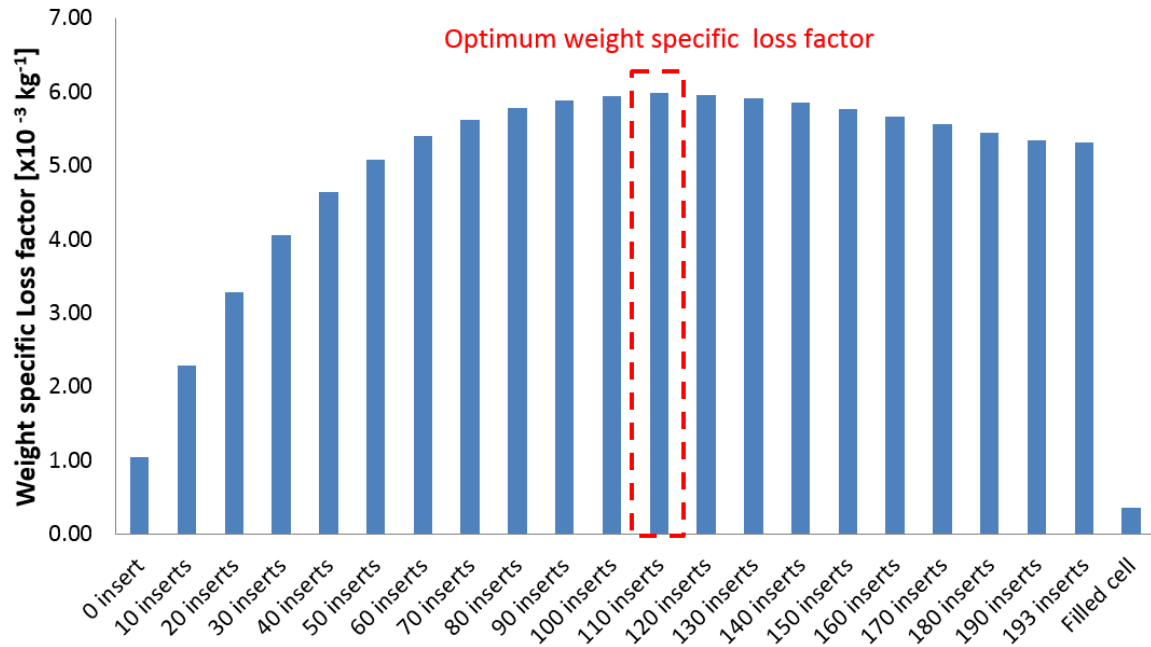
Figure 6.8: Weight-specific loss factor of a sandwich panel with cores exhibiting various numbers of DSLJ inserts and a core completely filled with viscoelastic material..

6.4 Discussion

6.4.1 Bending Stiffness of Sandwich Panel with DSLJ Damping Inserts

The bending stiffness of the sandwich panel has been shown to be almost independent of the number of embedded damping inserts (see Table 6.2 and Table 6.3). A maximum variation of 1% has been highlighted for the sandwich panel completely filled with DSLJ damping inserts compared to the sandwich panel with no insert. This is because the stiffness of the sandwich panel geometries is mostly dependent on the honeycomb sandwich panel host structure geometry, which is the same for all geometries studied in this chapter. The same applies to the bending stiffness of the sandwich panel filled with viscoelastic material.

The weight-specific bending stiffness has been shown to be maximal for the sandwich panel host geometry with no damping insert (see Figure 6.7). Since the variation of the bending stiffness has shown to be independent of the number of

Honeycombs with Structured Core for Enhanced Damping

embedded damping inserts inside the sandwich panel, any added mass caused by the addition of DSLJ damping inserts introduces a reduction of the weight-specific bending stiffness. The sandwich panel filled with viscoelastic material is characterised by the minimum weight-specific bending stiffness since this geometry gives the maximal weight increase.

6.4.2 Modal Frequency of Sandwich Panel with DSLJ Damping Inserts

Partial insertion of DSLJ damping inserts for up to 140 inserts has shown a frequency variation of up to 10% despite a maximum weight increase of 60% for the sandwich panel geometry with 140 inserts. Therefore, partial insertion of DSLJ damping inserts has a minor impact on the first bending mode frequency response of a sandwich panel. This is a consequence of the methodology used for partial filling and orientation of the DSLJ damping insert inside the sandwich host structure. As shown in Table 6.1, damping inserts are localised near the constrained edge of the panel where the relative displacement between opposite edges of the honeycomb unit cell wall is maximal (Chapter 2). Therefore, the added mass of the DSLJ insert does not have a significant impact on the dynamic behaviour of the panel. This is illustrated in Table 6.3, which shows a 10% variation of the transverse modal effective mass (z direction) for up to 70 added damping inserts.

Geometries with more than 140 damping inserts have higher impact on the frequency variation of the first bending mode of the honeycomb sandwich panel host structure. The first bending frequency of the panel with DSLJ damping inserts in each of its cells is decreased by 25% compared to the frequency of the sandwich panel host structure. The larger influence on the frequency variation with increasing numbers of DSLJ damping inserts is caused by the location of the damping insert. With increased numbers of damping inserts, cells further away from the constraining edge of the sandwich panel are filled. Therefore, these geometries have larger impact on the transverse modal effective mass of the panel, i.e. larger impact on the dynamical response of the structure. The sandwich panel filled with viscoelastic material is characterised by the maximum frequency variation since this geometry gives the maximal weight increase and transverse modal effective mass.

6.4.3 Loss Factor of Sandwich Panel with DSLJ Damping Inserts

The loss factor of the sandwich panels studied had a positive relationship with the number of DSLJ inserts used. The geometry filled with DSLJ damping inserts has shown an 825% loss factor increase compared to the sandwich panel geometry with no inserts. With increasing numbers of damping inserts inside the sandwich host structure, the total strain energy stored in the viscoelastic material of the damping inserts increases, and, therefore, the loss factor. It should be noted that the rate of the loss factor variation is maximal for small numbers of inserts added to the sandwich host structure (see Figure 6.6). This is because the first damping inserts are located in cells exhibiting maximum relative displacement between their opposite walls, therefore, storing more strain energy than the damping inserts placed in cells that have less relative displacements between their opposite walls. The loss factor of the panel filled with viscoelastic materials has shown a loss factor increase of 420%, reaching the loss factor of the geometry with 40 DSLJ damping inserts. Despite having more viscoelastic material to dissipate energy, the loss factor of the panel filled with viscoelastic material does not achieve the performance of the DSLJ damping inserts. This is because complete viscoelastic material filling of the cell is not an efficient method to add the damping material, since most of the material is not loaded by the surrounding walls of the honeycomb cell (Chapter 5). This also explains why the sandwich panel filled with viscoelastic material showed the minimal weight-specific loss factor with all the geometries studied (see Figure 6.8). The added damping provided by the viscoelastic material filling the cells does not balanced the added weight, hence, providing less energy dissipation on a density basis than the host sandwich panel. All geometries with DSLJ damping inserts have shown an increase of the weight-specific loss factor compared to the host sandwich panel with an optimum solution with 110 CLD damping inserts. This optimum configuration gives a 739% loss factor increase for a 47% added mass compared to the sandwich panel without damping inserts, with minimal impact on the bending stiffness and first natural frequency of the structure. Hence, partial filling of the honeycomb cells performs better on a density basis than the complete filling of all the cells of the sandwich panel.

184

6.5 Conclusion

Enhancement of the damping loss factor of the first bending mode of a honeycomb sandwich panel with CLD damping inserts has been investigated in this chapter and benchmarked against a honeycomb sandwich panel with no damping insert and a sandwich panel filled with viscoelastic material.

The sandwich panel completely filled with viscoelastic material is an inefficient way of improving the damping capacity of a sandwich panel on a density basis. The weight penalty of this solution has been shown to be too large to compensate for the added damping provided by the viscoelastic material.

On the other hand, partial filling with DSLJ damping inserts of the honeycomb sandwich panel have been shown to be a very effective solution for improving the damping capacity of a honeycomb sandwich panel on a density basis, with minimal influence on the stiffness and first frequency of the panel. An optimum configuration using 110 embedded DSLJ damping inserts has been found for the first bending mode of the panel, giving a 739% loss factor increase for a weight increase of only 47% compared to the host sandwich panel structure without DSLJ inserts.

Honeycombs with Structured Core for Enhanced Damping

Chapter 7. Discussion

Seminal work by Huang et al. [11] presented the enhanced damping properties of the honeycomb sandwich panel due to the introduction of viscoelastic material inside the hollow honeycomb core. This method, however, severely increased the weight of the sandwich panel, therefore mitigating the excellent density-specific properties. Subsequently, Woody et al. [47] and Wayne et al. [98] investigated the damping properties of honeycomb structures by respectively filling target cells within the honeycomb structure and partially filling the honeycomb cell voids with the use of damping inserts in the form of corner fillets in the corner of 'auxetic' honeycomb unit cells to reduce the weight increase. Both methods showed large enhancements of the damping properties of the honeycomb structure with reduced added mass. The aim of the current work has been to combine and develop both methods to investigate the competitive demand between increased damping properties and minimum added mass. The present work describes the optimisation of the location of the damping insert material for use within the honeycomb unit cell and presents an effective method for location of these damping inserts within a honeycomb sandwich panel. The loss factor of a honeycomb sandwich panel partially filled with DSLJ inserts has been evaluated at 0.084% for the first bending mode of the panel for a 47% added mass compared to the host sandwich panel without insert. The lost factor of the host sandwich panel was evaluated at 0.01%. Finite element models and analytical predictions have been developed to characterise honeycomb structures with damping inserts and have been validated against well-established analytical predictions [2] [18].

7.1   Location of Damping Material within a Honeycomb Unit Cell

As an initial step for characterising optimal locations for damping material within the void of a honeycomb unit cell, a study has been undertaken to understand the primary deformation mechanism of the unit cell within a honeycomb and sandwich panel subjected to vibration in Chapter 2. The local out-of-plane shear strains of the honeycomb unit cell within a honeycomb panel have been found to be two orders of magnitude lower than the in-plane strains for its first fundamental modes. This is

because bending is the principal deformation mechanism of the honeycomb unit cell within a honeycomb panel. Therefore, planes situated away from the neutral bending plane of the honeycomb panel exhibit larger in-plane tension/compression than transverse shear loading (see Table 2.6 to Table 2.9). For sandwich panels, in-plane tension/compression strains and transverse shear strains are of similar magnitude because the skins of the sandwich panel limit the bending deformation of the honeycomb core. It should be noted that, as a consequence, the bending stiffness of a sandwich panel is significantly higher than the honeycomb core panel itself, and is characteristic of the excellent density-specific properties of a sandwich structure.

The locations of the filling damping material, in this case a viscoelastic elastomer, within the honeycomb cell void have been studied in Chapter 3, assuming that the optimal locations for damping inserts lie where the relative displacements of the honeycomb cell walls are maximal. Damping inserts placed in these locations are deformed at the highest axial strain possible, therefore dissipating maximum energy. Analytical expressions have been derived using beam theory and assuming that the damping material does not contribute to the deformation of the unit cell. This approach ignores the stiffness of the viscoelastic insert assuming that the stiffness of the cell itself dominates, as supported by Abd El-Sayed et al. [99]. These expressions have been used to characterise these optimal locations under in-plane loading cases reflecting the deformation of core honeycomb cells in a range of possible structural vibration modes studied in Chapter 2. Out-of-plane transverse shear loading has not been studied since the relative cell walls motion is less than for in-plane loading as demonstrated in Chapter 2.. The optimal locations of inserts within cells have been demonstrated to be sensitive to both cell geometry and the in-plane loading directions, as illustrated in Figure 3.8, Figure 3.10, Figure 3.12 and Figure 3.13. The optimal location for a regular honeycomb cell loaded in tension compression forms a single horizontal ligament in the middle of the honeycomb cell void (see Figure 3.8), whereas, for in-plane shear loading, it forms a double cross ligament between the top and bottom walls of the honeycomb unit cell. These locations have been shown to be a consequence of the characteristic parameters

Honeycombs with Structured Core for Enhanced Damping

defining the honeycomb unit cell and were discussed in further detail in Chapter 3. The locations of damping materials predicted with the analytical model developed for this study have been found to be similar to the results of the topological optimisation run for regular and 'auxetic' honeycomb unit cells taking into account of the stiffness of the viscoelastic material, validating the assumptions made in the analytical model for predicting the best locations for damping inserts inside honeycomb cells. Specifically, the fact that the stiffness of the damping insert was not accounted in these analytical models. It should be noted that this will be invalid for cases where stiff or large inserts are used.

Regular honeycomb unit cells with damping material in the optimal location highlighted previously have been studied in Chapter 4 and showed a 26.7% increase of the density-specific loss modulus for in-plane axial loading and a 16% increase for in-plane shear loading compared to a honeycomb unit cell completely filled with viscoelastic material, as described by Huang et al. [11]. Despite having less damping material than a filled honeycomb unit cell, honeycomb unit cells partially filled with damping showed higher density-specific loss modulus because the ratio between the strain energy stored in the viscoelastic material and its volume is reduced between the optimum configuration for the damping insert and the filled honeycomb cell. Strain plots of the different insert geometries studied illustrated this characteristic in Figure 4.13, Figure 4.14 and Figure 4.20. Partial filling of the honeycomb unit cell in the form of fillets, as described by Miller et al. [98], has been shown to be an effective location for damping inserts in the very specific cases of an auxetic honeycomb with a large aspect ratio (α >3) as described in their patent application. Fabrication of metallic honeycomb panels with such unit cell geometries is, however, not possible using the current well-established expanded and corrugated manufacturing processes, therefore creating evident limitation in the case of mass production. Hence, these damping insert locations have not been further investigated. It should be noted that the results of this analysis have been derived from a linear static analysis using the modal strain energy method to quantify the damping properties of the honeycomb unit cell with damping inserts [2]. The

viscoelastic material dependency against frequency and temperature has not been analysed in this study. Generic viscoelastic properties have been used to quantify the density-specific loss modulus efficiency against honeycomb unit cells without inserts and completely filled with viscoelastic material. As defined, this analysis provides a methodology for comparison of the damping capability of honeycomb unit cells with different geometries of damping inserts.

7.2 Effective Damping Insert Geometry within a Honeycomb Unit Cell

Partial filling of the honeycomb unit cell with a unique damping material in the optimal locations highlighted has been shown previously to enhance the density-specific loss modulus of the honeycomb unit cell compared to a honeycomb unit cell completely filled with a damping material. Since the optimal location for damping inserts have been identified in locations where the relative displacement between opposite displacement of the honeycomb cell walls is maximal, this assumes that most of the dissipation by the damping insert is provided by its axial deformation. It is well known that shear deformation is very effective for dissipating energy and more efficient than tension/compression loadings [27] [109]. In order to enhance the energy dissipation of the damping insert made from a single damping material, the concept of SLJ damping inserts has been investigated in Chapter 5. These SLJ damping inserts are made from two different materials. A viscoelastic material forms a layer constrained between two or three thin sheets of a stiffer material, as illustrated in Figure 5.1. The SLJ damping inserts have shown significantly higher density-specific loss modulus for the smallest introduction of viscoelastic material (damping insert filling 5% of the honeycomb cell void). The density-specific in-plane and shear loss moduli have respectively been shown to be 280 and 100 times higher than a honeycomb unit cell completely filled with viscoelastic material as described by Huang et al. [11]. Since the SLJ inserts have been located in the optimal location for axial loading of the insert within the honeycomb cell void, the constrained layers load the viscoelastic layer in shear inducing a shear strain inversely proportional to the viscoelastic layer thickness, therefore providing higher energy dissipation for thinner viscoelastic layer thicknesses. This explains why these SLJ damping inserts are characterised by such

Honeycombs with Structured Core for Enhanced Damping

large improvement of the density-specific loss modulus compared to inserts made only from a viscoelastic material. This is illustrated in Figure 4.13 and Figure 5.15, where the maximal strain inside the viscoelastic material reaches 0.2% for simple damping inserts and 3% for DSLJ inserts under the same loading condition. It should be noted that the fatigue shear strength and adhesive strength of the viscoelastic material have not been investigated and are likely to impose constraints on the minimum thickness of the viscoelastic layer for a given fatigue life requirement, therefore limiting its damping capability.

7.3   Partial Filling of Sandwich Panel with Damping Inserts

The influence on the damping loss factor of the first bending mode of a sandwich structure with embedded DSLJ damping inserts has been investigated in Chapter 6. Partial filling of selected voids within the honeycomb panel exhibits the best weight-specific loss factor, which is 12% higher than the honeycomb sandwich panel filled with damping inserts in all of its cells, 4.7 times higher than the host honeycomb sandwich panel and 15.8 times higher than the honeycomb sandwich panel completely filled with viscoelastic material, as described by Huang et al. [11] (see Figure 6.8). The loss factor of the best weight specific loss factor configuration with 110 DSLJ inserts was evaluated at 0.084% for the first bending mode of the sandwich panel which compares with a loss factor of 0.01% for the host sandwich panel without inserts and a loss factor of 0.052% for the sandwich panel completely filled with viscoelastic material. The cell voids selected for partial filling of the honeycomb host structure resulted from the study in Chapter 2 of the modal deformation of the first bending mode of the structure. Cell voids with the highest local in-plane tension/compression have been progressively filled with DSLJ inserts and are, therefore, the best locations for damping inserts since they have been shown to be more effective when loaded axially. Since the local in-plane deformation of each cell within the sandwich structure is dependent on its location within the panel, this explains why partial filling of the sandwich structure has been shown to be more effective on a weight basis than complete occupation of all the cell voids with DSLJ damping inserts. It should be noted that the best locations of damping

Honeycombs with Structured Core for Enhanced Damping

inserts identified in Chapter 6 are valid only for the first bending mode of the sandwich structure since the local in-plane strain of the cells have been shown to be dependent on the mode shape of the host structure in Chapter 2. Therefore, damping inserts could be located within the sandwich panel to target specific modes of deformation and damp critical frequency ranges. This could be a very efficient way of designing next generations of gas turbine fan blades using DSLJ damping inserts embedded in a low-density honeycomb panel within the hollow structure of the blade. Significantly, since these damping inserts are located within the sandwich structure, they would have minimum impact on the aerodynamic performance of the blades and be protected from their harsh conditions of use (air flow speed, buzz saw, bird strike events, etc.).

Additionally, partial filling of a sandwich panel was demonstrated to have a marginal impact on the dynamical response of the sandwich structure with the first modal frequency varying only by 3.4% for the optimal partial filling solution with DSLJ inserts found in Chapter 6 (see Table 6.3). This is because partial filling of the honeycomb sandwich structure does not largely impact on the total weight and stiffness of the structure as opposed to complete filling of the honeycomb cell voids, which has been characterised by a frequency drop of 64.4% because of the large added mass caused by the introduction of the damping material in large quantities.

It is also important to note that the honeycomb sandwich structure simply filled with viscoelastic material as described by Huang et al. [11] was shown to have a weight-specific loss factor lower than the sandwich panel host structure itself. Since honeycomb sandwich panels are used in application where the weight penalty is critical, the attraction of this solution appears to be limited; for instance, in transport applications.

Manufacturing methods for the fabrication of sandwich panels with embedded SLJ inserts have not been investigated in this thesis and could potentially appear to be challenging given the complexity of the geometry and the fact that these inserts are not made from a sole material. It is believed that the recent development in additive

Honeycombs with Structured Core for Enhanced Damping

layer manufacturing processes, with the use of 3D printing technology, could result in very efficient processes for manufacturing SLJ inserts, which could then be embedded in the honeycomb core of a sandwich structure.

Honeycombs with Structured Core for Enhanced Damping

Honeycombs with Structured Core for Enhanced Damping

Chapter 8. Conclusion

This thesis focused on the vibration damping enhancement of honeycomb sandwich panels and explored the competing demands between damping and the addition of extra mass.

The problem was tackled by initially characterising the main local deformation mechanism of unit cells within a sandwich panel subjected to vibration. In-plane deformation of the honeycomb unit cell has been shown to be the predominant mode of deformation for honeycomb panels, whereas in-plane and transverse shear deformation have been shown to be the predominant mode of deformation for honeycomb sandwich structures. It was also highlighted that the magnitude and loading of the honeycomb unit cell are dependent on its location within the honeycomb or sandwich panel and the mode shape of the panel.

An optimisation study has been done on diverse honeycomb unit cell geometries for finding locations where the relative displacement between the honeycomb cell walls of the void is maximal under in-plane loadings. Therefore, these locations are valid for both honeycomb panel and sandwich panel together since in-plane loadings have been characterised as the main deformation mechanism for both structures. Transverse shear loading has not been studied in this work and could be used as a subject for further study for optimisation of the damping performance of a sandwich structure. These locations have shown to be dependent on the nature of the loading, i.e. in-plane tension/compression or in-plane shear loading of the honeycomb unit cell and the unit cell geometry.

Analytical expressions and finite element analysis have been used to investigate partial filling of the honeycomb unit cell with a damping material, in this case a viscoelastic elastomer, in the target locations identified previously where the relative displacement between the honeycomb cell walls is maximal. Damping inserts in the form of ligaments partially filling the honeycomb cell void have been characterised with a 26% increase of their density-specific loss modulus compared to cells filled with damping material for in-plane tension/compression loading.

Honeycombs with Structured Core for Enhanced Damping

The form of the damping insert itself has also been analysed for enhancement of the dissipation provided by the damping material. DSLJ damping inserts, placed in the location where the relative displacement between the honeycomb cell walls of the void is maximal under in-plane loadings, have been characterised with very significant damping improvements compared to honeycomb cells completely filled with viscoelastic material. This insert geometry showed a density-specific loss modulus for tension/compression loading increased by 280 compared to filled honeycomb unit cells. Such enhancement is provided by the use of SLJ inserts inside the honeycomb unit cell because the constrained layer of the damping insert introduced a high shear strain in the damping material layer, which is a very efficient mechanism for dissipation of vibrational energy.

The loss factor of the first bending mode of a cantilever sandwich panel has been shown to be significantly enhanced with the use of embedded SLJ inserts for a small addition of mass by the damping inserts. The loss factor of the sandwich structure filled with an SLJ insert in every cell was shown to be enhanced by 8.2 times for an 82% increase in mass compared to the honeycomb host sandwich panel. The solution described by Huang et al. consisting of a honeycomb sandwich panel completely filled with viscoelastic material gave a loss factor increase of 4.2 times for a 14 times increase in mass compared to the host sandwich panel, therefore not efficient on a density basis. Partial filling of target cells of the honeycomb sandwich structure with SLJ damping inserts orientated appropriately to maximise the shear strain of the viscoelastic layer has been shown to be the most efficient method for enhancement of the loss factor of the structure on a density basis. Partial filling solutions with SLJ inserts have also been shown to have a reduced impact on the dynamical behaviour of the host structure. The optimum partial filling solution identified on a density basis gave a first modal frequency reduction of only 3.5% compared to the host structure.

This thesis primarily focussed on developing a concept which enhances the damping properties of honeycomb sandwich panel without largely increasing the weight of the panel using analytical models and finite element analyses. Further work is required

Honeycombs with Structured Core for Enhanced Damping

so as to complete and validate the work presented in this thesis. Guideline for further is described subsequently.

- Analysis methods: a combination of analytical and FE linear static and modal analyses have been used in this thesis to demonstrate the concept of using viscoelastic damping insert. As such, the influence of the loading frequency and temperature have not been investigated in this thesis.

- Strength capability of the damping insert: stress analysis of detailed FE models of the different insert geometries presented in this thesis should be carried out to determine the maximum loading capability of the insert and investigate potential debonding of the insert with the honeycomb host structure.

- Manufacturability of the damping insert: investigation on the manufacturability of the insert should be carried out to understand the feasibility of manufacturing the damping inserts presented in this thesis.

- Experimental validation: experiments should be carried on sandwich panels with damping inserts to validate their damping enhancement.

- Optimisation of the number and location of damping inserts within sandwich panels: an engineered methodology has been presented in this thesis so as to optimise the number and location of damping inserts within a sandwich panel. Optimisation algorithms could be investigated so as to improve the result presented in this thesis. Furthermore, only the first bending mode of a sandwich panel has been investigated to quantify the damping enhancement given by the introduction of damping inserts. The optimisation of the number and location of damping inserts could be extended to investigate the damping enhancement of a multitude of natural modes of the panel, of different panel geometries and of different boundary conditions.

It should be noted that part of the above suggestions for further work are currently under investigation in another PhD research project by Pierre Amjaud from the University of Exeter, supervised by Prof. Chris Smith.

Honeycombs with Structured Core for Enhanced Damping

Honeycombs with Structured Core for Enhanced Damping

References

[1] Vinson, J. R., 2001. Sandwich Structures, *Applied Mechanics Review*, 54 (3).

[2] Gibson, L. J. and Ashby, M. F., 1997.*Cellular Solids: Structure and Properties_ Second Edition*, Cambridge.

[3] Bitzer, T. *Honeycomb Technology: Materials, Design, Manufacturing, Applications and Testing*, Chapman & Hall.

[4] Rao, M. D., 2003. Recent Applications of Viscoelastic Damping for Noise Control in Automobiles and Commercial Airplanes. *Journal of Sound and Vibration*, 262 (3), pp.457-474.

[5] Herrmann, A., Zahlen, P. and Zuardy, I., 2005. Sandwich Structures Technology in Commercial Aviation,*Sandwich Structures 7: Advancing with Sandwich Structures and Materials*, pp.13-26.

[6] Tomlinson, G. R., 1996. Overview of Active/Passive Damping Techniques Employing Viscoelastic Materials. *3rd International Conference on Intelligent Materials and 3rd European Conference on Smart Structures and Materials*, vol. 2779, pp.656-669.

[7] Park, G., 2007. The Use of Active Materials for Machining Processes: A Review. *International Journal of Machine Tools and Manufacturing*, p.47.

[8] Preumont, A., 2002. *Vibration Control of Active Structure: An Introduction*, Kluwer Academic Publishers.

[9] Romberg, O., 2007, Passive Damping of Spacecraft Sandwich Panels. *1st European Air and Space Conference, 10-13.*

[10] Michon, G., Almajid, A., Ferrero, J. F., Aridon, G., Fascio, V. and Heurteau, J. P., 2009. Dissipation Mechanisms Identification of Soft Hollow Particle-dampers in Honeycomb Structures for Micro-vibration Environments. *11th European Conference on Spacecraft Structures, Materials and Mechanical Testing*.

Honeycombs with Structured Core for Enhanced Damping

[11] Huang, H., Joe, C. R. and Kim, D. U., 2005. Mechanical Behavior of Rubberfilled Multifunctional Honeycomb Sandwich Composite. *Sandwich Structures 7: Advancing with Sandwich Structures and Materials*, pp.671-680.

[12] Lagoudas, D. C., 2008. *Shape Memory Alloys: Modelling and Engineering Applications*, Springer.

[13] Petras, A. and Sutcliffe, M. P. F., 1999. Failure Mode Maps for Honeycomb Sandwich Panels, *Composite Structures*, p.44.

[14] Akay, M. and Hanna, R., 1990. A Comparison of Honeycomb-core and Foam-core Carbon-fibre/Epoxy Sandwich Panels, *Composites,* 21(4), pp.325-331.

[15] Wadley, H. N. G., 2006. Multifunctional Periodic Cellular Metals. *Philosophical Transactions: Mathematical, Physical and Engineering Sciences*, 364(1838), pp.31-68.

[16] Lu T. J., 1998. Heat Transfer Efficiency of Metal Honeycombs. *International Journal of Heat and Mass Transfer*, 42, pp.2031-2040.

[17] Zhang, J. and Ashby, M. F., 1992. The Out-of-plane Properties of Honeycombs. *International Journal of Mechanical Sciences*, 34(6), pp.475-489.

[18] Master, I. G. and Evans, K. E., 1996. Models for the Elastic Deformation of Honeycombs. *Composite Structures*, 35(4), pp.403-422.

[19] Kim, B. and Christensen, R. M., 2000. Basic Two-dimensional Core Types for Sandwich Structures. *International Journal of Mechanical Sciences*, 42(4), pp.657-676.

[20] Mostafa, N. et al., 2009. A Study of Melt Flow Analysis of an ABS-Iron Composite in Fused Deposition Modelling Process. *Tsinghua Science and Technology*, 14(1), pp.29-37.

Honeycombs with Structured Core for Enhanced Damping

[21] Scott Burton, W. and Noor, A. K., 1997. Structural Analysis of the Adhesive Bond in a Honeycomb Core Sandwich Panel. *Finite Elements in Analysis and Design*, 26(3), pp.213-227.

[22] Hexcel, 1986. *The Basics of Bonded Sandwich Construction*. TSB 124 Hexcel Corporation, Dublin, CA.

[23] Noor, A. K., Burton, W. S. and Bert, C. W., 1996. Computational Models for Sandwich Panels and Shells. *Applied Mechanic Review*, 49(3).

[24] Gibson, L. J., 1989. Modeling the Mechanical Behavior of Cellular Materials. *Materials Science and Engineering*: A 110.

[25] Daniel, I. M. and Gdoutos, E. E., 2009. *Failure Modes of Composite Sandwich Beams, Major Accomplishments in Composite Materials and Sandwich Structures*, pp.197-227.

[26] Triantafillou, T. C. and Gibson, L. J., 1987. Failure Mode Maps for Foam Core Sandwich Beams. *Materials Science and Engineering*, 95, pp.37-53.

[27] Petras, A. and Sutcliffe, M. P. F., 1999. Failure Mode Maps for Honeycomb Sandwich Panels. *Composite Structures*, 44(4), pp.237-252.

[28] McCormach, T. M. et al., 2001. Failure of Sandwich Beams with Metallic Foam Cores. *International Journal of Solids and Structures*, 38(28-29), pp.4901-4920.

[29] Jones, D. I. G., 2001. *Handbook of Viscoelastic Vibration Damping*. Wiley.

[30] Morvan, O., 2008. *Cours de Vibration des Systèmes Discrets*, ENSMM.

[31] de Silva, C. W., 2007. Vibration Damping, Control, and Design. *Mechanical Engineering Series*, 1st ed., CRC Press.

[32] Tomlinson, G. R., 1990. The Use of Constrained Layer Damping in Vibration Control. *International Journal of Mechanical Sciences*, 32(3), pp.233-242.

Honeycombs with Structured Core for Enhanced Damping

[33] Chung, D. D. L., 2001. Review Material for Vibration Damping. *Journal of Material Science*, p.36.

[34] Chen Y. and Gibson R. F., 2003. Analytical and Experimental Studies of Composite Isogrid Structures with Integral Passive Damping. *Mechanics of Advanced Materials and Structures*, 10, pp.127-143.

[35] Oberst, H., 1956. Maximum Vibration Damping by Means of Suitably Composed High Polymers. *The Journal of the Acoustical Society of America*, 28(4), p.781.

[36] Oberst, H., 1952. Über die Dämpfung der Biegeschwingungen dünner Bleche durch fest haftende Belage, *Acustica* 2 (Akustische Beih. 4), pp.181-194.

[37] Kent, W. W., Frederick, A. J. and Lee, J. K. General Electric, 2007. Vibration Damper Coating for a Fan Blade, Patent Number: GB2430985..

[38] Kerwin, Jr., 1959. Damping of Flexural Waves by a Constrained Viscoelastic Layer. *The Journal of the Acoustical Society of America*, 31(7).

[39] Jung, W.-Y. and Aref, A. J., 2003. A Combined Honeycomb and Solid Viscoelastic Material for Structural Damping Applications. *Mechanics of Materials*, 35(8), pp.831-844.

[40] Bhattacharya, B., Tomlinson, G. R. and House, J. R., 1999. Effect of Shapes of Viscoelastic Inserts on Vibration Absorption in Laminated Composites, Smart Structures and Materials. Passive Damping and Isolation, 3672 (presented at the Smart Structures and Materials 1999: Passive Damping and Isolation, Newport Beach, CA, USA: SPIE), pp.316-323.

[41] Marvalova, B., 2008. Viscoelastic Properties of Filled Rubber. *Experimental Observations and Material Modelling, Constitutive Models for Rubber_Proceedings-,* Vol.5, Balkema.

[42] Burlayenko, V. N., Sadowski, T., 2010. Effective Elastic Properties of Foam-filled Honeycomb Cores of Sandwich Panels. *Comps Struct*, 92(12), pp.2890-2900.

Honeycombs with Structured Core for Enhanced Damping

[43] Reuterlöv, S., 2002. Causes for and Preventive Action to Avoid, Disbonds and Blistering. *DIAB Technologies*, Divinycell International AB, Laholm, Sweden.

[44] Reid, S. R., Reddy, T. Y. and Gray, M. D., 1986. Static and Dynamic Axial Crushing of Foam Filled Sheet Metal Tubes. *Int J Mech Sci*, 23, pp.295-322.

[45] Reddy, T. Y. and Wall, R. J., 1988. Axial Compression of Foam Filled Thin-walled Circular Tubes. *Int J Impact Eng*, 7, pp.151-166.

[46] Alavi Nia, A., Sadeghi, M. Z., 2010. The Effects of Foam Filling on Compressive Response of Hexagonal Cell Aluminum Honeycombs under Axial Loading - Experimental Study. *Materials and Design*, 31(3), pp.1216-1230.

[47] Woody, S. C., Smith, S. T., 2006. Damping of a Thin-walled Honeycomb Structure using Energy Absorbing Foam. *Journal of Sound and Vibration*, 291(1-2), pp.491-502.

[48] Saluena, C., Poschel, T., and Esipov, S. E., 1999. Dissipative Properties of Vibrated Granular Materials. *Physical Review*, 59(4), pp.4422-4425.

[49] Cempel, C. and Lotz, G., 1993. Efficiency of Vibrational Energy Dissipation by Moving Shot. *Journal of Structural Engineering*, 119(9), pp.2624-2652.

[50] Friend, R. D. and Kinra, V. K., 2000. Particle Impact Damping. *Journal of Sound and Vibration*, 233(1), pp.93-118.

[51] Simonian, S., 2004. Particle Damping Applications, 45th AIAA/ASME/ASCE/AHS/ASC Structures, Structural Dynamics and Materials Conference, Palm Springs, California.

[52] Yang, Y., 2003. *Development of Master Design for Particle Impact Dampers*. PhD thesis, Pennsylvania State University.

[53] Saeki, M., 2005. Analytical Study of Multi-particle Damping. *Journal of Sound and Vibration*, 281, pp.1133-1144.

Honeycombs with Structured Core for Enhanced Damping

[54] Liu, W., Tomlinson, G. R. and Rongong, J. A., 2004. The Dynamic Characterization of Disk Geometry Particle Dampers. *Journal of Sound and Vibration*, 280, pp.849-861.

[55] Ramachandran, S. and Lesieutre, G., 2008. Dynamics and Performance of a Harmonically Excited Vertical Impact Damper. *Journal of Vibration and Acoustics*, p.130.

[56] Xu, Z., Wang, M. Y. and Chen, T., 2004. An Experimental Study of Particle Damping for Beams and Plates, *Journal of Vibration and Acoustics*, 126, pp.141-148.

[57] Xu, Z., Wang, M. Y. and Chen, T., 2005. Particle Damping for Passive Vibration Suppression: Numerical Modelling and Experimental Investigation, *Journal of Sound and Vibration*, 279(3-5), pp.1097-1120.

[58] Schmidt, I. and Lammering, R., 2004. The Damping Behaviour of Superelastic NiTi Components, *Materials Science and Engineering*, A 378(1-2), pp.70-75.

[59] Piedboeuf, M. C., Gauvin, R. and Thomas, M., 1998. Damping Behaviour of Shape Memory Alloys: Strain Amplitude, Frequency and Temperature Effects. *Journal of Sound and Vibration*, 214(5), pp.885-901.

[60] M.R. Hassan, F. Scarpa, and N.A. Mohamed, 2009. In-plane Tensile Behavior of Shape Memory Alloy Honeycombs with Positive and Negative Poisson's Ratio, Journal of Intelligent Material Systems and Structures 20, no. 8:897-905.

[61] Hassan, M.R., Scarpa, F., Ruzzene, M. and Mohammed, N.A., 2008. Smart shape memory alloy chiral honeycomb. *Materials Science and Engineering: A*, *481*, pp.654-657.

[62] Hassan, M.R., Scarpa, F., Mohamed, N.A. and Ruzzene, M., 2008. Tensile properties of shape memory alloy chiral honeycombs. *physica status solidi (b)*, *245*(11), pp.2440-2444.

204

[63] Scarpa, F., Hassan, M. R. and Ruzzene, M., 2006. Modeling and Testing of Shape Memory Alloy Chiral Honeycomb Structures, in *Smart Structures and Materials 2006: Active Materials: Behavior and Mechanics*, 6170 (presented at Smart Structures and Materials 2006: Active Materials: Behavior and Mechanics, San Diego, CA, USA: SPIE, 2006), 61700W-8.

[64] Hassan, M. R., Scarpa, F. L. and Mohamed, N. A., 2004. Shape Memory Alloys Honeycomb: Design and Properties, in *Smart Structures and Materials 2004: Active Materials: Behavior and Mechanics*, 5387 (presented at Smart Structures and Materials 2004: Active Materials: Behavior and Mechanics, San Diego, CA, USA: SPIE, 2004), pp.557-564.

[65] Michailidis, P. A., et al., 2009. Superelasticity and Stability of a Shape Memory Alloy Hexagonal Honeycomb under In-plane Compression. *International Journal of Solids and Structures*, 46(13), pp.2724-2738.

[66] Yoji, O., et al., 2007. Smart Honeycomb Sandwich Panels with Damage Detection and Shape Recovery Functions. *Journal of the Japan Society for Composite Materials*, 33(1), pp.30-37.

[67] Boucher, M.-A. Smith, C. W., Scarpa, F., Miller, W. and Hassan, M. R., 2010.Damping Capacity in Shape Memory Alloy Honeycomb Structures, *SPIE Proceedings*, volume 7643

[68] Cameron, T. M., et al., 1990. An Integrated Approach for Friction Damper Design. *Journal of Vibration and Acoustics*, 112(2), pp.175-182.

[69] Earles, S. W. E. and Williams, E. J., 1972. A Linearized Analysis for Frictionally Damped Systems. *Journal of Sound and Vibration*, 24(4), pp.445-458.

[70] Hurlebaus, S. and Gaul, L., 2006. Smart Structure Dynamics. *Mechanical Systems and Signal Processing*, 20(2), pp.255-281.

[71] Mason, W. P., 1981. Piezoelectricity, Its History and Applications. *The Journal of the Acoustical Society of America*, 70(6), pp.1561-1566.

Honeycombs with Structured Core for Enhanced Damping

[72] Stanway, R., Rongong, J. and Sims, N., 2003. Active Constrained-layer Damping: A State-of-the-art Review. *Proceedings of the Institution of Mechanical Engineers, Part I: Journal of Systems and Control Engineering*, 217(6), pp.437-456.

[73] Muhammad, A., Yao, X.-L. and Deng, Z.-C., 2006. Review of Magnetorheological (MR) Fluids and its Applications in Vibration Control. *Journal of Marine Science and Application*, 5(3), pp.17-29.

[74] Kordomsky, W. O., Ashour, Rogers, C. A., 1996. Magnetorheological Fluids: Materials, Characterization, and Devices. *Journal of Intelligent Material Systems and Structures*, 7, pp.123-130

[75] Johnson, C. D., 1995. Design of Passive Damping Systems. *Journal of Mechanical Design* 117(B), p.171.

[76] Norton, M. P. and Karczub, D. G., 2003. *Fundamentals of Noise and Vibration Analysis for Engineers*. Cambridge University Press.

[77] Ewins, D. J., 2010. Control of Vibration and Resonance in Aero-engines and Rotating Machinery - An Overview. *International Journal of Pressure Vessels and Piping*, 87.

[78] C. Lira, F. L., Scarpa, R. and Rajasekaran, A., 2011. Gradient Cellular Core for Aero-engine Fan Blades Based on Auxetic Configurations. *Journal of Intelligent Materials Systems and Structures*, 22.

[79] Nashif, A. D., Jones, D. I. G. and Henderson, J. P., 1985. *Vibration Damping*. Wiley Interscience, New York.

[80] Lakes, R. S., 2002. High Damping Composite Materials: Effect of Structural Hierarchy. *Journal of Composite Materials*, 36.

[81] Chen, Y., Scarpa, F., Remillat, C., Farrow, I., Liu, Y. and Leng, J., 2013. Curved Kirigami SILICOMB cellular structures with zero Poisson's ratio for large deformations and morphing. *Journal of Intelligent Material Systems and Structures*, p.1045389X13502852.

[82] Virk, K., Monti, A., Trehard, T., Marsh, M., Hazra, K., Boba, K., Remillat, C.D.L., Scarpa, F. and Farrow, I.R., 2013. SILICOMB PEEK Kirigami cellular structures: mechanical response and energy dissipation through zero and negative stiffness. *Smart Materials and Structures*, *22*(8), p.084014.

[83] Alderson, K. L., Alderson, D., Di Maio, M. R., Haberman, T. A. M., Hewage, T., Klatt, A., Ragni and Scarpa, F. L., 2012. New Solutions for Energy Absorbing Materials: Auxetic Composites. *Proceedings of DYNACOMP*, Arcachon.

[84] Lakes, R. S., 1987. Foam Structures with a Negative Poisson's Ratio. *Science*, 235, pp.1038-1040.

[85] Wang, Y. C. and Lakes, R. S., 2004. Extreme Stiffness Systems due to Negative Stiffness Elements. *Am. J. Phys.* 72(1).

[86] Lakes, R. S., 2001. Extreme Damping in Compliant Composites with a Negative Stiffness Phase. *Philosophical Magazine Letters*, 81(2), pp.95-100.

[87] Gibson, L. J., Ashby, M. F., Schajer, G. S., Robertson, C. I., 1982. *Proc. R. Soc. Lond.*, A382, pp.25-42.

[88] Evans, K. E., 1990. Tailoring the Negative Poisson's Ratio. *Chem. Ind.*, 20, pp.654-657.

[89] Scarpa, F., Ciffo, L. G. and Yates, J. R., 2004. Dynamic Properties of High Structural Integrity Auxetic Open Cell Foam. *Smart Mater. Struct.*, 13(1), pp.49-56.

[90] ANSYS® Academic Research, Release 13.0.

[91] Chen, C. P., Lakes, R. S., 1993. Viscoelastic Behaviour of Composite Materials with Conventional or Negative Poisson's Ratio Foam as One Phase. *J. Materials Science*, 28(16), pp.4288-4298.

[92] Scarpa, F., Remillat, C., Landi, P., Tomlinson, G., 2000. Damping Modelization of Auxetic Foams. *Proc. SPIE*, 3989, p.336.

[93] Wu, C., Weeks, C. and Sun, C., 1995. Improving Honeycomb Core Sandwich Structures for Impact Resistance. *J Adv Mater*, 26(4), pp.41-47.

[94] Vaidya, U., Kamath, M., Mahfuz, H. and Jeelani, S., 1998. Low Velocity Impact Response of Resin Infusion Molded Foam Filled Honeycomb Sandwich Composites. *J Reinf Plast Compos*, 17(9), pp.819-849.

[95] Vaziri, A., Xue, Z. and Hutchinson, J., 2006. Metal Sandwich Plates with Polymer Foam-filled Cores. *J Mech Mater Struct*, 1(1), pp.95-125.

[96] Wang, B. and Yang, M., 2000. Damping of Honeycomb Sandwich Beams. *Journal of Materials Processing Technology*, 105(1–2), pp.67-72.

[97] Wong, C. X., Daniel, M. C., Rongong, J. A., 2009. Energy Dissipation Prediction of Particle Damper. *Journal of Sound and Vibration*, 319(1-2), pp.91-118.

[98] Rajasekaran R., Scarpa, F., Smith, C., Miller, W. and Evans, K., 2011. *Vibration Damping Structure*. Rolls-Royce plc, University of Exeter, University of Bristol, Patent WO2011104112 (A1).

[99] Abd El-Sayed, F. K., Jones, R. and Burgess, I. W., 1979. A Theoretical Approach to the Deformation of Honeycomb Based Composite Materials. *Composites*, 10(4), pp.209-214.

[100] Gibson, R. F., 1992. Damping Characteristics of Composite Materials and Structures. *Journal of Materials Engineering and Performance*, 1(1), pp.11-20.

[101] Matlab 7.9.0, The MathWorks Inc., 2009.

[102] Johnson, C. D. and Kienholz, D. A., 1982. Finite Element Prediction of Damping in Structures with Constrained Viscoelastic Layers, *AIAA Journal*, 20(9), pp.1284-1290.

[103] Landi, F. P., Scarpa, F., Rongong, J. A. and Tomlinson, G., 2002. Improving the Modal Strain Energy Method for Damped Structures using a Dyadic Matrix

Honeycombs with Structured Core for Enhanced Damping

Perturbation Approach. *Proceedings of the Institution of Mechanical Engineers, Part C: Journal of Mechanical Engineering Science*, 216, p.12.

[104] Warren, C. Y. and Budynas, R. G., 2011. *Roak's Formulas for Stress and Strain*, 8th edition, McGraw Hill Professional.

[105] HexWeb, T. M., 1999. Honeycomb Attributes and Properties, *Hexcel Composites.*

[106] Sun, C. T. and Vaidya, R. S., 1996. Prediction of Composite Properties from a Representative Volume Element. *Composites Science and Technology*, 56(2).

[107] Odegard, G. M., 2004. Constitutive Modeling of Piezoelectric Polymer Composites, *Acta Materialia*, 52(18).

[108] Lakes, R. S., 2009. *Viscoelastic Materials*, Cambridge University Press.

[109] Mentel, T. J. and Fu, C. C. Damping Energy Dissipation at Support Interfaces of Square Plates. Materials Laboratory, Contract no. AF33 (616)-5426, Project no. 7360.

[110] Technical Data, 2012. 3M Viscolestic Damping Polymers 112- 130-, *Electronics Markets Materials Division,* 3M.

[111] Gere, J. M. and Goodno, B. J., 2009. *Mechanics of Materials, Seventh Edition (SI Edition)*, Cengage Learning.

Honeycombs with Structured Core for Enhanced Damping